INTEGRATED INVESTIGATION OF NATURAL

ATTENUATION IN A PETROLEUM HYDROCARBON

CONTAMINATED AQUIFER

by

RICHARD THEODULE AMOS

B.Sc., University of Toronto, 2001

A THESIS SUBMITTED IN PARTIAL FULFILMENT OF

THE REQUIREMENTS FOR THE DEGREE OF

DOCTOR OF PHILOSOPHY

in

THE FACULTY OF GRADUATE STUDIES

(Geological Sciences)

THE UNIVERSITY OF BRITISH COLUMBIA

July 2006

Abstract

This research investigates natural attenuation processes at a crude oil spill site near Bemidji, MN, with a focus on the contribution of methanogenesis. An important aspect of this work is evaluating the use of naturally occurring gases in the saturated and unsaturated zones to aid in the assessment of methane production rates, the fate of methane, and more generally to quantitatively assess the effect of gas production in source zones on contaminant release and attenuation.

Field data from the Bemidji site demonstrate that naturally occurring stable gases such as Ar and N_2 can be effectively used to better understand and quantify physical and chemical processes related to methanogenic activity. These include biochemically induced gas advection in the unsaturated zone, degassing and gas bubble formation due to methanogenic gas production in the saturated source zone, and attenuation of dissolved gases in the groundwater plume. To allow a more quantitative assessment, the reactive transport code MIN3P has been enhanced to simulate bubble growth due to in-situ gas production, bubble entrapment due to water table rise, and permeability changes due to trapped bubbles. Simulations for a hypothetical case study suggest that these processes work to attenuate the dissolved gas plume emanating from the source zone. A detailed simulation, constrained by Bemidji field data, is conducted to provide an integrated assessment of natural attenuation processes in the unsaturated and saturated zones. Although gas bubble ebullition is potentially an important process at the site, it could not be included in the site-specific simulations, because this process is poorly understood and not well constrained by field data. To investigate this process, column experiments were conducted that show clear evidence for ebullition from a methanogenic environment,

using dissolved gas concentrations to monitor the extent and rate of ebullition. An empirically derived formulation describing ebullition, integrated into MIN3P, provides insights into the parameters controlling ebullition and allows the process to be quantified.

Overall, this work contributes to a better understanding of natural attenuation processes in contaminated aquifers and offers novel field and modeling techniques to investigate and quantify these processes.

Table of Contents

List of Tables

List of Figures

xi

List of Abbreviations

NAPL – non-aqueous phase liquid

LNAPL - light non-aqueous phase liquids

BTEX – benzene, toluene, ethylbenzene, xylenes

TEAP – terminal electron accepting process

DNAPL – dense non-aqueous phase liquid

MPN – most probable number

WEA – water in equilibrium with the atmosphere

MASL – meters above sea level

Acknowledgements

To my friends in Vancouver, I would like to say thanks for all the beers and barbeques along with the hiking, sailing, kayaking, hockey and the occasional golf game. This includes in no particular order, Edmo, Dave, Cindy, Jon, Craig, Randi, Sergi and

1 Introduction

The contamination of aquifers by petroleum hydrocarbons from pipeline breaks, leaky underground storage tanks, and other sources is a widespread environmental problem. In Canada, the Federal Contaminated Sites and Solid Waste Landfills Inventory lists 1,396 sites contaminated with hydrocarbons, which is by far the largest group of contaminated sites listed. In 2003, The Canadian Association of Petroleum Producers reported three spills, on average equivalent to 60 m^3 of oil, per 1000 km of pipeline. Traditional methods of remediation, such as pump and treat, can be very costly and are often unable to meet regulatory requirements. An alternative approach is monitored natural attenuation, which has gained regulatory acceptance and has become an important remediation technology (National Research Council (U.S.), 2002). In general, regulations are based on showing that contaminant plumes have ceased growing or are shrinking in size and that downgradient receptors will not be affected by the contaminant.

Despite the extensive research conducted in this area, key questions remain, particularly with respect to quantification of the rates of biodegradation and longevity of the source zone, although it is generally acknowledged that large source zones will persist for long periods of time, i.e. tens to hundreds of years. EPA guidelines stipulate that remediation objectives must be attained in a reasonable timeframe and further recommends use of source control measures in conjunction with natural attenuation (EPA, 1999). In light of the lack of research documenting the potential for contaminant mass removal from source zones, and reliable estimates of source zone longevity under natural attenuation conditions, it is not surprising that regulators tend to opt for more conventional source control methods. Understandably these issues are of particular concern where large spills have occurred and the accumulation of non-aqueous phase

2

liquids (NAPL) pose a long-term environmental concern, as is the case at the Bemidji site.

The petroleum hydrocarbon contaminated site near Bemidji, Minnesota has presented an ideal natural laboratory to study natural attenuation processes. The crude oil spill occurred in 1979 due to a ruptured underground pipeline and left ~400,000 L of oil in the subsurface after initial clean-up efforts (Delin et al., 1998). Two main oil pools formed on the water table of which the north pool is the largest and the most intensively studied. An extensive investigation has been conducted at the site involving many researchers from the U.S. Geological Survey and several universities over a period of approximately 20 years.

Previous research at the Bemidji site has included organic and inorganic geochemistry in the saturated zone, mineralogy (Bennett et al., 1993; Baedecker et al., 1993; Eganhouse et al., 1993), detailed investigation of the progression of microbially mediated redox processes (Bekins et al., 1999; Cozzarelli et al., 2001; Bekins et al., 2001), isotope analysis of petroleum degradation pathways in the saturated and unsaturated zones (Revesz et al., 1995), oil phase saturation studies (Dillard et al., 1997), and several modeling studies in the saturated and unsaturated zones (Essaid et al., 1995; Chaplin et al., 2002; Essaid et al., 2003). These studies have been successful in elucidating the evolution of the degradation processes over the history of the site. However, previous studies have not considered the saturated and unsaturated zones in an integrated manner and have not explicitly considered mass transfer between the zones, and the related affect on biogeochemical processes. Furthermore, given that methanogenesis is an important degradation pathway, key processes related to CH_4

production, transport, and degradation have not been adequately investigated and quantified.

Modeling studies at Bemidji have included both the saturated and unsaturated zones. Essaid et al. (1995) simulated biodegradation of volatile and nonvolatile dissolved organic matter and the geochemical evolution of the groundwater plume, including the progression of redox processes, up to 1990 and showed that anaerobic degradation processes accounted for more than half of the dissolved organic carbon removal at the site. Essaid et al. (2003) used inverse modeling to estimate BTEX dissolution and degradation rates in the saturated zone and determine mass removal from the oil body. Using measured oil saturation data and effective solubilities they determined that 18 years after the spill 10.2% of benzene, 8.6% of toluene, 1.2% of ethylbenzene, 1.4% of *m,p*-xylene and 2.7% of *o*-xylene had been removed from the oil body. They estimated that 77% of the benzene would remain in the oil body after 50 years. Chaplin et al. (2002) simulated vertical 1D mass flux of gases through the vadose zone based on 1985 and 1992 data to determine rates of volatilization and biodegradation. Based on O_2, CO_2 and CH_4 concentration data they found that hydrocarbon mass loss decreased from 10.52 kg day^{-1} in 1985 to 1.99 kg day^{-1} in 1997, with most of this decrease due to a reduction in volatilization while degradation rates remained relatively constant. These studies do not consider mass flux across the water table; although, each makes assumptions or note discrepancies in the model due to this simplification. For example, Chaplin et al. (2002) used CH_4 mass fluxes through the vadose zone to quantify degradation rates but have assumed that all the CH_4 was produced in the vadose zone and ignored the potential for degassing from the saturated zone. Essaid et al. (1995) noted that simulated CH_4

4

concentrations downgradient of the floating oil body are lower than those measured in the field. These authors suggest that recharge water may contain high levels of CH_4 due to methanogenesis occurring in the highly contaminated section of the unsaturated zone. These assumptions and simplifications highlight the need for a more integrated approach.

Methanogenesis has been identified as an important degradation process at the Bemidji site since early in the evolution of the plume. Baedecker et al. (1993) found that dissolved CH_4 concentrations in wells immediately downgradient of the floating oil body increased sharply from 1984 to 1987. Furthermore, concentrations measured in 1987 and 1988 were sufficient to exceed total gas solubility, and suggest that degassing and possibly ebullition may occur. This hypothesis is supported by Revesz et al (1995), who measured dissolved Ar and N_2 directly below the floating oil body in June 1991 and found concentrations 25 times lower than in background wells. This suggests that degassing and consequent stripping of non-reactive gases was occurring due to CH_4 production from methanogenesis. The formation of gas bubbles can provide a significant sink for CH_4 and other gases and can also affect the hydraulic properties of the aquifer (Ryan et al, 2000). The formation of gas bubbles below the water table can also lead to ebullition, which may provide a source of CH_4 to the unsaturated zone, providing another link between the two zones. Considering the importance of methanogenesis as a degradation pathway and the potential for gas bubble formation, a more rigorous investigation of the processes affecting CH_4 production, transport, and degradation, along with the potential effects of gas bubbles on natural attenuation processes, is warranted.

1.1 Objectives

The objectives of this study are defined by four key research questions. These are; 1) What is the potential for contaminant mass removal through biodegradation, and specifically methanogenesis, at the Bemidji site in both the saturated and unsaturated zones? 2) What is the relationship between saturated and unsaturated zone processes and geochemistry? 3) What are the processes responsible for CH_4 production, transport, and degradation, and what are their rates? 4) What are the effects of gas bubbles on natural attenuation processes and how can these effects be quantified in the field and in modeling studies?

This thesis has been organized into four main research chapters (Chapters 2-5), each outlining a specific component of the research. Chapter 2 covers fieldwork conducted at the Bemidji site. This study involved the collection of dissolved and vapor phase gases in the saturated and unsaturated zones, and employs the use of non-reactive and relatively stable gases, Ar and N_2 respectively, to identify important processes related to the fate and transport of CH_4 in the groundwater and vadose zone plume. Specifically, in the vadose zone Ar and N_2 are used to identify reactive zones, including production of CH_4 by methanogens and the oxidation of CH_4 by aerobic methanotrophs, and assess the relative importance of advective and diffusive gas fluxes. In the saturated zone, dissolved Ar and N_2 concentrations are used to quantify degassing and bubble formation in the source zone, providing a better estimate of CH_4 production in the methanogenic zone, and evaluate gas transport processes downgradient of the source.

Chapter 3 outlines the development of a reactive transport model to simulate gas bubble formation/dissolution due to changes in dissolved gas pressure, and

6

entrapment/release of gas bubbles due to water table fluctuations. This model provides a means of quantitatively assessing the conceptual model of CH_4 fate and transport in the saturated zone developed in Chapter 2. Simulations are conducted for a hypothetical case study based on a simplified representation of the Bemidji site to demonstrate that bubble formation below the water table, and bubble entrapment near the water table can significantly affect the hydrogeochemistry of the contaminant plume. In the source zone, the formation of gas bubbles provides a large sink for CH_4 and reduces the hydraulic conductivity of this zone. Downgradient of the source zone, gas bubbles of atmospheric composition trapped near the water table can potentially be a significant source of O_2 to the aquifer providing oxidation potential for CH_4 or organic contaminants.

In Chapter 4, the newly developed model is used to simulate the evolution of petroleum hydrocarbon degradation at the Bemidji site. This study integrates the important processes identified in Chapters 2 and 3 into a comprehensive site-specific model that includes the saturated and unsaturated zone. This simulation includes a detailed representation of the initial oil distribution, including representative fraction of the important contaminants, a detailed representation of the progression of terminal electron accepting processes (TEAPs) consistent with observed degradation pathways at the field site, and integrates saturated and unsaturated zone processes to investigate mass transfer across the water table and important processes in the capillary fringe. The simulation offers insights into physical and chemical processes at the site, provides an estimate of total hydrocarbon degradation and source longevity, and highlights limitations in the current state of knowledge with respect to hydrogeological and

geochemical processes at the site, and the interpretation of these processes using reactive transport modeling.

In Chapter 5, the process of gas bubble ebullition is investigated using column experiments and reactive transport modeling. Ebullition is potentially an important process at sites like Bemidji where significant biogenic gas production occurs, but is difficult to asses at the field scale. The experiments and modeling are aimed at determining the important parameters controlling ebullition, and investigating the potential importance of this process at sites where biogenic gas production is significant.

1.2   References

Baedecker, M.J., Cozzarelli, I.M., Eganhouse, R.P., Siegel, D.I., Bennett, P.C. (1993), Crude oil in a shallow sand and gravel aquifer - III. Biogeochemical reactions and mass balance modeling in anoxic groundwater, *Appl. Geochem.*, *8*, 569-586.

Bekins, B.A., Godsy, E.M., Warren, E. (1999), Distribution of microbial physiologic types in an aquifer contaminated by crude oil, *Microbial Ecology*, *37*, 263-275.

Bekins, B.A., Cozzarelli, I.M., Godsy, E.M., Warren, E., Essaid, H.I. Tuccillo, M.E. (2001), Progression of natural attenuation processes at a crude oil spill site: II: Controls on spatial distribution of microbial populations, *J. Contam. Hydrol.*, *53*, 387-406.

Bennett, P.C., Siegel, D.E., Baedecker, M.J., and Hult, M.F. (1993), Crude oil in a shallow sand and gravel aquifer – I. Hydrogeology and inorganic geochemistry, *Appl. Geochem.*, *8*, 529-549.

Chaplin, B.P., Delin, G.N., Baker, R.J., Lahvis, M.K. (2002), Long-term evolution of biodegradation and volatilization rates in a crude oil-contaminated aquifer, *Bioremediation Journal*, *6*, 237-255.

Cozzarelli, I.M., Bekins, B.A., Baedecker, M.J., Aiken, G.R., Eganhouse, R.P., Tuccillo, M.E. (2001), Progression of natural attenuation processes at a crude-oil spill site I. Geochemical evolution of the plume, *J. Contam. Hydrol.*, *53*, 369-385.

Delin, G.N., Essaid, H.I., Cozzarelli, I.M., Lahvis, M.H., Bekins, B.A. (1998), USGS Fact Sheet 084-98, Ground Water Contamination by Crude Oil near Bemidji, Minnesota. http://mn.water.usgs.gov.

Dillard, L.A., Essaid, H.I., Herkelrath, W.N. (1997), Multiphase flow modeling of a crude-oil spill site with a bimodal permeability distribution, *Water Resour. Res.*, *33*, 1617-1632.

Eganhouse, R.P., Baedecker, M.J., Cozzarelli, I.M., Aiken, G.R., Thorn, K.A. (1993), Crude oil in a shallow sand and gravel aquifer - II. Organic geochemistry, *Appl. Geochem.*, *8*, 551-567.

EPA (1999), Use of monitored natural attenuation at Superfund, RCRA corrective action, and underground storage tank sites, Directive number 9200.4.17P, Washington, D.C., EPA, Office of Solid Waste and Emergency Response.

Essaid, H.I., Bekins, B.A., Godsy, E.M., Warren, E., Baedecker, M.J., Cozzarelli, I.M. (1995), Simulation of aerobic and anaerobic biodegradation processes at a crude oil spill site, *Water Resour. Res.*, *31*, 3309-3327.

Essaid, H.I., Cozzarelli, I.M., Eganhouse, R.P., Herkelrath, W.N., Bekins, Delin, G.N. (2003). Inverse modeling of BTEX dissolution and biodegradation at the Bemidji, MN crude-oil spill site, *J. Contam. Hydrol.*, *67*, 269-299.

National Research Council (U.S.), Committee on Intrinsic Remediation (2000), Natural attenuation for groundwater remediation. Washington D.C., National Academy Press.

Revesz, K., Coplen, T.B., Baedecker, M.J., Glynn, P., and Hult, M. (1995), Methane production and consumption monitored by stable H and C isotope ratios at a crude oil spill site, Bemidji, Minnesota. *Appl. Geochem.*, *10*, 505-516.

Ryan, M.C, MacQuarrie, K.T.B., Harman, J., Mclellan, J. (2000), Field and modeling evidence for a "stagnant flow" zone in the upper meter of sandy pheatic aquifers, *J. Hydrol.*, *233*, 223-240.

2 Use of Dissolved and Vapor Phase Gases to Investigate Methanogenic Degradation of Petroleum Hydrocarbon Contamination in the Subsurface

2.1 Introduction

The use of monitored natural attenuation has become an accepted remediation strategy for treatment of petroleum hydrocarbon contaminated groundwater plumes (National Research Council (U.S.) 2000). Despite this general acceptance, many regulatory agencies still require source removal of mobile light non-aqueous phase liquids (LNAPL) to ensure timely elimination of all subsurface contaminants (e.g. EPA, 1999). This is not surprising considering the lack of reliable estimates of source longevity, and the difficulties involved in making such estimates. It is therefore important to understand the physical and geochemical processes that control the fate of contaminants and their biodegradation by-products in the source zone and downgradient plume, and identify means of quantifying these processes. (The term *source zone* is used in this paper to describe the subsurface area that contains free-phase oil, including the saturated and unsaturated zones). Where significant hydrocarbon mass exists, methanogenesis can become the dominant long-term degradation pathway as more thermodynamically favored electron acceptors become depleted from the aquifer. In a survey of 38 sites, Wiedemeier et al. (1999) estimated that methanogenesis was responsible for 16% of petroleum hydrocarbon degradation, confirming the general importance of this degradation pathway.

Natural attenuation processes at petroleum hydrocarbon contaminated sites, and methanogenic degradation in particular, have been previously studied using a variety of techniques. These include, organic and inorganic aqueous geochemistry (Bennett et al., 1993; Eganhouse et al., 1993; Cozzarelli et al., 2001), isotope geochemistry (Revesz et al., 1995; Conrad et al., 1997, Bolliger et al., 1999), laboratory microcosm experiments

(Baedecker et al., 1993; Weiner and Lovley, 1998; Shubal et al., 2001), microbial data (Bekins et al., 1999; Bekins et al., 2001), redox indicators such as E_h and H_2 measurements (Vroblesky and Chapelle, 1994; Chapelle et al, 1996), vapor phase reactive gases such as CH_4, CO_2, O_2 and hydrocarbons (Lahvis and Baehr, 1996; Hers et al., 2000, Chaplin et al., 2002), and dissolved reactive gases such as CH_4 and CO_2 (Revesz et al., 1995; Skubal et al., 2001).

Despite this extensive research, quantification of various processes, including the rate of methane production, consumption, and transport in the saturated and unsaturated zones, as well as mass transfer between the zones, has been difficult. Methane production below the water table may be significant, and because methane is fairly insoluble, formation of gas bubbles and ebullition may be possible (Reeburgh, 1972; Kipphut and Martens, 1982; van Breukelen et al., 2003). As a point of clarification, the process of bubble formation and partitioning of gases into the bubble as described in this paper is referred to as *'degassing'*. This is distinguished from the term *'ebullition'* which refers to the transport of gas bubbles to the unsaturated zone. This distinction is made because, although these processes are closely related to each other, the effects of each process on groundwater chemistry may differ. Methane may also be produced in the vadose zone or may be re-oxidized by ingress of atmospheric oxygen from the ground surface (Hers et al., 2000; Chaplin et al., 2002). Better quantification of these processes would lead to more accurate estimates of methane production, transport, and consumption rates, thus leading to a better carbon mass balance of the system and improved estimates of total hydrocarbon degradation.

Previous studies have shown that non-reactive dissolved and vapor phase gases can be used to investigate physical and chemical processes affecting dissolved gas concentrations in the subsurface. For example, Blicher-Mathieson et al. (1998) showed that in the saturated zone naturally occurring dissolved Ar could be used to quantify degassing occurring in response to denitrification in a Danish riparian wetland. Other workers have observed depleted concentrations of Ar and N_2 in methanogenic aquifers, which has been interpreted as being due to degassing as a result of production of methane (Revesz et al., 1995; van Breukelen et al., 2003). Researchers have also used stable gases to investigate transport processes in saturated media. For example, Jardine et al. (1999) injected helium and neon as tracers to investigate transport processes in fractured media; Semprini et al. (2000) used naturally occurring Radon-222 to locate NAPL saturation in field and laboratory experiments; and Divine et al. (2003) investigated residual DNAPL distribution using helium and neon in laboratory partitioning tracer tests. In the unsaturated zone, Thorstenson and Pollock (1989) demonstrated theoretically that Ar and N_2 concentrations could be used to estimate total gas fluxes of reactive gases, including diffusive and advective components.

The objective of this research is to demonstrate that non-reactive and relatively inert dissolved and vapor phase gases, such as Ar and N_2 respectively, can be used to gain a more complete understanding of the physical and chemical processes within the saturated and unsaturated zones at a petroleum-hydrocarbon contaminated site, where methanogenesis is a significant biodegradation pathway. To our knowledge a comprehensive study involving dissolved and vapor phase gases has not been previously undertaken at any field site, and more specifically, various processes related to

14

methanogenic degradation have not been thoroughly investigated using Ar and N_2 as indicators.

Using field data collected at an oil spill site near Bemidji, MN, we aim to show that several processes can be identified using Ar and N_2 as indicators, and that these processes can potentially be quantified using the data. Specifically, we will show that; 1) In the vadose zone, regions of depletion and enrichment in Ar and N_2 can be used to identify reactive zones, including production of CH_4 by methanogens and the oxidation of CH_4 by aerobic methanotrophs. Furthermore, the concentration gradients of Ar and N_2 can be used to assess the relative importance of advective and diffusive gas fluxes. 2) In the saturated zone, dissolved Ar and N_2 concentrations can be used to quantify degassing, thus providing a better estimate of methane production in the methanogenic zone. Downgradient of the source, trends in dissolved Ar and N_2 concentrations can be used to evaluate gas transport processes. 3) Comparison of the Ar and N_2 data in both the saturated and unsaturated zones can be used to assess the reactivity of N_2 and the importance of chemical processes such as nitrogen fixation.

2.2 Site Description

In 1979, an underground crude oil pipeline burst near Bemidji, Minnesota and three large bodies of oil accumulated in the subsurface. These are referred to as the south, middle, and north pools, with the north pool, originally containing an estimated ~80,000 to 160,000L of oil (Bennett et al., 1993), being the subject of this study. Figure 2-1 shows a cross section of the contaminated aquifer parallel to the groundwater flow direction through the north pool, and delineates the major geochemical zones that have developed as a result of the contamination. A comprehensive site overview and a detailed

description of the geochemical zones can be found in Bennett et al. (1993), Baedecker et al. (1993), Bekins et al. (1999), Bekins et al. (2001), Cozzarelli et al. (2001), and Chaplin et al. (2002). Here we focus on information that is relevant to the generation and fate of methane.
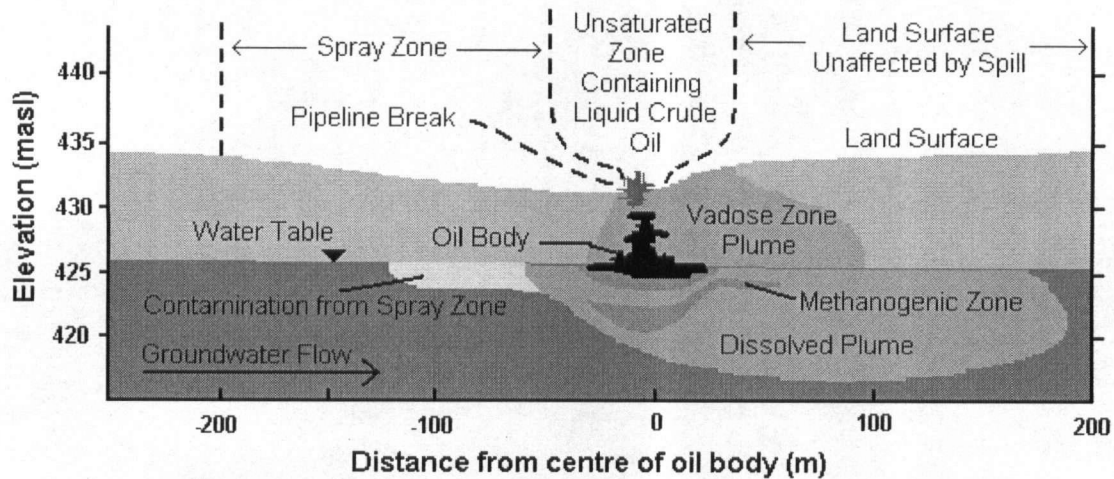
Figure 2-1. Cross section of contaminated aquifer showing major geochemical zones. Modified from Delin et al. (1998).

The oil body sits on the water table of a surficial glacial outwash aquifer 6-9 m below land surface. The saturated and unsaturated zones consist of moderately to poorly sorted sandy gravel, gravely sand, and sand with thin interbeds of fine sand and silt, and are moderately calcareous (Franzi, 1988). Groundwater velocities have been measured and range from 18 m y^{-1} in the fine sand layers to 180 m y^{-1} in coarser material (Bennett et al., 1993). Uncontaminated groundwater is oxic and does not contain methane.

Zones of methane production have been identified in previous studies, both in the saturated zone directly underlying and down gradient of the oil body (Baedecker et al., 1993; Cozzarelli et al., 2001; Bekins et al., 2001), and in the unsaturated zone containing

16

liquid crude oil (Hult and Grabbe, 1988; Chaplin et al., 2002). The saturated zone

contaminant plume is anoxic and contains two distinct zones of methanogenic activity

(Bekins et al. 1999) with CH_4 concentrations greater than 15 mg L^{-1} in both zones

(Cozzarelli et al., 2001). Using the most probable number (MPN) method on wet

sediment samples, Bekins et al. (1999) defined a zone as methanogenic if attached total

methanogens were greater than 10 per gram; maximum observed numbers were

approximately 10^2 cells per gram. Although these numbers are relatively low compared

to other physiologic types (i.e. iron reducers range between 10^2 and 10^6 per gram), they

represent a distinct increase over background samples where methanogens were

nondetectable. The methanogenic zones are also characterized by decreased numbers of

iron reducers and increased numbers of fermenters. Methane concentrations in pore water

farther down gradient decrease, while oxygen concentrations increase to near background

levels.

The vadose zone vapor plume near the oil body is characterized by low O_2

concentrations (less than 2 % of atmospheric) and high levels of CO_2 (>10%) and CH_4

(>15%). In wet sediment samples from locations in the oil body, Bekins et al. (1999,

2002) found greater methanogen numbers (10^2 to 10^4 per gram) than found in the

saturated zone, suggesting that methanogenesis is a significant degradation pathway in

the unsaturated zone. Gas concentrations transition to near atmospheric levels away from

the oil body (Hult and Grabbe, 1988; Chaplin et al., 2002).

2.3 Methods

2.3.1 Dissolved gas sampling:

Monitoring wells are constructed of 5 cm ID PVC tubing with stainless steel screens as described by Bennett et al. (1993). Water samples for dissolved gas sampling were collected using down-hole positive displacement pumps at a rate of approximately 2-4 L min^{-1}. A minimum of 3 well volumes was purged from each well before sampling. In 2002, water samples from within the source zone were analyzed using a bubble-stripping technique (Chapelle and McMahon, 1991), while outside the source zone the samples were analyzed using a static headspace technique (e.g. Risgaard-Peterson and Rysgaard, 1995; Blicher-Mathieson et al.,1998). In 2003, all samples were analyzed using the static headspace technique. Briefly, both methods made use of a 500 mL Erlenmeyer flask fitted with a three-hole rubber stopper. The stopper was fitted with an inlet tube, an outlet tube, and a rubber septum. The stoppered flask was carefully filled through the inlet tube to ensure that no air bubbles were trapped; and purged for approximately 5 minutes to further reduce the possibility of air contamination. With the flask inverted a 15 ml aliquot of UHP helium was injected through the rubber septum. For the bubble stripping technique, water continued to be flushed through the flask for a minimum of 30 minutes to allow the dissolved gases to equilibrate with the He headspace. For the static headspace technique the flask was sealed, then shaken vigorously for ten minutes to equilibrate the gases. After equilibration, a 10 ml gas sample was collected with a gas-tight syringe for injection into the field GC.

For both methods, the volumes used, i.e. a 500 ml water sample and a 10 ml gas sample, are generally much larger than other values quoted in the literature. However, we

found the 10 ml gas sample necessary to facilitate adequate flushing of the water vapor filter and sample loop fitted to our particular GC model (see section 3.3). Due to the large gas volume necessary, a large water sample was used to maximize analytical accuracy. The bubble-stripping method was chosen for the source zone wells in 2002 because theoretically this method should provide a higher degree of accuracy. However, in practice this method was more cumbersome and time consuming and was therefore abandoned the subsequent year.

Accuracy and precision of the static headspace method was tested in the lab using water equilibrated with the atmosphere (WEA). The standard deviation of 6 samples was 0.013, 0.15 and 0.16 mg L^{-1} for Ar, O_2 and N_2 respectively. Assuming mole fractions of 0.0093, 0.21 and 0.78 for Ar, O_2 and N_2 in air, the accuracy of the 6 samples was -2.1%, -3.2% and -3.4% for the three gases respectively. This negative bias appears to be due to an increase in pressure in the sampling flask, which is difficult to measure accurately.

At the Bemidji site in 2003, source zone well 420d (33 m downgradient of well 421) was sampled using both the bubble stripping and static headspace methods 3 times each within a 4 h period. The difference between the means of the two methods was 0.23, 27.4, 0.04, 0.02 and 0.84 mg L^{-1} for CH_4, CO_2, Ar, O_2 and N_2 respectively, which is equivalent to 2.7%, 19%, 7.5%, 5.0% and 7.3% of the mean values from the static headspace method for the five gases respectively. Although these differences are not insignificant, they are small in comparison to the large changes in dissolved gas composition along the flow path, and the general trends observed can be defended with reasonable certainty.

19

2.3.2 Vapor phase gas sampling

Vapor sampling wells are constructed of 6.4-mm OD stainless steel tubing with a 10 cm screen as described by Hult and Grabbe (1988) and Chaplin et al. (2002). Gas samples were collected in a 50 ml gas tight syringe using a peristaltic pump after purging a minimum of 3 well volumes.

2.3.3 Gas analysis

Analysis for Ar, O_2, N_2, CH_4, and CO_2, was performed on a Varian CP-4900 dual channel gas chromatograph equipped with TCD detectors, a molsieve 5A PLOT column to separate Ar, O_2, and N_2 and a PoraPLOT U column to separate CH_4 and CO_2. The carrier gas used for both columns was helium. The molsieve column is capable of baseline separation of Ar and O_2 at ambient temperatures. This instrument was calibrated with air and Supelco calibration mix #234 consisting of approximately 5 % N_2, 5 % O_2, 4 % CH_4, and 5 % CO_2 in He.

2.4 Results

2.4.1 Spatial Distribution of Dissolved and Vapor Phase Gases

Cross-sections of the vapor phase and dissolved gas data along a transect parallel to the groundwater flow through the source zone are shown in Figure 2-2A-E for CH_4, CO_2, O_2, Ar and N_2 respectively. Dissolved gas data collected in 2002 showed similar trends to the 2003 data and are therefore not displayed graphically. Also shown in the figures is the location of the free-phase oil based on data from Dillard et al. (1997).
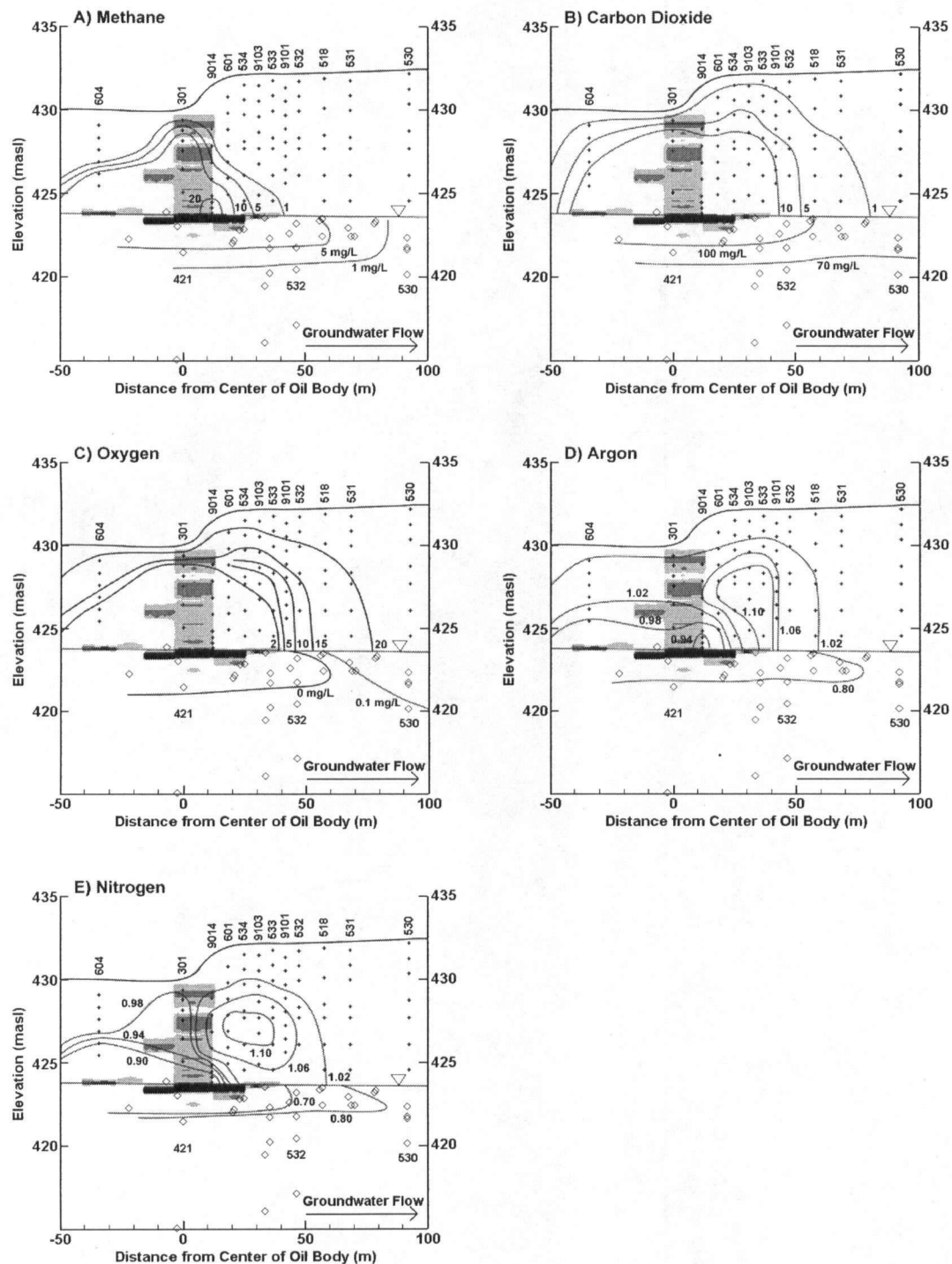
Figure 2-2. Cross sections of aquifer showing dissolved and vapor phase gas data collected in 2003. Vapor phase contours are in % mole fractions except for N_2 and Ar which are in fraction of atmospheric concentrations. Dissolved N_2 and Ar contours are in fraction of average background concentrations. Oil body saturation contours are from light to dark, 0.1, 0.2 and 0.3 and are based on data from Dillard et al. (1997). Well numbers for each vapor well and selected saturated zone wells are shown.

21

2.4.2 Vapor Phase

Vapor phase CH_4, CO_2 and O_2 data (Figures 2-2A-C) show expected trends based on previous data collected at the Bemidji site (Hult and Grabbe, 1988; Chaplin et al., 2002). Namely, O_2 concentrations are depleted surrounding the suspended free-phase oil in the unsaturated zone and above the floating oil, with an anoxic zone nearest the free-phase oil. Methane concentrations are elevated in the anoxic area near the free-phase oil and CO_2 concentrations are elevated in the area of O_2-depletion. In agreement with the findings of Chaplin et al. (2002), the vapor phase plume continues to grow with time. The plume shown here (i.e. area of low O_2 concentrations and high CH_4 and CO_2 concentrations) from 2003 data is larger than in 1997 (Chaplin et al., 2002), which is in turn larger than in 1985 (Hult and Grabbe, 1988).

Although argon is a non-reactive gas, vapor phase Ar concentrations distinctly show an enrichment above atmospheric levels throughout most of the vapor phase plume with an area of Ar-depletion directly above the floating oil (Figure 2-2D). Generally the trends in the N_2 data are similar to the Ar data; however, there tends to be less enrichment and greater depletion in comparison to Ar (Figure 2-2E).

2.4.3 Dissolved Gases

Dissolved CH_4, CO_2 and O_2 data also show trends consistent with the existing conceptual model and previously collected data (Baedecker et al., 1993; Revesz et al., 1995, Cozzarelli et al., 2001; Bekins et al., 2001; Figure 2-2A-C). A large suboxic plume (DO <1 mg L^{-1}) extends approximately 200m downgradient from the center of the oil body with a more anoxic core. Methane concentrations are high in the source zone but quickly decrease down gradient. The area of highest CH_4 concentrations, i.e. within the 1

mg L^{-1} contour, lies within the anoxic portion of the plume. Concentrations of CO_2 are high in the source zone and in the downgradient plume.

Despite its non-reactive nature, dissolved Ar concentrations in the source zone show depletion compared to background concentrations, but quickly return to background levels ~100 m downgradient of the source. The area of Ar depletion roughly corresponds to the area of high CH_4 concentrations. Dissolved nitrogen concentrations follow a similar trend, although they tend to show a greater depletion than Ar.

2.5   Discussion

2.5.1   Unsaturated zone gas transport

2.5.1.1   Evidence for advective gas flux

Thorstenson and Pollock (1989) demonstrated through theoretical analysis that the concentration of a non-reactive gas will be enriched in the direction of net mass flux, and depleted where the net mass flux is away from the region. This result also implies that there must be an advective component to the net mass flux where there is an enrichment or depletion of non-reactive gases. Data for a vertical section at vapor well 601 (Figure 2-3) shows areas of both enrichment and depletion, indicating that gas advection is taking place in the unsaturated zone at Bemidji.

At the lowest sampling point of well 601 (425 masl), N_2 concentrations are below atmospheric levels implying a net mass flux away from this region. However, because the N_2 concentration decreases downward, driving a downward diffusive flux, an advective flux in the upward direction must exist to maintain the observed depletion in N_2. The opposite effect is apparent in the middle section of the vertical profile (426-429 masl).

The maximum concentration of N_2 is in the center, driving diffusive flux outward from this zone so that an inward advective flux must exist to maintain the observed enrichment in N_2. The net mass flux is also toward this zone. Although the net flux may not be entirely vertical at this location (Figure 2-2), the principles discussed here are not significantly altered by this simplification. Argon is not shown in the diagram; however, the vertical concentration profile follows the same general trend as for N_2 (see Figure 2-2), and the same arguments apply.
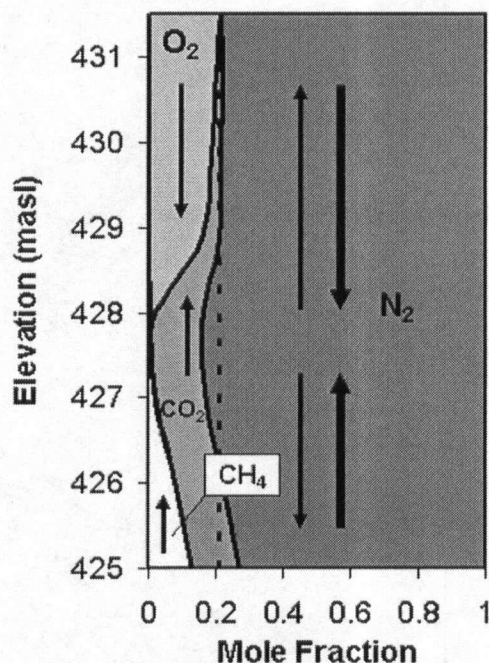
Figure 2-3. Mole fractions of major gases, represented by the shaded areas, at vapor well 601 in 2003. Argon fractions are too low to be shown on this scale and are therefore excluded. Direction of diffusive gas flux for each gas shown by fine arrows. Direction of advective gas flux shown by bold arrows. The dashed line represents the mole fraction of N_2 in the atmosphere for comparison.

To induce an advective flux a pressure gradient must exist. Our data indicate, that a total pressure decrease in the N_2 and Ar enrichment zone results from the aerobic

oxidation of CH_4 (Figure 2-2) and hydrocarbon vapors. However, vapor pressures of volatile hydrocarbons decreased significantly between 1985 and 1997 (Chaplin et al., 2002) so that the influence of these compounds on total vapor pressure in the unsaturated zone is insignificant. Therefore, the main sink for O_2 is the microbial oxidation of CH_4 according to the reaction;

$$2O_2 + CH_4 \rightarrow CO_2 + 2H_2O \qquad (1)$$
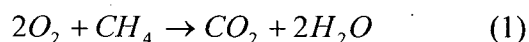
where 3 moles of gas ($O_2 + CH_4$) react to produce 1 mole of CO_2. Furthermore, the solubility of CO_2 is an order of magnitude greater than that of O_2 or CH_4, so that even more gas is removed from the gas phase by dissolution of the produced gas into infiltrating water. Microbial oxidation of CH_4 in the unsaturated zone at Bemidji is also supported by isotopic evidence. Revesz et al. (1995) determined carbon isotope fractionation factors, $(^{13}C/^{12}C)_{CO2}/(^{13}C/^{12}C)_{CH4}$, above the floating oil ranging from 1.028 at 5.5 m depth to 1.008 at 0.5 m depth. This is in good agreement with values given by Whiticar and Faber (1986) for oxidation of methane in aerobic culture studies. Although these data cannot distinguish between aerobic and anaerobic oxidation of CH_4, the sharp O_2 gradients (Figure 2-2C) and low sulfate concentrations observed at Bemidji (e.g. Bennett et al., 1993) strongly indicate an aerobic process. In addition, most probable numbers for methanotrophic microbes from wet sediment samples in a core taken in 2003 near vapor well 534 (see Figure 2-2) ranged from 1×10^4 to 2×10^6 per gram over an elevation range from 424.5 to 429.5 masl, while numbers from a core taken mid-way between vapor wells 604 and 301 (see Figure 2-2) ranged from 1.4×10^3 to 2.6×10^6 per gram over an elevation range from 424.5 to 428.5 masl (unpublished data). Consistent with our interpretation from vapor phase gas concentrations, these data indicate that

significant methanotrophic activity, i.e. aerobic methane oxidation, is occurring in the zone of Ar and N_2 enrichment.

A pressure increase results from production of CH_4 and CO_2 by biodegradation of the hydrocarbons in the unsaturated zone, primarily in sediments containing free-phase oil near the water table and in sediments with residual oil above the water table. High rates of methanogenic activity in the oil are consistent with MPN data showing that the microbial population in the oil body is dominated by methanogens and fermenters (Bekins et al., 2002). Significant methanogenic activity also has been documented in the saturated zone (Baedecker et al., 1993; Bekins et al, 1999). This activity may cause ebullition of gas bubbles containing CH_4, CO_2, N_2 and Ar.

2.5.1.2 Direction of advective gas flux

The Ar data can be used to infer the direction of advective flow. We assume that the areas of greatest Ar enrichment represent the areas of maximum gas consumption and lowest total pressure; and the areas of greatest depletion are the largest source areas for gas and highest total pressure. Thus, the Ar contours can be used as proxies for total pressure. Flow lines of inferred gas advection are drawn perpendicular to the contours as shown in Figure 2-4. These flow lines indicate that advection is ubiquitous throughout the unsaturated zone plume, and that the advection often has a significant horizontal component.

Argon

Ar Enrichment
$2O_2 + CH_4 \rightarrow CO_2 + 2H_2O$

Ar Depletion
$2CH_2O_{(aq)} \rightarrow CO_2 + CH_4$

435

435

9014 601 534 9103 533 9101 532 518 531 530

430

430

60 30

1.02

0.98

1.10

425

1.06

1.02

425

0.94

Elevation (masl)

0.80

420

420

421 532 530

Groundwater Flow

-50 0 50 100

Distance from Center of Oil Body (m)

Figure 2-4.Cross section of aquifer showing argon data collected in 2003, inferred direction of advective fluxes (arrows), and inferred reactive zones (see text for explanation). Bold arrow shows linear segment used for advective flux calculations. Vapor phase argon data in fraction of atmospheric concentrations.

2.5.1.3   Magnitude of advective gas flux

By making some simplifying assumptions we can calculate a rough estimate of the advective flux in order to comment on its relative importance compared to diffusive fluxes. The most important assumption is that the vapor phase plume is at steady state. Although this is not likely the case, changes in the system occur slowly enough that the steady state assumption is reasonable as a first-order approximation. This is because the largest and most permanent perturbations result from methanogenic production of CH_4 and methanotrophic consumption of CH_4 and O_2; and the evolution of the biodegradation processes (i.e. the transition from aerobic to anaerobic and methanogenic conditions)

27

occurs over a period of years, which is much longer than the time needed for gases to redistribute in the unsaturated zone.

We further assume that processes such as Knudsen diffusion and barometric pumping do not significantly influence the distribution of gases. Given that the unsaturated zone at Bemidji is relatively thin and highly permeable these assumptions seem reasonable (Massman and Farrier, 1992).

For the flux calculation, we chose the transect defined by the bold arrow in Figure 2-4, from sampling point 9014-3 to 9103-3 (the suffix '-3' refers to the third sample point from the bottom of the well nest), because the direction of advective flow appears to be relatively constant and the concentration gradients for Ar, N_2 and CH_4 are relatively uniform. The distance between these wells is 20.3 m. The diffusive flux (mol cm^{-2} s^{-1}) is calculated by;

$$F_{diff,i} = D_{eff,i} \frac{dC_i}{dx} \qquad (2)$$

where C_i (mol L^{-1}) is the concentration of gas i, and x (m) is the distance between the sampling points. As an approximation, we assume dC/dx to be constant over the distance x for the gases CH_4, Ar and N_2. Inspection of Figures 2-2A, D and E suggests that this assumption is reasonable. The effective diffusion coefficient D_{eff} (cm s^{-1}) can be calculated by (e.g.: Chaplin et al., 2002);

$$D_{eff,i}(x,y,z) = D_i\theta(x,y,z)\tau(x,y,x) \qquad (3)$$

where D_i (cm s^{-1}) is the binary gas-phase diffusion coefficient of each gas given in Table 2-1, θ (-) is the air-filled porosity as function of spatial coordinates, and τ (-) is the gas phase tortuosity also as a function of spatial coordinates. Here we assume constant values of θ and τ for simplicity, and adopt the average values measured by Chaplin et al. (2002)

for the unsaturated zone, between 0.72 m and 2.72 m above the water table, of 0.286 and

0.393 for θ and τ respectively. The calculated diffusive gas fluxes are given in Table 2-1.

Table 2-1. Parameters and results of advective gas flux calculations.

Gas	D_i (cm² s⁻¹)	C_i^1 (mol L⁻¹)	C_i^2 (mol L⁻¹)	$F_{diff,i}$ (mol cm⁻² s⁻¹)	v^1 (cm s⁻¹)	v^2 (cm s⁻¹)	v^m (cm s⁻¹)
Ar	0.148	3.65×10^{-04}	4.51×10^{-04}	-7.02×10^{-13}	6.72×10^{-06}	5.44×10^{-06}	6.01×10^{-06}
N$_2$	0.202	3.05×10^{-02}	3.53×10^{-02}	-5.40×10^{-11}	6.20×10^{-06}	5.35×10^{-06}	5.75×10^{-06}
					F^1_{adv} (mol cm⁻² s⁻¹)	F^2_{adv} (mol cm⁻² s⁻¹)	F^m_{adv} (mol cm⁻² s⁻¹)
CH$_4$	0.106	7.67×10^{-03}	2.63×10^{-07}	4.50×10^{-11}	1.42×10^{-11}	4.06×10^{-16}	6.45×10^{-12}

D_i is the diffusion coefficient of Ar and CH$_4$ in air and N$_2$ in O$_2$ at 293 K from CRC handbook (2001), C_i^1 and C_i^2 are concentrations of gas i at sampling point 9014-3 and 9103-3 respectively, v^1 and v^2 are velocities calculated using C_i^1 and C_i^2 respectively and v_m is the velocity calculated using C = average of C_i^1 and C_i^2. F^j_{adv} is the advective flux calculated using velocity v^j (average of Ar and N$_2$ data) and CH$_4$ concentration C^j.

Given the assumption of steady state, and the non-reactive nature of Ar and N$_2$, their

advective fluxes must be of equal magnitude and opposite direction to the diffusive

fluxes. The linear velocity of gas advection can then be calculated from;

$$F^j_{adv} = v\theta C_i^j \qquad (4)$$

where F^j_{adv} (mol cm⁻² s⁻¹) is the advective gas flux for gas i, v (cm s⁻¹) is the linear

velocity and C_i is the concentration of gas i at point j. The calculated velocities based on

Ar and N$_2$ concentrations using C_i^j equal to C_i^1, C_i^2 and C_i^m (average of C_i^1 and C_i^2) are

shown in Table 2-1. Note that the calculated velocities vary by less than 20% using the

different concentrations of Ar and N$_2$ in the calculation, indicating that the advective

velocity is fairly uniform along the chosen transect. Also, the velocities calculated using

the Ar and N$_2$ values are similar with differences of less than 10%.

Advective mass fluxes of CH_4 for a given point can be calculated with Equation 4, using the CH_4 concentration at that point, and the advective velocities obtained from the Ar and N_2 data (Table 2-1). The resulting estimates vary by several orders of magnitude due to the large gradient in CH_4 concentration. At the low end of the scale, i.e. at sampling point 9103-3, the calculated CH_4 advective flux is 4×10^{-16} mol cm^{-2} s^{-1}, which is approximately 5 orders of magnitude less than the diffusive flux and can be considered inconsequential. However, near sampling point 9014-3 the advective flux of 1.5×10^{-11} mol cm^{-2} s^{-1} is of the same order of magnitude as the diffusive methane flux

2.5.1.4 Effect of heterogeneity in sediment properties

Spatial heterogeneity, anisotropy, and soil moisture content will have a significant impact on the distribution of soil gases. For example, Figure 2-2A shows a sharp CH_4 concentration gradient at vapor well 604, dropping from above 10% to below 1% mol fraction, over a short depth interval between 426.2 and 426.9 masl. There is a similarly sharp O_2 concentration gradient in the opposite direction. The depth of this gradient change corresponds to the top of a fine grained layer (Dillard et al., 1997), which inhibits upward methane flux and downward oxygen flux, so that steep gradients are created in the zone of lower permeability and methane oxidation is limited to a narrow zone where oxygen and methane co-exist.

In general, where significant discontinuities in sediment properties exist, observed gradients will tend to be non-linear and will show pronounced changes near the discontinuity. Heterogeneities in sediment properties do not affect our interpretations regarding the occurrence and direction of advective fluxes. On the other hand, to determine the magnitude of gas fluxes, sediment properties must be well defined. In our

30

quantitative assessment of diffusive and advective fluxes (section *5.1.3*), porosity and gas phase tortuosity used in the calculations were measured properties in the area under consideration (Chaplin et al., 2002).

2.5.1.5 Importance of advective gas transport

These results show that reaction-induced gas advection is a significant process in the unsaturated zone at the Bemidji site. Advection occurs throughout the vapor phase plume and has a notable non-vertical component in places. Furthermore, first estimates indicate that the magnitude of the advective flux can be similar to that of diffusive fluxes. As the source zone redox conditions evolve, methanogenesis is expected to become a more important degradation pathway and therefore gas advection will also likely become a more significant process. Previously, Chaplin et al. (2002) used 1997 CH_4, CO_2 and O_2 data from the Bemidji site to determine volatilization and biodegradation rates. They assumed that gas flux was by diffusion only and mainly in the vertical direction. The above analysis shows that these assumptions may no longer be valid, and that a similar analysis based on the 2003 data will require consideration of advective fluxes.

2.5.2 Saturated Zone Degassing

2.5.2.1 Evidence for degassing

Figures 2-5A-D compare dissolved methane concentrations to Ar and N_2 depletion for background wells, wells from within the source zone, and wells down gradient of the source zone for data collected in 2002 and 2003. Depletion is calculated by:

31

$$Depletion = 1 - \frac{Dissolved\ Gas\ Concentration}{Average\ Background\ Dissolved\ Gas\ Concentration} \quad (5)$$

Background wells show a considerable scatter in depletion, indicating that Ar and N_2 concentrations are highly variable in unaffected wells, potentially due to temperature differences at the time of recharge, or entrapment of excess air (Heaton and Vogul, 1981). A negative depletion refers to Ar or N_2 concentrations that are higher than the average background value.
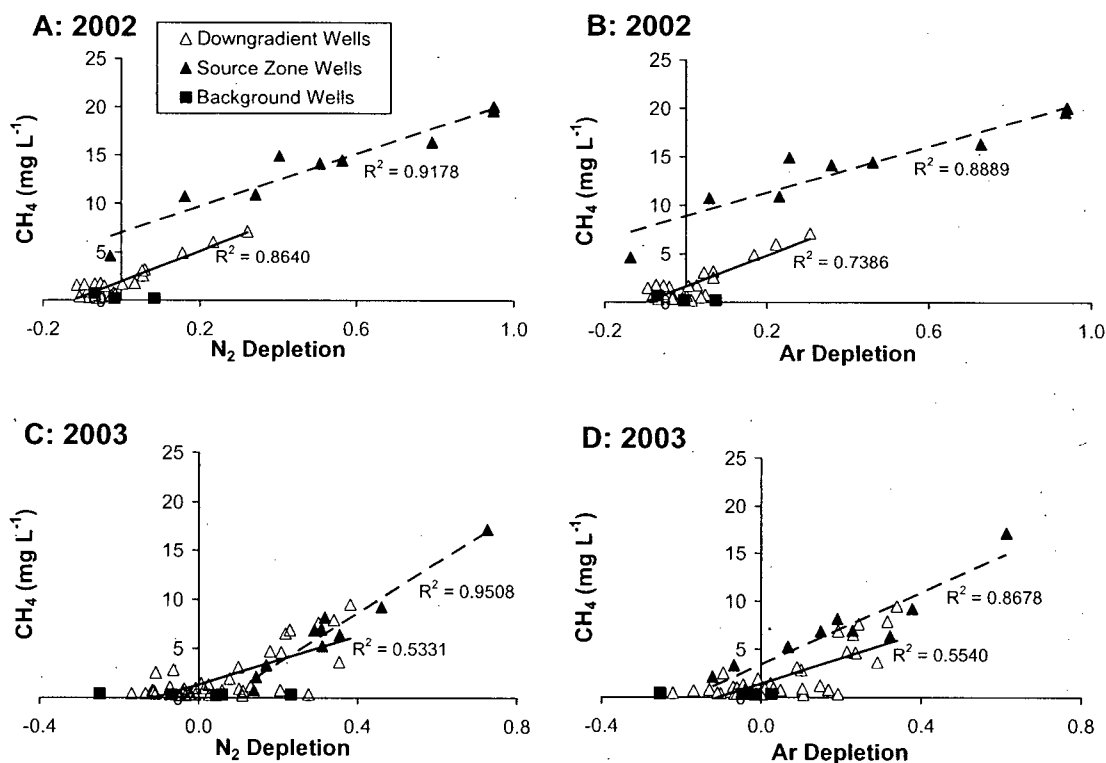
Figure 2-5. Dissolved CH_4 concentrations versus depletion of Ar and N_2. Depletion calculated as shown in text. Lines are least squares linear regressions for source zone wells (dashed) and downgradient wells (solid). Background wells are 200 m upgradient from the centre of the oil body, beyond the edge of the spray zone. Source zone wells are within ~40 m of the centre of the oil body and generally contain free phase oil. Downgradient wells are beyond the source zone.

Despite this uncertainty in background concentrations, both the 2002 and 2003 data show considerable depletion in Ar and N_2 in relation to background values, particularly for the source zone wells. A significant correlation exists between increased CH_4 concentrations and increased levels of depletion suggesting that the depletion is due to degassing caused by methane production.

Methanogenic degradation of organic matter can be described by the equation;

$$2CH_2O_{(aq)} \rightarrow CO_{2(g)} + CH_{4(g)} \qquad (6)$$
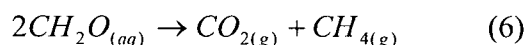
where CH_2O refers to readily degradable organic substrates produced by the fermentation of petroleum hydrocarbons. Most notably, the reaction produces CH_4 and CO_2, which both will increase the total gas pressure in the dissolved phase. However, a pressure increase is primarily caused by the production of CH_4 due to its lower solubility in relation to CO_2 and the tendency of CO_2 for speciation. Before the onset of methanogenesis, the total pressure in the pore water will typically be lower than WEA due to the removal of O_2 by aerobic degradation of hydrocarbons. The production of CH_4 and CO_2 will then increase the total pressure until a critical threshold is reached and bubble formation occurs. Typically the threshold pressure is considered to be the hydrostatic pressure plus a nucleation barrier (Li and Yortsos, 1995), although high levels of supersaturation are not observed here, so that the nucleation barrier is considered to be negligible. Upon bubble formation, all gases dissolved in the water, including Ar and N_2, will partition into the bubble according to Henry's Law, neglecting any kinetic considerations. Assuming that the water is isolated from the atmosphere and no other source of Ar and N_2 exists; dissolved concentrations of these gases will be depleted in comparison to background concentrations.

2.5.2.2 Degassing batch model

The degree of Ar and N_2 depletion measured in the source zone has important implications for quantifying the amount of methanogenesis that has occurred and the rate at which it has taken place. If only the existing dissolved CH_4 concentrations are used to determine the rates and extent of methanogenic degradation, an underestimation of both will occur because a considerable amount of CH_4 has been lost to the gas phase during degassing. However, by using Ar and N_2 concentrations to quantify the amount of degassing, an estimate of total CH_4 production can be made. This is similar to the approach used by Blicher-Mathiesen et al. (1998) to estimate denitrification rates using Ar.

A simple analytical batch model for a system undergoing methanogenesis, considering the partitioning of CH_4, CO_2, N_2 and Ar into the gas phase, can be used to demonstrate this principle. The model is based on the formulation of Cirpka and Kitanidis (2001) and solves the gas composition analytically for a 1 L system at 286 K. The formulation is given in Appendix 2-1. The initial condition used in the model assumes that Ar and N_2 are in equilibrium with the atmosphere and CH_4 or CO_2 are not present. Therefore, the total pressure is under the assumed threshold pressure of 0.93 atm, the average atmospheric pressure at an elevation of 425 m. It is assumed that no oxygen is present in the water.

The production of gases by methanogenesis and other biodegradation reactions is simulated by incremental additions of CH_4 and CO_2. Because the methanogenic degradation of organic matter may not always result in the 1:1 CH_4 to CO_2 ratio shown in Equation 6, and CO_2 may also be produced as a result of other hydrocarbon

34

biodegradation reactions, or carbonate dissolution, a CH_4 to CO_2 ratio of 1:4 was determined to best represent the observed gas data collected in this study. At each 'reaction progress step', 6 x 10^{-5} moles of CH_4 and 2.4 x 10^{-4} moles of CO_2 are added. A reaction step does not specifically represent a given time period, but reaction progress could theoretically be converted to time by dividing by a pseudo first order rate constant. However, considering that the methanogenic reaction rate is not well defined in this system, we do not attempt to correlate reaction progress to time in this study.

The batch model results shown in Figure 2-6A and B demonstrate the effects of degassing on gas composition. Initially, as CH_4 and CO_2 are produced, no degassing takes place as the total pressure is below the threshold pressure, N_2 and Ar partial pressures remain constant and the CH_4 partial pressure is equal to the total CH_4 introduced to the system. Once the total pressure reaches the threshold pressure of 0.93 atm (reaction progress step 4), bubble formation begins to occur, N_2 and Ar partial pressures drop, CH_4 is lost due to degassing, and the CH_4 partial pressure begins to deviate from the total amount of CH_4 produced. Note that although on a mole basis four times more CO_2 is produced than CH_4, the CO_2 partial pressure remains much lower than that of CH_4 due to the higher solubility of CO_2. Additional effects of CO_2-speciation were neglected.

2.5.2.3   Comparison of model and field results

Data collected in the source zone at the Bemidji site in 2003 are shown in Figures 2-6A and B while down gradient data are shown in Figures 2-6C and D. The field data are plotted along the horizontal axis, independent of location along the flow path, such that for each well the measured CH_4 concentration corresponds to the modeled

concentration. Measured CO_2, N_2, Ar and total pressure data are plotted at the corresponding reaction progress step. For example, the partial pressure of CH_4 measured in 2003 for well 423 is 0.35 atm, which corresponds to the methane partial pressure at reaction progress step 16. All measured data points for well 423, including CH_4, CO_2, N_2, Ar and total pressure are therefore plotted along the horizontal axis at reaction progress step 16.
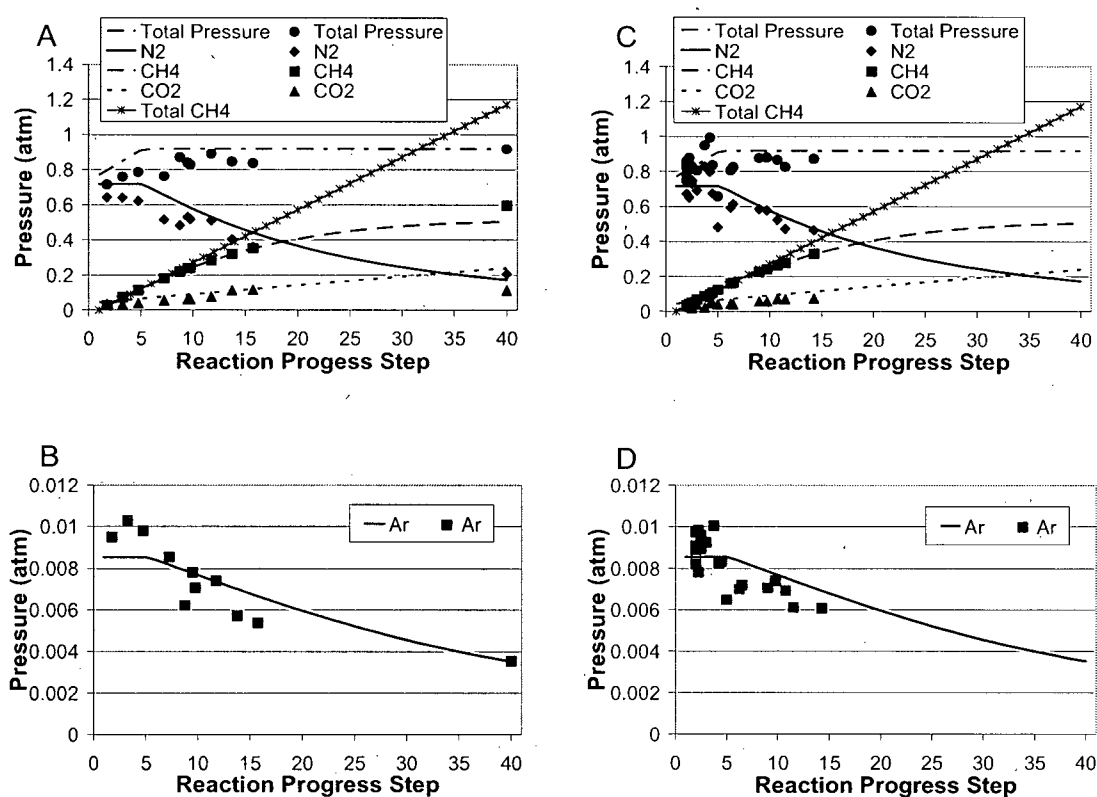
Figure 2-6. Model results (lines) showing evolution of dissolved gases in response to CH_4 and CO_2 production. On the horizontal axis each 'reaction step' refers to the addition of 6 x 10^{-5} moles of CH_4 and 2.4 x 10^{-4} moles of CO_2 to the 1 L batch system. Field data (symbols) for source zone wells (A and B) and downgradient wells (C and D) are plotted at a specific reaction progress step so that measured CH_4 concentration for a given sample point matches the modeled CH_4 concentration. Ar, N_2 and CO_2 data from that sample point are plotted at the corresponding reaction progress step so that data in a vertical column represent one sample point. See text for further explanation.

In general, measured N_2, Ar, CO_2 and total pressure data from the source zone and downgradient wells are close to the predicted pressures from the model, confirming that the model incorporates the important features of the geochemical system controlling the degassing process. The data from each well can then be correlated to a certain degree of CH_4 and CO_2 production, causing a certain degree of degassing. For example, pore water from well 423 has been exposed to the production of 9.6×10^{-4} mol of CH_4 (16 steps x 6 $\times 10^{-5}$ mol CH_4 per step) and 3.84×10^{-3} mol of CO_2 (16 step x 2.4×10^{-4} mol CO_2 per step) and has degassed to the point where N_2 and Ar are reduced to approximately 70% of their background concentrations.

An important process not taken into account in the batch model is groundwater flow and transport of dissolved gases. In the methanogenic region of the aquifer, groundwater flowing into the area, either horizontally or vertically from recharge, will have background levels of Ar and N_2 which will tend to replenish the Ar and N_2 and mask the depletion to some extent. Therefore, in order to produce the observed levels of depletion, a greater amount of degassing will be required in the aquifer than is demonstrated by the above batch model. This hypothesis is supported by observation of cores from the source zone at the Bemidji site. The batch model suggests that a gas saturation of only 1.9 % is required to achieve 50 % N_2 depletion, and even at the highest depletion simulated the model predicts a gas saturation of only 6 %. Although the majority of the sampled wells showed N_2 depletion below 50 %, core samples from the methanogenic area show significant gas saturations, well above the levels predicted by the model (Figure 2-7).
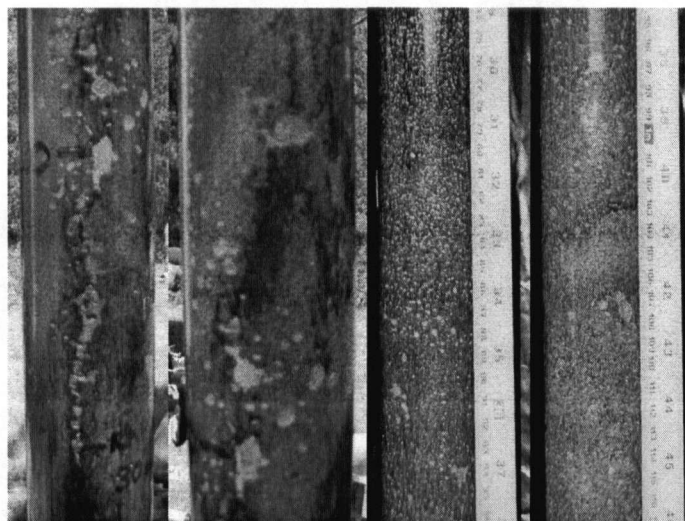
Figure 2-7. Cores from source zone at Bemidji. A and B; Core recovered approximately at location of vapor well 9014 in 2002 from depth interval 421.3 to 423.5 masl. C and D: Core recovered approximately 10 m upgradient from well 421 in 1997. Oil shown at top of photo C indicates that the core was taken directly below the water table. Cores are 47 mm in diameter.

At the final reaction progress step the model calculated a CH_4 partial pressure of ~ 0.5 while the maximum measured value in 2003 was ~0.6 (Figure 2-6A). Although the model could be run for additional steps to increase the CH_4 partial pressure, this would also increase the discrepancy between the measured and modeled CO_2 partial pressure. The discrepancy in the CO_2 partial pressure is at least in part a result of the inability of the model to account for the complexities of carbonate speciation and carbonate mineralogy. This in turn is certain to affect the modeled CH_4 partial pressures.

Although the model described here is somewhat simplistic, it clearly shows that the assumption of equilibrium partitioning provides a reasonable representation for the degassing process. More importantly, the model demonstrates that Ar and N_2 concentrations can be used to quantify degassing processes, better constrain total gas loss from the water phase, and therefore provide a better estimate of methanogenic degradation rates and gas phase saturation in the saturated zone. This latter point is

38

important in that gas saturation will affect aquifer permeability and also potentially be a source of mass transfer to the unsaturated zone through ebullition.

2.5.3 Ebullition

Ebullition will occur if the gas bubbles become sufficiently large such that buoyancy forces can overcome capillary forces. However, this process is difficult to quantify in that capillary forces can vary significantly depending on the grain size distribution and the potential for bubble channels to form. Although gas saturations predicted by the batch model seem too low for ebullition to occur, cores from the source zone at the Bemidji site show higher gas saturations and evidence of ebullition in the form of bubble channels (Figure 2-7A). In some source zone wells Ar and N_2 depletion was well above 50 % (Figure 2-5), indicating that near these wells gas saturations may exceed those predicted by the batch model, and that the potential for ebullition will be greater. Also, as methanogenesis continues at the Bemidji site the potential for ebullition will likely further increase.

2.5.4 Saturated zone gas transport

Based on measured linear ground water velocities, ranging from approximately 18 m yr^{-1} to 180 m yr^{-1} (Bennett et al., 1993), and the time that methane was first observed in the aquifer, ~1987 (Baedecker et al., 1993), elevated methane concentrations should have been observable hundreds of meters downgradient of the source zone in 2003. However, methane concentrations return to near zero about 130 m from the source zone.

A more detailed illustration of the observed trends in CH_4 concentrations with distance along the flow path, along with Ar and N_2 depletion, are shown in Figures 2-8A

and B for 2002 and 2003 respectively. For both years, the general trend in the data shows CH_4 concentrations reaching a maximum at the centre of the source zone and decreasing sharply, reaching concentrations near zero, approximately 100 m downgradient in 2002 and 130 m downgradient in 2003. Trends in Ar and N_2 depletion mimic the trends in the CH_4 concentrations in that the highest depletion is observed in the centre of the oil body and decreases to near background values coincident with the decrease in CH_4 concentrations.
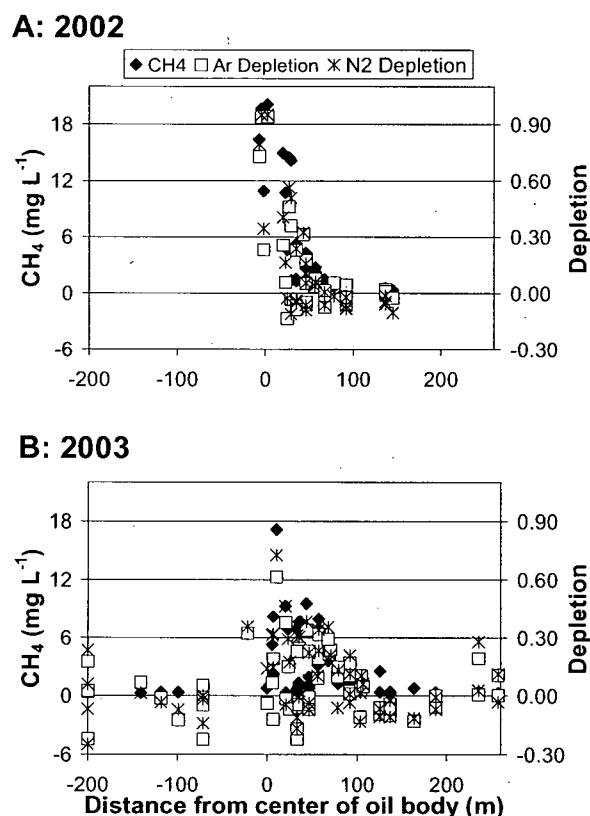
Figure 2-8. Methane concentration and Ar and N_2 depletion with distance along the north pool flow path for 2002 and 2003 data. Note the different horizontal scales for each of the figures.

A possible explanation for this observation is the oxidation of CH_4 by O_2 or potentially other oxidants in the aquifer. However, this mechanism is not likely an important contributor to the observed trend because the methane plume does not interact

40

with oxygenated portions of the aquifer, as is shown in Figures 2-2A and C. In addition, isotope data collected in 1990 did not show any significant fractionation in $\delta^{13}C$ and δD of CH_4 along the flowpath (Revesz et al., 1995); also suggesting that methane oxidation is not significant.

Because Ar and N_2 are for the most part non-reactive, it can be surmised that the reduction in Ar and N_2 depletion along the flowpath is due to physical processes, and since the trends in Ar and N_2 depletion are very similar to the trends in CH_4 concentrations, these observed CH_4 trends must also in large part be due to physical processes. The similarity of the CH_4 concentration and Ar and N_2 depletion trends may be coincidental; however, both trends migrated ~30 m downgradient between 2002 and 2003 suggesting that this is not the case.

Possible physical processes that may be contributing to the observed trends in the CH_4, Ar and N_2 data include dispersive mixing, hydraulic isolation of the source zone due to the presence of NAPL (Essaid et al., 1995, 2003) or the formation of gas bubbles (Ryan et al., 2000), solute attenuation downgradient of the source zone due to aquifer heterogeneity (Feehley et al., 2000; Harvey and Gorelick, 2000), or partitioning of Ar, CH_4 and N_2 into entrapped gas bubbles due to water table fluctuations (Fry et al., 1995; Fry et al., 1996; Donaldson et al., 1998; Williams and Oostrom, 2000). It is likely that a combination of these processes is controlling the transport of dissolved gases at Bemidji.

2.5.5   Differential depletion in Ar and N_2

Up to this point we have assumed that both Ar and N_2 are non-reactive gases. The data, however, suggests that this is not entirely true. Plots of dissolved Ar vs N_2 concentrations for source zone and downgradient wells are shown in Figures 2-9A and B

for data collected in 2002 and 2003 respectively. Argon vs N_2 concentrations are also shown for WEA over a range of temperatures for comparison. Note that the trend for the source zone wells is different than that for the downgradient wells. For the downgradient wells the trend deviates from the WEA line, approximately at the average groundwater temperature of 282 K observed at the site, and in general continues along an expected path for depletion of Ar and N_2 by degassing. That is, the trend shows a concurrent reduction in Ar and N_2 but tends toward a preferential decrease in N_2 due to the lower solubility of N_2. On the other hand, the trend in the source zone wells appears to be displaced from the WEA line indicating that the Ar:N_2 ratio of the least depleted source zone wells is different than that of WEA, and a process other than degassing must be occurring. The noted trends are important because they show that; 1) the preferential depletion of N_2 over Ar in the source zone wells is not due to the solubility of the gases alone and 2) the preferential depletion of N_2 and/or enrichment of Ar appear to be restricted to the source zone only. Possible explanations for the difference in the source zone Ar and N_2 depletion can either involve a source of Ar, which would tend to shift the trend line upward (arrow A in Figure 2-9B), or removal of N_2 independently of Ar, which would tend to shift the trendline to the left (arrow C in Figure 2-9B).

Unsaturated zone data also suggest a discrepancy in the Ar:N_2 ratio. Note that in Figure 2-2E the N_2 fraction above the upgradient end of the oil body is reduced to less than 0.90 while for Ar (Figure 2-2D) the fraction only drops below 0.94 in a very small area. Furthermore, above the downgradient end of the oil body the elevated argon contours (i.e. above 1.06 and 1.10) extend down to the water table, while for N_2 these contours do not reach the water table. In both cases the observed Ar/N_2 ratios are greater

than in the atmosphere, suggesting a preferential depletion in N_2 or an independent source of Ar.
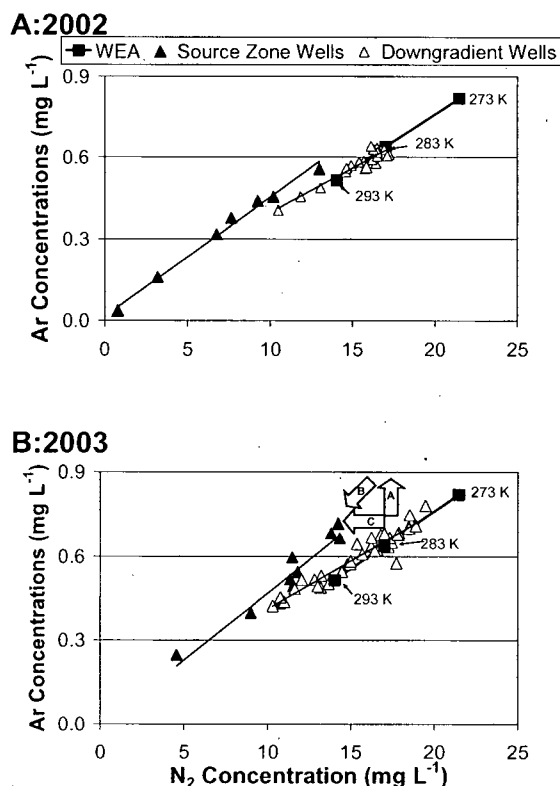
Figure 2-9. Argon versus N2 concentrations for source zone and downgradient wells in 2002 and 2003. Also shown are the concentrations of Ar and N2 for water in equilibrium with the atmosphere (WEA) at a range of temperatures. Arrows in Figure B represent expected trends for various processes which affect Ar and N_2 concentrations (see text for explanation).

A possible explanation for the discrepancy between Ar and N_2 depletion in the source zone is the removal of N_2, specifically, as a result of nitrogen fixation by methanogens or iron reducing bacteria. When other sources of nitrogen have been depleted, these microbes are able to use N_2 as their nitrogen source (Lobo and Zinder, 1992). No conclusive evidence of nitrogen fixing methanogenic strains at Bemidji is available; however, nitrogen fixation by methanogens is widespread, existing within all

three orders (Leigh, 2000), and large populations of methanogens are observed at Bemidji (Bekins et al., 1999). Furthermore, conditions at the Bemidji site point to nitrogen fixation as a likely source of nitrogen for microbes. Nitrate levels are very low in the groundwater and drop to below detection limit in the core of the saturated plume (Bennett et al., 1993). Bekins et al. (1999) found greater numbers of anaerobic bacteria in the unsaturated source zone than in the saturated source zone and suggested that this may be due to nutrient limitations at depth. Recent studies have demonstrated nitrogen fixation by iron reducing bacteria at the Bemidji site. Holmes et al. (2004) found expression of *Geobacteraceae* nifD, the dinitrogenase gene involved in nitrogen fixation, under Fe(III)-reducing conditions in unaltered Bemidji sediment, and nifD expression decreased more than 100-fold within two days following the addition of 100 μM ammonium.

Ammonium data from the saturated and unsaturated zones at Bemidji suggest that nitrogen fixation is widespread throughout the source zone. The first product of nitrogen fixation is NH_3 (Postgate, 1998), which will protonate to form NH_4^+ in neutral pH environments. Saturated zone ammonium concentrations are shown in Figure 2-10. A zone of elevated ammonium concentrations is apparent below the floating oil and to a lesser extent, in the plume downgradient of the source. In this zone, CH_4 and Fe^{2+} concentrations are also elevated so that it is not possible to distinguish between ammonia production by methanogens or iron reducing bacteria. Ammonium concentrations from unsaturated zone water samples are shown in Table 2-2. In general, NH_4^+ concentrations increase with proximity to the free phase oil (i.e. in deeper samples, or those closer to the center of the source zone), indicating that NH_3 production is greatest where biodegradation activity is highest, and thus where nutrients are most limited. Although

the evidence suggests that nitrogen fixation is occurring at the site, quantification of its impact on dissolved and gaseous N_2 concentrations is difficult. To our knowledge, data that relates CH_4 production rates to N_2 uptake rates is not available in the literature.
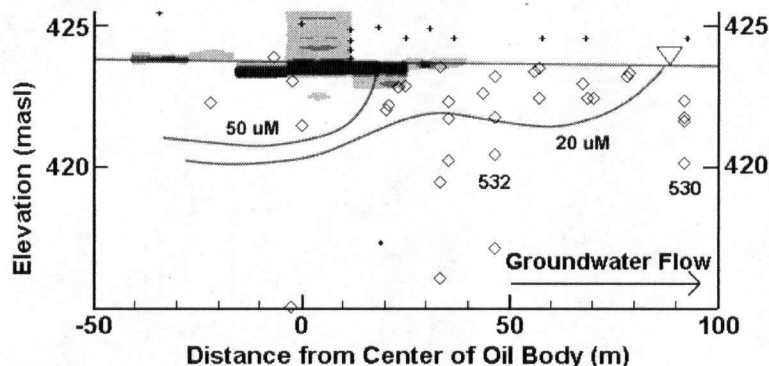
Figure 2-10. Cross section of aquifer showing dissolved NH4+ concentrations from 2004.

Other possible explanations of the discrepancy in the Ar and N_2 depletion values include alternative sources of Ar, such as radiogenic ^{40}Ar from radioactive decay of ^{40}K in potassium bearing aquifer minerals, or potentially the crude oil acts as a source of Ar or sink for N_2. However, the radioactive decay of ^{40}K is too slow to account for any significant accumulation of ^{40}Ar since the time of the spill. It is possible that the oil is acting to enrich Ar or deplete N_2 from the groundwater, but this is difficult to assess since the gas content of the oil at the time of the spill is unknown, and has not been monitored over the time period since. Additionally, other factors such as diffusion coefficients and solubilities of gases in crude oil are poorly defined.

Even considering the potential reactivity of N_2, this does not significantly detract from the utility of N_2 as an indicator of the other processes described in this paper. For example, with respect to the degassing process in the saturated zone, a strong correlation

45

exists between CH_4 concentrations and depletion of both Ar and N_2, especially for the wells in the source zone where the strongest Ar/N_2 discrepancy exists (Figure 2-5). This suggests that degassing due to CH_4 production is the dominant process. Similarly, in the unsaturated zone the main features of the Ar and N_2 concentration profiles, i.e. depletion in the methanogenic zone near the free-phase oil and enrichment in the zone of CH_4 oxidation, appear to be strongly controlled by the CH_4 chemistry (Figures 2-2 and 2-4).

Table 2-2. Ammonium data from lysimeters in 2004.

Lysimeter ID	NH_3 (μM)	Distance from Well 421 (m)	Notes
L9014-1.5	2	21.0	East of Well 421
L9014-3.0	8	21.0	Above floating oil
L9014-4.5	71	21.0	
LT-1.5N	206	10.4	South of Well 421
LT-3.0N	252	10.4	Above floating oil
LT-4.5N	133	10.4	
LT-1.5S	1	15.4	South of Well 421
LT-3.0S	0	15.4	
LT-4.5S	117	15.4	
L303-1.4	55	22.7	North of Well 421
L303-3.0	79	22.7	Above floating oil
L303.4.4	68	22.7	
L310	0	200.0	Background well

Groundwater flow direction is from west to east so that the L9014 lysimeter nest is downgradient of the center of the source zone (Well 421), while the other nests are located away from Well 421 perpendicular to the groundwater flow direction.

2.6 Summary and Conclusions

The use of dissolved and vapor phase gas data, and particularly by employing non-reactive or relatively inert gases such as Ar and N_2 as indicators, has resulted in a more complete understanding of the physical and chemical processes occurring in a crude-oil contaminated aquifer undergoing methanogenesis. In the unsaturated zone, non-

reactive gases can be used to determine the direction and magnitude of advective gas fluxes. Our data suggest that reaction-induced advective gas transport of CH_4 and O_2 may enhance CH_4 oxidation in the unsaturated zone. Consideration of advective fluxes may therefore be an important aspect of quantifying the carbon balance of the system.

In the saturated zone, CH_4 production due to methanogenesis is the driving force behind degassing and stripping of Ar and N_2 from the contaminated pore water. By applying a degassing model, which accounts for losses of all gases to the gaseous phase, a more accurate accounting of the methanogenic process can be obtained. If degassing is neglected, and historical rates of methanogenesis are determined based only on measured CH_4 concentrations, both methanogenesis and contaminant degradation is under-predicted. Under-prediction may be even more pronounced, if ebullition of gas bubbles is occurring.

Furthermore, the Ar and N_2 depletion, caused by degassing in the source zone, can be used to investigate transport of dissolved solutes from the source zone. The data show that the slow advance of the methane plume correlates with that of the depleted Ar/N_2 plume and must therefore be in large part due to physical processes. Distinguishing between physical and chemical attenuation processes has obvious, yet significant implications on natural attenuation at the site, particularly in determining biodegradation rates and contaminant mass loss.

Comparison of Ar and N_2 data in both the saturated and unsaturated zones indicates a preferential depletion of N_2 near the free-phase oil. This is consistent with other evidence from the Bemidji site indicating nutrient limitations near the free-phase oil and suggests that nitrogen fixation is an important microbial process.

47

Although N_2, unlike Ar, appears to be slightly reactive, it is still a useful indicator for the processes of degassing and gas transport in the saturated and unsaturated zones. This is likely true for aquifers that do not undergo a significant amount of denitrification. N_2 may therefore be a particularly attractive indicator gas as its concentrations in air and water are generally much higher than Ar, and analytical detection methods are more straightforward.

Appendix 2-1

After Cirpka and Kitanidis (2001), the following formulation is used to calculate gas phase saturation and equilibrium partitioning of gases into the gas phase. The total concentration of each gas in the system is calculated by;

$$T_i = C_{i(aq)}S_w + C_{i(g)}S_g \qquad \text{(A1)}$$

where T_i (mol L^{-1}) is the total mass of gas i per pore volume, $C_{i(aq)}$ (mol L^{-1}) is the concentration of the gas in the aqueous phase, $C_{i(g)}$ (mol L^{-1}) is the concentration of the gas in the gas phase and S_w and S_g are the water and gas saturations respectively. Given the total concentration, a theoretical gas pressure for each gas can be calculated assuming $S_g = 0$;

$$\overline{p}_i = T_i / K_i \qquad \text{(A2)}$$

where K_i is the Henry's law constant (mol L^{-1} atm^{-1}) of gas i. If the sum of the theoretical gas pressures of all the gases present in the system is less than the threshold pressure, P_T, then no gas phase is present. If the sum of the theoretical pressures exceeds the threshold pressure then a gas phase is present and S_g can be calculated so that the following condition is satisfied;

$$P_T = \sum_{i=1}^{ng} p_i \qquad \text{(A3)}$$

where p_i (atm) is the partial pressure of gas i and ng is the number of gases in the system.

Substituting the relations;

$$C_{i(aq)} = p_i K_i \qquad \text{(A4)}$$

and

$$C_{i(g)} = p_i / RT \qquad \text{(A5)}$$

into Equation A1 and solving for p_i yields;

$$p_i = \frac{T_i}{K_i S_w + S_g / RT} \qquad \text{(A6)}$$

where R is the gas constant (0.08206 atm L mol^{-1} K^{-1}) and T (K) is the temperature. Substituting in Equation A6, Equation A3 can be solved for S_g and subsequently $C_{i(aq)}$ and $C_{i(g)}$ can be calculated using Equations A4 and A5 respectively.

Due to the incompressibility of water, the formation of a gas phase displaces a volume of water equal to the gas saturation so that at each reaction progress step the water saturation is updated by;

$$S_w = 1 - S_g \qquad \text{(A7)}$$

maintaining a constant volume of the control volume. This results in a loss of gas from the system equal to $S_g \times C_{i(aq)}$ at each step

2.7 Acknowledgements

2.8 References

Baedecker, M.J., Cozzarelli, I.M., Eganhouse, R.P., Siegel, D.I., Bennett, P.C. (1993), Crude oil in a shallow sand and gravel aquifer - III. Biogeochemical reactions and mass balance modeling in anoxic groundwater, *Appl. Geochem.*, *8*, 569-586.

Bekins, B.A., Godsy, E.M., Warren, E. (1999), Distribution of microbial physiologic types in an aquifer contaminated by crude oil, *Microbial Ecology*, *37*, 263-275.

Bekins, B.A., Cozzarelli, I.M., Godsy, E.M., Warren, E., Essaid, H.I. Tuccillo, M.E. (2001), Progression of natural attenuation processes at a crude oil spill site: II: Controls on spatial distribution of microbial populations, *J. Contam. Hydrol.*, *53*, 387-406.

Bekins, B.A., Cozzarelli, I.M., Warren, E., Godsy, E. M. (2002), Microbial ecology of a crude-oil contaminated aquifer, in *Groundwater Quality: Natural and Enhanced Restoration of Groundwater Pollution*, edited by S.F. Thornton and S. E. Oswald, International Association of Hydrological Sciences Publication, *275*, 57-63.

Bennett, P.C., Siegel, D.E., Baedecker, M.J., and Hult, M.F. (1993), Crude oil in a shallow sand and gravel aquifer – I. Hydrogeology and inorganic geochemistry, *Appl. Geochem.*, *8*, 529-549.

Bilir, S.H. (1992). Hydrogeologic characterization of a glacial aquifer contaminated by crude oil near Bemidji, Minnesota, M.A. thesis, The University of Texas at Austin.

Blicher-Mathiesen, G., McCarty, G.W., Nielsen, L.P. (1998), Denitrification and degassing in groundwater estimated from dissolved dinitrogen and argon, *J. Hydrol.*, *208*, 16-24.

Bolliger, C., Höhener, P., Hunkeler, D., Haberli, K., Zeyer, J. (1999), Intrinsic bioremediation of a petroleum hydrocarbon-contaminated aquifer and assessment of mineralization based on stable carbon isotopes, *Biodegradation, 10*, 201-217.

Chapelle, F.H., McMahon, P.B. (1991), Geochemistry of dissolved inorganic carbon in a coastal plain aquifer. 1. Sulfate from confining beds as an oxidant in microbial CO_2 production, *J. Hydrol., 127*, 85-108.

Chapelle, F.H., Haack, S.K., Adriaens, P., Henry, M.A., Bradley, P.M. (1996), Comparison of E_h and H_2 measurements for delineating redox processes in a contaminated aquifer, *Environ. Sci. Technol., 30*, 3565-3569.

Chaplin, B.P., Delin, G.N., Baker, R.J., Lahvis, M.K. (2002), Long-term evolution of biodegradation and volatilization rates in a crude oil-contaminated aquifer, *Bioremediation Journal, 6*, 237-255.

Cirpka, O.A., Kitanidis, P.K. (2001). Transport of volatile compounds in porous media in the presence of a trapped gas phase, *J. Contam. Hydrol., 49*, 263-285.

Conrad, M.E., Daley, P.F., Fischer, M.L., Buchanan, B.B., Leighton, T., Kashgarian, M. (1997), Combined 14C and δ13C monitoring of in situ biodegradation of petroleum hydrocarbons, *Environ. Sci. Technol., 31*, 1463-1469.

Cozzarelli, I.M., Bekins, B.A., Baedecker, M.J., Aiken, G.R., Eganhouse, R.P., Tuccillo, M.E. (2001), Progression of natural attenuation processes at a crude-oil spill site I. Geochemical evolution of the plume, *J. Contam. Hydrol., 53*, 369-385.

CRC Press (2004), *CRC Handbook of Chemistry and PhysicsI*, 84th ed., Boca Raton, Fla.

Delin, G.N., Essaid, H.I., Cozzarelli, I.M., Lahvis, M.H., Bekins, B.A. (1998), USGS Fact Sheet 084-98, Ground Water Contamination by Crude Oil near Bemidji, Minnesota. http://mn.water.usgs.gov.

Dillard, L.A., Essaid, H.I., Herkelrath, W.N. (1997), Multiphase flow modeling of a crude-oil spill site with a bimodal permeability distribution, *Water Resour. Res.*, *33*, 1617-1632.

Divine, C.E., Sanford, W.E., McCray, J.E. (2003), Helium and neon groundwater tracers to measure residual DNAPL: laboratory investigation, *Vadose Zone Journal*, *2*, 382-388.

Donaldson, J.H., Istok, J.D., O'Reilly, K.T. (1998), Dissolved gas transport in the presence of a trapped gas phase: experimental evaluation of a two-dimensional kinetic model, *Ground Water*, *36*, 133-142.

Eganhouse, R.P., Baedecker, M.J., Cozzarelli, I.M., Aiken, G.R., Thorn, K.A. (1993), Crude oil in a shallow sand and gravel aquifer - II. Organic geochemistry, *Appl. Geochem.*, *8*, 551-567.

EPA (1999), Use of monitored natural attenuation at Superfund, RCRA corrective action, and underground storage tank sites. Directive number 9200.4, 17 pp, Washington, D.C., EPA, Office of Solid Waste and Emergency Response.

Essaid, H.I., Bekins, B.A., Godsy, E.M., Warren, E., Baedecker, M.J., Cozzarelli, I.M. (1995), Simulation of aerobic and anaerobic biodegradation processes at a crude oil spill site, *Water Resour. Res.*, *31*, 3309-3327.

Essaid, H.I., Cozzarelli, I.M., Eganhouse, R.P., Herkelrath, W.N., Bekins, Delin, G.N. (2003). Inverse modeling of BTEX dissolution and biodegradation at the Bemidji, MN crude-oil spill site, *J. Contam. Hydrol.*, *67*, 269-299.

Feehley, C.E., Zheng, C., Molz, F.J. (2000), A dual-domain mass transfer approach for modeling solute transport in heterogeneous aquifers: Application to the Macrodispersion Experiment (MADE) site, *Water Resour. Res.*, *36*, 2501-2515,

Franzi, D.A. (1988), Surficial and subsurface distribution of aquifer sediments at the Bemidji, Minnesota research site, in U.S. Geological Survey Toxic Waste--Ground Water Contamination Program--Proceedings of the technical meeting, Cape Cod, Massachusetts, October 21-25, 1985: U.S. Geological Survey Open-File Report 86-481, edited by S.E. Ragone, p.C5-C10.

Fry, V.A., Istok, J.D., Semprini, L., O'Reilly, K.T., Buscheck, T.E. (1995), Retardation of dissolved oxygen due to a trapped gas phase in porous media, *Ground Water*, *33*, 391-398.

Fry, V.A., Istok, J.D., O'Reilly, K.T. (1996), Effect of trapped gas on dissolved oxygen transport – implications for in situ bioremediation, *Ground Water*, *34*, 200-210.

Harvey, C., Gorelick, S.M. (2000), Rate-limited mass transfer or macrodispersion: Which dominates plume evolution at the Macrodispersion Experiment (MADE) site?, *Water Resour. Res.*, *36*, 637-650.

Heaton, T.H.E., Vogel, J.C. (1981), "Excess air" in groundwater, *J. Hydrol.*, *50*, 201-216.

Hers, I., Atwater, J., Li, L., Zapf-Gilje, R. (2000), Evaluation of vadose zone biodegradation of BTX vapors, *J. Contam. Hydrol.*, *46*, 233-264.

Hess, K.M., Herkelrath, W.N., Essaid, H.I. (1992), Determination of subsurface fluid contents at a crude-oil spill site, *J. Contam. Hydrol.*, *10*, 75-96.

Hult, M.F., Grabbe, R.R. (1988), Distribution of gases and hydrocarbon vapors in the unsaturated zone, in U.S. Geological Survey Toxic Substances Hydrology Program;

Proceedings of the Technical Meeting, Cape Cod, Massachusetts, October 21 –25, 1985: U.S. Geological Survey Water Resources Investigations Report 81 –4188 , edited by S.E. Ragone, p.C21 –C26.

Holmes, D.E., Nevin, K.P., Lovley, D.R. (2004), In situ expression of Geobacteraceae nifD in subsurface sediments. *Appl. Environ. Microbiol.* (submitted).

Jardine, P.M., Sanford, W.E., Gwo, J.P., Reedy, O.C., Hicks, D.S., Riggs, J.S., Bailey, W.B. (1999), Quantifying diffusive mass transfer in fractured shale bedrock. *Water. Resour. Res., 35,* 2015-2030.

Kipphut, G.W., Martens, C.S. (1982), Biogeochemical cycling in an organic-rich coastal marine basin, Part 3: Dissolved gas transport in methane-saturated sediments, *Geochimica et Cosmochica Acta, 46,* 2049-2060.

Lahvis, M.A., Baehr, A.L. (1996), Estimation of rates of aerobic hydrocarbon biodegradation by simulation of gas transport in the unsaturated zone, *Water. Resour. Res., 32,* 2231-2249.

Leigh, J.A. (2000), Nitrogen fixation in methanogens: The archaeal perspective, *Curr. Issues. Mol. Biol., 2,* 125-131.

Li, X., Yortos, Y.C. (1995), Theory of multiple bubble growth in porous media by solute diffusion, *Chem. Eng. Sci., 50,* 1247-1271.

Lobo, A.L., Zinder, S.H. (1992), Nitrogen fixation by methanogenic bacteria, in *Biological nitrogen fixation,* edited by G. Stacey, R.H. Burris, H.J. Evans, Chapman and Hall, New York, pp. 191-211.

Massmann, J., Farrier, D.F. (1992), Effects of atmospheric pressure on gas transport in the vadose zone. *Water. Resour. Res., 28,* 777-791.

National Research Council (U.S.), Committee on Intrinsic Remediation (2000), Natural attenuation for groundwater remediation, Washington D.C., National Academy Press.

Postage, J. (1998), *Nitrogen Fixation,* Cambridge University Press, New York, N.Y.

Reeburgh, W.S. (1972), Processes affecting gas distribution in estuarine sediments, in Memoir - Geological Society of America, no.133, Environmental framework of coastal plain estuaries, pp.383-389.

Revesz, K., Coplen, T.B., Baedecker, M.J., Glynn, P., and Hult, M. (1995), Methane production and consumption monitored by stable H and C isotope ratios at a crude oil spill site, Bemidji, Minnesota. *Appl. Geochem., 10,* 505-516.

Risgaard-Petersen, N., Rysgaard, S. (1995), Nitrate reduction in sediments and waterlogged soil measured by ^{15}N techniques, in *Methods in applied soil microbiology and biochemistry,* edited by K. Alef and P. Nannipien, Academic Press, New York, pp. 287-295.

Ryan, M.C, MacQuarrie, K.T.B., Harman, J., Mclellan, J. (2000), Field and modeling evidence for a "stagnant flow" zone in the upper meter of sandy pheatic aquifers, *J. Hydrol., 233,* 223-240.

Semprini, L., Hopkins, O.S., Tasker, B.R. (2000), Laboratory, field and modeling studies of radon-222 as a natural tracer for monitoring NAPL contamination, *Transport in Porous Media, 38,* 223–240.

Shubal, K.L., Barcelona, M.J., Adriaens, P. (2001), An assessment of natural biotransformation of petroleum hydrocarbons and chlorinated solvents at an aquifer plume transect, *J. Contam. Hydrol., 49,* 151-169.

Thorstenson, D.C., Pollock, D.W. (1989), Gas transport in unsaturated zones: multicomponent systems and the adequacy of Fick's Laws, *Water. Resour. Res.*, *25*, 477-507.

van Breukelen, B.M., Roling, W.F.M., Groen, J., Griffioen, J., van Verseveld, H.W. (2003), Biogeochemistry and isotope geochemistry of a landfill leachate plume, *J. Contam. Hydrol.*, *65*, 245-268.

Vroblesky, D.A., Chapelle, F.H. (1994), Temporal and spatial changes of terminal electron-accepting processes in a petroleum hydrocarbon-contaminated aquifer and the significance for contaminant biodegradation, *Water Resour. Res.*, *30*, 1561–1570.

Whiticar, M.J., Faber, E. (1987), Methane oxidation in sediment and water column environments – Isotope evidence, *Org. Geochem.*, *10*, 759-768.

Wiedemeier, T.H., Rifai, H.S., Newell, C.J., Wilson, J.T. (1999), *Natural Attenuation of Fuels and Chlorinated Solvents in the Subsurface*. John Wiley & Sons, New York.

Weiner, J.M., Lovley, D.R. (1998), Rapid benzene degradation in methanogenic sediments from a petroleum-contaminated aquifer, *Appl. Environ. Microbiol.*, *64*, 1937-1939.

Williams, M.D., Oostrom, M. (2000), Oxygenation of anoxic water in a fluctuating water table system: an experimental and numerical study, *J. Hydrol.*, *230*, 70-85.

3 Investigating the Role of Gas Bubble Formation and Entrapment in Contaminated Aquifers: Reactive Transport Modelling

3.1 Introduction

The formation of gas bubbles in groundwater may be a result of exsolution due to biogenic gas production or bubble entrapment due to a water table rise. Because most naturally occurring gases are relatively insoluble, the presence of gas bubbles can have a significant effect on groundwater geochemistry. Furthermore, the formation of gas bubbles can also affect the effective hydraulic properties of porous media.

The generation of gas bubbles due to biogenic gas production has been known to occur extensively in natural settings where high levels of methanogenesis occur, such as marine sediments (Reeburgh, 1969; Martens and Berner, 1977), peats (Fecher-Levy and Hemond, 1996; Beckwith and Baird, 2001; Rosenberry et al., 2003), estuaries (Reeburgh, 1972; Chanton and Martens, 1988) and organic rich aquifers in the Netherlands (Fortuin and Willemsen, 2005), but has also been shown to occur where groundwater contamination leads to high levels of denitrification or methanogenesis (Revesz et al., 1995; Blicher-Mathiesen et al., 1998; van Breukelen et al., 2003, Amos et al., 2005). Where bubble formation occurs, other non-reactive gases such as Ar or N_2 will partition into the bubbles resulting in depleted concentrations of these gases in the groundwater (Reeburgh, 1969; 1972; Martens and Berner, 1977). Blicher-Mathiesen et al. (1998) showed that depleted Ar concentrations could be used to quantify denitrification, and Amos et al. (2005) and Fortuin and Willemsen (2005) used a similar approach to quantify methanogenesis using Ar and N_2 concentrations. In column experiments, Beckwith and Baird (2001) and Reynolds et al. (1992) both showed permeability reductions of up to 50% in peat associated with the formation of biogenic gas bubbles.

In multi-phase systems, infiltration of the wetting phase (i.e. water) will lead to entrapment of the non-wetting phase (i.e. gas). This process is important in unconfined aquifers where infiltration and water table fluctuations can lead to entrapped air and can provide a significant amount of O_2 to oxygen-depleted waters (Williams and Oostrom, 2000) or affect the hydraulic properties of an aquifer (Ryan et al., 2000; Heilweil et al., 2004). Previous studies have documented bubble saturation ranging from ~2 to 26% of porosity in a variety of porous materials (Fayer and Hiller, 1986; Williams and Oostrom, 2000; Heilwell et al. 2004), representing a significant reservoir of gas compared to the amount dissolved in the water. Ryan et al. (2000) presented field and modelling evidence which suggests that the presence of trapped bubbles in the upper meter of sandy unconfined aquifers creates a low conductivity layer where groundwater flow tends toward vertical. At a field site in Strathroy, Ontario they found hydraulic conductivity was reduced by a factor of 35 in the bubble-induced low conductivity layer directly below the water table relative to the underlying aquifer.

The objective of this study is to investigate the processes that control bubble formation and dissolved gas concentrations, as well as solute transport in the presence of gas bubbles, in an effort to better understand the evolution of dissolved gases observed in the field, and to provide a basis for quantifying the various processes involved. This is carried out through the development of a reactive transport model capable of simulating the formation of gas bubbles, from biogenic gas production or entrapment near the water table, and equilibrium partitioning of gases between the aqueous and gaseous phases. The model is used to simulate biogenic gas bubble formation in a hydrocarbon contaminated aquifer. Our simulations are based on observations from a crude oil spill site near

Bemidji, MN) but do not attempt to quantitatively reproduce the system evolution at Bemidji; the focus of the work is rather to qualitatively and conceptually investigate the role of dissolved gases in natural attenuation processes.

At the Bemidji site, an aquifer contaminated by a crude oil spill has undergone natural attenuation since 1979 and methanogenesis has been a significant degradation pathway since approximately 1987 (Baedecker et al., 1993). Amos et al. (2005) demonstrated qualitatively that CH_4 and CO_2 production has led to the formation of gas bubbles that have had a significant effect on groundwater chemistry and potentially solute transport. This study showed that the concentration of dissolved Ar and N_2 were significantly lower in the methanogenic source zone, implying that gas bubble formation due to methanogenesis has led to the stripping of the non-reactive gases Ar and N_2. Field observations by Amos et al. (2005) also showed that gas concentrations returned to near background level approximately 100 m dowgradient of the source, despite advection rates which predict a transport distance of greater than 250 m. Because Ar and N_2 are non-reactive, attenuation of the depleted Ar and N_2 plumes must be due to physical processes. Furthermore, Ar and N_2 concentrations return to background levels concurrently with CH_4, suggesting that the physical processes acting to attenuate the depleted Ar and N_2 plumes must also be acting to attenuate the CH_4 plume. These processes may include partial hydraulic isolation of the source zone as a result of a reduction in relative permeability due to the presence of free phase oil and gas bubbles, or interaction with entrapped bubbles near the water table as a result of water table fluctuations.

The reactive transport code MIN3P (Mayer et al., 2002) is applicable to geochemical problems involving kinetically controlled redox and mineral

dissolution/precipitation reactions, along with equilibrium hydrolysis, aqueous complexation, ion exchange and surface complexation reactions. Here, MIN3P is enhanced to include changes in gas saturation below the water table (i.e. the formation and collapse of gas bubbles) in response to changes in dissolved gas concentrations, entrapment of gas bubbles due to water table rise, and permeability changes as a function of gas saturation below the water table. The formulation for gas saturation changes as a result of changes in dissolved gas partial pressures generally follows the work of Cirpka and Kitanidis (2001), but is incorporated into the multicomponent framework of MIN3P. This approach is advantageous in that it allows for the simulation of bubble growth and partitioning of gaseous species into the bubbles in a broader geochemical context, where overall solution chemistry, including reaction-induced gas production, speciation of gaseous species (particularly CO_2), and changes in pH and alkalinity can be monitored. These features can be important when evaluating the effects of bubble formation in geochemically complex aquifers. The formulation for gas bubble entrapment as a result of water table rise follows the example of Williams and Oostrom (2000) and adopts the formulation of Kaluarachchi and Parker (1992) first applied to two phase oil/water systems. When combined with the reactive transport code and the above mentioned gas partitioning enhancements, a more complete and versatile model is obtained that facilitates study of the role of gases in groundwater systems.

3.2   Model Formulation

3.2.1   Conceptual Model

In the current context, the interaction of groundwater with gas bubbles can be described by essentially three separate, yet related processes: 1) gas bubble formation,

growth and shrinkage resulting from changes in dissolved gas pressure; 2) entrapment and release of gas bubbles during imbibition and drainage; and 3) permeability changes due to changes in gas bubble saturation. In the saturated zone, i.e. where the hydrostatic pressure is greater than zero, gases may be produced or consumed by a number of chemical or biogenic processes. This results in changes in the partial pressure of individual dissolved gases, and consequently in the total dissolved gas pressure. If the total gas pressure exceeds a threshold pressure a gas bubble may form (Li and Yortsos,1995). Once the bubble is formed, gases partition between the aqueous and gas phases according to an equilibrium relationship and the bubble may grow or shrink depending on whether gases are produced or consumed. If the total dissolved gas pressure drops below the threshold pressure the bubble will disappear. Gas bubbles may also form near the water table as a result of entrapment during imbibition (Parker and Lenhard,1987; Williams and Oostrom, 2000). Once the bubble is trapped below the water table, gases in the bubble will partition into the groundwater, and vice versa, so that the size of the bubble is again determined by the total dissolved gas pressure. Conversely, if a gas bubble is present near the water table and drainage occurs, gas bubbles will be released to the unsaturated zone. In the formulation presented here, individual bubbles are not modelled explicitly but are instead represented by the trapped gas phase saturation, S_{gt}. This does not affect the conceptualization and facilitates its implementation into the code. Given that the trapped gas phase saturation is known, the permeability of the porous media can be determined based on generally accepted saturation/permeability relations (Wösten and van Genuchten, 1988), which have been shown to be applicable to quasi-saturated porous media (Fry et al., 1997).

3.2.2 Governing Equations

The following section outlines the formulation describing the equilibrium partitioning of dissolved gases into a discontinuous gas phase present below the water table, entrapment and release of a discontinuous gas phase below the water table due to water table fluctuations, and the resulting changes in permeability. The detailed formulation of MIN3P is presented by Mayer et al. (2002). Here we outline specific additions to the model formulation that are relevant to the current problem.

3.2.2.1 Gas pressure induced changes in gas phase saturation

The mass conservation equation for a system with N_C components can be written as:

$$
\frac{\partial}{\partial t}\left[S_a \phi T_j^a\right] + \frac{\partial}{\partial t}\left[S_g \phi T_j^g\right]
$$
$$
+ \nabla \cdot \left[v_a T_j^a\right] - \nabla \cdot \left[S_a \phi D_a \nabla T_j^a\right] - \nabla \cdot \left[S_g \phi D_g \nabla T_j^g\right] - Q = 0 \qquad j = 1, N_C, \tag{1}
$$

where t is time, S_a [m^3 water m^{-3} pore space] is the water saturation, and S_g [m^3 gas m^{-3} pore space] is the gas phase saturation, which can be further subdivided into:

$$
S_g = S_{gt} + S_{gc}, \tag{2}
$$

where S_{gt} and S_{gc} [m^3 gas m^{-3} pore space] are the trapped and connected gas phase saturations, respectively, where in this context, the connected gas phase is defined as a continuous gas phase that allows gas transport through the unsaturated zone to and from the ground surface , ϕ is the porosity, v_a [m s^{-1}] is the Darcy flux vector, D_a and D_g [m^2 s^{-1}] are the hydrodynamic dispersion tensors for the aqueous and gas phases, respectively, Q [mol L^{-1} porous medium] represents a variety of source-sink terms, and N_C is the

l

number of components. T_j^a [mol L^{-1} H$_2$O] and T_j^g [mol L^{-1} gas] are the total component

concentrations in the aqueous and gas phases given by

$$T_j^a = C_j^C + \sum_{i=1}^{N_x} v_{ij}^x C_i^x,$$ (3)

and

$$T_j^g = \sum_{l=1}^{N_g} v_{lj}^g C_l^g,$$ (4)

where C_j^C [mol L^{-1} H$_2$O] is the concentration of component j as a species in solution, C_i^x

[mol L^{-1} H$_2$O] is the concentration of aqueous complex i, C_l^g [mol L^{-1} gas] is the

concentration of gaseous species l, N_x and N_g are the number of aqueous complexes and

gaseous species, respectively, and v_{ij}^x and v_{lj}^g are the stoichiometric coefficients relating

component j to complexes i and gases l, respectively. The concentrations of the aqueous

complexes are related to the primary unknowns C_j^C by the following expressions:

$$C_i^x = \left(K_i^x \gamma_i^x\right)^{-1} \prod_{j=1}^{N_c} \left(C_j^C \gamma_j^C\right)^{v_{ij}^x},$$ (5)

where K_i^x is the equilibrium constant for the dissociation of aqueous complex i, and the γ-

terms represent the activity coefficients. The concentrations of gaseous species are given

by

$$P_l = \left(K_l^g\right)^{-1} \prod_{j=1}^{N_c} \left(C_j^C \gamma_j^C\right)^{v_{lj}^g};$$ (6)

$$C_l^g = \frac{P_l}{RT},$$ (7)

where P_l (atm) and K_l^g (mol atm^{-1}) are the partial pressure and Henry's Law constant for

gas species l, respectively, R is the gas constant [0.08206 L atm mol^{-1} K^{-1}] and T [K] is

the temperature.

64

The nucleation and growth of gas bubbles is considered to occur when the total dissolved gas pressure exceeds the sum of the hydrodynamic and capillary pressures (Li and Yortsos, 1995). For simplicity we neglect capillary forces such that a gaseous phase will form under the condition:

$$\sum P_l > P_H \qquad P_H > 0, \qquad (8)$$

where P_H (atm) is the hydrodynamic pressure equal to the sum of the atmospheric pressure and water pressure. Neglecting capillary forces may underestimate the total gas pressure required to produce a gas bubble and potentially overestimate bubble growth. However, this simplification is reasonable for sand and gravel aquifers considering that observed total gas pressures are not significantly above hydrodynamic pressures (e.g. Bemidji site; Amos et al., 2005), but may be less adequate in finer grained sediments where bubble growth is restricted by capillary forces (e.g. van Breukelen et al, 2003). The condition $P_H > 0$ implies that the process of bubble formation occurs only below the water table. Under equilibrium conditions the following condition must apply:

$$\sum_{l=1}^{N_g} P_l - P_H = 0 \qquad if\ S_{gt} > 0, \qquad (9)$$

noting that below the water table $S_g = S_{gt}$. The solution to Equation 1 does not implicitly conform to this condition so that a relationship must be sought which links Equations 1 and 9. Considering that at a given moment (i.e. any solution to Equation 1) the total mass of each gas in the aqueous and gaseous phases together is fixed, then the partial pressure of each gas is given by the concentration of the gas in the aqueous phase (Equation 6) and also by the gas saturation S_{gt}. The formulation of Cirpka and Kitanidis (2001) provides an expression that relates the partial pressure P_l to S_{gt}, and is adapted here into a

65

multicomponent framework. The total component concentrations T_k^T [mol L^{-1} pore

space], accounting for gases present in both the aqueous and gas phase, are defined as:

$$T_k^T = S_a T_k^a + S_{gt} T_k^g, \qquad (10)$$

where the subscript k refers to a specific component associated with each gas. For

example, the gas O_2 would be associated with the component $O_2(aq)$ while the gas CO_2

would be associated with the component HCO_3^-. The next step is to express the total

aqueous and gaseous component concentrations in terms of partial pressures. By

substituting Equation 4 into Equation 10 we obtain:

$$T_k^T = \left(1 - S_{gt}\right)T_k^a + S_{gt}\sum_{l=1}^{N_g} v_{lk}^g C_l^g, \qquad (11)$$

with $S_a = (1 - S_{gt})$. By choosing each gas-related component k, such that it is only

associated with one gas with a stoichiometric coefficient $v_{lk}^g = 1$, the expression

simplifies to:

$$T_k^T = \left(1 - S_{gt}\right)T_k^a + S_{gt} C_{l(k)}^g, \qquad (12)$$

where the subscripts k and $l(k)$ refer to a specific component and the associated gas

species, respectively. Substituting in Equation 7 yields:

$$T_k^T = \left(1 - S_{gt}\right)T_k^a + S_{gt} \frac{P_{l(k)}}{RT}. \qquad (13)$$

To express the total aqueous component concentrations in terms of partial pressures we

start by substituting Equation 3 into 13:

$$T_k^T = \left(1 - S_{gt}\right)\left(C_k^C + \sum_{i=1}^{N_x} v_{ik}^x C_i^x\right) + S_{gt} \frac{P_{l(k)}}{RT}, \qquad (14)$$

followed by substitution of Equation 5 to express each species in terms of components:

$$T_k^T = \left(1 - S_{gt}\right)\left(C_k^C + \sum_{i=1}^{N_x} v_{ik}^x \left(\left(K_i^x \gamma_i^x\right)^{-1} \prod_{j=1}^{N_C}\left(C_j^C \gamma_j^C\right)^{v_{ij}^x}\right)\right) + S_{gt}\frac{P_{l(k)}}{RT}. \quad (15)$$

Using Equation 6 with $v_{lk}^g = 1$, the following expression can be derived:

$$T_k^T = \left(1 - S_{gt}\right)P_{l(k)}\left[\frac{K_{l(k)}^g}{\prod\limits_{j=1;j\neq k}^{N_C}\left(C_j^C \gamma_j^C\right)^{v_{ij}^x}}\left(\frac{1}{\gamma_k^C} + \left(C_k^C \gamma_k^C\right)^{(v_{ik}^x - 1)}\sum_{i=1}^{N_x} v_{ik}^x\left(\left(K_i^x \gamma_i^x\right)^{-1}\prod_{j=1;j\neq k}^{N_C}\left(C_j^C \gamma_j^C\right)^{v_{ij}^x}\right)\right)\right] + S_{gt}\frac{P_{l(k)}}{RT}.$$
$$(16)$$

Note that the solution to this equation is only possible if $v_{ik}^x = 1$, implying that all gas components k must have a stoichiometric coefficient of less than or equal to 1 in the aqueous complex i. This assumption, and the condition that $v_{lk}^g = 1$, restricts the use of the model from the general case; however, inspection of standard geochemical databases suggests that these limitations are minor and in practice do not limit the applicability of this formulation. Defining the term in square brackets as Ψ_k and rearranging yields:

$$P_{l(k)} = \frac{T_k^T}{\left(1 - S_{gt}\right)\Psi_k + \dfrac{S_{gt}}{RT}}. \quad (17)$$

A solution for S_{gt} can be obtained by minimizing Equation 9 with $P_{l(k)}$ given by Equation 17.

In the multicomponent framework of MIN3P, components other than those associated with a specific gas are also considered and must be updated appropriately. For many components the stoichiometric coefficient v_{lj}^g will be zero for all gases, so that T_j^g will also be zero, and the update is straightforward by maintaining mass balance in the aqueous phase. For other components v_{lj}^g may not be zero. For example, the coefficient for H^+ in $CO_{2(g)}$ is equal to one. In this case, $T_{H^+}^g$ will be non-zero as $CO_{2(g)}$ partitions into

the gas phase. Update of these components is accomplished by iteration between the bubble solution (Equations 9 and 17) and the reactive transport solution (Equation 1, subject to the relationships defined by Equations 3, 4, and 5), to ensure that all components are appropriately distributed between the aqueous and gas phases.

3.2.2.2 Bubble Entrapment

The model presented by Parker and Lenhard (1987), describing hysteretic saturation-capillary pressure relationships in three phase air-oil-water porous media, distinguishes between pore-geometry related hysteresis (Type I) and hysteresis due to non-wetting phase fluid entrapment (Type II). Previous work has shown that consideration of only Type II hysteresis provides an accurate representation of saturation-capillary pressure relations in two and three phase systems, without the additional complexities associated with Type I hysteresis (Lenhard et al., 1995; Oostrom et al 1997; Williams and Oostrom, 2000). After Kaluarachchi and Parker (1992), the effective trapped gas saturation is given by

$$S_{egt} = \left\{ \frac{1 - S_{ea}^{min}}{1 + R_L (1 - S_{ea}^{min})} - \frac{1 - S_{aa}}{1 + R_L (1 - S_{aa})} \right\}, \qquad (18)$$

where S_{ea}^{min} is the minimum effective aqueous saturation, S_{aa} is the apparent aqueous phase saturation, and R_L is the empirically derived Land's parameter given by

$$R_L = \frac{1}{S_{egt}^{max}} - 1, \qquad (19)$$

where S_{egt}^{max} is the maximum effective trapped gas saturation. Visual conceptualization of this hysteretic model is shown in Figure 3-1A. Assuming that the porous medium is at saturation, upon a decrease in pressure head (increase in capillary head), the

saturation/pressure head relationship follows the main drainage curve. If at a given point the pressure head increases, such as that marked as point 'A' in Figure 3-1A, imbibition occurs along the scanning imbibition curve, and S_{ea}^{min} corresponds to the minimum effective aqueous saturation prior to imbibition. At any point during imbibition, point 'B' in Figure 3-1A for example, S_{aa} corresponds to the saturation given by the main drainage saturation/pressure head relationship, S_{egt} is calculated according to Equation 18, and the effective aqueous phase saturation is given by

$$S_{ea} = S_{aa} - S_{egt}.$$ (20)

If drainage resumes before full saturation is reached, the saturation/pressure head relation follows the scanning curve in reverse. With this formulation, the only additional parameter needed to determine the trapped gas saturation, beyond the parameters already needed to determine non-hysteretic aqueous phase saturations, is S_{egt}^{max}, which must be determined empirically for particular porous media. Effective saturations are related to actual saturations by (Parker and Lenhard, 1987)

$$S_{ea} = \frac{S_a - S_{ra}}{1 - S_{ra}},$$ (21)

and

$$S_{egt} = \frac{S_{gt}}{1 - S_{ra}},$$ (22)

where S_{ra} is the residual saturation, and the gas phase saturation is given by $S_g = 1 - S_a$.
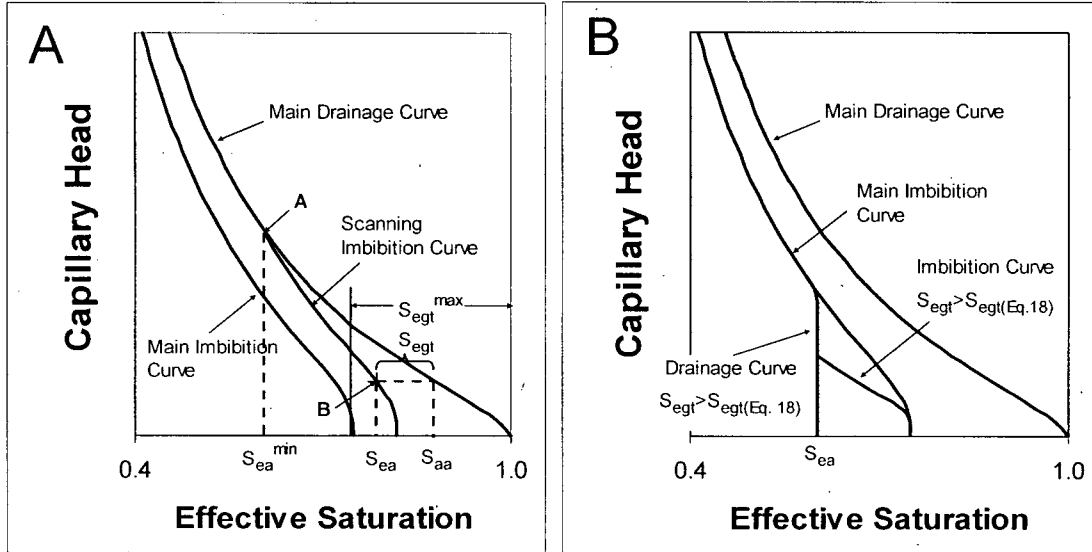
Figure 3-1. A) Schematic representation of hysteretic bubble entrapment model. B) Representation of drainage and imbibition curves where S_{egt} is greater than S_{egt} predicted by Equation 18 (see text for explanation).

Once a particular control volume becomes saturated ($S_{aa} = 1$), S_{gt} is no longer controlled by the saturation/pressure head relation but is instead a function of total dissolved gas pressure as described in the preceding section. Upon drainage this presents a problem in that Equation 18 and possibly Equation 19 are undefined. If S_{egt} is less than S_{egt}^{max}, due to dissolution of entrapped gases into the groundwater, then Equation 18 is undefined because S_{ea}^{min} is unknown. However, this can be easily rectified using Equation 18 to calculate a value for S_{ea}^{min}, taking S_{egt} to be the value prior to drainage, and S_{aa} equal to 1. If drainage occurs when S_{egt} exceeds S_{egt}^{max}, which may occur due to in-situ gas production, the problem becomes more complex in that both Equations 18 and 19 are undefined. As a remedy, we propose the scheme depicted graphically in Figure 3-1B. If drainage occurs when S_{egt} exceeds S_{egt}^{max}, then S_{ea} is held constant until S_{egt}, calculated by $S_{aa} - S_{ea}$, is less than S_{egt} predicted by Equation 18 with S_{ea}^{min} equal to 0 (i.e. a saturation/pressure head relation corresponding to the main imbibition branch). If

70

imbibition occurs when S_{egt} exceeds the value for S_{egt} calculated by Equation 18 with S_{ea}^{min} equal to 0, then S_{egt} is held constant until it becomes equal to the value predicted by Equation 18. Although there is no experimental evidence to support or refute this scheme, we believe it is a reasonable representation, and a necessary addition to allow the model to be generally applicable to problems involving in-situ gas production and exsolution.

3.2.2.3 Relative Permeability Relationship

In MIN3P the equation relating relative permeability, k_{ra}, to aqueous phase saturation is currently expressed as:

$$k_{ra} = S_{ea}^{l}\left(1 - \left[1 - S_{ea}^{1/m}\right]^{m}\right)^{2},$$ (23)

where l and m are soil hydraulic function parameters (Wösten and van Genuchten, 1988). This equation is typically applied to unsaturated porous media where the gas exists as a connected phase. However, Fry et al. (1997) showed that this relationship is valid in quasi-saturated sands (i.e. where a trapped gas phase exists) ranging from fine to coarse grained, with gas saturations ranging from ~ 10 to 60%. Therefore, this relation is applied here to both the saturated and unsaturated zones, irrespective of whether the gas phase is trapped or not.

3.2.3 Numerical Implementation

Geochemical interactions of trapped gases in quasi-saturated porous media also have an impact on groundwater flow. Flow is affected by growth and contraction of the bubbles displacing water, and more importantly by changes in permeability due to changes in gas phase saturation. Because of this, the presence of a trapped gas phase affects both the reactive transport and transient flow equations in MIN3P, and the non-

71

linear coupling between these processes requires an iterative solution. Figure 3-2 shows a schematic diagram of the numerical approach.

The aqueous phase mass conservation equation for variably saturated flow is described as:

$$S_a S_s \frac{\partial h}{\partial t} + \phi \frac{\partial S_a}{\partial t} - \nabla \cdot [k_{ra} K \nabla h] - Q_a = 0, \qquad (24)$$

where h, hydraulic head [m], is the primary unknown, S_s is the specific storage coefficient [m^{-1}], K is the hydraulic conductivity tensor [m s^{-1}], and Q_a is a source sink term [s^{-1}]. In any control volume, at a given timestep, Equation 24 is initially solved giving values of hydraulic head dependent variables such as P_H, S_a, S_g and S_{gl} (Figure 3-2, Box (1)). For saturated control volumes, i.e. $P_H > 0$, S_a, S_g, and S_{gl} are not a function of hydraulic head and remain unchanged in the flow solution. For unsaturated control volumes, $P_H \leq 0$, these variables are a function of hydraulic head and are updated as outlined in section 3.2.2.2.

Given an initial flow solution, the reactive transport solution (Equation 1) is solved giving values of the primary unknowns (C_j^C), and therefore total aqueous and gaseous component concentrations (T_j^a and T_j^g) along with initial values of S_a, S_g and S_{gl} (Figure 3-2, Box (2)). In the bubble module (Figure 3-2, Box (3)), if the control volume is saturated ($P_H > 0$), values of T_k^T and Ψ_k are calculated and the term $\sum P_l$ is evaluated using Equation 17. If the sum of the partial pressures is less than P_H, then no gas phase is present and S_{gl} is zero. If the sum of the partial pressures is greater than P_H, then a gas phase is present, the condition expressed in Equation 9 must hold, and S_g is solved for
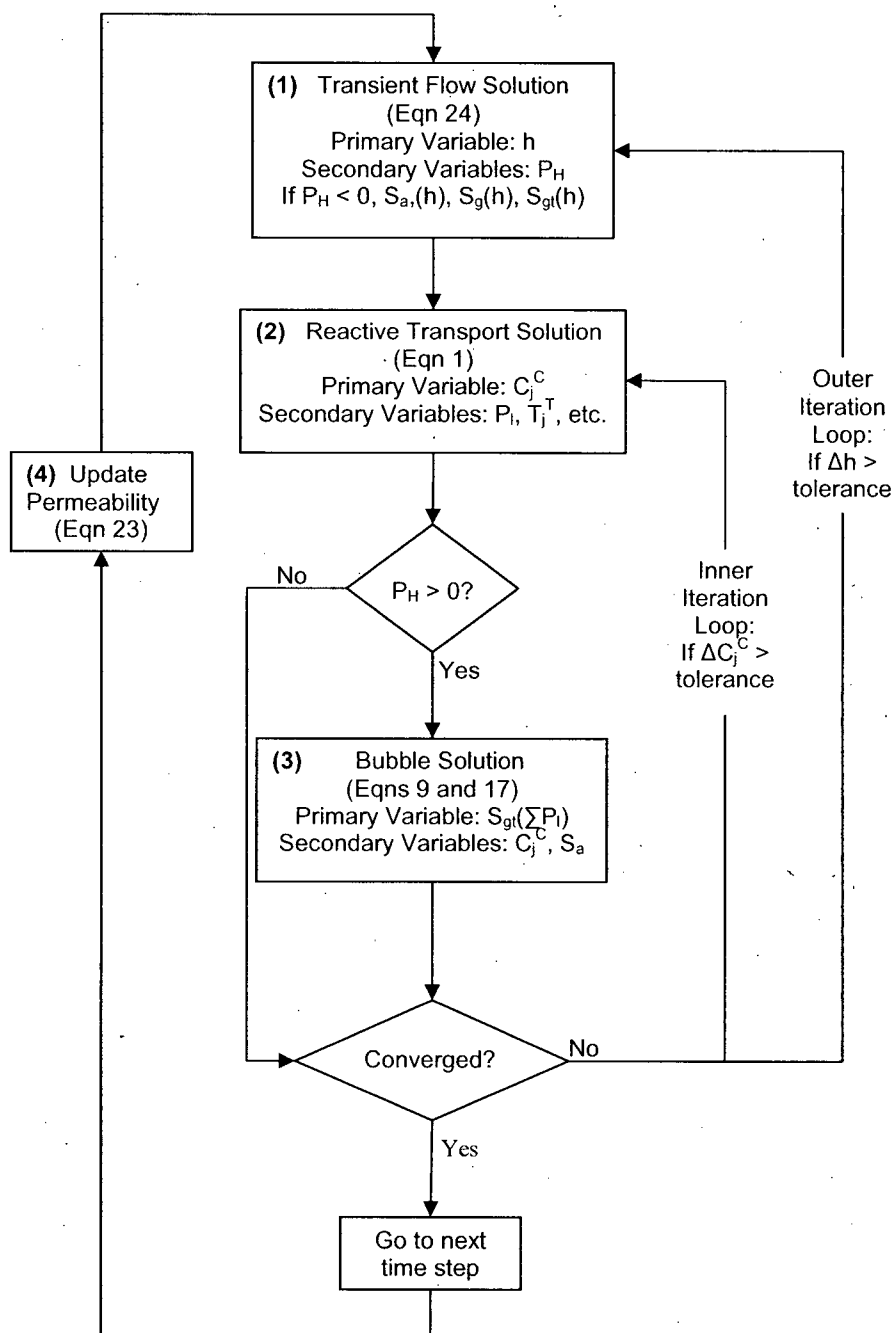
Figure 3-2. . Schematic diagram showing numerical implementation of the MIN3P bubble model.

73

using Newton's method using analytical derivatives to Equation 17. If a control volume is unsaturated ($P_H < 0$), the bubble module is skipped and S_{gt} is unchanged. This is based on the assumption that above the water table S_{gt} is controlled by the saturation/pressure head relationship, and that the trapped and connected gas phases remain in equilibrium with the dissolved gas concentration according to Equation 6.

With the updated values for S_{gt}, S_a is updated, partial pressures for each gas can be calculated using Equation 17, where Ψ_k is evaluated before updating S_{gt}, and the dissolved gas concentrations (C_k^C) are recalculated using Equation 6. These intermediate results are returned to the reactive transport solution and the inner iteration loop is continued until changes in the primary unknowns, C_j^C, are less than the user-defined convergence tolerance.

If S_{gt} and S_a in saturated control volumes have changed in the inner iteration loop, the flow solution must be updated. The solution to Equation 24 is used to determine new values for v_a [m s^{-1}], the Darcy flux vector, which are then used in re-evaluating the reactive transport solution (Equation 1). Near the water table, changes in S_{gt} and S_a in saturated control volumes may also affect unsaturated control volumes so that saturations are also recalculated for unsaturated control volumes as part of the solution to Equation 24. The outer iteration loop continues until changes in h are less than the user-defined convergence tolerance.

Once the outer and inner loops have converged the model updates relative permeability according to Equation 23 (Figure 3-2, Box(4)) and proceeds to the next time step. This explicit update is adequate because permeability changes are small at each timestep. An option exists in the code to iterate through the outer loop only, which

implicitly incorporates the inner loop. This option is less stable under certain conditions but reduces computer time when the conditions are appropriate. Both methods adhere to the same convergence criteria and therefore produce the same degree of numerical accuracy.

3.2.4 Model Limitations

MIN3P is a single phase model in the sense that the flow solution is solved for the water phase only. The resulting primary limitation is that advective gas transport is not considered in the model, which can have serious implications under certain conditions. To examine this we refer to Equation 1, the MIN3P mass conservation equation for reactive transport. For the case of a rapidly falling water table, we can consider a control volume where the aqueous phase saturation will decrease and the gas phase saturation will increase. For any non-volatile component j, the solution to Equation 1 will maintain mass balance and will yield adequate results. However, for volatile components, the increase in gas phase saturation may yield a decrease in T_j^g to maintain mass balance. This may result in an unrealistically low value for T_j^g, and therefore T_j^a since the two are related by Henry's law, and is due to neglecting the downward advective gas transport that is likely induced by a rapid drop of the water table. To provide a more realistic representation under these conditions we apply the following optional modification to the code. Applying the chain rule to the second term in Equation 1, and assuming constant porosity for simplicity, yields:

$$\phi S_g \frac{\partial T_j^g}{\partial t} + \phi T_j^g \frac{\partial S_g}{\partial t} \qquad\qquad j = 1, N_c, \qquad (25)$$

75

showing that the gas phase storage term is composed of two components. The first is a change in storage due to a change in T_j^g, primarily related to concentration changes in the aqueous phase and diffusive gas fluxes, and the second is a change in storage related to a change in gas phase saturation, which is the problematic term. The code includes an option to neglect the contribution of the latter term for unsaturated control volumes, which effectively provides an approximation for the advective response of the gas phase to water table fluctuations. Although this modification does not strictly honour the mass balance of the governing equations, and does not describe advective gas transport based on physical principles, it provides a more realistic representation for volatile components. Note that this modification is only required in cases where water table fluctuations are rapid in comparison to the time scale of diffusive gas transport, and only has to be employed in special cases. Where this modification is used we will discuss the implications and validity.

3.3   Verification

3.3.1   1-D Column Example

An analytical solution to the bubble problem is relatively straight forward for simple problems where groundwater flow is negligible and the number of gases is small. Here we compare the results of a four-gas, 1-D problem simulated using MIN3P and an analytical model (Amos et al., 2005) to show that the numerical solution to Equations 9 and 17, including feedback to the transport and flow equations, is accurate. In this example groundwater flow is only in response to bubble growth and not due to a hydraulic gradient across the model domain. The simulation represents a 1-D vertical column, 1.2 m in height and discretized into 0.1 m control volumes with half-cells at the

76

boundaries (Figure 3-3). The initial hydraulic head in the column is set to 1 m so that the column is initially saturated from the bottom up to 1 m. Relevant model parameters are given in Table 3-1. Initially the total pressure of the four gases, N_2, O_2, CH_4 and Ar, is 1.04 atm so that it exceeds P_H and forces a bubble to form in control volumes 7, 8, 9, 10 and 11, which are centered at elevations of 0.6, 0.7, 0.8, 0.9 and 1.0 m, respectively. Control volumes 1 through 6 are sufficiently deep, i.e. > 0.4 m below the water table, that P_H is greater than 1.04 atm and no bubble forms. Control volumes 12 and 13 are unsaturated. No sources or sinks for gases are simulated so that the model achieves a steady state solution. Comparison of the MIN3P and analytical solutions, including gas phase saturations and aqueous concentrations of the gases, indicate that the two solutions give very similar results (Table 3-1).

Table 3-1. Parameters, MIN3P simulation results and analytical model results (A) for 4 gas, 1-D column verification example.

K_i^g (mol L^{-1} atm^{-1})	z (m)	P$_H$ (atm)	S$_{gt}$		N$_2$ 5.9090 x 10^{-04}	
			MIN3P (x 10^{04})	A (x 10^{04})	MIN3P (atm)	A (atm)
Initial Condition			0		0.78	
Volume 7	0.6	1.0387	0.22286	0.22427	0.77888	0.77888
Volume 8	0.7	1.0290	1.9341	1.9353	0.77052	0.77052
Volume 9	0.8	1.0193	3.6804	3.6809	0.76216	0.76216
Volume 10	0.9	1.0096	5.4625	5.4626	0.75382	0.75382
Volume 11	1.0	1.0000	7.2814	7.2810	0.74550	0.74550

K_i^g (mol L^{-1} atm^{-1})	O$_2$ 1.2687 x 10^{-03}		CH$_4$ 1.4117 x 10^{-03}		Ar 1.2719 x 10^{-03}	
	MIN3P (atm)	A (atm)	MIN3P (atm)	A (atm)	MIN3P (atm)	A (atm)
Initial Condition	0.05		0.2		0.01	
Volume 7	0.049963	0.049963	0.19986	0.19986	0.009993	0.009993
Volume 8	0.049689	0.049689	0.19887	0.19887	0.009943	0.009943
Volume 9	0.049413	0.049413	0.19788	0.19788	0.009892	0.009892
Volume 10	0.049135	0.049134	0.19687	0.19687	0.009841	0.009841
Volume 11	0.048853	0.048853	0.19585	0.19585	0.009789	0.009789

h = 1.0 m, z = 1.2 m

Unsaturated Control Volume

Saturated Control Volume, P_H < 1.04 atm

Saturated Control Volume, P_H > 1.04 atm

0.1 m

h = 1.0 m, z = 0 m
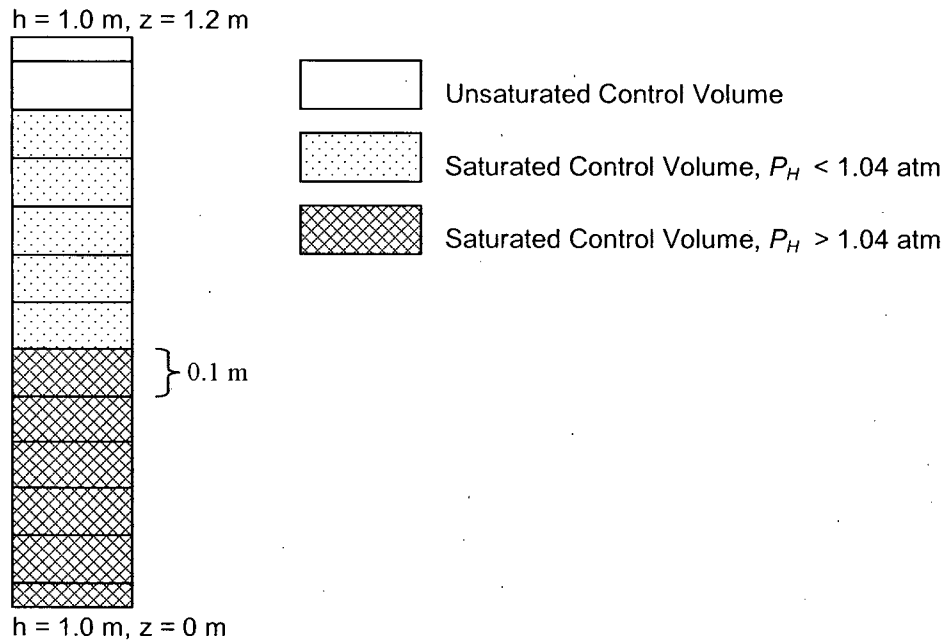
Figure 3-3. Schematic representation of 1-D column verification example showing model domain and boundary conditions.

3.3.2   1-D Flow Problem

Cirpka and Kitanidis (2001) developed a 1-D numerical model that describes the partitioning of gas species between gas bubbles and flowing groundwater, and verified their model against a semi-analytical solution based on coherence theory. We attempted to reproduce results presented by Cirpka and Kitanidis (2001) to verify our solution in saturated media with groundwater flow and gas bubble dissolution. The example is a 1-D flow problem where the initial dissolved gas partial pressures are 0.8 atm N_2 and 0.2 atm O_2 in equilibrium with a gas phase saturation, S_{gt}, of 0.25. The inflow dissolved gas partial pressures are 0.24 atm N_2, 0.06 atm O_2, and 0.35 atm SF_6 so that the total dissolved gas pressure in the inflow is less than P_H, the gas phase is unstable, and S_{gt} decreases through the course of the simulations. The temperature is 298 K, the specific

78

discharge is 3.66×10^{-5} m s^{-1}, and the porosity is 0.36. The Henry's law constants used for the simulations are those given by Cirpka and Kitanidis (2001) of 1.53×10^5, 8.04×10^4, and 4.21×10^5 Pa m^3 mol^{-1} for N_2, O_2, and SF_6, respectively.

The MIN3P model domain consisted of a 90 cm long horizontal section discretized into 901 control volumes to minimize numerical dispersion, which is consistent with the Cirpka and Kitanidis (2001) numerical simulations. Specified flux boundaries were set for the flow solution at either end of the domain. For the transport problem a specified aqueous mass flux was specified at the inflow end of the domain and a Neuman type boundary was set at the outflow end of the domain. The results, in terms of dissolved gas concentrations and S_{gt} at the outflow end of the model domain, are shown in Figure 3-4 for the MIN3P and the Cirpka and Kitanidis (2001) models. Both models produce very similar results which demonstrates the ability of the updated MIN3P code to accurately simulate partitioning of gases into an immobile gas phase within a flow field, including reliable representation of the corresponding changes in S_{gt}.

3.3.3   Bubble entrapment

In an effort to verify the bubble entrapment formulation we attempted to simulate the work of Williams and Oostrom (2000) who presented experimental and modelling results of a fluctuating water table experiment. The experiment was conducted in a 90 cm high flow cell packed with fine-grained 30/40 mesh quartz sand and fitted along its height with dissolved oxygen (DO) probes and a gamma radiation system to measure saturation. The experiment started with the flow cell fully saturated with de-oxygenated water (obtained by flushing with He), followed by six, ~ 24 hr, drainage/imbibition cycles during which water was either drained from the bottom of the flow cell, at a specific

79

discharge of ~ 1.6 x 10^{-6} m s^{-1}, or pumped into the bottom of the flow cell at a similar

rate. After the sixth imbibition cycle, water was drained continually from the flow cell.

The top of the flow cell was open to the atmosphere to allow the ingress of oxygen. For

further details on experimental conditions, experimental methods, and numerical

simulations using the multi-phase flow and transport code STOMP, the reader is referred

to Williams and Oostrom (2000).
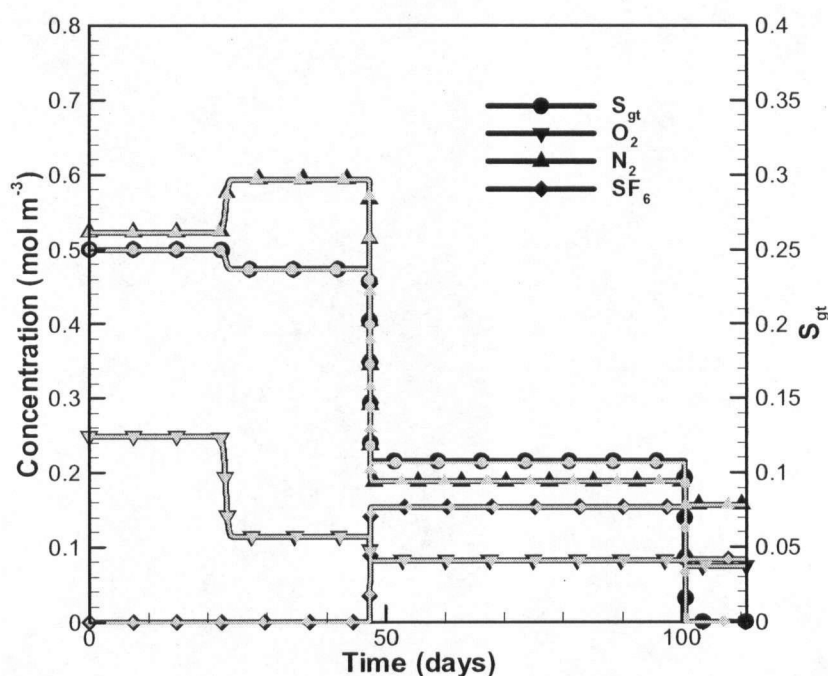
Figure 3-4. Model results at outflow end of the simulated columns from MIN3P (grey lines and symbols) and Cirpka and Kitanidis (2001) model (black lines and symbols).

The MIN3P simulations consisted of a 90 cm vertical domain discretized into 91

control volumes. For the flow solution, a specified flux boundary was set at the bottom of

the domain corresponding to flow rates used in the experiment. At the top of the domain

a no-flow boundary was set. The porosity used in the simulations was 0.325, which was experimentally determined, and the Van Genuchten soil hydraulic function parameters were set to 6.65 for alpha and 10.35 for n, which were chosen to best represent the experimentally determined Brooks-Corey parameters of 13.0 cm for the air entry pressure and 5.0 for lambda (Figure 3-5). For transport, the initial composition of dissolved gases in the water consisted of 1.0 atm He only. A Dirichlet type boundary was used for the aqueous phase at the bottom of the model domain and for the gas phase at the top of the domain. Boundary concentrations at the bottom of the domain were the same as initial conditions, and set to atmospheric concentrations for N_2, Ar and O_2 at the top boundary.
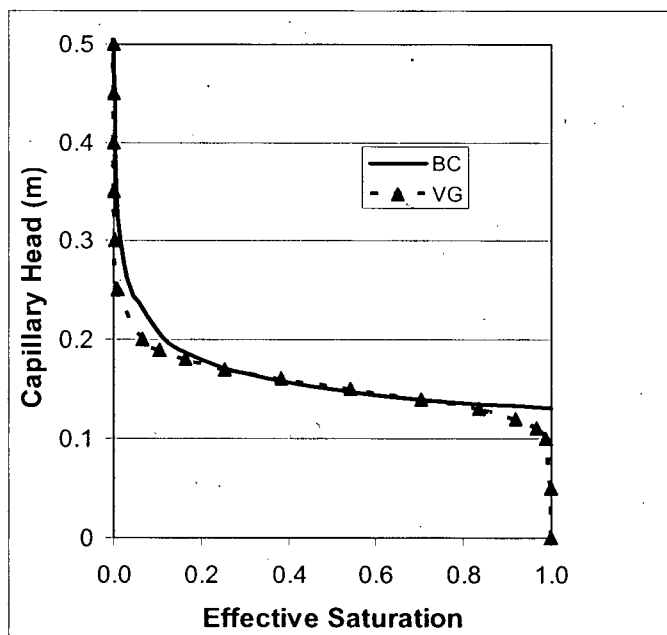
Figure 3-5. Saturation-pressure relationships determined by Brooks-Corey (BC) parameters used in STOMP simulations and Van Genuchten (VG) parameters used in MIN3P simulations of water table fluctuation experiments run by Williams and Oostrom (2000).

In MIN3P, to represent the total pressure of the gas phase, all major gases must be included. The free phase diffusion coefficients used for all gases were 2×10^{-9} m^2 s^{-1} for

81

the aqueous phase and 2.0 x 10^{-5} m^2 s^{-1} for the gas phase. These are reasonable average values for all gases considered in the simulations (CRC press, 2004). Effective diffusion coefficients were calculated internally based on saturations and porosity using the relationships provided by Millington (1959). Because of the rapid water table fluctuations in the experiment, advective gas fluxes are of importance. This necessitates use of the simplified formulation discussed in section 2.4, which ignores changes in gas phase storage as a result of gas phase saturation changes.

Saturation versus time data from the MIN3P simulations, STOMP simulations and the experimental results are presented in Figure 3-6 for various levels within the flow cell. In general, the agreement between MIN3P and STOMP are good suggesting that the numerical implementation of the trapped gas formulation in MIN3P is satisfactory. Furthermore, the agreement between MIN3P and the experimental data suggests that our formulation is a reasonable representation of the physical system. Much of the difference between the MIN3P and STOMP simulations can be attributed to the different saturation-pressure relationships used in the codes (Figure 3-5). Although the relationships are very similar, they do differ, especially at high and low saturations where the Van Genuchten parameters tend to predict slightly lower saturations for a given capillary head. The effect of these differences is especially noticeable in Figure 3-6B between ~66 and 90 hours. Here MIN3P under-predicts saturation by about 5 %, but note that only a small difference in capillary head, ~1-2 cm, is required to change the saturation from 1 to 0.95 as is shown in Figure 3-5.
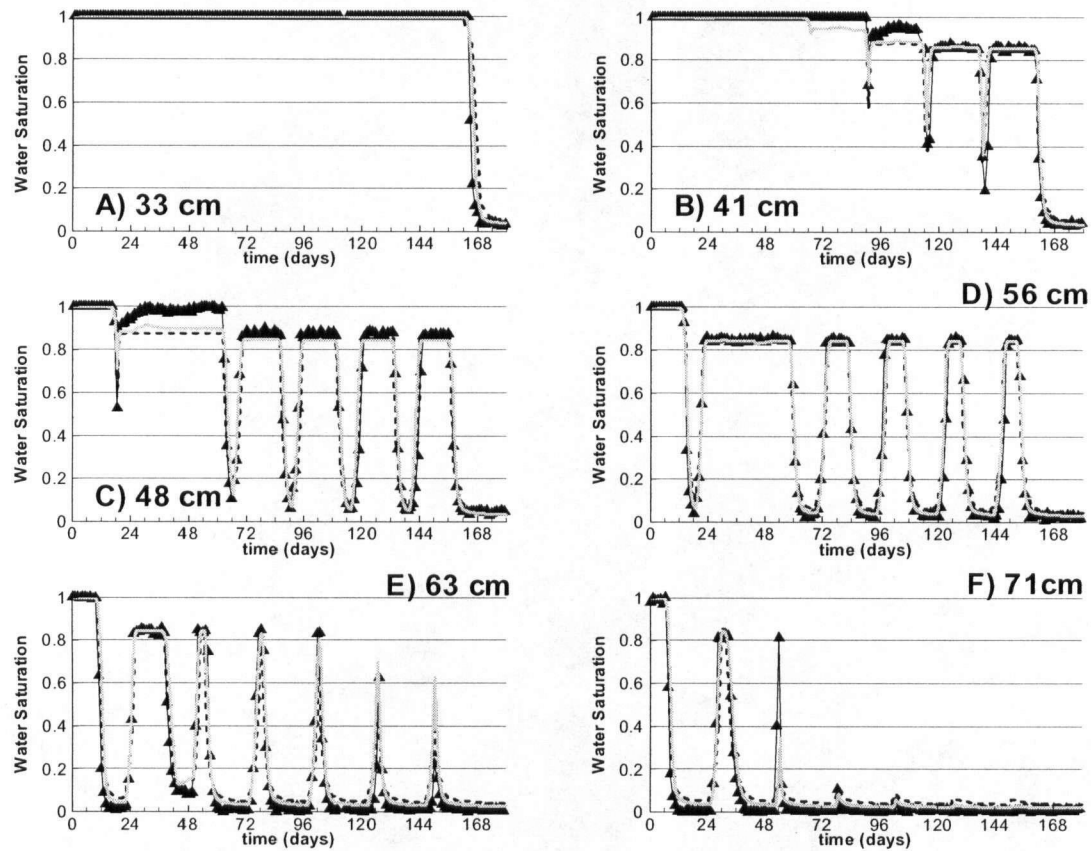
Figure 3-6. Water saturation vs time data at various locations along the column for MIN3P simulations (solid grey lines), STOMP simulations (dashed black lines) and experimental results (symbols with solid black lines) of water table fluctuation experiments run by Williams and Oostrom (2000).

Plots of dissolved oxygen concentrations versus time from the MIN3P simulations, STOMP simulations and the experimental results are shown in Figure 3-7 for various levels within the flow cell. In general, the MIN3P results closely match the STOMP results, and both are good representations of the experimental data. Figure 3-8 shows dissolved O_2 and water saturation profiles through the column at 79 hrs for the MIN3P simulations, STOMP simulations and experimental results. It is important to note that in the unsaturated zone, i.e. above ~ 50 cm, and in the quasi-saturated zone, i.e. between ~ 50 and 60 cm, experimentally observed O_2 concentrations are near saturation

suggesting that O_2 transport by advection and diffusion is rapid in the unsaturated zone.

Similarly, the MIN3P simulation shows O_2 concentrations near saturation in the

unsaturated and quasi-saturated zones, indicating that our simplified formulation provides

a reasonable representation of this system. Given that this is the case, we can be confident

that the simulations accurately represent the experimental conditions in the aqueous

phase.
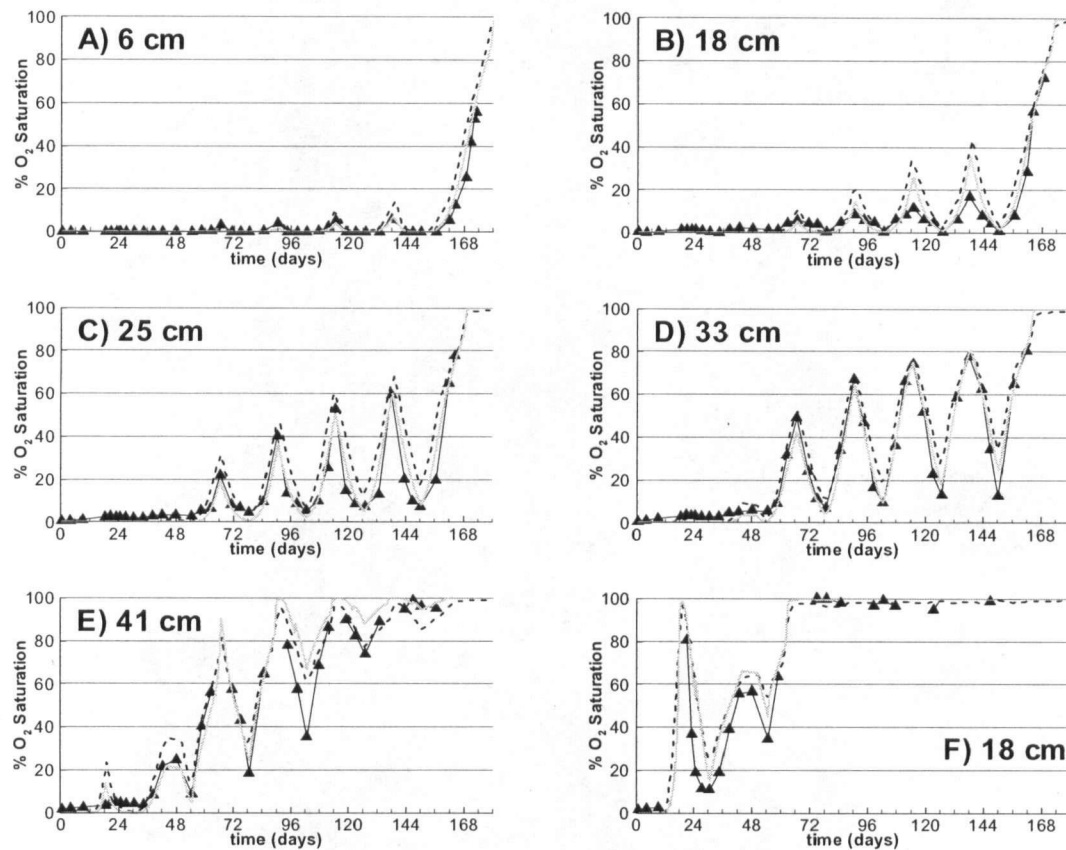
Figure 3-7. Oxygen saturation vs time data at various locations along the column for MIN3P simulations (solid grey lines), STOMP simulations (dashed black lines) and experimental results (symbols with solid black lines) of water table fluctuation experiments run by Williams and Oostrom (2000).
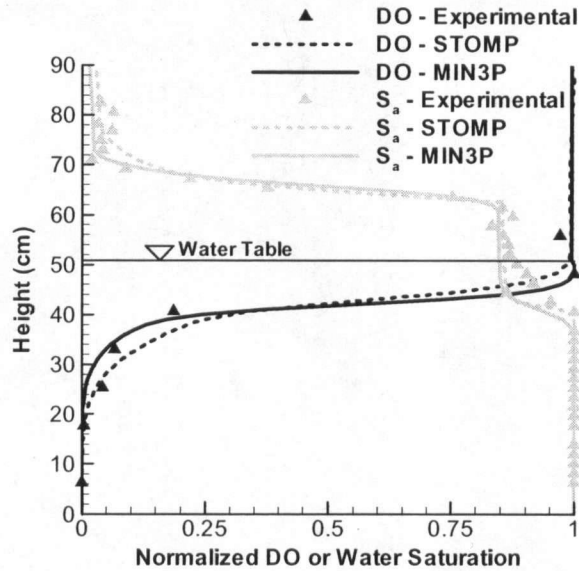
Figure 3-8. Spatial profile of dissolved O₂ (DO) and water saturations (S_a) at 79 hrs for MIN3P simulations, STOMP simulations and experimental results of water table fluctuation experiments run by Williams and Oostrom (2000).

3.3.4 Other Considerations

It is difficult to diligently verify the numerical solution to the bubble problem involving gases that speciate in solution (such as CO_2) due to the non-linear dependence on other components (e.g. pH in the case of CO_2). However, it is possible to verify that any solution given by the model, for any particular control volume, is in chemical equilibrium with respect to the various components and species, in both the aqueous and gaseous phases. Given that this is the case, this is a strong indication that the implementation of Equation 17 with respect to speciated gases is correct.

We have not attempted to verify the permeability relationship given above; however, this relationship is not new to MIN3P, and straightforward in terms of numerical implementation.

3.4   Field Scale Investigation of a Methanogenic Aquifer

The intent of this section is to investigate the role of gas bubble formation and water table fluctuations on aqueous chemistry and hydraulic properties in a methanogenic aquifer. Physical and chemical parameters used in the simulations have been based on observed data from the petroleum hydrocarbon spill site near Bemidji, MN. However, it must be emphasized that our intention is to focus on the processes related to bubble production and their effects on aquifer chemistry and hydrology. It is not our intent to simulate the complete geochemical evolution at the site, which is complex and beyond the scope of this work.

3.4.1   Bemidji Field Data

Dissolved CH_4, N_2 and Ar data collected from the Bemdji site in 2003 are shown in Figure 3-9 (Amos et al., 2005). The data were collected along a transect through the source zone, parallel to the groundwater flow direction. Dissolved gas data collected in 2002 are similar to those found in 2003 and are therefore not shown here (see Amos et al., 2005). N_2 and Ar data are shown as depletion which is given by 1-(dissolved gas partial pressure/average background dissolved gas partial pressure). Most notably, CH_4 concentrations peak near the centre of the source zone, corresponding to the highest measured N_2 and Ar depletions, then return to near zero approximately 130 m downgradient of the centre of the source zone, coinciding with a return to background levels of Ar and N_2 (i.e. zero depletion). The strong correlation of CH_4 concentrations to Ar and N_2 depletion suggest that the depletion in Ar and N_2 is due to degassing as a result of CH_4 production (Amos et al., 2005). Amos et al. (2005) reasoned that the zone of high CH_4 and depleted Ar and N_2 should have migrated 100's of meters downgradient given

that significant CH_4 concentrations were observed in the source zone in 1987, and

average groundwater velocity estimates range from ~18 m yr^{-1} in fine sand layers to 180

m yr^{-1} in coarser materials (Bennett et al., 1993). Furthermore, because Ar and N_2 are

non-reactive, attenuation of the depleted Ar and N_2 plumes must be due to physical

processes, that in turn must also be relevant for the attenuation of the CH_4 plume. The

purpose of the following modelling study is to quantitatively evaluate the role of gas

exsolution, water table fluctuations, gas exchange across the capillary fringe, and

permeability reduction due to entrapped gas bubbles as potential explanations for the

observed behaviour.
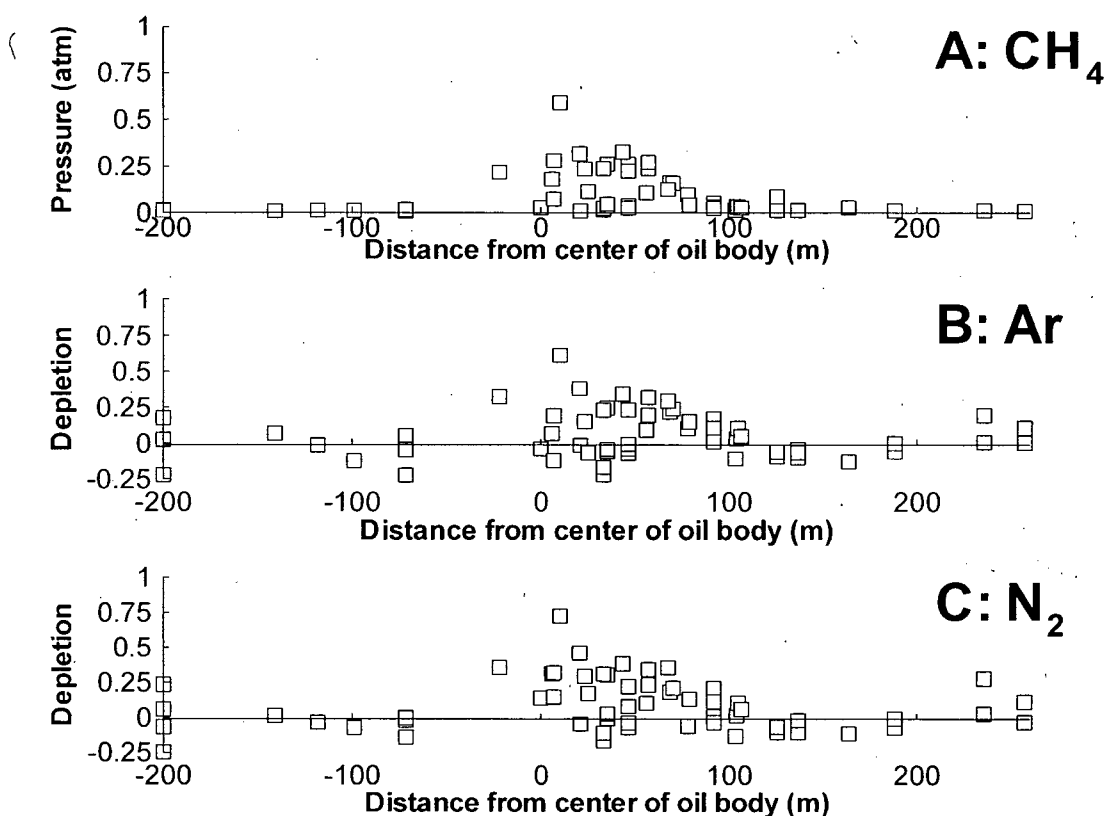
Figure 3-9. Methane concentration and Ar and N_2 depletion with distance along the north pool flow path at Bemidji in 2003. Depletion is defined as 1-(dissolved gas partial pressure/average background dissolved gas partial pressure).

87

3.4.2 Model Parameters

The model domain, shown in Figure 3-10, is 150 m long and 7 m deep, discretized into 1 m horizontal and 0.10 m vertical control volumes. The maximum time step used for the simulations was 0.05 years, limiting the Courant number to <1 in order to minimize numerical dispersion. Other physical parameters used in the simulations are shown in Table 3-2. The simulations include 7 primary components: HCO_3^-, N_2, Ar, CH_4, H^+, O_2 and benzene (C_6H_6); 3 secondary species: CO_3^{2-}, $H_2CO_3(aq)$, and OH^-; one NAPL phase to represent the free phase organic compounds; and 5 gases: CO_2, N_2, Ar, O_2 and CH_4. The source zone contains a NAPL phase with an initial mole fraction of 10% benzene. The dissolution of free phase benzene produces dissolved benzene with a rate of reaction given by

$$R_{C_6H_6-diss} = -k_{C_6H_6-diss}\left[X_{C_6H_6} K^S_{C_6H_6} - T^a_{C_6H_6}\right]$$ (26)

where $k_{C_6H_6-diss}$, the effective rate constant, equals 2×10^{-9} L H_2O L^{-1} bulk s^{-1}, $X_{C_6H_6}$ is the mole fraction of benzene in the organic mixture, and $K^S_{C_6H_6}$ equals 2.29×10^{-3} mol L^{-1} H_2O, is the solubility of pure benzene in water. The term in brackets ensures that the concentration of benzene does not exceed the solubility limit as dictated by Raoult's Law.
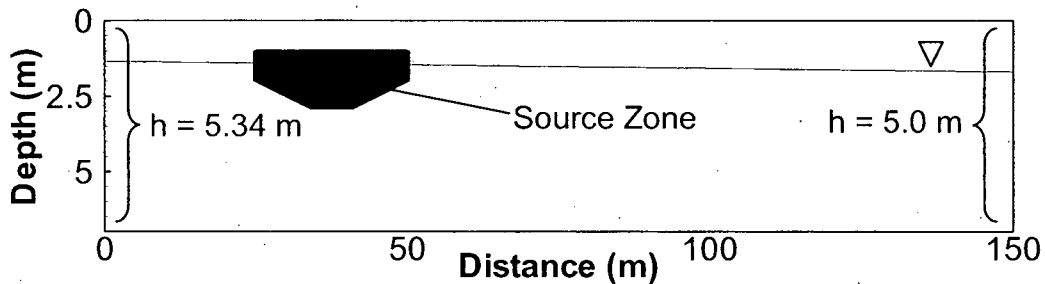
Figure 3-10. Schematic representation of MIN3P model domain for field scale simulations.

Table 3-2. Physical parameter for field scale simulations.

		Source
Hydraulic conductivity (m day^{-1})	8.64	Essaid et al., 1995
Porosity	0.38	Essaid et al., 1995
van Genuchten - alpha	3.5	Dillard et al., 1997
van Genuchten - n	4	Dillard et al., 1997
residual saturation	0.05	Estimated
longitudinal dispersivity (m)	0.1	Essaid et al., 1995
transverse dispersivity (m)	0.001	Essaid et al., 1995
atmospheric pressure (atm)	0.93	Calculated; Langmuir, 1997
diffusion coefficient - aqueous phase (m^2 s^{-1})	2.00×10^{-09}	CRC press, 2004
diffusion coefficient - gas phase (m^2 s^{-1})	1.00×10^{-05}	CRC press, 2004
Temperature (K)	282	Amos et al., 2005

Parameters were chosen to best represent conditions at the Bemidji site and were determined as shown.

Once dissolved, benzene will undergo methanogenesis according to the reaction:

$$C_6H_6 + 6.75H_2O \rightarrow 3.75CH_4 + 2.25HCO_3^- + 2.25H^+ , \qquad (27)$$
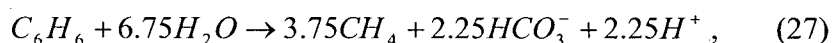
where the reaction is expressed in terms of the components used in the model, and the reaction rate is given by

$$R_{C_6H_6-CH_4} = -k_{C_6H_6-CH_4}\left[\frac{[C_6H_6]}{K_{C_6H_6} + [C_6H_6]} \right], \qquad (28)$$

where $K_{C_6H_6}$ is the half saturation constant. Note that benzene is used as a model organic compound to represent the complex mixture of organics observed at the field site. It is more likely that compounds undergoing methanogenesis are alkylbenzenes or short chain alkanes which are more readily degradable under anaerobic conditions (Eganhouse et al., 1993; 1996). The choice of benzene as a surrogate compound does not significantly affect the results of the simulations except that the ratio of CH_4 to HCO_3^- produced may be somewhat altered. For simplicity, the presence of NAPL is not considered to affect

Table 3-3. Initial conditions, boundary conditions and reaction parameters for field scale simulations.

	Saturated Zone Chemistry	Unsaturated Zone Chemistry	K_i^g (mol L^{-1} atm^{-1})
N_2	0.725	0.725	8.569×10^{-04}
Ar	0.00865	0.00865	1.894×10^{-03}
CH_4	0.00	0.00	1.990×10^{-03}
O_2	0.00	0.195	1.742×10^{-03}
HCO_3^-	1.365×10^{-02}	0.00	9.667×10^{-02}
pH	7	7	

	C_6H_6-CH_4	CH_4-O_2	C_6H_6-O_2
k - Simulation 1	1.4×10^{-6}	8.6×10^{-05}	
k - Simulation 2	6.9×10^{-6}	8.6×10^{-05}	
k - Simulation 3	2.6×10^{-5}	8.6×10^{-05}	8.6×10^{-05}
$K_{C_6H_6}$	1.00×10^{-3}		1.00×10^{-3}
K_{CH_4}		1.00×10^{-05}	
K_{O_2}		3.125×10^{-06}	3.125×10^{-06}
$^a K_{O_2}^I$	3.125×10^{-06}		

Saturated zone chemistry is used for initial conditions for saturated control volumes and for Dirichlet type boundary condition on left hand side of domain below 2.5 m depth. Unsaturated zone chemistry is used for initial conditions for unsaturated control volumes and for fixed concentration boundary for gaseous species at the top boundary for Simulation 3. Concentration of gaseous species are given in partial pressures (atm) except for bicarbonate which is given in total aqueous component concentrations (mol L^{-1}). Initial and boundary conditions from Bennett et al. (1993) and Amos et al. (2005). Henry's law constants from CRC Press (2004). Effective rate constants, k, given in mol L^{-1} bulk day^{-1}. Half saturation constants K, and inhibition constants K^I, in mol L^{-1}. a) Applies to simulation 3 only.

permeability in the simulations. The only other redox reaction included in the simulations

is the aerobic oxidation of CH_4 according to the reaction:

$$CH_4 + 2O_2 \rightarrow HCO_3^- + H^+ + H_2O, \qquad (29)$$
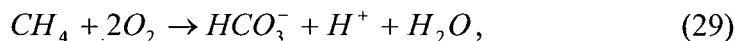
where the reaction rate is given by the expression:

$$R_{CH_4-O_2} = -k_{CH_4-O_2} \left[\frac{[CH_4]}{K_{CH_4} + [CH_4]} \right]\left[\frac{[O_2]}{K_{O_2} + [O_2]} \right]. \qquad (30)$$

Henry's law constants, effective rate constants, half saturation constants, initial

conditions, and boundary conditions for the various simulations are given in Table 3-3.

The results are shown after 15 years of simulation time to facilitate comparison to the field data (1988 – 2003).

3.4.3 Biogenic Bubble Formation

Gas bubbles will form in groundwater if the total pressure of the dissolved gases exceeds the threshold pressure, which we have considered here to be the hydrostatic pressure. In anaerobic systems the total gas pressure tends to be lower than the hydrostatic pressure, due to the removal of oxygen, so that in order for a bubble to form significant gas production must occur. The condition for bubble formation is that the net amount of gas produced in any particular volume of water, i.e. the total produced through reaction minus the amount of gas removed through reaction and mixing processes, must be sufficient to exceed the hydrostatic pressure. The formation of a bubble is therefore dependent on a number of factors including the rate of gas production, groundwater flow rate, the extent of the reaction zone, and the degree of mixing, which is dependent on the dispersion and diffusion coefficients. This is relatively intuitive but becomes somewhat more complicated when considering a dynamic system. As water travels through the source zone, dissolved organic contaminants will undergo methanogenesis, consuming the organic contaminants and producing CH_4. As the organics are consumed, dissolution is enhanced providing more substrate for the reaction. The amount of CH_4 added to a particular volume of water passing through the source zone is related to the groundwater flow rate and the rate of the gas producing reaction. Once the water has left the source zone, dissolved organic matter will continue to undergo methanogenesis but no more contaminant will dissolve into the water. This principle is demonstrated in the results of Simulation 1, which are shown in Figure 3-11. Methane concentrations increase through

the source zone (Figure 3-11A) and continue to increase while C_6H_6 concentrations remain high (Figure 3-11C). Note that the area of bubble formation, shown in Figure 3-11F, is displaced downgradient of the source zone. Here the effective rate constant, 1.4×10^{-6} mol L^{-1} H_2O day^{-1}, is relatively slow so that a gas phase does not form until the water has traveled through most of the horizontal thickness of the source zone and beyond.

Due to the insolubility of most dissolved gases, the formation of a gas phase can have a significant effect on the dissolved gas concentrations. Most notably, concentrations of non-reactive dissolved gases will decrease as they partition into the bubbles. This is shown in Figure 3-11B for N_2. This effect has been observed at many field sites as noted above (Reeburgh, 1969; 1972; Martens and Berner, 1977; Revesz et al., 1995; Blicher-Mathiesen et al., 1998; van Breukelen et al., 2003; Amos et al., 2005; Fortuin and Willemsen, 2005). Another important point is that the formation of gas bubbles does not necessarily decrease the concentration of the reactive gases downgradient. Previous researchers have hypothesized that an observed trend of decreasing CH_4 concentrations along the flow path downgradient of a source zone may be due to degassing (i.e. Revesz et al., 1995; van Breukelen et al., 2003); however, the simulations show that this is not the case if degassing is induced by the production of CH_4. Comparing Figures 3-11A and F, note that CH_4 concentrations reach a maximum where the gas phase is formed. As methanogenesis proceeds, CH_4 concentrations increase until the threshold pressure is reached. At this point additional gas produced will preferentially partition into the gas phase along with other dissolved gases. This will slow down the accumulation of dissolved CH_4 but will not cause dissolved CH_4 concentrations to decrease. In fact, as long as CH_4 is being produced, the dissolved CH_4 concentration
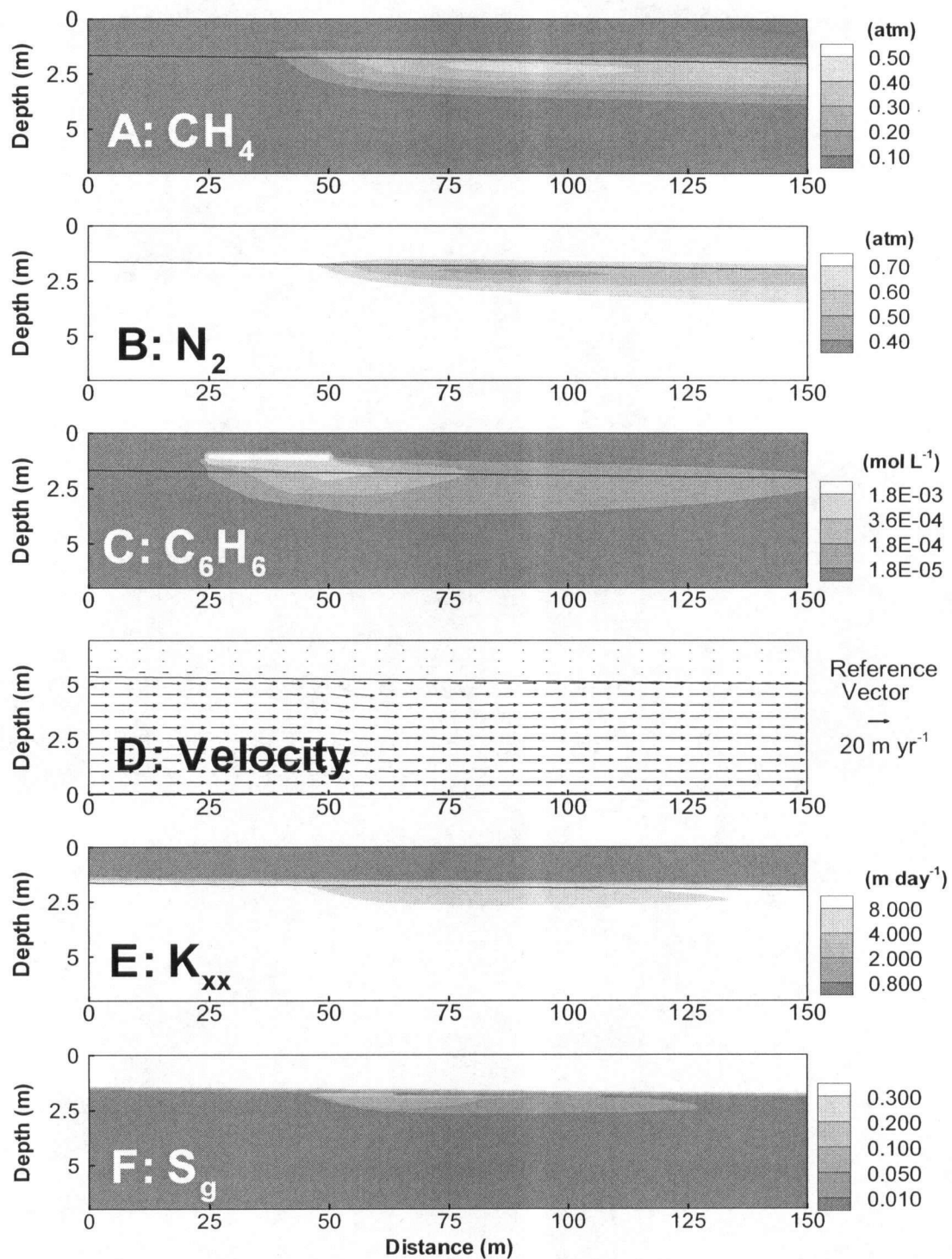
Figure 3-11. MIN3P results for Simulation 1 after 15 years simulation time. The water table is indicated by the solid line in each figure.

93

will tend to increase as other gases, particularly N_2, partition into the gas phase and reduce their contribution to the total gas pressure. It is possible for degassing to cause a decrease in CH_4 concentrations if degassing is induced by the production of other gases such as CO_2 (Van Breukelen et al., 2004). However, this is not the case in the present simulations. The small decrease in CH_4 along the flow path in the simulation is due to dispersive mixing. Although a gas phase forms, the resulting decrease in permeability (Figures 3-11E) does not have a significant effect on the flow through the aquifer in this simulation because the trapped gas phase saturation remains low. This is demonstrated by the nearly uniform flow field shown in Figure 3-11D.

The simulation results presented here show some similarity to the observed field data at Bemidji, namely the corresponding peaks in CH_4 concentrations and N_2 depletion, but fail to capture important aspects of the observed data. Most notably, the peak in simulated CH_4 concentration and N_2 depletion are not as high as those observed, and contrary to the field results, these peaks are displaced downgradient of the source zone. (Figure 3-9). Furthermore, elevated CH_4 concentrations and N_2 depletion persist much further into the downgradient area than observed. These discrepancies are an indication that the simulations do not capture important processes occurring in the field.

3.4.4   Permeability Changes

As noted above, the reduction in hydraulic conductivity due to the presence of gas bubbles is well documented, but it is also important to note that the resulting change in groundwater flow can have a significant impact on geochemistry as well. This effect is demonstrated by Simulation 2, shown in Figure 3-12, where the effective rate constant

94

for methanogenesis used, 6.9×10^{-6} mol L^{-1} H_2O day^{-1}, is 5 times higher than in Simulation 1 to emphasize the potential effects of permeability changes.

As is shown in Figure 3-12F, after 15 years simulation time an area of significant gas saturation has formed in the source zone, with the maximum saturation exceeding 30 %. Note that the highest saturations are just below the water table and sharply decrease in the capillary fringe. This is because our assumption in the model is that in the capillary fringe, part of the gas phase is connected, so that CH_4 formed is free to diffuse away. Gas bubbles will only form in the capillary fringe due to entrapment from water table fluctuations. This sharp gradient is not very realistic. In fact, it is likely that high levels of gas saturation near the water table will lead to ebullition. However, the process of ebullition is complex, not well understood, and difficult to quantify, and therefore was not included in the model.

In areas where a gas phase has formed below the water table, hydraulic conductivity has decreased to less than 25% of the initial value (Figure 3-12E), which has resulted in a deflection of the groundwater flow around the area where bubbles have formed (Figure 3-12D). The diversion of water flow around the source zone has a significant impact on the geochemistry, resulting in the highest observed CH_4 concentrations, and lowest observed N_2 concentrations, being restricted to the source zone area (Figures 3-11A and 3-11B). This can be attributed mostly to a significant reduction of water flow through the source zone such that release of CH_4 out of the source zone, and transport of N_2 into the source zone are limited. Although of lesser importance, dispersive mixing of contaminated water leaving the source zone with uncontaminated water, low in CH_4 and high in N_2, flowing around the source zone,
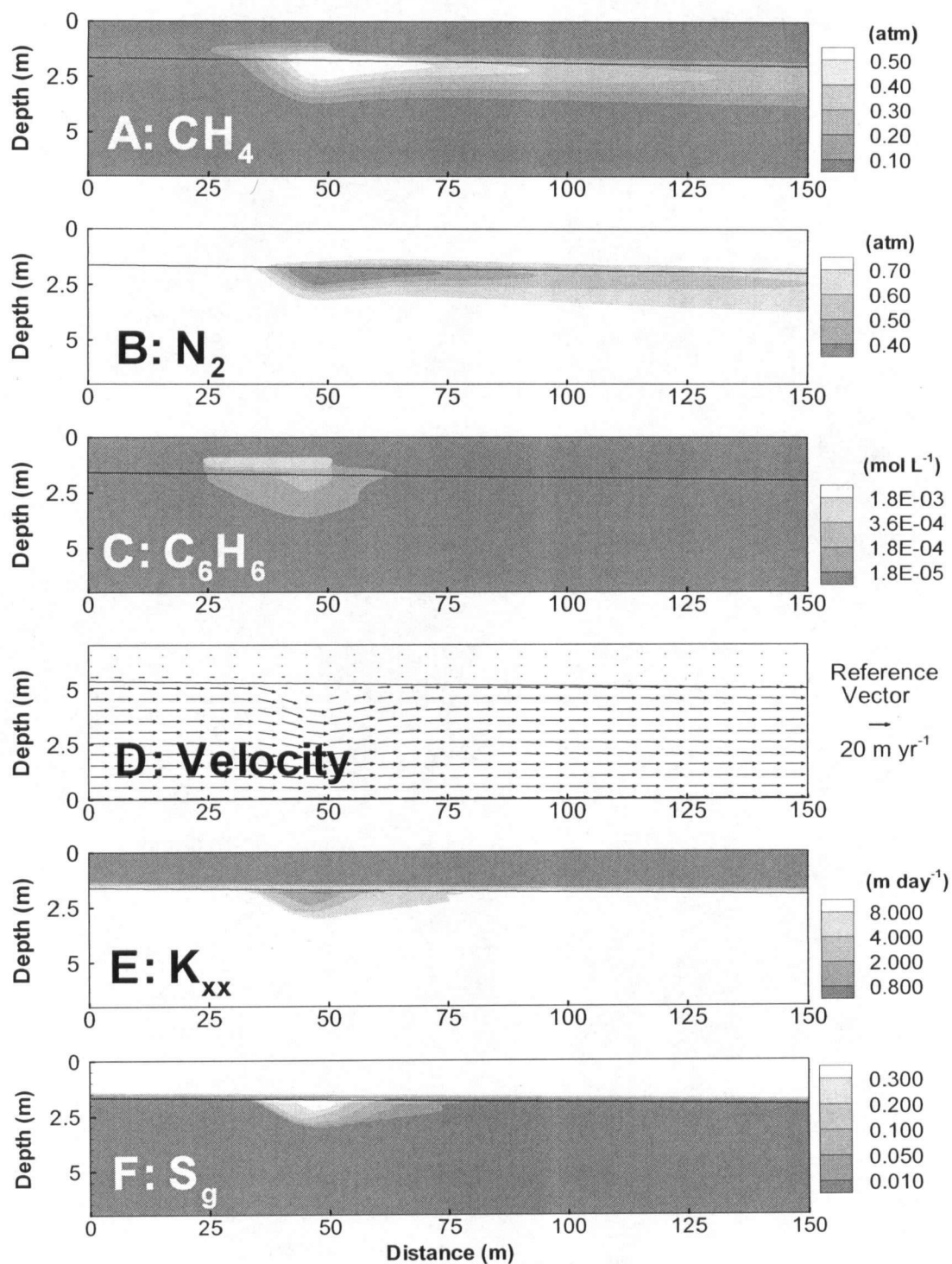
Figure 3-12. MIN3P results for Simulation 2 after 15 years simulation time. The water table is indicated by the solid line in each figure.

contributes to the dilution of the contaminated water. If permeability changes did not occur, the contaminated water, with high concentrations of CH_4 and low concentrations of N_2, would travel at the average linear groundwater velocity, which is ~ 20 m yr^{-1}, so that high CH_4 concentrations and low N_2 concentrations would be observed 100's of meters downgradient.

Shown in Figure 3-13 are CH_4, N_2 and Ar profiles through the model domain after 15 years, superimposed with field data collected in 2003 for comparison. Each line represents a horizontal transect through the model domain at 20 cm intervals. The data are aligned horizontally so that the downgradient edge of the oil body in the field (~ meter 30 in Figure 3-9) is aligned with the downgradient edge of the simulated oil body (meter 50 in Figure 3-10). The majority of the simulated transects will show only background concentrations and cluster around $y = 0$ (see also Figure 3-12); however, the transects near the water table, and through the source zone, show the highest deviations from zero and will be most representative of the observed data, which is generally collected within 2 m of the water table. In this simulation, concentrations of CH_4, and depletion of N_2 and Ar, peak in the source zone and decrease significantly with distance downgradient of the source, providing a more favourable comparison to the observed data than Simulation 1. The permeability decrease in the source zone and resulting deflection of groundwater flow tend to limit the release of contaminated water from the source zone and also somewhat enhance dispersive mixing with cleaner water from the upgradient region, and provide a potential explanation for the observed trend. However, the simulation also shows that these mechanism do not appear to fully account for the observed CH_4 attenuation and increase in Ar and N_2. A higher rate of methanogenesis

would increase the amount of gas produced, further decrease the relative permeability, and provide greater attenuation of the gas plumes. However, this would tend to produce unrealistically high CH_4 concentrations in the source zone.

Figure 3-13. CH_4, Ar and N_2 profiles through the model domain for Simulation 2 at 15 years (lines) and field data from 2003 (open squares). Each line represents a horizontal transect through the model domain at 20 cm intervals. The data are aligned horizontally so that the downgradient edge of the oil body in the field (~ meter 30 in figure 9) is aligned with the downgradient edge of the simulated oil body (meter 50 in figure 10). Depletion is defined as 1-(dissolved gas partial pressure/average background dissolved gas partial pressure).

The simulation also shows that attenuation of the depleted Ar and N_2 plumes appears to be greater than that of the CH_4 plume. This can only be related to mixing processes since CH_4 is not produced down gradient of the source zone (see Figure 3-12C, C_6H_6 is fully degraded with ~ 15m of the source zone), and degassing is occurring mainly

near the source zone. A process that may be reflected in the field data but not in the simulation is the aerobic oxidation of CH_4 as oxygenated background water dispersively mixes with the contaminated water downgradient of the source. This would tend to enhance the depletion of the CH_4 plume. Two additional simulations were run with O_2 concentration in the background water equal to 25 and 50 % of saturation (results not shown). Both simulations showed enhanced attenuation of the CH_4 plume, but CH_4 concentrations remained elevated, i.e. > 0.2 atm, throughout the model domain, again showing that a reduction in CH_4 release due to isolation of the source zone combined with dispersive mixing is not sufficient to account for the observed attenuation of the gas plumes.

3.4.5 Water Table Fluctuations

The experiments conducted by Williams and Oostrom (2000) show that fluctuations of the water table, and the resulting entrapment of gas bubbles, can lead to oxygenation of oxygen-depleted water. It can be envisioned that the same process causes the replenishment of other gases such as Ar and N_2 where these gases have been depleted. To investigate this process, Simulation 3 was run with a fluctuating water table, based on observed water table fluctuations at the Bemidji site to provide a realistic scenario. A comparison of simulated and observed hydraulic heads is shown in Figure 3-14 for a well upgradient of the source zone and a well ~50 m downgradient of the source zone. Although the simulated results are a simplification of the observed water table fluctuations, the main features of the overall trend in water levels are generally well represented. The water table was varied by increasing or decreasing the flow rate into the model domain as appropriate. The maximum trapped gas saturation was set to 10% of

porosity. This value is somewhat uncertain, but given the broad range of values quoted in the literature (Fayer and Hiller, 1986; Williams and Oostrom, 2000; Heilwell et al. 2004), appears to be a reasonable approximation. Results of simulations using a maximum trapped gas saturation of 5% of porosity (not shown) did not show significantly different results.
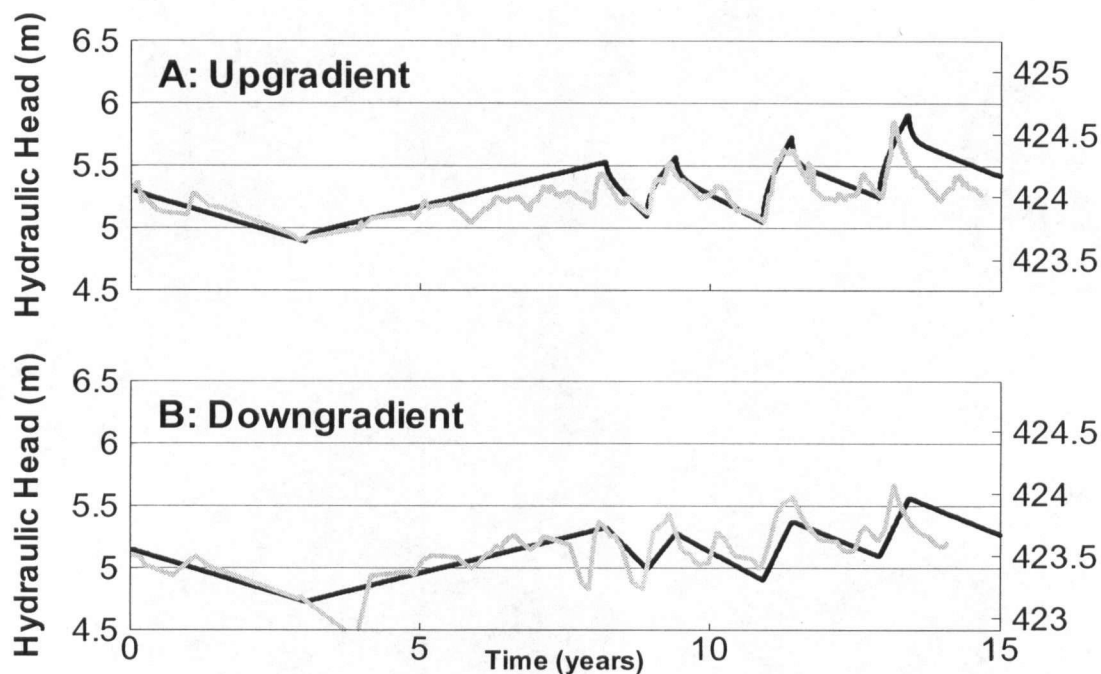
Figure 3-14. Water table fluctuations for Simulation 3 (black lines) compared to observed field data at Bemidji (grey lines). Hydraulic head is shown on the left axis for Simulation 3 and on the right axis for the field data. Time zero is assumed to be January 1, 1987. A: Upgradient of the source at x = 20 m for Simulation 3 and well 310, 200 m upgradient of the source for the field data. B: Downgradient of the source at x = 100 m for Simulation 3 and well 519, 50 m downgradient of the source for the field data.

Because a decrease in water levels may expose methanogenic sediments to atmospheric O_2, we have included aerobic oxidation of organic matter and inhibition of methanogenesis by O_2 in simulation 3. Aerobic oxidation of organic matter is described by the equation;

100

$$C_6H_6 + 7.5O_2 + 3H_2O \rightarrow 6HCO_3^- + 6H^+, \qquad (31)$$
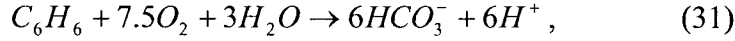
where the reaction rate is given by the expression;

$$R_{C_6H_6-O_2} = -k_{C_6H_6-O_2} \left[\frac{[C_6H_6]}{K_{C_6H_6} + [C_6H_6]} \right] \left[\frac{[O_2]}{K_{O_2} + [O_2]} \right]. \qquad (32)$$

The inhibition of methanogenesis by O_2 is represented by adding an inhibition term to the rate expression (Equation 28);

$$R_{C_6H_6-CH_4} = -k_{C_6H_6-CH_4} \left[\frac{[C_6H_6]}{K_{C_6H_6} + [C_6H_6]} \right] \left[\frac{K_{O_2}^I}{K_{O_2}^I + [O_2]} \right], \qquad (33)$$

where K^I is the inhibition constant. This conceptual model does not strictly represent the conditions at the Bemidji site since at the field site the unsaturated zone above the source is anaerobic. However, this conceptual model allows the quantification of CH_4 production and aerobic degradation in the groundwater.

The results of this simulation show that the interaction of the dissolved gas plume with entrapped bubbles can have a significant effect on the concentrations of the various gases (Figure 3-15). For the non-reactive gas N_2, the concentration returns to background levels approximately 50 m downgradient from the source, whereas without the water table fluctuations, the N_2 concentrations remain somewhat depleted throughout the model domain (compare Figures 3-12B and 3-15B). This enhanced replenishment of N_2 concentrations is caused by the dissolution of entrapped gas bubbles high in N_2. The attenuation of the CH_4 plume is also greatly enhanced in Simulation 3 (compare Figures 3-12A and 3-15A). This is in part due to physical processes, i.e. partitioning of CH_4 into entrapped gas bubbles, but is also due to aerobic oxidation of CH_4 as O_2 is introduced into the groundwater.
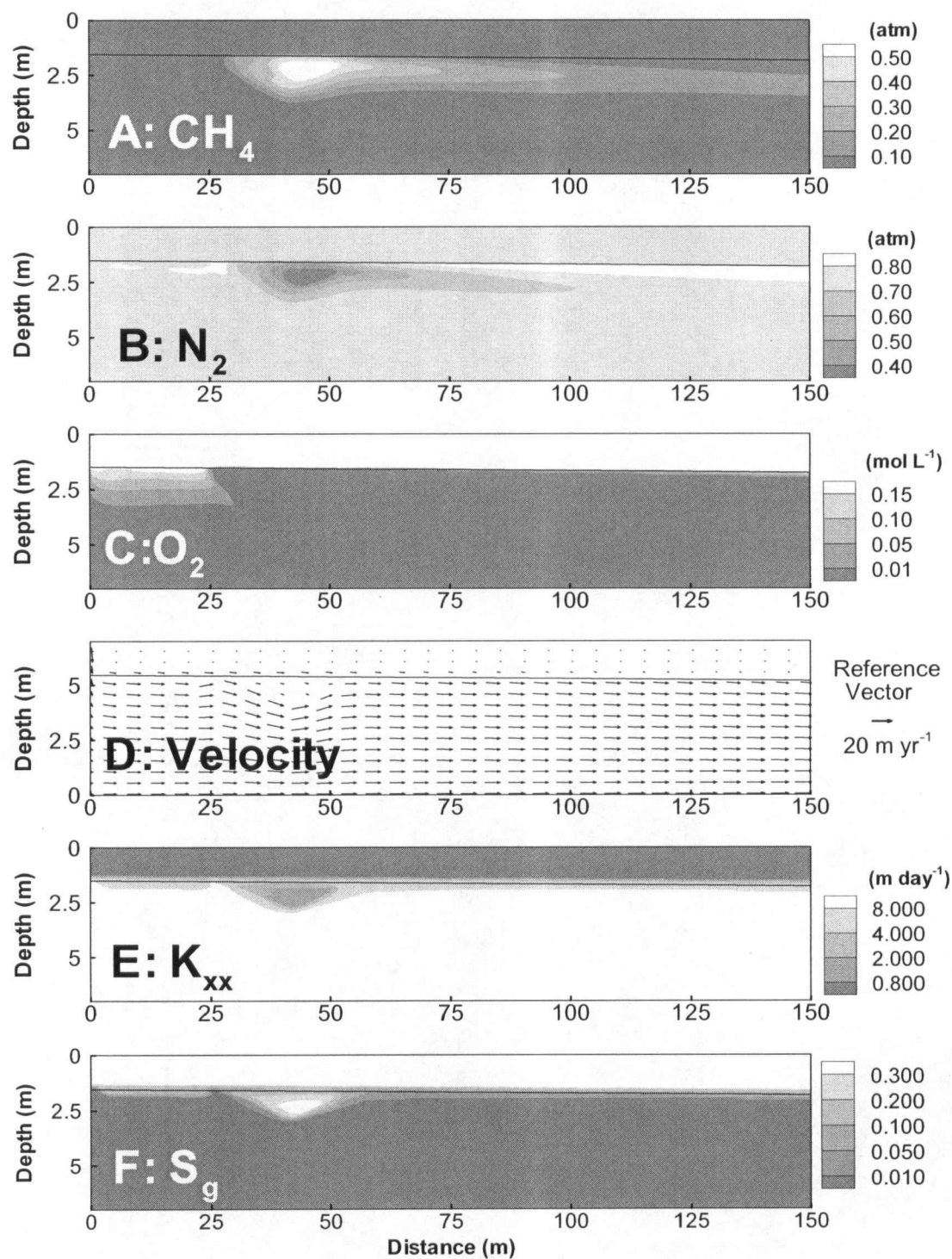
Figure 3-15. MIN3P results for Simulation 3 after 15 years simulation time. The water table is indicated by the solid line in each figure.

The effects of the water table fluctuations are not limited to the downgradient end of the plume. As shown in Figures 3-15B and C, N_2 and O_2 concentrations are enriched upgradient of the source zone, and although it is not immediately apparent in the figures, atmospheric gases are also introduced in the source zone area. As a result, in the source zone methanogenesis is periodically suppressed, CH_4 is consumed by aerobic degradation, and N_2 is replenished due to dissolution of gas bubbles of atmospheric composition. Therefore, in order to reproduce similar concentrations of CH_4 and N_2 in the source zone for Simulation 3, compared to Simulation 2, the rate of methanogenesis had to be increased by a factor of 3.75 to 2.6×10^{-5} mol L^{-1} H_2O day^{-1}.

Upgradient and downgradient of the source zone, N_2 concentrations are above atmospheric levels, i.e. partial pressures in excess of 0.73 atm. This cannot be due entirely to excess air since the bubbles always remain near the water table, and the excess pressure created is not enough to increase the partial pressure of the gases to the levels shown in the simulations. Instead, the increase in the partial pressure of N_2 is caused by the preferential removal of O_2 from the entrapped bubbles. Upgradient of the source the groundwater is depleted in O_2, so that O_2 in the bubbles will quickly dissolve into the water. As the O_2 partial pressure in the bubbles decreases, the partial pressures of the remaining gases must increase, coinciding with a decrease in bubble volume. This leads to an increase in the partial pressure of N_2 in the bubble, and therefore, also in the groundwater. Downgradient of the source, O_2 is removed more quickly due to aerobic oxidation of CH_4, but here the dissolved N_2 concentrations are also depleted, resulting in less enrichment of N_2 downgradient of the source zone compared to the upgradient region.
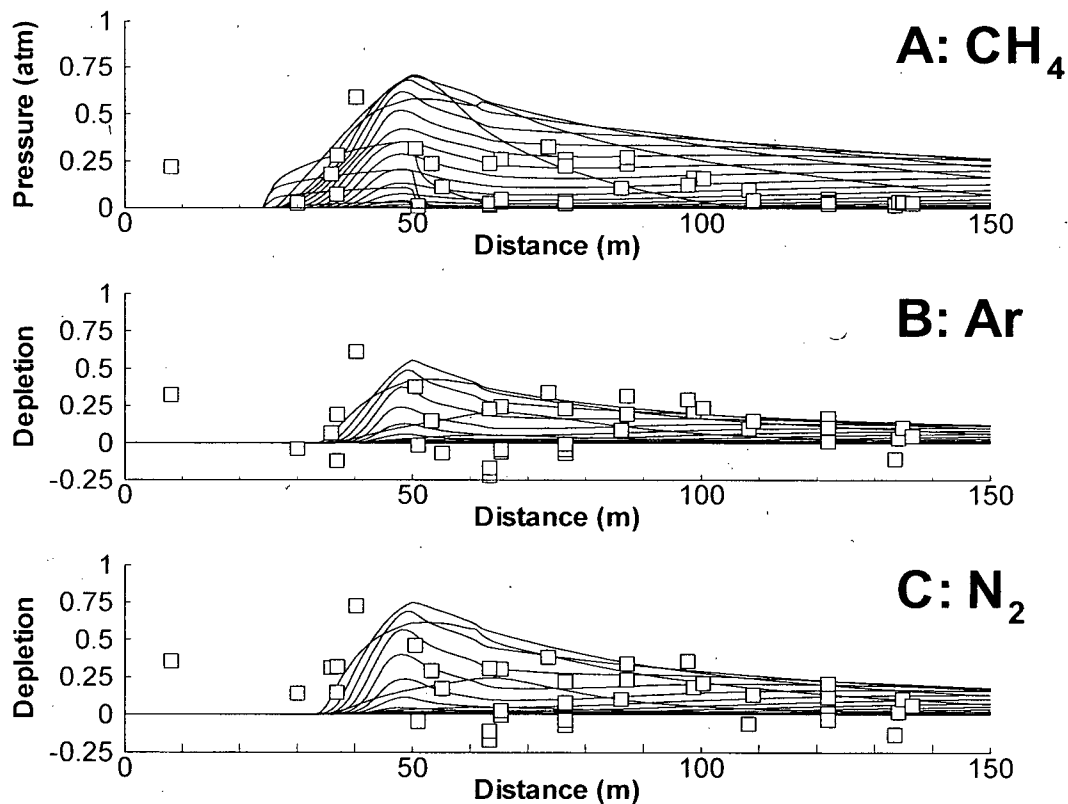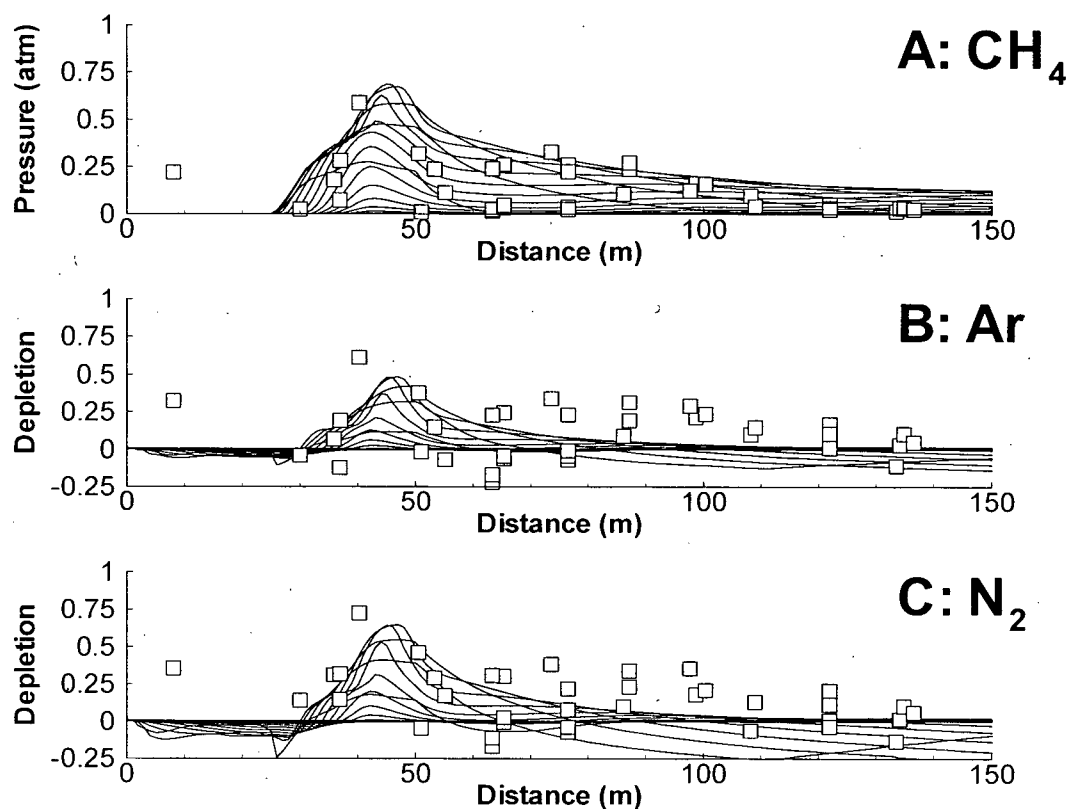
Figure 3-16. CH_4, Ar and N_2 profiles through the model domain for Simulation 3 at 15 years (lines) and field data from 2003 (open squares). Each line represents a horizontal transect through the model domain at 20 cm intervals. The data are aligned horizontally so that the downgradient edge of the oil body in the field (~ meter 30 in figure 3-9) is aligned with the downgradient edge of the simulated oil body (meter 50 in figure 3-10). Depletion is defined as 1-(dissolved gas partial pressure/average background dissolved gas partial pressure).

Simulated CH_4, N_2 and Ar spatial profiles after 15 years compared to the field data are shown in Figure 3-16. In general the simulations reproduce the attenuation of the CH_4 plume well, but exaggerate the attenuation of the Ar and N_2 depleted plume. There are several simplifications used in the model that would affect the simulation results. These include anoxic background water in saturated zone, atmospheric gas concentrations above the source zone, a simplified geometry of the NAPL distribution, no consideration of the permeability effects of NAPL saturation, and a simplified

104

representation of water table fluctuations. Each of these simplifications will affect the distribution of the gas plumes in varying and inter-related manners. However, given the magnitude of the observed water table fluctuations at Bemidji, over 0.5 m on a seasonal basis and over 1 m overall, the entrapment of bubbles is very likely, and the simulations indicate that the potential for attenuation of CH_4 and Ar and N_2 replenishment is significant.

3.4.6 Implications

Gas bubble formation is a well documented phenomenon where CH_4 production is significant. Therefore, the mass of CH_4 released to the gas phase must be accounted for if rates of methanogenesis are to be determined accurately. In Simulation 2 the total amount of CH_4 produced after 15 years of simulation time was 260 moles, while the amount lost to the gas phase was 122 moles, so that if the gas phase was not considered, the rate of methanogenesis would be underestimated by almost 50 %. Similarly, the entrapment of bubbles near the water table is a well documented occurrence and can introduce O_2 into the aquifer near the water table. For simulation 3, the total amount of CH_4 produced after 15 years of simulation was 171 moles, while the amount lost to the gas phase was 40 moles and the amount consumed by aerobic oxidation was 83 moles, so that the amount remaining in the aqueous phase was only 49 moles. In this case, if only the aqueous phase CH_4 concentrations were considered, the rate and extent of methanogenesis would be underestimated by more than 70%. Both of these examples demonstrate the importance of considering gas bubbles when assessing geochemical and hydrological processes in a methanogenic aquifer. Furthermore, the simulations highlight

the effectiveness of N_2 and Ar as tracers to quantify gas bubble formation and gas transport mechanisms, allowing the rates of methanogenesis to be better constrained.

The processes described in the model have a significant impact on the evolution of the dissolved gas plume which is due to partitioning of gases between the aqueous and gas phases, introduction of oxygen and reaction with CH_4, hydraulic isolation of the source zone, and enhanced mixing at the leading edge of the plume as a result of permeability restrictions in the source zone. These processes can potentially also affect other dissolved constituents and may be important when assessing natural attenuation degradation pathways in an aquifer. Introduction of oxygen near the water table can enhance degradation of other contaminants in the groundwater plume. Hydraulic isolation of the source will potentially limit inflow of oxidants or nutrients to the source, limiting degradation, but may also reduce the release of contaminants from the source, thus decreasing contaminant loading to the downgradient plume. Furthermore, as contaminated water from the source zone dispersively mixes with less contaminated water which has flowed around the source zone the potential exists for enhanced degradation of the downgradient plume as electron acceptors or nutrients are brought in contact with the contaminants. Each of these processes needs to be considered to fully assess the natural attenuation capacity of an aquifer.

3.5   Summary and Conclusions

The reactive transport code MIN3P was enhanced to include formulations describing the formation of gas bubbles below the water table due to biogenic gas production or entrapment during water table fluctuations. The formulations account for equilibrium partitioning of multiple gases between the aqueous and gas phases, and also

106

include permeability changes as a function of gas phase saturation. The resulting model allows for a comprehensive accounting of gaseous species in complex biogeochemical and hydrological environments.

Simulations were run that demonstrate various processes related to gas bubble and gas transport in a methanogenic aquifer. Simulation 1 demonstrated the relationship between biogenic gas bubble formation and source zone dynamics, and showed that CH_4 concentrations continue to rise while degassing occurs. The simulation reproduced the depletion of the non-reactive gases N_2 and Ar where gas bubbles form, as has been reported previously. Simulation 2 showed that permeability decreases due to biogenic gas bubble formation in the source zone may significantly reduce water flow through the source zone, and may enhance the relative contribution of dispersive mixing downgradient from the source. These effects combine to enhance attenuation of the CH_4 plume and replenish dissolved N_2 and Ar downgradient from the source. Simulation 3 investigated the interaction of the dissolved gas plume with bubbles entrapped near the water table. The simulations suggest that entrapment of bubbles of atmospheric composition may significantly contribute to the attenuation of the gas plume through aerobic oxidation of CH_4, partitioning of CH_4 into existing bubbles, and replenishment of N_2 and Ar previously lost to degassing. Comparison of the simulations with field data from a petroleum contaminated site near Bemidji, MN suggests that hydraulic isolation of the source zone and interaction with entrapped bubbles are likely important processes at the site.

The results of this study have important implications to other sites where biogenic gas formation or water table fluctuations occur. In particular, the simulations showed that

degassing and bubble entrapment may significantly contribute to natural attenuation in shallow unconfined aquifers. In addition, by not accounting for bubble-related processes, the rate and extent of biogeochemical processes may be significantly underestimated.

3.6 Acknowledgements

3.7 References

Amos, R.T., Mayer, K.U., Bekins, B.A., Delin, G.N., Williams, R.L. (2005), Use of dissolved and vapor-phase gases to investigate methanogenic degradation of petroleum hydrocarbon contamination in the subsurface, *Water Resour. Res.*, *41*, W02001, doi:10.1029/2004WR003433.

Baedecker, M.J., Cozzarelli, I.M., Eganhouse, R.P., Siegel, D.I., Bennett, P.C. (1993), Crude oil in a shallow sand and gravel aquifer - III. Biogeochemical reactions and mass balance modeling in anoxic groundwater, *Appl. Geochem.*, *8*, 569-586.

Beckwith, C.W., Baird, A.J. (2001), Effect of biogenic gas bubbles on water flow through poorly decomposed blanket peat, *Water Res. Res.*, *37*, 551-558.

Bennett, P.C., Siegel, D.E., Baedecker, M.J., Hult, M.F. (1993), Crude oil in a shallow sand and gravel aquifer – I. Hydrogeology and inorganic geochemistry, *Appl. Geochem.*, *8*, 529-549.

Blicher-Mathiesen, G., McCarty, G.W., Nielsen, L.P. (1998), Denitrification and degassing in groundwater estimated from dissolved dinitrogen and argon, *J. Hydrol.*, *208*, 16-24.

Chanton, J.P., Martens, C.S. (1988), Seasonal variations in ebullitive flux and carbon isotopic composition of methane in a tidal freshwater esturary, *Global Biochem. Cy.*, *2*, 289-298.

Cirpka, O.A., Kitanidis, P.K. (2001), Transport of volatile compounds in porous media in the presence of a trapped gas phase, *J. Contam. Hydrol.*, *49*, 263-285.

CRC Press (2004), *CRC Handbook of Chemistry and PhysicsI*, 84th ed., Boca Raton, Fla.

Dillard, L. A., Essaid, H. I., Herkelrath, W. N., 1997. Multiphase flow modeling of a crude-oil spill site with a bimodal permeability distribution. Water Resour. Res. 33, 1617-1632.

Eganhouse, R.P., Baedecker, M.J., Cozzarelli, I.M., Aiken, G.R., Thorn, K.A. (1993), Crude oil in a shallow sand and gravel aquifer - II. Organic geochemistry, *Appl. Geochem.*, *8*, 551-567.

Eganhouse, R.P., Dorsey, T.F., Phinney, C.S., Westcott, A.M. (1996), Processes affecting the fate of monoaromatic hydrocarbons in an aquifer contaminated by crude oil, *Environ. Sci. Technol.*, *30*, 3304-3312.

Essaid, H.I., Bekins, B.A., Godsy, E.M., Warren, E., Baedecker, M.J., Cozzarelli, I.M. (1995), Simulation of aerobic and anaerobic biodegradation processes at a crude oil spill site, *Water Resour. Res.*, *31*, 3309-3327.

Fayer, M.J., Hiller, D. (1986), Air encapsulation: I. Measurement in a field soil, *Soil Sci. Soc. Am. J., 50*, 668-572.

Fechner-Levy, E.J., Hemond, H.F. (1996), Trapped methane volume and potential effects on methane ebullition in a northern peatland, *Limnol. Oceanogr., 41*, 1375-1383.

Fortuin, N.P.M., Willemsem, A. (2005), Exsolution of nitrogen and argon by methanogenesis in Dutch ground water, *J. Hydrol., 301*, 1-13.

Fry., V.A., Selker, J.S., Gorelick, S.M. (1997), Experimental investigations for trapping oxygen gas in saturated porous media for in situ bioremediation, *Water Resour. Res., 33*, 2687-2696.

Heilweil, V.M., Solomon, D.K., Perkins, K.S., Ellett, K.M. (2004), Gas-partitioning tracer test to quantify trapped gas during recharge, *Ground Water, 42*, 589-600.

Kaluarachchi, J.J., Parker, J.C. (1992), Multiple flow with a simplified model of oil entrapment, *Transp. Porous Media, 7*, 1-14.

Langmuir, D. (1997), *Aqueous Environmental* Geochemistry, Prentice-Hall, Upper Saddle River, New Jersey.

Lenhard, R.J., Oostrom, M., White, M.D. (1995), Modeling fluid flow and transport in variably saturated porous media with the STOMP simulator. 2. Verification and validation exercises, *Adv. Water Resour., 18*, 365-373.

Li, X., Yortsos, Y.C. (1995), Theory of multiple bubble growth in porous media by solute diffusion, *Chem. Eng. Sci., 50*, 1247-1271.

Martens, C.S., Berner, R.A. (1977), Interstitial water chemistry of anoxic Long Island Sound sediments. 1. Dissolved gases, *Limnol. Oceanogr., 22*, 10-25.

Mayer, K.U., Frind, E.O., Blowes, D.W. (2002), A numerical model for the investigation of reactive transport in variably saturated media using a generalized formulation for kinetically controlled reactions, *Water Resour. Res.*, *38*, 1174-1194.

Millington, R.J. (1959), Gas diffusion in porous media, *Science*, *130*, 100-102.

Oostrom, M., Hofstee, C., Dane, J.H. (1997), Light nonaqueous-phase liquid movement in a variably saturated sand, *Soil Sci. Soc. Am. J.*, *61*, 1547-1554.

Parker, J.C., Lenhard, R.J. (1987), A model for hysteretic constitutive relations governing multiphase flow 1. Saturation-pressure relations, *Water Resour. Res.*, *23*, 2187-2196.

Reeburgh, W.S. (1969), Observation of gases in Chesapeake Bay sediments, *Limnol. Oceanogr.*, *14*, 368-375

Reeburgh, W.S. (1972), Processes affecting gas distribution in estuarine sediments. Memoir - Geological Society of America, no.133, Environmental framework of coastal plain estuaries, p.383-389.

Revesz, K., Coplen, T.B., Baedecker, M.J., Glynn, P., Hult, M. (1995), Methane production and consumption monitored by stable H and C isotope ratios at a crude oil spill site, Bemidji, Minnesota, *Appl. Geochem.*, *10*, 505-516.

Reynolds, W.D., Brown, D.A., Mathur, S.P., Overend, R.P. (1992), Effect of in-situ gas accumulation on the hydraulic conductivity of peat, *Soil Sci.*, *153*, 397-408.

Rosenberry, D.O., Glaser, P.H., Siegel, D.I., Weeks, E.P. (2003), Use of hydraulic head to estimate volumetric gas content and ebullition flux in a northern peatlands, *Water Resour. Res.*, *39*, 1066, doi:10.1029/2002WR001377.

Ryan, M.C, MacQuarrie, K.T.B., Harman, J., Mclellan, J. (2000), Field and modeling evidence for a "stagnant flow" zone in the upper meter of sandy pheatic aquifers, *J. Hydrol.*, *233*, 223-240.

van Breukelen, B.M., Roling, W.F.M., Groen, J., Griffioen, J., van Verseveld, H.W. (2003), Biogeochemistry and isotope geochemistry of a landfill leachate plume, *J. Contam. Hydrol.*, *65*, 245-268.

van Breukelen, B.M., Griffioen J. (2004), Biogeochemical processes at the fringe of a landfill leachate pollution plume: potential for dissolved organic carbon, $Fe(II)$, $Mn(II)$, $NH4$, and $CH4$ oxidation, *J. Contam. Hydrol.*, *73*, 181-205.

Williams, M.D., Oostrom, M. (2000), Oxygenation of anoxic water in a fluctuating water table system: an experimental and numerical study, *J. Hydrol.*, *230*, 70-85.

Wösten, J.H.M., van Genuchten, M.T. (1988), Using texture and other soil properties to predict the unsaturated soil hydraulic functions, *Soil Sci. Soc. Am. J.*, *52*, 1762-1770.

4 Reactive Transport Modeling of Coupled Saturated and Unsaturated Zone Processes Affecting Natural Attenuation of Petroleum Hydrocarbons

4.1   Introduction

When spilled on land or in the subsurface, light non-aqueous phase liquids (LNAPLs) are retained in the unsaturated zone at residual saturation and can form a pool on the water table if the quantity is large. As a result, both saturated and unsaturated zone processes can contribute to the natural attenuation of these contaminants. In the unsaturated zone, contaminants may volatilize into the vapour phase or biodegrade. In the saturated zone, dissolution and biodegradation are the dominant processes. Furthermore, infiltration of recharge water through the contaminated unsaturated zone and entrapment of gas bubbles near the water table link the hydrogeochemical evolution in the saturated and unsaturated zones. Few studies have investigated the interactions between processes in these two zones.

This study focuses on a contaminated site near Bemidji, MN where a large crude oil spill occurred in 1979. Several previous studies have simulated the geochemical evolution at the site in either the saturated (Essaid et al., 1995; 2003; Curtis et al., 1999) or the unsaturated zones (Chaplin et al., 2002). These studies have provided important insights into natural attenuation processes; however, given the availability of data from both zones, an integrated modeling effort may provide additional insights.

One limitation of previous models is that static boundary conditions were assumed at the water table. For example, Essaid et al. (1995) accounted for spatial variation in dissolved oxygen and nutrient concentrations, assuming anoxic recharge water with elevated nutrient concentrations above the floating oil, and oxygenated water with limited nutrient supply elsewhere, but did not consider temporal variations in dissolved concentrations at the water table boundary. Furthermore, their analysis did not

consider the transfer of other important redox-related species, such as CH_4 or CO_2, across the water table. These simplifications may be unrealistic at the Bemidji site, because hydrogeochemical conditions in both the saturated and unsaturated zones have, and continue to, evolve over time.

In the unsaturated zone, Chaplin et al. (2002) simulated 1-D vertical fluxes of O_2, CH_4 and CO_2 to obtain estimates of aerobic and anaerobic degradation rates at specific times. Their study, based on steady state simulations of 1985 and 1997 vapour phase data, showed that the dominant processes evolved from volatilization to methanogenic degradation over this time period; however, the mechanism of the transition was not investigated. Furthermore, the study by Chaplin et al. (2002) assumed that the hydrocarbon source is only near the water table and does not account for contaminants suspended above the water table at residual saturation.

Previous studies at the Bemidji site have indicated that biogenic CH_4 production has led to the production of gas bubbles below the water table (Revesz et al., 1995, Amos et al., 2005), and that these bubbles can provide a significant sink for CH_4, possibly resulting in reduced hydraulic conductivity in the zone of bubble formation (Amos et al., 2005; Amos and Mayer, 2006a). Furthermore, the entrapment of gas bubbles near the water table may enhance gas transport into the saturated zone, providing additional O_2 for aerobic degradation of CH_4 or organic contaminants (Amos and Mayer, 2006a). Modeling of a hypothetical scenario suggests that gas bubble entrapment may have significant impact on natural attenuation at the Bemidji site (Amos and Mayer, 2006a).

In the current study, we present a 2-D model that simultaneously considers the saturated and unsaturated zones. Water table fluctuations are simulated dynamically, as is

mass transfer of geochemical species across the water table. The processes of gas bubble formation and entrapment below the water table, including permeability effects of the trapped bubbles, is also considered. Furthermore, this study explicitly simulates the geochemical evolution of degradation processes in the unsaturated zone including aerobic degradation, Mn and Fe reduction, and methanogenesis, and includes the distribution of hydrocarbons based on field observations (Dillard et al., 1997). The objective of the study is to integrate available saturated and unsaturated zone data into a single model to; 1) gain insights into the relevant geochemical processes affecting natural attenuation with a focus on interactions between the saturated and unsaturated zones, 2) estimate the mass of hydrocarbons that have degraded from the source zone, accounting for both saturated and unsaturated zone processes, to provide an estimate of source longevity, 3) evaluate the effectiveness of this coupled modeling approach in comparison to previous more simplified modeling efforts.

4.2   Site Description

In 1979, near Bemidji, MN, an underground crude oil pipeline burst spilling approximately 1.7 million litres of oil. A portion of the spilled oil was sprayed under high pressure over the land surface hydraulically upgradient of the pipeline. This area is referred to as the spray zone (Figure 4-1) and contains oil contamination in the unsaturated zone but no free phase oil on the water table. Near the pipeline two large bodies of oil accumulated where sufficient oil percolated through the unsaturated zone. These are referred to as the south pool and north pool, with the north pool being the subject of this study and originally consisting of ~80,000 to 160,000 L of oil (Bennett et al., 1993). The oil bodies are perched on the water table of a surficial glacial outwash

aquifer 6-9 m below land surface. The saturated and unsaturated zones consist of moderately to poorly sorted sandy gravel, gravely sand, and sand with thin interbeds of fine sand and silt, and are moderately calcareous (Franzi, 1988). Groundwater velocities have been estimated from 0.05 md^{-1} in the silty layers to 0.5 md^{-1} in coarser material.
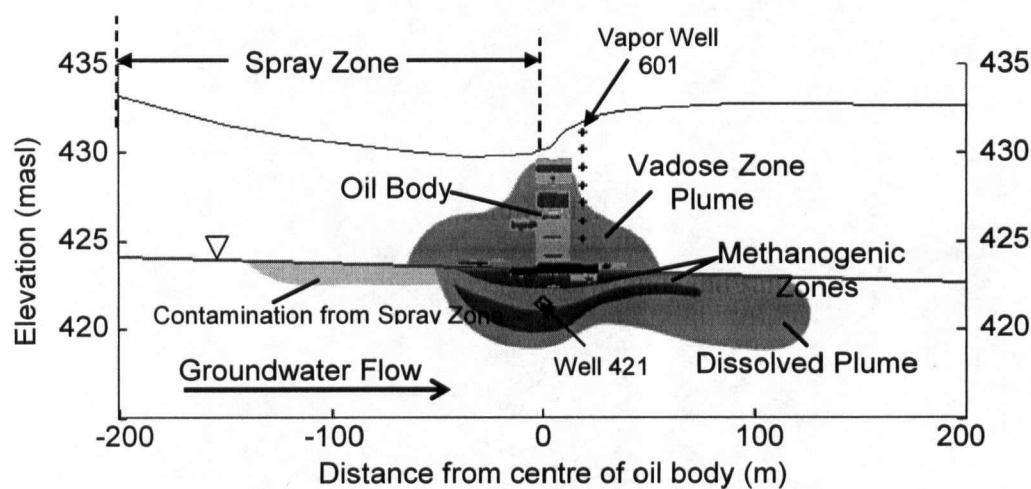
Figure 4-1.Cross section of contaminated aquifer showing major geochemical zones. Vadose zone plume based on 1 atm CH$_4$ contour in 2003 (Amos et al., 2005), dissolved plume based on 0.05 mg L^{-1} BTEX contour in 1995 (Cozzarelli et al., 2001), methenogenic zones based on populations of methanogens sampled in cores collected from 1994-1197 (Bekins et al., 1999), contamination from spray zone inferred from 1987 geochemical data (Bennett et al., 1993) and oil saturation contours interpolated from data collected from core samples collected in 1990 (Dillard et al., 1997). Oil saturation contours, from lightest to darkest, are 0.1, 0.2 and 0.3.

Figure 4-1 shows a cross section of the contaminated aquifer parallel to the groundwater flow direction and defines the major geochemical zones that have developed as a result of the contamination. The vadose zone plume has evolved over time; in 1985 the vapour phase plume was characterized by high concentrations of hydrocarbons, due to a high rate of volatilization, and aerobic respiration was the dominant biodegradation process. By 1997 the vapour phase is characterized by low levels of O$_2$, and high levels

117

of CO_2 and methane near the oil, while gas concentrations transition to near atmospheric levels with increasing distance from the oil body. Volatilization decreased significantly, and >50 % of biodegradation was attributed to methanogenesis (Hult and Grabbe, 1988; Chaplin et al., 2002).

In the saturated zone background water is uncontaminated and oxygenated (Figure 4-1). The region underlying the spray zone is characterized by reduced oxygen concentrations, increased levels of dissolved organic and inorganic carbon, and a decrease in pH of ~0.5 to 1 compared to background water. The contaminant plume is the area which has been most heavily affected by the dissolution of the free phase oil from the source zone. This area has undergone a progression of biodegradation reactions including aerobic, manganese reduction, iron reduction, and methanogenesis. The plume is anoxic and contains increased levels of hydrocarbons, Mn^{2+}, Fe^{2+} and CH_4 (Bennett et al., 1993; Delin et al., 1998). The methanogenic zone within the contaminant plume is the area of highest concentrations of methane and methanogenic bacteria, although iron reduction is also an important biodegradation pathway within this zone (Bekins et al., 1999; 2001).

4.3   Relevant Studies at Bemidji

4.3.1   Degradation Estimates

Several previous studies of the Bemidji site have endeavoured to estimate hydrocarbon degradation rates and source longevity in the saturated or unsaturated zones. Revesz et al. (1995) estimated an upward carbon flux to the land surface at vapor well 601, which is located above the floating oil, (see Figure 4-1) of 0.28 mol m^{-2} d^{-1}, and a horizontal flux in the saturated zone beneath the oil at well 421 (see Figure 4-1) of 0.24

mol m^{-2} d^{-1}. Given an estimated carbon reservoir of 20 x 10^3 mol per meter squared of horizontal surface area they estimated source longevity to be a minimum of 110 years. These estimates were based on 1990 data and inherently include volatilization and aerobic/anaerobic degradation, but do not include spatial or temporal variation in degradation rates.

Essaid et al. (2003) used inverse modeling to estimate BTEX dissolution and degradation rates and determine mass removal from the oil body. Using measured oil saturation data and effective solubilities they determined that 18 years after the spill 10.2% of benzene, 8.6% of toluene, 1.2% of ethylbenzene, 1.4% of m,p-xylene and 2.7% of o-xylene had been removed from the oil body. They estimated that 77% of the benzene would remain in the oil body after 50 years. These simulations are limited to saturated zone processes.

In the unsaturated zone, Chaplin et al. (2002) modeled total hydrocarbon, CH_4, O_2, and CO_2 distributions to estimate volatilization and biodegradation rates. They estimated the total hydrocarbon mass loss to be 10.52 kg day^{-1} in 1985, 97% by volatilization and 3% by aerobic degradation. This is approximately equivalent to 1% yr^{-1} of the original hydrocarbon mass. By 1997 volatilization had decreased significantly so that the total hydrocarbon mass loss was estimated to be 1.99 kg day^{-1}, 48% by volatilization, 29% by aerobic degradation and 23% by methanogenesis. This is equivalent to approximately 0.2% yr^{-1} of the original oil mass.

Landon (1993) used physical and chemical properties of oil samples collected from the north pool in 1989 to estimate that 2.5% of the oil by volume had been degraded in the 10 years since the time of the spill. However, most of the hydrocarbon removal was

of volatile hydrocarbons so that the rate of removal would be expected to slow down considerably as volatilization becomes a less important process.

It is difficult to directly compare these estimates given that the conceptual models used are generally limited in spatial or temporal scale, or do not take into account all relevant processes.

4.3.2 Calibration Data

At the Bemidji site an abundance of geochemical and hydrogeological data has been collected. To facilitate calibration of the model discussed here we have chosen data sets that provide good spatial coverage and have attempted to calibrate each geochemical parameter at two or more times spanning the site history where the data is available. The data sets used for calibration are listed in Table 4-1.

To provide current pH and cation data, particularly Mn, Fe and Ca, samples were collected from lysimeters in the unsaturated zone in 2002, 2003 and 2004 and from groundwater wells in 2004. Samples were analyzed immediately in the field for pH. Cation samples were filtered through 0.22 μm syringe filters and preserved with nitric acid. The samples were analyzed with ICP/MS at the University of British Columbia.

4.4 Numerical Model

An enhanced version of the reactive transport code MIN3P (Mayer et al., 2002) is used in this study (Amos and Mayer, 2006a). This code includes gas bubble growth and contraction below the water table in response to changes in dissolved gas pressure, gas bubble entrapment and release due to water table fluctuations, and relative permeability changes due to bubble accumulation within a generalized geochemical framework

involving kinetically controlled redox and mineral dissolution/precipitation reactions along with equilibrium hydrolysis and aqueous complexation reactions. The reader is referred to Mayer et al. (2002) and Amos and Mayer (2006a) for detailed descriptions of the model formulation.

Table 4-1. Unsaturated and saturated zone data sets used for model calibration.

| | Unsaturated Zone | | | | |
	1985 Hult and Grabbe, 1988	1991 Revesz et al., 1995	1997 Chaplin et al., 2002	2003 Amos et al, 2005	2004 This Study
CH_4	✓	✓	✓	✓	
CO_2	✓	✓	✓	✓	
O_2	✓		✓	✓	
N_2				✓	
pH					✓
Ca					✓
Alkalinity					✓
Total HC	✓		✓		

| | Saturated Zone | | | | | |
	1986 Cozzarelli, unpublished	1987 Bennett et al., 1993	1990 Revesz et al., 1995	1995 Cozzarelli et al, 2001	2003 Amos et al, 2005	2004 This Study
CH_4	✓		✓		✓	
CO_2	✓				✓	
O_2	✓			✓	✓	
N_2	✓				✓	
pH		✓				✓
Ca		✓				✓
Alkalinity		✓				✓
BTEX (Essaid et al, 2003)	✓		✓	✓		

Total HC refers to total hydrocarbons.

4.5 Conceptual Model

4.5.1 Physical System

At the Bemidji site the water table is located approximately 6-9 meters below land surface with a gradient of ~0.003 (Bennett el al., 1993). Above the north pool oil body, the ground surface elevation increases steeply from ~ 430 masl on the upgradient end to ~ 432.5 masl on the downgradient end. Due to the finite volume formulation used in MIN3P this feature cannot be reproduced in the simulations. Therefore, it was assumed that the ground surface elevation was constant at 430 masl.

Hydraulic conductivity has been determined at the site by several researchers and varies over several orders of magnitude (Bilir, 1992; Dillard et al., 1997). Bilir (1992) conducted permeameter tests on intact cores from throughout the site and measured hydraulic conductivities in the range of 5×10^{-8} to 2.8×10^{-4} m s^{-1} with the majority of the samples, 78 out of 87, ranging between 10^{-6} and 10^{-4} m s^{-1}. This study estimated anisotropy ratios (horizontal hydraulic conductivity/vertical hydraulic conductivity) to range between 0.8 and 76, with a mean of 15 and a median of 2. The author suggests that the lower vertical hydraulic conductivity is due to sporadically placed thin silt layers. Grain size analysis on the same cores yielded calculated hydraulic conductivities of 1.4×10^{-5} to 1.4×10^{-3} m s^{-1} with anisotropy ratios of 0.4 to 6.9. However, the author argues that the thin silt layers are under-represented using this method, yielding higher hydraulic conductivities and lower anisotropy. Dillard et al. (1997) estimated hydraulic conductivity from grain size analysis on 6 cores along a 90 m transect parallel to the groundwater flow direction through the north pool oil body. Their results showed

hydraulic conductivities ranging from 1.6×10^{-7} to 8.1×10^{-4} m s^{-1} with a mean of 5.0×10^{-5} m s^{-1}.

The groundwater flow at Bemidji is primarily horizontal so that flow would occur through the coarse grained material and the fine grained silt layers would have limited effect on the ground water velocity. Therefore, for the simulation conducted here we have chosen a horizontal hydraulic conductivity, K_x, of 1×10^{-4} m s^{-1}, which is at the higher end of the experimentally determined range. This value yields a linear groundwater velocity of ~25 m yr^{-1}, which is consistent with other reactive transport models conducted of the site (Essaid et al., 1995; Essaid et al., 2003) and a bromide tracer test conducted 57 m downgradient of the center of the oil body (Essaid et al., 2003). For the vertical hydraulic conductivity, K_z, we have assumed a value of 1×10^{-5} m s^{-1} giving an anisotropy ratio of 10.

The cores collected by Dillard et al. (1997) were also used to determine soil hydraulic function parameters. Mean values of the van Genuchten parameters α and n were 3.53 and 3.98 respectively with ranges of 0.77 to 9.34 for α and 1.77 to 11.88 for n. Porosity values ranged from 0.26 to 0.54 with a mean of 0.38. Residual saturation is estimated to be 0.05. Preliminary simulations using the mean values for α and n yielded water saturations in the unsaturated zone that were much lower than observed, suggesting that finer grained material, and possibly fine grained lenses, control unsaturated zone flow. Therefore values of α and n where set to 1.5 and 2.0 respectively yielding water saturations between ~25 and 50%, which is more consistent with observed values (Dillard et al., 1997).

Recharge rates of 0.2 to 0.3 m yr^{-1} have been measured at the site using soil-moisture measurements, and between 0.1 and 0.2 m yr^{-1} using water level changes observed in hydrographs (Herkelrath and Delin, 2001). Furthermore, soil moisture profiles show that recharge is concentrated in the spring months due to snowmelt, and peaks at several times during the summer months, presumably due to storm events. Recharge is limited in the winter months. Essaid et al. (2003) estimated average annual recharge at 0.178 m yr^{-1} using inverse modeling. These variations in recharge also create large variations in soil moisture content, ranging from < 0.1 to > 0.4. Recharge rates will affect contaminant transport in a variety of ways. In the unsaturated zone, increases in soil moisture content will slow the diffusion of gases including O_2 and CH_4 through the soil and therefore affect reaction rates. The rate of recharge will also control the transport of solutes and gases from the unsaturated zone to the saturated zone. This may have important implications on the progress of redox reactions in the contaminated groundwater. For the simulations, monthly recharge was estimated by scaling the recorded monthly precipitation by the ratio of average annual precipitation to the average annual recharge rate estimated by Essaid et al. (2003), which is 0.28. Furthermore, it is assumed that all precipitation in the winter months (December to February) resulted in recharge in the month of March.

Dillard et al. (1997) determined oil saturations on 269 samples from 6 cores through the oil body. The oil saturation contours obtained from interpolation of the data are shown in Figure 4-1.

The presence of oil and soil gas restricts the movement of water so that the relative permeability for water, k_{ra}, is reduced according to the function (Wösten and van Genuchten, 1988):

$$k_{ra} = S_{ea}{}^{l}\left(1 - \left[1 - S_{ea}{}^{1/m}\right]^{m}\right)^{2}, \qquad (1)$$

where l and m are soil hydraulic function parameters and S_{ea} is the effective aqueous saturation given by;

$$S_{ea} = \frac{S_a - S_{ra}}{1 - S_{ra}}, \qquad (2)$$

where S_{ra} is the residual saturation and S_a is the aqueous phase saturation given by;

$$S_a = 1 - S_o - S_g, \qquad (3)$$

where S_o and S_g are the oil saturation and gas phase saturation respectively. In the simulation presented here, it is assumed that relative permeabilities due to oil saturation are constant. This is not unreasonable since the oil saturation does not change significantly throughout the simulations as a result of the large non-degradable fraction, as will be discussed below. As such, the initial effective horizontal hydraulic conductivities were calculated based on the equation:

$$K_{x,eff} = K_x k_{ra}, \qquad (4)$$

where k_{ra} is determined using equations 1 to 3 with $S_g=0$. Initial vertical hydraulic conductivities were calculated in an analogous manner. Subsequently, throughout the simulation relative permeabilities are calculated assuming $S_o = 0$, and K_x equal to the initially calculated $K_{x,eff}$.

In the saturated zone the production of CH_4 and CO_2 due to methanogenic degradation of the oil may result in the formation of gas bubbles. The nucleation and

growth of gas bubbles is considered to occur when the total dissolved gas pressure

exceeds the sum of the hydrodynamic and capillary pressures (Li and Yortsos,1995). For

simplicity we neglect capillary forces such that a gaseous phase will form under the

condition:

$$\sum P_l > P_H \qquad P_H > 0, \qquad (5)$$

where P_l (atm) is the partial pressure of gas l, and P_H (atm) is the hydrodynamic pressure

equal to the sum of the atmospheric pressure and water pressure. This simplification is

reasonable for the sand and gravel aquifer at Bemidji where observed total gas pressures

are not significantly above hydrodynamic pressures (Amos et al., 2005). Under

equilibrium conditions the condition;

$$\sum_{l=1}^{N_g} P_l - P_H = 0 \qquad if \ S_{gt} > 0, \qquad (6)$$

must apply where gas bubbles are represented by the saturation of the trapped gas phase,

S_{gt}, N_g is the number of gases, and P_l is given by;

$$P_{l(k)} = \frac{T_k^T}{\left(1 - S_{gt}\right)\Psi_k + \dfrac{S_{gt}}{RT}}. \qquad (7)$$

where Ψ_k is an equilibrium term allowing gas pressures to be related to component and

species concentrations in the multicomponent framework of MIN3P, R (0.08206 L atm

mol^{-1} K^{-1}) is the ideal gas constant, T(K) is temperature, and T_k^T (mol L^{-1} porosity) is the

total component concentration of component k given by

$$T_k^T = S_a T_j^a + S_{gt} T_j^g, \qquad j = k, \qquad (8)$$

where T_j^a [mol L^{-1} H$_2$O] and T_j^g [mol L^{-1} gas] are the total component concentrations in

the aqueous and gas phases, respectively, and the subscript j refers to the entire pool of

126

components while the subscript k refers to a specific set of components, each associated with a specific gas. A solution for S_{gt} can be obtained by minimizing equation 6 with P_l given by equation 7 (Amos and Mayer, 2006a).

Records of water table levels at the Bemidji site are shown in Figure 4-2A and B for wells upgradient and downgradient of the source zone, respectively. The records show water table fluctuations up to 0.5 m on a seasonal basis and 1 m overall. A fluctuating water table may also have an effect on the transport of dissolved gases in an aquifer. Where gas bubbles are trapped below the water table, a decrease in water table elevation may release gases to the unsaturated zone. Conversely, a rising water table can trap gas bubbles, potentially supplying a significant amount of gases such as O_2 to the saturated zone (Williams and Oostrom, 2000; Amos and Mayer, 2006a). In the simulations conducted here, gas bubble entrapment and release due to water table fluctuations is considered using the formulation of Amos and Mayer (2006a), which includes the parameter S_{gt}^{max}, defining the maximum effective trapped gas saturation. S_{gt}^{max} was estimated at 10 %, which is an intermediate value of measured trapped gas saturations found in the literature (Fayer and Hiller, 1986; Williams and Oostrom, 2000; Heilwell et al. 2004). Once gas bubbles are entrapped, the bubble can dissolve or grow according to the equilibrium expression described by equations 6 and 7.

Previous research has shown that the presence of gas bubbles below the water table can affect the hydraulic conductivity of the aquifer (Ryan et al., 2000; Heilweil et al., 2004). Fry et al. (1997) showed that the relationship described in equation 1, 2 and 3, where;

$$S_g = S_{gt} + S_{gc}, \qquad (9)$$

and S_{gc} is the connected gas phase saturation, is valid in quasi-saturated sands (i.e. where a trapped gas phase exists) ranging from fine to coarse grained, with gas saturations ranging from ~ 10 to 60%.
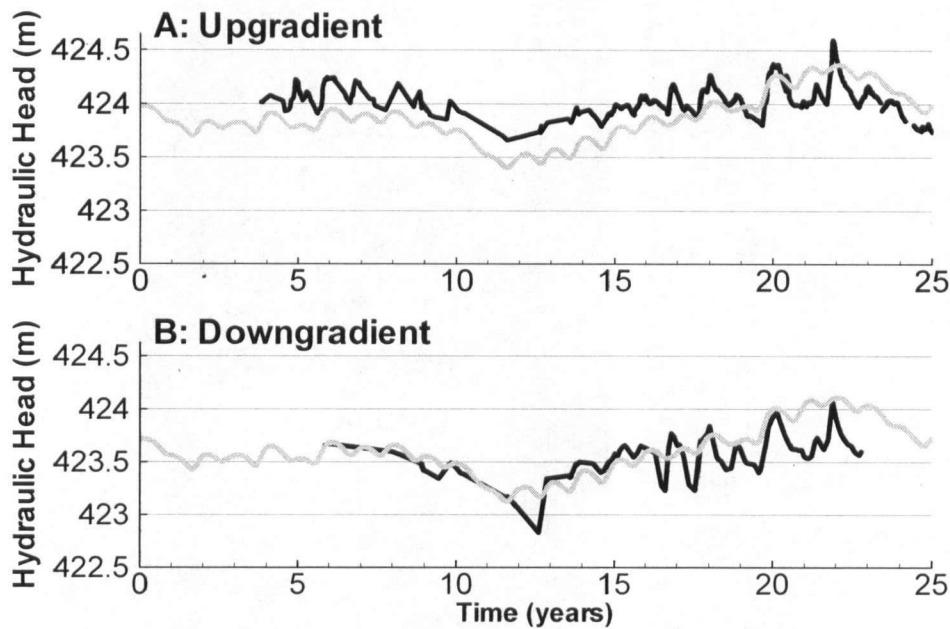
Figure 4-2.Observed (back lines) and simulated (grey lines) water levels for A) well 301, 200 m upgradient from the centre of the source zone, and simulations at x = -50, and B) Well 519, 56 m downgradient from the centre of the source zone and simulations at x = 50 m. Time zero is taken to be July, 1979.

In the unsaturated zone, gas transport can potentially be through diffusion or advection. Amos et al. (2005) showed that at Bemidji, the production of CH_4 and CO_2 by methanogenesis and the consumption of CH_4 and O_2 through methanotrophy create pressure gradients that drive advective gas flux. While advective gas fluxes, in general, appear to be much lower than diffusive fluxes (Amos et al., 2005), gas advection is an important process for controlling the partial pressures of individual gases and the total gas pressure in the system. This is illustrated by the vertical transect at well 601 (Figure

128

4-3). Near the water table, CH_4 and CO_2 are produced through methanogenesis so that

both of these gases diffuse upward past the lowest sampling point of well cluster 601.

Part way up the transect, CH_4 and O_2 come in contact, creating a zone of methanotrophic

activity and resulting in a consumption of both gases. Although CO_2 will be produced by

this reaction the net result is a consumption of gases and a reduction in total gas pressure.

This reduction in gas pressure drives an inward advective gas flux resulting in an

enrichment of N_2 in the methanotrophic zone. Note that the N_2-enrichment makes up for

the depletion in other gases so that the total gas pressure remains near 1 atm.
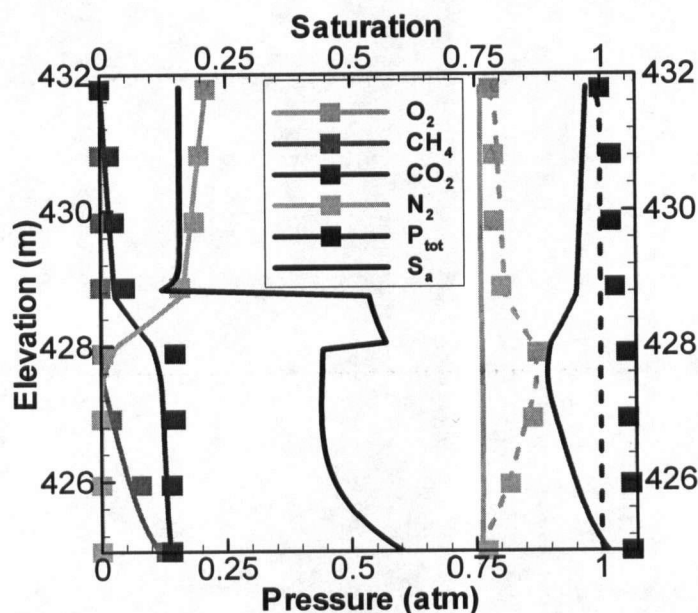
Figure 4-3. Observed partial pressures of major gases at well 601 (symbols), and simulated partial pressures of gas species (solid lines) and simulated aqueous saturation (S_w) for diffusion-only simulation. Dashed lines for N_2 and total pressure (P_{tot}) show results using the N_2 approximation described by equation 10 in the text.

The current version of MIN3P simulates transport of gases in the unsaturated zone

by diffusion only and is not capable of simulating advective transport. This results in an

inaccurate representation of N_2 partial pressures and total gas pressure in the unsaturated zone. To demonstrate this point we simulated gas transport by diffusion only along the 1-D vertical transect represented by well 601. The model domain used in these simulations is shown in Figure 4-4. At the top boundary, gas partial pressures are set to atmospheric concentrations, while at the bottom boundary gas pressures are set equal to those observed at the bottom sampling point of well 601. Gases are allowed to diffuse inward with the only reaction being the aerobic oxidation of CH_4. The aqueous saturation profile (Figure 4-3) was calibrated using the soil hydraulic properties shown in Figure 4-4 to match the simulated diffusion profiles to the observed data. As can be seen in Figure 4-3, the reactive gases can be reasonably simulated using a diffusion-only conceptual model. However, because N_2 is non-reactive the concentration is uniform along the simulated transect and the N_2 partial pressure is drastically under-predicted by the model, and as a result, so is the total gas pressure.

The inaccurate representation of N_2 and total gas pressure creates problems with the quality of the simulation results, as shown above, but also can create technical problems with the model if total simulated gas pressures deviate too far from 1 atm. To resolve this problem, we have adopted the assumption that in the unsaturated zone;

$$P_{N_2} = P_A - P_T' \qquad (10)$$

where P_{N_2} is the partial pressure of N_2, P_A is atmospheric pressure and P_T' is the total pressure of all gases other than N_2. The effect of using this approximation is demonstrated in Figure 4-3. For the reactive gases, the concentrations remain the same as with the diffusion-only conceptual model, but for N_2 the partial pressure is much closer to the observed, and the total pressure remains near atmospheric. This assumption provides

130

realistic N_2 concentrations because in a system affected by advective gas fluxes, and

assuming near steady state conditions, the advective and diffusive fluxes of non-reactive

gases will tend to reach an equilibrium, being equal in magnitude but opposite in

direction, so that the net N_2 flux is zero, but the size of the advective and diffusive

gradients is driven by the total pressure of the other gases in the system (Thorstenson and

Pollock, 1989). In the field total gas pressures in the unsaturated zone are not expected to

deviate far from atmospheric, so that the assumption used here provides a more realistic

representation of the gas pressure in the system.
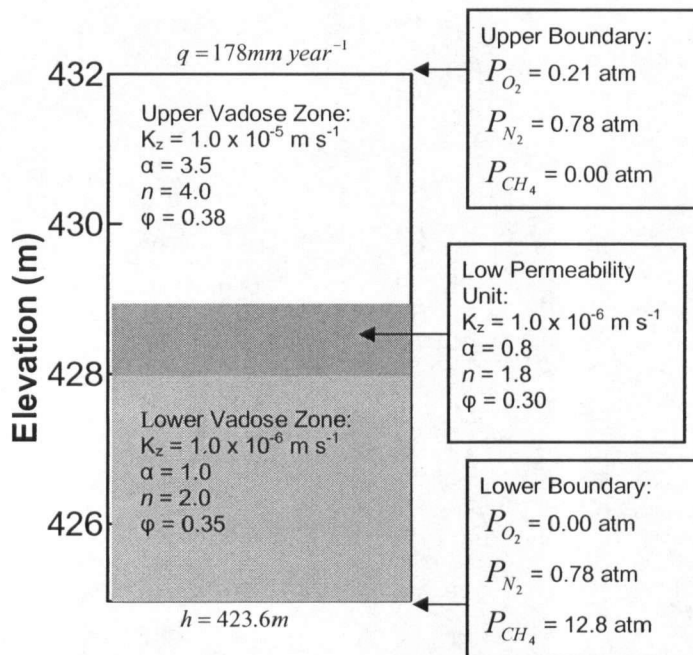
Figure 4-4. Model domain for 1-D gas transport simulations of vapour well 601. Initial conditions for reactive transport are the same as for upper boundary. Hydraulic properties are within the range of measured values but are calibrated to obtain an appropriate saturation profile which is in turn needed to simulate the observed reactive gas profiles. The diffusion coefficient used for all gases in the simulation is 1.0×10^{-5} m^2 s^{-1}.

4.5.2 Reaction Network

The contaminant at the Bemidji site is crude oil, which is a complex mixture of hydrocarbons too numerous to simulate as individual compounds. Furthermore, the CPU requirements of the model make it advantageous to limit the number of organic components to as few as possible. Research at the site has shown that the most prominent components dissolved in the groundwater are by far BTEX compounds with lesser amounts of low-molecular-weight alkanes (C4-7). For example, in 1987 the dissolved benzene concentration in well 522 (at the leading edge of the oil body) was 9.9 mg L^{-1}, alkylbenzene concentrations totalled ~2.1 mg L^{-1} and alkane concentrations totalled ~ 1.7 mg L^{-1} (Eganhouse et al., 1993). Given these observations, it is apparent that the geochemistry of the groundwater plume at Bemidji will be predominantly controlled by the BTEX compounds and to a lesser extent by low-molecular-weight alkanes.

Cozzarelli et al. (1990) demonstrated the differences in persistence of the various BTEX compounds in the anoxic groundwater at Bemidji. Toluene and o-xylene tend to degrade quickly, with concentrations decreasing to below detection limits less than 40 m from the centre of the oil body. Benzene and ethylbenzene concentrations decrease by only 20 and 35 % respectively, relative to 1,2,3,4-tetramethylbenzene, in the core of the anoxic portion of the plume, but decrease significantly 60-80 m from the centre of the oil body. Cozzarelli et al. (2001) showed that the extent of benzene and ethylbenzene migration corresponds to the zone of Fe(III) oxide depletion in the aquifer sediment, suggesting that Fe(III) reduction is an important degradation pathway controlling the transport of these compounds.

132

In the unsaturated zone volatilization of light alkane (i.e. C3-5) is an important process. In 1985, Hult and Grabbe (1988) measured volatile hydrocarbon concentration greater than 1000 g m^{-3} directly above the floating oil. However by 1997 maximum total hydrocarbon concentrations decreased to ~50 g m^{-3} (Chaplin et al., 2002).

Given these observations, the oil is represented by four compounds in the simulations. The component 'toluene' is used to represent readily degradable alklylbenzenes such as toluene and xylenes, 'benzene' is used to represent compounds that are somewhat less degradable such as benzene and ethylbenzene, and 'butane' is used to represent volatile alkanes. These compounds represent a good compromise between a realistic representation of the oil and maintaining manageable simulation times. The remainder of the oil is represented by a non-degradable, non-volatile, insoluble residual.

In the simulations dissolution of component j from the organic mixture is controlled by the following kinetic expression;

$$R^o_{diss,j} = k^o_{diss,j} \left(1 - \frac{\gamma^c_j C^c_j}{K^o_{diss,j} X^o_j} \right) \tag{11}$$

where k^o_{diss} (mol L^{-1} day^{-1}) are the dissolution rate constants, γ^C, C^C (mol L^{-1}) are the activity coefficients and aqueous concentrations for the organic components, respectively, K^o_{diss} (mol L^{-1}) are the solubilities, and X^o_j is the mole fraction of component j in the organic mixture. The expression in brackets ensures that the dissolved concentration of the organic compound does not exceed the solubility limit as dictated by Raoult's Law. The mole fraction of 'benzene' and 'toluene' used in the simulations are determined from equilibration experiments conducted by Eganhouse et al. (1996) on oil

from well 534 at the leading edge of the oil body, which is considered to be the least degraded oil at the time of the sampling in 1987. Measured equilibrium benzene and ethylbenzene concentrations are summed by weight and an equivalent 'benzene' mole fraction is determined by Raoult's law using the solubility of benzene. Similarly, toluene and xylene concentrations are summed to determine an equivalent mole fraction of 'toluene'. Initial mole fractions of 'benzene' and 'toluene' in the organic mixture were determined to be 0.007 and 0.015, respectively.

The initial volume fraction of volatile components in the oil is not well established. Therefore, to determine the initial 'butane' mole fraction, we assumed that at equilibrium the vapor phase concentration was 1000 g m^{-3}, equivalent to the maximum observed hydrocarbon concentrations in the unsaturated zone at the site (Hult and Grabbe, 1988). This yields a 'butane' mole fraction of 0.3 in the organic mixture. This value appears high; however, assuming that the predominant hydrocarbons measured in the unsaturated zone were C2-C5 alkanes (Hult and Grabbe, 1988), the mole fraction of these compounds in the oil could possibly have ranged from 0.09, if the majority of the C2-C5 mixture was propane, to 0.48, if the majority of the mixture was pentane. Laboratory-aging experiments showed that 15% of the oil from Bemidji well samples evaporated within 24 hours, mainly due to the loss of C3-C5 hydrocarbon (Hult and Grabbe, 1988). This value falls in the range of calculated mole fractions for C3-C5 hydrocarbons.

Vapor phase concentrations are determined in MIN3P by;

$$C_l^g = \frac{P_l}{RT}, \qquad\qquad (12)$$

134

$$P_l = \left(K_l^g\right)^{-1} \prod_{j=1}^{N_C} \left(C_j^C \gamma_j^C\right)^{v_{lj}^g}, \qquad (13)$$

where P_l (atm) and K_l^g (mol atm^{-1}) are the partial pressure and Henry's Law constant for gas species l respectively, v_{lj}^g is the stoichiometric coefficient relating component j to gas l, R is the gas constant [0.08206 L atm mol^{-1} K^{-1}] and T [K] is the temperature. Note that this formulation, in contrast to the dissolution of organic compounds into water, implies that the partitioning of components between the aqueous and gas phase is at equilibrium.

The degradation of organic compounds, including hydrocarbons, generally follows a series of microbially mediated terminal electron accepting processes (TEAPs) based on the availability of electron acceptors. This sequence starts with the most energetically favorable reaction, reduction by O_2, followed by progressively less energetically favorable reactions involving NO_3^-, Mn(IV), Fe(III), SO_4^{2-}, and ending with methanogenesis. At the Bemidji site average background NO_3^- and SO_4^{2-} concentrations are generally low, 0.02 and 0.003 mM respectively, so that these components are unimportant electron acceptors in this system (Bennett et al., 1993, Baedecker et al., 1993). However, Mn(IV) and Fe(III) reduction, and methanogenesis have proven to be important. Baedecker et al. (1993) showed that at the downgradient end of the oil body between 1984 and 1988, Fe(III) reduction and methanogenesis were becoming significantly more important processes while the zone of Mn(IV) reduction was moving further downgradient. Subsequently, Fe(III) reduction and methanogenesis have proven to be important degradation processes in the saturated zone (Revesz et al., 1995; Bekins et al., 1999; Cozzarelli et al., 2001; Bekins et al., 2001; Amos et al., 2005). Aerobic oxidation of the oil will also be important in the saturated zone but will be generally limited to the edges of the plume due to the limited supply of O_2 into groundwater.

135

To determine the rate of hydrocarbon degradation, Monod type rate expressions are used where the rate is controlled by availability of reaction substrate, and inhibition terms are included to restrict reaction rate when more energetically favorable electron acceptors are present. In the simulations all anaerobic reactions are inhibited by the presence of O_2 while both Fe(III)-reduction and methanogenesis are inhibited in the presence of Mn(IV) minerals. In sampling conducted between 1994 and 1997, using most probable number analysis (MPN), Bekins et al. (1999) showed an inverse correlation between iron reducers and methanogens, but also showed that zones dominated by either Fe(III) reduction or methanogenesis vary on small spatial scales on the order of cm's. Furthermore, Baedecker et al. (1993) showed significant increases in both Fe(II) and CH_4 concurrently in groundwater at the downgradient edge of the source zone. These data suggest that, on the scale of interest for this study, Fe(III) reduction and methanogenesis occur simultaneously in the aquifer, and although there may be inhibition of methanogenesis by Fe(III) reduction, it is on a spatial scale too small to represent in the current model. As such, the inhibition of methanogenesis by Fe(III) reduction is neglected in the model which is consistent with other modeling efforts at the site (Essaid et al., 1995).

The sequence of TEAPs in the unsaturated zone is generally less well studied than saturated zone processes. At the Bemidji site, the data available for the unsaturated zone is somewhat sparse, but in general points to a similar progression of TEAPs as observed in the saturated zone. Existing unsaturated zone data was supplemented by water sample collection from unsaturated zone lysimeters in 2002, 2003 and 2004. Analyses indicate that both Mn(IV) and Fe(III) reduction are occurring in the unsaturated zone (Figure 4-5).
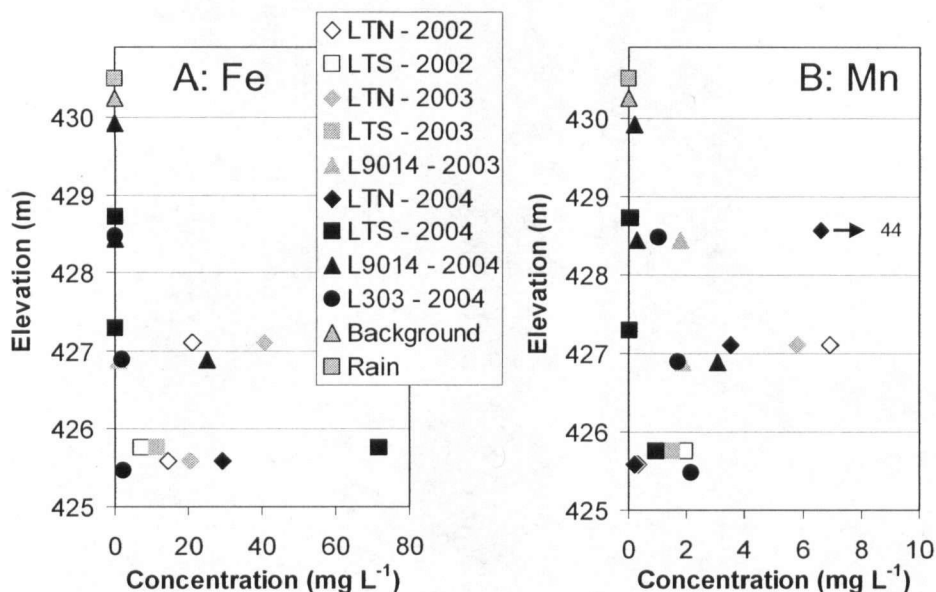
Figure 4-5. Fe and Mn concentrations measured in samples from unsaturated zone lysimeters in 2002, 2003 and 2004. Land surface elevation are; LTN – 430.1 m, LTS – 430.2 m, L9015 - 431.4 m, and L303 - 429.9 m. Water table elevation is ~423.5 m. Background and rain concentrations are plotted at arbitrary elevations. Actual elevation of background lysimeter is 430.1 m, 3.0 m below land surface.

Lysimeter nests LTN, L9014 and L303 are above the floating oil body while LTS is just off the transverse edge of the oil body. The data shows that dissolved Mn and Fe concentrations, byproducts of both Mn(IV) and Fe(III) reduction, respectively, are well above background. For Fe the concentrations generally increase with time and depth, although for LTN the highest concentrations are at an elevation of 427 m. For Mn there is a peak in the concentrations at 427 m of elevation, but the concentrations tend to decrease with time. Although the data are spatially and temporally sparse, they suggest that Mn(IV) and Fe(III) reduction occur most prominently at depth, corresponding to the anaerobic portion of the unsaturated zone, and that there is an inverse correlation between Mn(IV) and Fe(III) reduction. Measurement of vapor phase gas data in 1997 and 2003 show high methane concentration above the floating oil pool and around the oil present at residual saturation, indicating that methanogenesis is an important degradation

137

mechanism in the unsaturated zone (Chaplin et al., 2002; Amos et al., 2005). Furthermore, Bekins et al. (1999) found greater number of methanogens than Fe(III) reducers in two unsaturated zone sediment samples confirming that methanogenesis is an important process in the vadose zone.

Organic degradation reactions along with rate expressions and kinetic rate parameters are shown in Table 4-2. It is assumed that all organics are degraded fully to CO_2 or CH_4. This is a valid assumption in this case given that reaction intermediates are generally found at low concentrations in the Bemidji aquifer and appear to be readily degraded (Cozzarelli et al., 1990; Eganhouse et al., 1993). In addition to hydrocarbon degradation reactions, aerobic oxidation of CH_4 is also included in the simulations (Table 4-2, Reaction 4).

More rigorous representations of microbial degradation have been used in models at Bemidji and other sites. These include Monod kinetic formulations dependent on microbial growth and decay as well as nutrient limitations (Essaid et al., 1995) and formulations based on thermodynamic constraints (Postma and Jakobsen, 1996, Jakobsen and Postma, 1999, Curtis, 2003). While these alternative formulations have merit, the additional complexity is not required to attain the goals of this study, which focuses on interactions of unsaturated and saturated zone processes. Here we have attempted to reproduce the rate of contaminant degradation by calibrating the TEAPs to observed concentrations of reactants and products, and calibrating the dissolution of organic compounds to observed dissolved concentrations. This method is capable of reproducing the amount of contaminant degradation and production of reactions products adequately,

Table 4-2. Reaction stoiciometries, rate expression and constants used for reactions in the simulation.

Reaction	Rate Expression	Constants
Aerobic Oxidation Reactions:		
1. $C_6H_{6(aq)} + 7.5O_{2(aq)} + 3H_2O \rightarrow 6HCO_3^- + 6H^+$	$R_2 = k_2 \left(\dfrac{\{C_7H_{8(aq)}\}}{K_{C_6H_6}^S + \{C_7H_{8(aq)}\}} \right) \left(\dfrac{\{O_{2(aq)}\}}{K_{O_2}^S + \{O_{2(aq)}\}} \right)$	$k_1 = 5.0 \times 10^{-09}$ $K_{C_6H_6}^S = 1.40 \times 10^{-06}$ $K_{O_2}^S = 3.414 \times 10^{-0}$
2. $C_7H_{8(aq)} + 9O_{2(aq)} + 3H_2O \rightarrow 7HCO_3^- + 7H^+$	$R_2 = k_2 \left(\dfrac{\{C_7H_{8(aq)}\}}{K_{C_7H_8}^S + \{C_7H_{8(aq)}\}} \right) \left(\dfrac{\{O_{2(aq)}\}}{K_{O_2}^S + \{O_{2(aq)}\}} \right)$	$k_2 = 5.0 \times 10^{-09}$ $K_{C_7H_8}^S = 8.65 \times 10^{-07}$ $K_{O_2}^S = 3.414 \times 10^{-06}$
3. $C_4H_{10(aq)} + 6.5O_{2(aq)} \rightarrow 4HCO_3^- + H_2O + 4H^+$	$R_3 = k_3 \left(\dfrac{\{C_4H_{10(aq)}\}}{K_{C_4H_{10}}^S + \{C_4H_{10(aq)}\}} \right) \left(\dfrac{\{O_{2(aq)}\}}{K_{O_2}^S + \{O_{2(aq)}\}} \right)$	$k_3 = 5.0 \times 10^{-09}$ $K_{C_4H_{10}}^S = 9.95 \times 10^{-06}$ $K_{O_2}^S = 3.414 \times 10^{-06}$
4. $CH_{4(aq)} + 2.0O_{2(aq)} \rightarrow HCO_3^- + H^+ + H_2O$	$R_4 = k_4 \left(\dfrac{\{CH_{4(aq)}\}}{K_{CH_4}^S + \{CH_{4(aq)}\}} \right) \left(\dfrac{\{O_{2(aq)}\}}{K_{O_2}^S + \{O_{2(aq)}\}} \right)$	$k_4 = 5.0 \times 10^{-09}$ $K_{CH_4}^S = 1.00 \times 10^{-06}$ $K_{O_2}^S = 3.414 \times 10^{-06}$
Mn(IV) Reduction:		
5. $MnO_{2(s)} + 0.067C_6H_{6(aq)} + 1.6H^+ \rightarrow Mn^{2+} + 0.4HCO_3^- + 0.8H_2O$	$R_5 = k_5 \left(\dfrac{\{C_6H_{6(aq)}\}}{K_{C_6H_6}^S + \{C_6H_{6(aq)}\}} \right) \left(\dfrac{K_{O_2}^I}{K_{O_2}^I + \{O_{2(aq)}\}} \right)$	$k_5 = 5.0 \times 10^{-12}$ $K_{C_6H_6}^S = 1.40 \times 10^{-06}$ $K_{O_2}^I = 3.414 \times 10^{-06}$
6. $MnO_{2(s)} + 0.0556C_7H_{8(aq)} + 1.61H^+ \rightarrow Mn^{2+} + 0.389HCO_3^- + 0.833H_2O$	$R_6 = k_6 \left(\dfrac{\{C_7H_{8(aq)}\}}{K_{C_7H_8}^S + \{C_7H_{8(aq)}\}} \right) \left(\dfrac{K_{O_2}^I}{K_{O_2}^I + \{O_{2(aq)}\}} \right)$	$k_6 = 5.0 \times 10^{-12}$ $K_{C_7H_8}^S = 8.65 \times 10^{-07}$ $K_{O_2}^I = 3.414 \times 10^{-06}$
7. $MnO_{2(s)} + 0.0769C_4H_{10(aq)} + 1.69H^+ \rightarrow Mn^{2+} + 0.308HCO_3^- + 1.077H_2O$	$R_7 = k_7 \left(\dfrac{\{C_4H_{10(aq)}\}}{K_{C_4H_{10}}^S + \{C_4H_{10(aq)}\}} \right) \left(\dfrac{K_{O_2}^I}{K_{O_2}^I + \{O_{2(aq)}\}} \right)$	$k_7 = 5.0 \times 10^{-12}$ $K_{C_4H_{10}}^S = 9.95 \times 10^{-06}$ $K_{O_2}^I = 3.414 \times 10^{-06}$

Reaction	Rate Expression	Constants

Fe(III) Reduction:

8. $FeOOH_{(s)} + 0.0333C_6H_{6(aq)} + 1.8H^+ \rightarrow Fe^{2+} + 0.2HCO_3^- + 1.4H_2O$

$$R_8 = k_8\left(\frac{\{C_6H_{6(aq)}\}}{K^S_{C_6H_6} + \{C_6H_{6(aq)}\}}\right)\left(\frac{K^I_{O_2}}{K^I_{O_2} + \{O_{2(aq)}\}}\right)\left(\frac{K^I_{MnO_2}}{K^I_{MnO_2} + \phi_{MnO_2}}\right)$$

$k_8 = 5.0\times10^{-12}$
$K^S_{C_6H_6} = 1.40\times10^{-06}$
$K^I_{O_2} = 3.414\times10^{-06}$
$K^I_{MnO_2} = 3.0\times10^{-07}$

9. $FeOOH_{(s)} + 0.0278C_7H_{8(aq)} + 1.806H^+ \rightarrow Fe^{2+} + 0.194HCO_3^- + 1.417H_2O$

$$R_9 = k_9\left(\frac{\{C_7H_{8(aq)}\}}{K^S_{C_7H_8} + \{C_7H_{8(aq)}\}}\right)\left(\frac{K^I_{O_2}}{K^I_{O_2} + \{O_{2(aq)}\}}\right)\left(\frac{K^I_{MnO_2}}{K^I_{MnO_2} + \phi_{MnO_2}}\right)$$

$k_9 = 5.0\times10^{-12}$
$K^S_{C_7H_8} = 8.65\times10^{-07}$
$K^I_{O_2} = 3.414\times10^{-06}$
$K^I_{MnO_2} = 3.0\times10^{-07}$

10. $FeOOH_{(s)} + 0.0385C_4H_{10(aq)} + 1.846H^+ \rightarrow Fe^{2+} + 0.154HCO_3^- + 1.538H_2O$

$$R_{10} = k_{10}\left(\frac{\{C_4H_{10(aq)}\}}{K^S_{C_4H_{10}} + \{C_4H_{10(aq)}\}}\right)\left(\frac{K^I_{O_2}}{K^I_{O_2} + \{O_{2(aq)}\}}\right)\left(\frac{K^I_{MnO_2}}{K^I_{MnO_2} + \phi_{MnO_2}}\right)$$

$k_{10} = 5.0\times10^{-12}$
$K^S_{C_4H_{10}} = 9.95\times10^{-06}$
$K^I_{O_2} = 3.414\times10^{-06}$
$K^I_{MnO_2} = 3.0\times10^{-07}$

Methanogenesis:

11. $C_6H_{6(aq)} + 6.75H_2O$
$\rightarrow 3.75CH_4 + 2.25HCO_3^- + 2.25H^+$

$$R_{11} = k_{11}\left(\frac{\{C_6H_{6(aq)}\}}{K^S_{C_6H_6} + \{C_6H_{6(aq)}\}}\right)\left(\frac{K^I_{O_2}}{K^I_{O_2} + \{O_{2(aq)}\}}\right)\left(\frac{K^I_{MnO_2}}{K^I_{MnO_2} + \phi_{MnO_2}}\right)$$

Sat: $k_{11} = 5.0\times10^{-13}$
Unsat: $k_{11} = 5.0\times10^{-11}$
$K^S_{C_6H_6} = 1.40\times10^{-06}$
$K^I_{O_2} = 3.414\times10^{-06}$
$K^I_{MnO_2} = 3.0\times10^{-07}$

12. $C_7H_{8(aq)} + 7.5H_2O$
$\rightarrow 4.5CH_4 + 2.5HCO_3^- + 2.5H^+$

$$R_{12} = k_{12}\left(\frac{\{C_7H_{8(aq)}\}}{K^S_{C_7H_8} + \{C_7H_{8(aq)}\}}\right)\left(\frac{K^I_{O_2}}{K^I_{O_2} + \{O_{2(aq)}\}}\right)\left(\frac{K^I_{MnO_2}}{K^I_{MnO_2} + \phi_{MnO_2}}\right)$$

Sat: $k_{12} = 5.0\times10^{-12}$
Unsat: $k_{12} = 5.0\times10^{-10}$
$K^S_{C_7H_8} = 8.65\times10^{-07}$
$K^I_{O_2} = 3.414\times10^{-06}$
$K^I_{MnO_2} = 3.0\times10^{-07}$

Reaction	Rate Expression	Constants

Methanogenesis: continued.

13. $C_4H_{10(aq)} + 2.25H_2O$
$\rightarrow 3.25CH_4 + 0.75HCO_3^- + 0.75H^+$

$R_{13} = k_{13}\left(\dfrac{\{C_4H_{10(aq)}\}}{K_{C_4H_{10}}^S + \{C_4H_{10(aq)}\}}\right)\left(\dfrac{K_{O_2}^I}{K_{O_2}^I + \{O_{2(aq)}\}}\right)\left(\dfrac{K_{MnO_2}^I}{K_{MnO_2}^I + \phi_{MnO_2}}\right)$

Sat: $k_{13} = 5.0\times10^{-12}$

Unsat: $k_{13} = 5.0\times10^{-10}$

$K_{C_4H_{10}}^S = 9.95\times10^{-06}$

$K_{O_2}^I = 3.414\times10^{-06}$

$K_{MnO_2}^I = 3.0\times10^{-07}$

Mineral Dissolution/Precipitation:

14. $CaCO_{3(s)} + H^+ \rightarrow Ca^{2+} + HCO_3^-$

$R_{14} = k_{14}\left(\dfrac{IAP}{K_{CaCO_3}^m}\right)$

$k_{14} = 1.0\times10^{-09}$

$K_{CaCO_3}^m = 10^{1.855}$

Dissolution of organic compounds from NAPL:

15. $C_6H_{6(NAPL)} \rightarrow C_6H_{6(aq)}$

$k_{15} = 3.5\times10^{-08}$

$K_{C_6H_6}^o = 10^{-1.698}$

16. $C_7H_{8(NAPL)} \rightarrow C_7H_{8(aq)}$

$R_{diss,j}^o = k_{diss,j}^o\left(1 - \dfrac{\gamma_j^c C_j^c}{K_{diss,j}^o X_j^o}\right)$

$k_{16} = 1.75\times10^{-08}$

$K_{C_7H_8}^o = 10^{-2.239}$

17. $C_4H_{10(NAPL)} \rightarrow C_4H_{10(aq)}$

Sat: $k_{17} = 3.5\times10^{-10}$

Unsat: $k_{17} = 4.0\times10^{-06}$

$K_{C_4H_{10}}^o = 10^{-2.479}$

k = effective rate constant (mol L^{-1} s^{-1})
K^I = inhibition constant (mol L^{-1})
K^S = half saturation constant (mol L^{-1})
K^o = solubility of organic compound (mol L^{-1}) (CRC Press, 2004)
K^m = mineral solubility (mol L$^-$) (Allison et al., 1991)
X^o = fraction of compound in organic mixture
φ = mineral volume fraction
n = reaction number
j = component name

provides and overall mass balance, but does not investigate the mechanisms of microbial processes.

For the simulation of Mn(IV) and Fe(III) reduction of hydrocarbons, the minerals MnO_2 and FeOOH are assumed to be initially present throughout the aquifer. The morphology of these minerals is unimportant in these simulations since thermodynamic constraints are neglected. Iron extractions using 0.5 M HCl performed on Bemidji sediment showed an average of 8 μmol g^{-1} difference between background and source zone sediment suggesting that this amount of poorly crystalline Fe-oxide was available for microbial reduction (Tuccillo et al., 1999). Assuming a mineral density for FeOOH of 4.37 g cm^{-3}, an average sediment grain density of 2.65 g cm^{-3}, and a porosity of 0.38 results in a bio-available FeOOH volume fraction of ~2.5 x 10^{-4} m^3 mineral m^{-3} aquifer. This value was used as the initial condition throughout the model domain. The bio-available fraction of Mn(IV) minerals is not well constrained. Results from extractions using 0.5 M HCl from background samples and samples from within the contaminated portion of the aquifer ranged from 1 to 3 μmol g^{-1} (equivalent to 3 x10^{-5} to 9 x 10^{-5} m^3 MnO_2 m^{-3} aquifer), but show no clear trend (Tuccillo, unpublished data). These data will be used to constrain the calibration of the initial volume fraction of MnO_2.

Calcite is the only other mineral included in the simulation. Calcite remains near saturation along the entire sampled groundwater flowpath in both 1987 and 2004 (Figure 4-6), suggesting that calcite is a primary buffering mineral in this aquifer. Bennett et al. (1993) showed that dolomite and magnesian calcites also play a role in the aquifer geochemistry; however, to minimize CPU requirements we have chosen to not include Mg^{2+} as a component in the simulation and therefore neglect Mg containing minerals.

This simplification should not significantly affect the redox chemistry in the system but may produce inaccurate simulated Ca^{2+} concentrations and possibly alkalinity. Saturation indices calculated from unsaturated zone samples taken in 2004 also indicate the importance of calcite. Calcite is undersaturated in infiltrating water and approaches saturation with depth, suggesting kinetically controlled dissolution of calcite into recharge water, or potentially depletion of calcite at shallow depth. (Figure 4-7).
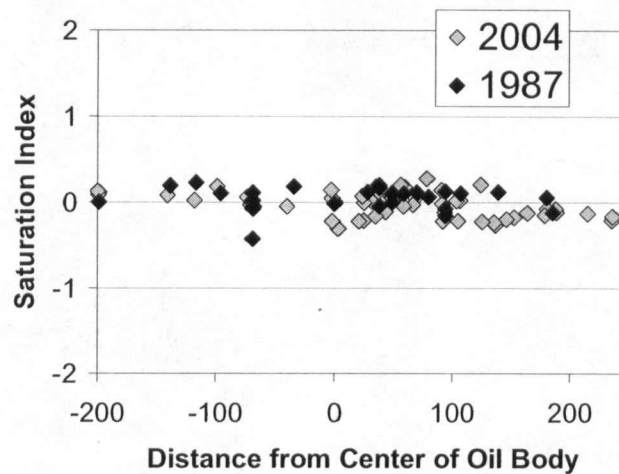
Figure 4-6. Saturation indices for calcite from groundwater samples collected along the north pool transect in 1987 (Bennett et al., 1993) and 2004.

The cycling of Fe and Mn in redox controlled environments is complex. At the Bemidji site, siderite, ferroan calcite and organically bound iron have been reported as potential sinks for iron (Baedecker et al., 1992; Tuccillo et al., 1999). Authigenic magnetite was also found in core samples, although in low abundance (Baedecker et al., 1992). However, Zachara et al. (2004) found little evidence for authigenic mineral formation and suggested that ion exchange could provide a potential explanation for the decrease in aqueous Fe^{2+} and accumulation of sediment bound Fe^{2+} downgradient of the

source. Geochemical modeling of 1987 and 2004 field data show that both siderite and rhodochrosite become oversaturated in the source zone, and in the downgradient groundwater plume, suggesting that these minerals have the potential to precipitate. However, preliminary simulations showed that these minerals did not provide a good control on Fe^{2+} and Mn^{2+}, underestimating Fe^{2+} by an order of magnitude and overestimating Mn^{2+} to a similar degree. Due to these uncertainties we have chosen not to simulate Fe^{2+} and Mn^{2+} sinks as they will not provide meaningful constraints on the model in light of the stated objectives. Instead, the constraint on the extent of Mn(IV) and Fe(III) reduction will be the availability of $MnO_{2(s)}$ and $FeOOH_{(s)}$ in the aquifer.
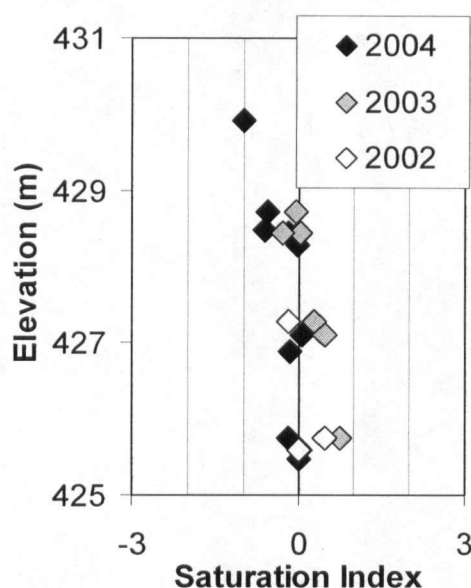
Figure 4-7. Saturation indices for calcite from unsaturated zone lysimeter data collected around the north pool oil body in 2002-2004.

4.6   Model Parameters

The 2-D model domain, shown in Figure 4-8, is 225 m long and 15 m high, representing an elevation of 415 to 430 meters above sea level (masl). The model is discretised into 1 m horizontal and 0.2 m vertical control volumes. The maximum time step used for the simulations was 0.01 years, limiting the Courant number to <1, in order to minimize numerical dispersion. Physical parameters used in the simulations are summarized in Table 4-3. The water table initially slopes from 424.1 m on the upgradient side of the domain to 423.3 m on the downgradient side giving a slope of 0.0035; water flow is simulated left to right.
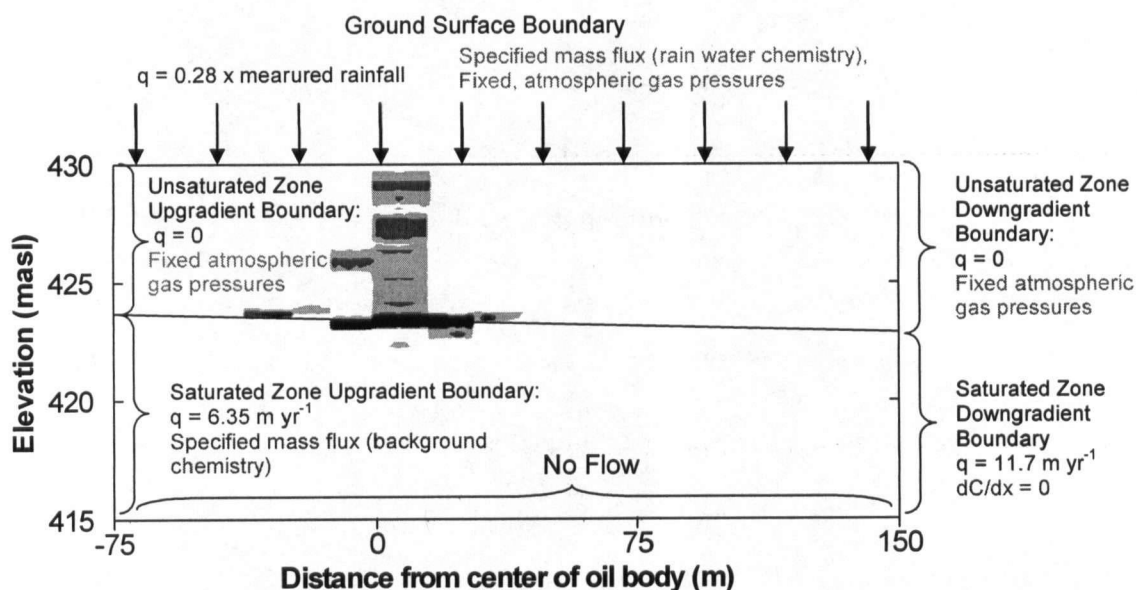
Figure 4-8. Model domain for reactive transport simulation showing initial oil saturations, initial water table and both flow (blue) and transport (red) boundary conditions. For the ground surface and unsaturated zone boundaries fixed concentrations of gaseous species, equivalent to atmospheric concentrations, are assumed on a dummy node outside the model domain. Oil saturation contours, from lightest to darkest, are 0.1, 0.2 and 0.3.

The simulations include 11 primary components; HCO_3^-, N_2, CH_4, H^+, O_2, Ca^{2+}, Fe^{3+}, Mn^{2+}, benzene (C_6H_6), toluene (C_7H_8) and butane (C_4H_{10}), and 7 gases; CO_2, N_2,

145

O_2, CH_4, C_6H_6, C_7H_8, and C_4H_{10}. Henry's Law constants used in the simulations are published values corrected to the average groundwater temperature observed at Bemidji of 9 ^0C (Table 4-4).

Table 4-3. Physical parameter used in simulation.

Parameter	Value	Source
Hydraulic conductivity (m day^{-1})	8.64	Essaid et al., 1995
Porosity	0.38	Essaid et al., 1995
van Genuchten - alpha	3.5	Dillard et al., 1997
van Genuchten - n	4	Dillard et al., 1997
residual saturation	0.05	Estimated
longitudinal dispersivity (m)	0.1	Essaid et al., 1995
transverse dispersivity (m)	0.001	Essaid et al., 1995
atmospheric pressure (atm)	0.93	Calculated; Langmuir, 1997
diffusion coefficient - aqueous phase (m^2 s^{-1})	2.00×10^{-09}	CRC press, 2004
diffusion coefficient - gas phase (m^2 s^{-1})	1.00×10^{-05}	CRC press, 2004
Temperature (K)	282	Amos et al., 2005

Parameters were chosen to best represent conditions at the Bemidji site and were based on the reference listed. Hydraulic conductivity shown is the initial background hydraulic conductivity.

Initial non-aqueous phase hydrocarbon distributions are determined by multiplying the calculated mole fraction of each hydrocarbon, as described in the previous section, by the measured oil saturation (Dillard et al, 1997). Initial water chemistry for the saturated zone is determined by averaging observed background concentrations (Table 4-4). For the unsaturated zone, initial chemistry is assumed to be that of observed rainwater chemistry; however, this pore water quickly equilibrates with calcite, providing more realistic unsaturated zone geochemistry (Table 4-4). The mineral volume fraction of FeOOH is set to 2.5 x 10^{-4} m^3 mineral m^{-3} aquifer to represent the bio-available fraction of Fe(III) minerals in the aquifer as determined by 0.5 M HCl extraction (Tuccillo et al., 1999). The mineral volume fractions of MnO_2 (Table 4-4) is calibrated to represent the biologically available fraction as described below. The volume

fraction of calcite is set to 1%, which is a sufficient amount to avoid depletion of this mineral in any part of the aquifer.

Table 4-4. Initial and boundary conditions used for reactive transport simulation.

	Background Chemistry Saturated Zone	Background Chemistry Unsaturated Zone	Atmospheric Partial Pressure (atm)	K_i^g (mol L^{-1} atm^{-1})
HCO$_3^-$ (mol L^{-1})	2.8×10^{-03}	6.0×10^{-5}	7.17×10^{-2}	1.48×10^{-8}
pH	7	7		
N$_2$ (atm)	0.725	0.725	0.725	8.599×10^{-04}
O$_2$ (atm)	0.0165	0.195	0.195	1.748×10^{-03}
CH$_4$ (atm)	0.00	0.00	0.00	1.998×10^{-03}
Ca^{2+} (mol L^{-1})	1.8×10^{-3}	2.0×10^{-3}		
C$_6$H$_6^-$ (mol L^{-1})	0.00	0.00	0.00	0.3555
C$_7$H$_8$ (mol L^{-1})	0.00	0.00	0.00	0.1535
C$_4$H$_{10}$ (mol L^{-1})	0.00	0.00	0.00	2.378×10^{-3}
MnO$_{2(s)}$ (mol fraction)	4.33×10^{-5}	4.33×10^{-5}		
FeOOH$_{(s)}$ (mol fraction)	2.5×10^{-4}	2.5×10^{-4}		
Calcite (mol fraction)	0.01	0.01		

Saturated zone background chemistry is used for initial conditions below the water table and for the saturated zone inflow boundary. Unsaturated zone background chemistry is used for initial conditions in the unsaturated zone and for the ground surface boundary. Atmospheric partial pressures are fixed on a dummy node outside the model domain for unsaturated zone and ground surface boundaries. Henry's Law constants from CRC Press (2004), Weiss (1970), and Yamamoto et al. (1976).

A no flow boundary condition is assumed for the bottom of the domain while specified flux boundaries are set on all other boundaries (Figure 4-8). The upgradient and down gradient flow boundaries are set to achieve a flow rate of ~25 m yr^{-1} at the upgradient end of the domain, while taking recharge into account. The ground surface flow boundary (Figure 4-8) is set to achieve recharge rates of 28% of measured rainfall as described in Section 4.5.1. Monthly rainfall is averaged over three months and the boundary condition is updated accordingly. The use of specified fluxes for all inflow and outflow boundaries was found to provide the best representation of the fluctuating water

147

table and provided the least interference with transport boundary conditions; however, the use of specified fluxes at all model boundaries is problematic from a numerical point of view. To achieve a meaningful result, the total inflow at the left boundary was set to equal the difference between the total outflow and total recharge over the duration of the simulation. This approach ensures that the transient simulations conducted represent perturbations of a system at quasi steady state.

Specified mass flux reactive transport boundary conditions are set for the aqueous phase on the upgradient and ground surface boundaries (Figure 4-8). Concentrations at the saturated zone upgradient boundary are assumed to be equivalent to the saturated zone initial conditions while the concentrations at the ground surface are set to the average of measured rain water samples (Table 4-4). For the ground surface boundary and the upgradient and downgradient unsaturated zone boundaries, fixed concentrations of gaseous species, equivalent to atmospheric concentrations, are assumed on a dummy node outside the model domain (Table 4-4). This allows diffusion of gaseous species into and out of the model domain.

Rate parameters, including effective rate constants, half saturation constants and inhibition constants are given in Table 4-2. All effective rate constants are calibrated to the observed data. Where possible we have attempted to maintain consistency between the rate constants to reduce the number of adjustable model parameters. For example, all aerobic, Mn(IV) reduction, and Fe(III) reduction rates are the same for each compound, and Mn(IV) and Fe(III) reduction rates are also identical. Rates of methanogenesis were decreased by an order of magnitude for 'benzene' compared to the other organic compound, which is consistent with field observations that suggest that benzene and

ethylbenzene are more recalcitrant under methanogenic conditions (Cozzarelli et al., 1990). The rate constants for saturated and unsaturated zone processes have also been kept consistent, except for methanogenesis which was set two orders of magnitude higher in the unsaturated zone, consistent with the MPN analysis of Bekins et al. (1999), who observed up to 30 times more methanogens in the unsaturated zone than in the saturated zone. The dissolution rate of 'butane' was set four orders of magnitude higher in the unsaturated zone to represent the process of volatilization, which is not explicitly simulated in MIN3P.

Half saturation constants have all been set two orders of magnitude below the maximum concentrations of the various components (defined by the solubility of the component) so that if a component is present at any significant concentration, i.e. >2% of the maximum concentration, then the reaction rate is essentially zero order, defined by the effective rate constant. This approach limits the tunability of the half saturation constants and places greater importance on the effective rate constants. Inhibition constants are defined in a similar manner so that the inhibiting substance must appraoch ~2 orders of magnitude below the maximum concentration (Defined as the solubility of O_2 or the initial volume fraction for $MnO_{2(s)}$) before the inhibited process begins to progress. An exception to this approach is that for Fe(III) reduction, the inhibition constant for $MnO_{2(s)}$ is set to only one order of magnitude below the initial volume fraction of $MnO_{2(s)}$, so that the Fe(III) reduction is initiated prior to complete depletion of $MnO_{2(s)}$. This also allows Fe(III) reduction to begin prior to methanogenesis, which appears to be consistent with observations at Bemidji (Baedecker et al., 1993).

4.7 Results and Discussion

4.7.1 Water table fluctuations

A potentially important control on hydrology and geochemistry in this system is the fluctuation of the water table (Figure 4-2), which can introduce gas bubbles into the saturated aquifer, affecting hydraulic conductivity and providing a source of oxygen, or alternatively, gas bubbles previously trapped below the water table can be released to the unsaturated zone. It is therefore important to accurately simulate the observed water table fluctuation. The simulations capture the longer term water table fluctuations, specifically, the ~0.5 m decrease in water levels from 10-12 years simulation time, followed by a period of increasing water levels, increasing the water table elevation to ~ 1 m above the recorded low in this period (Figure 4-2). Furthermore, the simulations reproduce seasonal fluctuations that are generally representative of the magnitude of the observed fluctuations. However, at later times, i.e. between 16 and 23 years, the simulations do not capture the large ~0.5 m seasonal fluctuations. The underestimation of the magnitude of these seasonal fluctuations will lead to less entrapment and release of gas bubbles and may potentially underestimate the effects of these processes. Despite these discrepancies, the generally good agreement between simulated and observed water levels should, therefore, provide a reasonable approximation of bubble entrapment and release.

4.7.2 Geochemical Evolution of Saturated and Unsaturated Zone Plumes

As a basis for discussion and to demonstrate that the calibrated model captures the major geochemical changes observed at the field site, we compare the simulation results

150

to field data at four times that have been chosen based on the availability of data. These are 7, 11, 17 and 24 years of simulation time.

4.7.2.1   7 years simulation time

The simulation results at 7 years simulation time reproduce the general nature of the vapour phase and dissolved plumes observed between 1985 and 1987 (6-8 years after the spill). Specifically, in the unsaturated zone the simulations reproduce the high volatile hydrocarbon ('butane') concentrations (>750 g m^{-3}), corresponding to a zone of elevated CO_2 (>10% by volume) and depleted O_2 (<2% by volume). CH_4 concentrations remain low (<1% by volume) in the vadose zone at this time (Figures 4-9A-D). This compares well with total hydrocarbon, CH_4, CO_2, and O_2 data collected in 1985 (Figure 4-10A-D; Hult and Grabbe, 1988; total hydrocarbons shown by Hult and Grabbe (1988) are primarily volatile C2-C5 hydrocarbons which are represented in the simulation results as VHC).

The simulation is consistent with the findings of Chaplin et al. (2002), who showed that volatilization and aerobic oxidation were the primary hydrocarbon attenuation mechanisms in 1985; however, the simulation shown here provides additional insights that are not captured by the 1-D steady state simulations of Chaplin et al. (2002), specifically with respect to the development of the anaerobic plume and transition to more reducing conditions. In the unsaturated zone the relatively high transport rate of gases requires a high concentration of volatile hydrocarbons to prevent the ingress of O_2 and create an anaerobic plume. Furthermore, the extended period of time over which volatilization occurs, i.e. > 7 years, allows the anaerobic plume to be maintained, and provides a suitable environment for the evolution of degradation processes to more

151
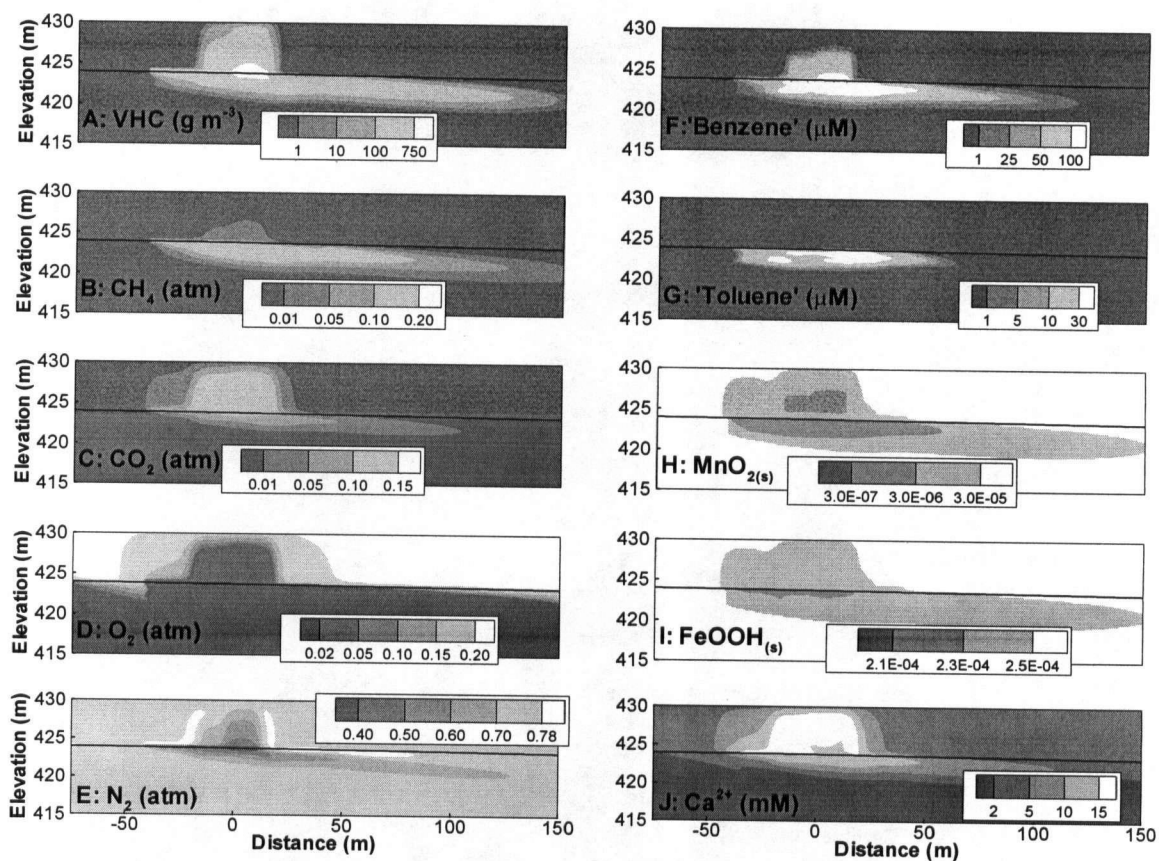
Figure 4-9. 2-D plots of geochemical results at 7 years of simulation time. Distance is from the center of the oil body. VHC refers to volatile hydrocarbons. $MnO_{2(s)}$ and $FeOOH_{(s)}$ in volume fraction (m^3 mineral m^{-3} aquifer).

reducing conditions. The simulations indicate that a significant volume fraction of the initial $MnO_{2(s)}$ has been depleted (Figure 4-9H) which has allowed the Fe(III) reduction and methanogenesis to begin. However, note that Fe(III) reduction and methanogenesis are of only minor importance in the unsaturated zone at this time (Figures 4-9B and I), suggesting that inhibition by $MnO_{2(s)}$ is an important aspect in the geochemical evolution of the plume. This aspect of plume evolution has not been previously investigated. These results show that the extended period of high volatilization rates is an important aspect of the unsaturated zone plume development at the Bemidji site, and offer an explanation for the delayed development of an unsaturated methanogenic zone.

The simulation does not reproduce specific features of the observed vadose zone plume. Specifically, the simulated volatile hydrocarbon concentrations are somewhat lower than the observed concentrations (maximum simulated is 750 g m^{-3}; maximum observed 1000 g m^{-3}; Figures 4-9A and 4-10A), and the lateral extent of the observed plume, and the sharp chemical gradients between the aerobic and anaerobic zones, is not accurately represented (Figures 4-9B-D and 4-10B-D). These inaccuracies are likely due to the simplified representation of volatile organic components, and the homogenous representation of the soil hydraulic properties used in the model. However, the simulations do reproduce the main geochemical processes in the vadose zone at this time, namely, volatilization of low molecular weight hydrocarbons, and degradation of hydrocarbons dominated by aerobic processes but transitioning to more reducing conditions in the core of the plume.

In the saturated zone, the simulations reproduce the anaerobic plume transitioning from Mn(IV) reduction to Fe(III) reduction and methanogenesis (Figure 4-9). In the core
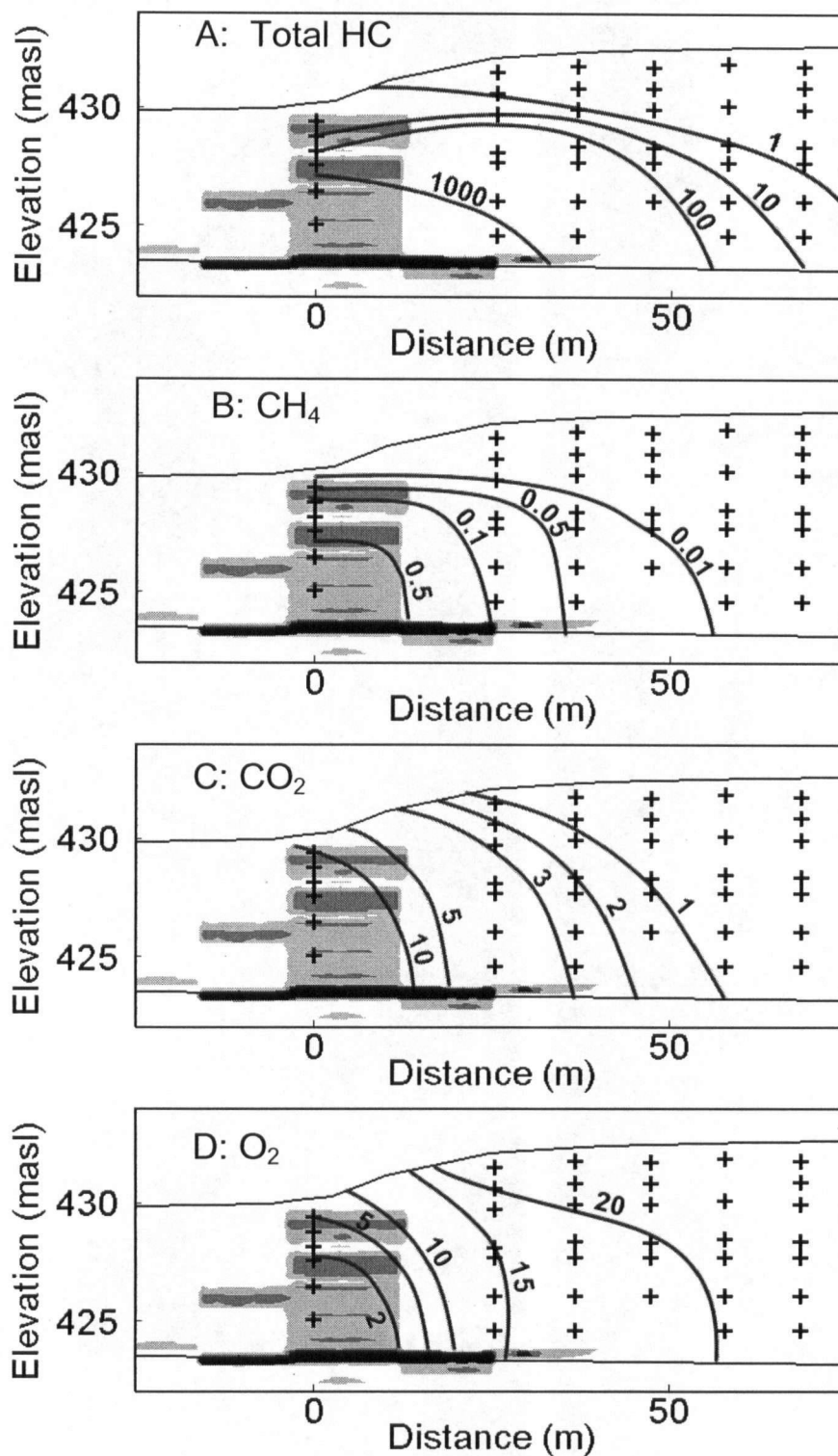
Figure 4-10. Cross sections of unsaturated zone showing contours of vapour phase data collected in 1985. All data is in percent by volume except total hydrocarbons (A) which is in g m^{-3}. Modified from Hult and Grabbe (1988). Oil saturation contours, from lightest to darkest, are 0.1, 0.2 and 0.3. Sampling points are marked with '+'.

154

of the saturated zone plume, $MnO_2(s)$ is being depleted (Figure 4-9H; 0.1 times the initial value) resulting in the onset of Fe(III) reduction, demonstrated by the slight depletion in initial volume fraction of FeOOH(s) (Figure 4-9I), and methanogenesis, shown by the elevated levels of CH_4 in the groundwater plume (Figure 4-9B). The 'benzene' plume, defined by the 1 μM contour, extends ~100 m downgradient, while the 'toluene' plume is restricted to the area below the floating oil (Figures 4-9F and G) due to it's higher reactivity under methanogenic conditions. Ca^{2+} concentrations are elevated in the plume due to the increased solubility of calcite brought on by the changing geochemical conditions. These features of the simulated groundwater plume are consistent with the observed geochemistry in 1986 and 1987 (Figure 4-11), and the previously developed conceptual model of plume evolution at the site (Bennett et al., 1993; Baedecker et al., 1993; Eganhouse et al., 1996; Essaid et al., 1995).

A fundamental difference between the simulation presented here and previous simulations of the groundwater plume at the Bemidji site (i.e. Essaid et al., 1995; 2003; Curtis et al., 1999) is that here the process of bubble formation and degassing in the source area is explicitly considered. The simulations suggest that at 7 years simulation time N_2 concentrations have already been depleted to less than 0.5 atm below the floating oil (Figure 4-9E), which is consistent with field observations (Figure 4-11D; Cozzarelli, unpublished data), suggesting that gas bubbles are being formed at this early stage of plume evolution. The formation of gas bubbles has several potential effects on plume evolution, which will be discussed in detail below.

The direct comparison of observed and simulated data along the groundwater flowpath shown in Figure 4-11 highlights some inconsistencies between the simulated
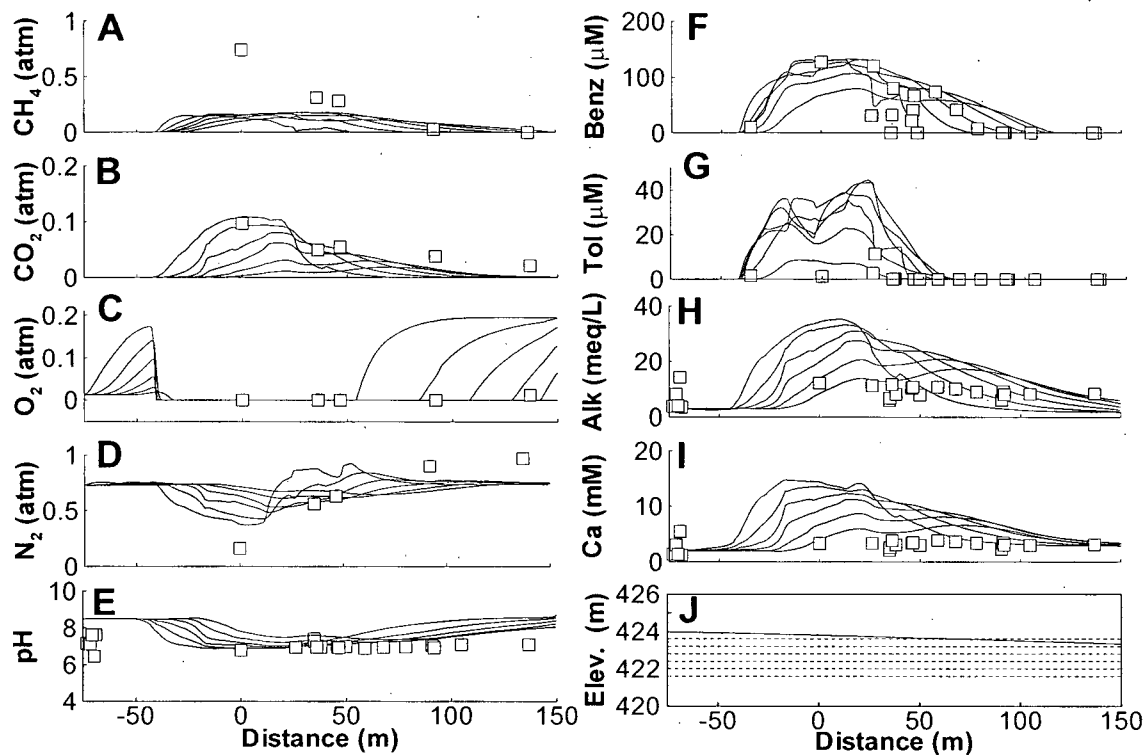
Figure 4-11. Profiles of geochemical constituents along the groundwater flow path for 7 years simulation time (lines) compared to observed data from 1986 for dissolved gases (A-D; Cozzarelli, unpublished), 'benzene' (F; Essaid et al., 2003) and 'toluene' (G; Essaid et al., 2003) and 1987 for all other data (E, H, I; Bennett et al., 1993). For observed data, 'benzene' and 'toluene' refers to the sum of benzene and ethylbenzene, and the sum of toluene and xylenes, respectively. For simulated data, each line represents a horizontal transect through the model domain as shown by the dashed lines in L. The selected transects are 2 meters below the water table which corresponds to the area of the aquifer where most of the sampling wells are screened. The simulated water table at 7 years is shown in J as a solid line.

and observed data. Firstly, the simulations predict a rebound in O_2 concentrations approximately 50 m downgradient from the center of the source zone that is not reflected in the observed data. The elevated levels of O_2 in the simulations are a result of O_2 rich recharge water entering the aquifer, and the entrapment of O_2-rich bubbles near the water table; however, observation wells near the water table at the field site generally have 1.5 m long screens, which would make detection of these variations in O_2, on a small spatial scale, difficult. Note that the simulations show that this replenishment in O_2 is restricted to a thin layer immediately below the water table, while the remainder of the aquifer

156

remains anoxic (Figure 4-9D). Nevertheless, because this feature cannot be confirmed with field data, we emphasize that the effects of O_2 entrapment near the water may be overestimated in the simulation results.

Other discrepancies in the simulated and observed data include overestimated 'toluene' concentrations, which highlights the difficulty in accurately simulating this highly reactive compound at low concentrations, and the over-prediction of alkalinity and Ca^{2+} concentrations. Although it is not immediately apparent due to the scale of the figures, observed alkalinity and Ca^{2+} concentrations peak above average background concentrations in the source zone (maximum alkalinity is 12 meq L^{-1}, maximum Ca^{2+} is 4 mM) and return to background ~100 to 150 m downgradient. So although the magnitude of the increase in alkalinity and Ca^{2+} is not well reproduced by the simulation, the general trend is. The discrepancy in the magnitude of these geochemical changes reflects the difficulty in accurately simulating alkalinity and its sensitivity to small variations in pH. The simplified geochemical conceptual model, including the limited number of components and neglecting potentially important minerals such as dolomite, also contributes to the noted discrepancies in alkalinity and Ca^{2+}.

The degradation of volatile alkanes in the groundwater is not well constrained by field data. However, the representation shown in Figure 4-9A overestimates observations reported by Eganhouse et al. (1993) who measured alkane concentration at 1.5 mg L^{-1} (26 g m^{-3}), 26 m downgradient of the center of the oil body, and at <0.1 mg L^{-1} (1.7 g m^{-3}), 57 m downgradient of the center of the oil body, in 1987 (8 years after the spill). This is due to the high rate of 'butane' dissolution in the unsaturated zone, which results in high dissolved concentrations in pore water recharging the saturated portion of the aquifer.

This discrepancy is difficult to correct in the simulation given that the component 'butane' is used to represent volatile, short chain alkanes ranging from C2 to C5 with solubilities and volatilities varying over several orders of magnitude.

4.7.2.2   11 years simulation time

At 11 years of simulation time the vadose zone plume is evolving to more reducing conditions as Fe(III) reduction and methanogenesis becomes more prominent degradation pathways. This is demonstrated by higher concentrations of CH_4 and depletion of $MnO_{2(s)}$ in the unsaturated zone (Figure 4-12B and H). Furthermore, the concentration of total volatile hydrocarbons is decreasing, suggesting that the supply of these compounds in the free phase oil is diminishing. The anaerobic plume is still maintained above the floating oil; however, at this stage O_2 consumption is due to aerobic degradation of CH_4 as well as the volatile hydrocarbons from the oil. The simulated vadose zone geochemistry at this point is constrained only by the CH_4 and CO_2 concentrations along a 1-D vertical transect at well 301, which is at the center of the oil body, collected in 1991 (Figure 4-13; Revesz et al., 1995). The simulation reasonably reproduces the observed CH_4 and CO_2 concentrations; although, the simulated CH_4 concentrations are lower than observed. This is a result of a delayed onset of methanogenesis, likely due to a somewhat overestimated initial $MnO_{2(s)}$ volume fraction.

Data from the Bemidji site suggest that the onset of methanogenesis is delayed in the unsaturated zone compared to the saturated zone. In the saturated zone CH_4 concentrations are elevated in 1986 (Figure 4-11A; Cozzarrelli, unpublished data), while elevated CH_4 concentrations are not observed in the unsaturated zone until 1991 (Figure 4-13; Revesz et al., 1995). An interesting outcome of the simulation is that this delayed
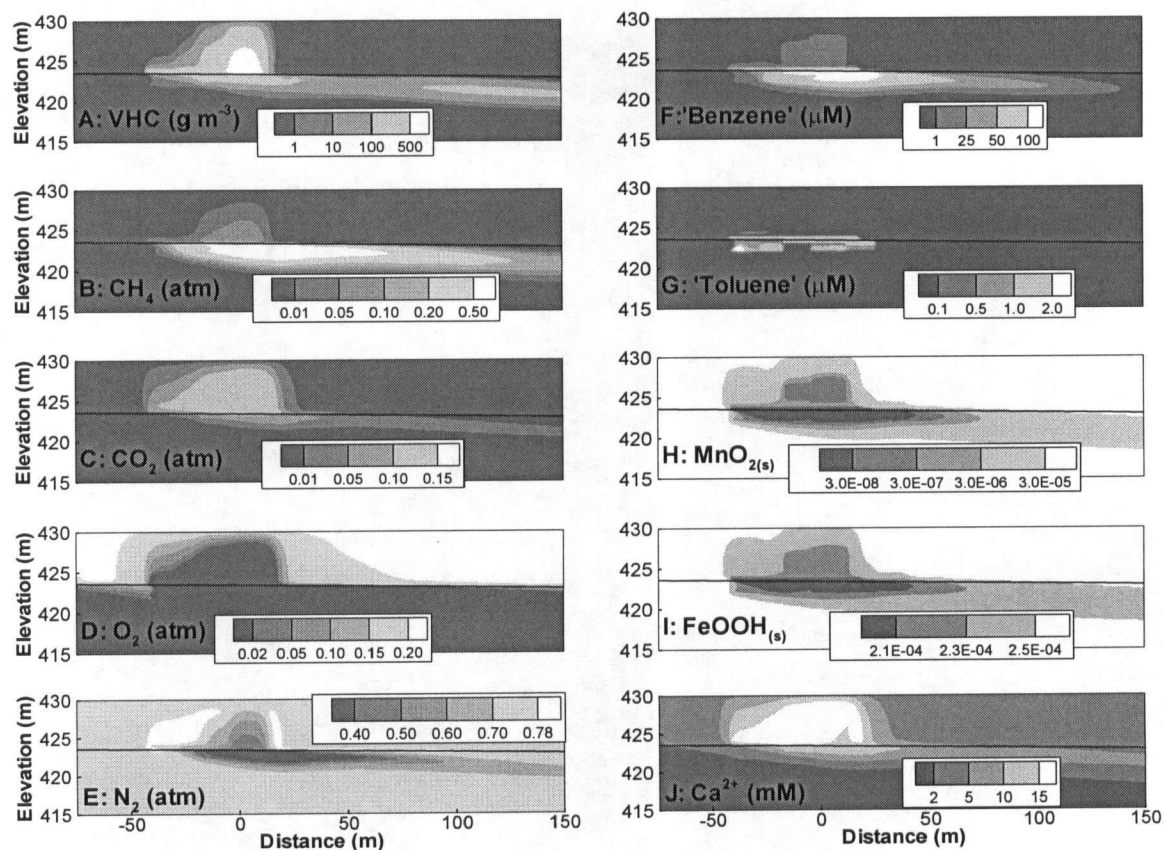
Figure 4-12. 2-D plots of geochemical results at 11 years of simulation time. Distance is from the center of the oil body. VHC refers to volatile hydrocarbons.

159
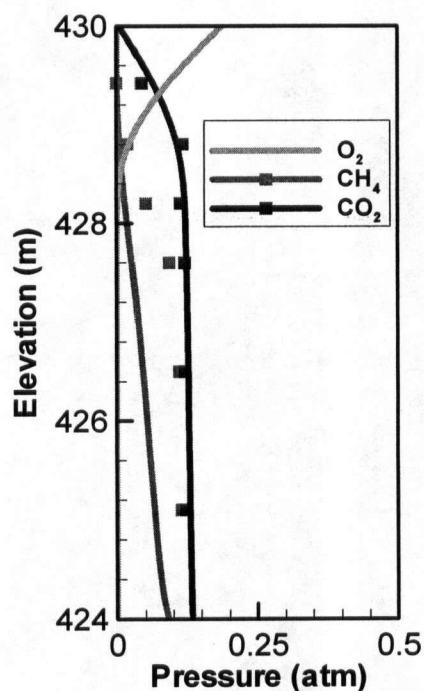
Figure 4-13. 1-D Vapour phase partial gas pressures from 1991 data collected at vapour well 301 (Symbols; Revesz et al., 1995) and simulated data along a vertical transect through the unsaturated zone at 0 m, 11 years simulation time (lines). Vapour well 301 is above the center of the floating oil body.

transition to methanogenesis in the unsaturated zone is accurately reproduced, despite

using similar conceptual models for both zones. In fact, the higher simulated rates of

volatile hydrocarbon dissolution (Table 2, Reaction 17) and methanogenic degradation

(Table 2, Reaction 11-13) used in the unsaturated zone would tend to suggest that

methanogenesis should begin earlier here. Comparison of the simulated 'toluene'

degradation rates at 7 and 11 years (Figure 4-14A and B) shows that not only are the

methanogenic rates higher in the unsaturated zone than in the saturated zone, but also that

the rates in the unsaturated zone are very similar for the two times shown. These data

suggest that the delay in observed high CH_4 concentrations in the unsaturated zone is not

necessarily a result of a delay in the onset of methanogenesis, but rather a function of the

time required for CH_4 to build up in the unsaturated zone and reflects the higher mobility

of gases in the unsaturated zone. This suggests that the build up of CH_4 in the unsaturated

zone is a process that may take several years to develop, despite significant production of

CH_4 at earlier times. A further point to note here is that rates of methanogenesis are

significant well above the water table, at both 7 and 11 years, even though high CH_4

concentrations may not be detected at the same elevation (Figure 4-10B and 4-13). This

example highlights the benefits of this integrated modeling approach that simulates the

evolution of both the saturated and unsaturated zone plumes over time.
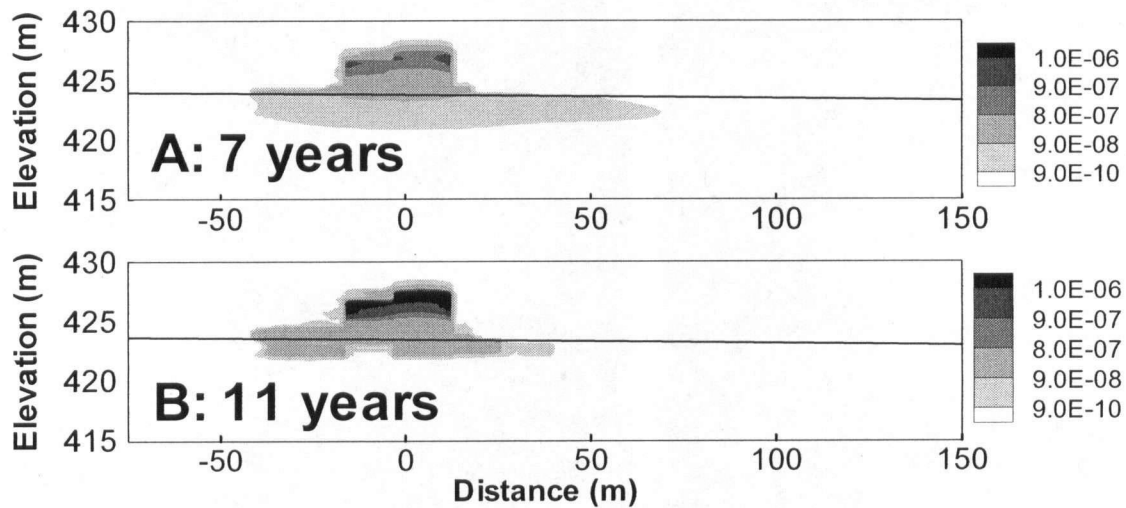
Figure 4-14. Simulated rates of methanogenic 'toluene' degradation (mol L^{-1} s^{-1}) at A) 7 years, and B) 11 years. Note the close spacing of the three highest contours.

The groundwater plume at 11 years simulation time does not change drastically

from that at 7 years. However, at this time the supply of $MnO_{2(s)}$ in the contaminated

portion of the aquifer is nearly depleted (Figure 4-12H) so that methanogenesis and iron

reduction are more prominent degradation pathways, resulting in greater depletion in

$FeOOH_{(s)}$ (Figure 4-12I) and increased CH_4 concentrations (Figure 4-12B). The higher

161

CH$_4$ concentrations have also led to further decreases in the N$_2$ concentrations due to in-situ gas bubble formation. Groundwater geochemistry is compared to the available observed spatial data from 1990 in Figure 4-15. The simulated and observed CH$_4$ and 'benzene' data are in good agreement; however, the simulations under-estimate 'toluene' concentrations. As noted earlier, due to the low concentrations and reactivity of 'toluene', the concentration of this component is difficult to accurately reproduce.
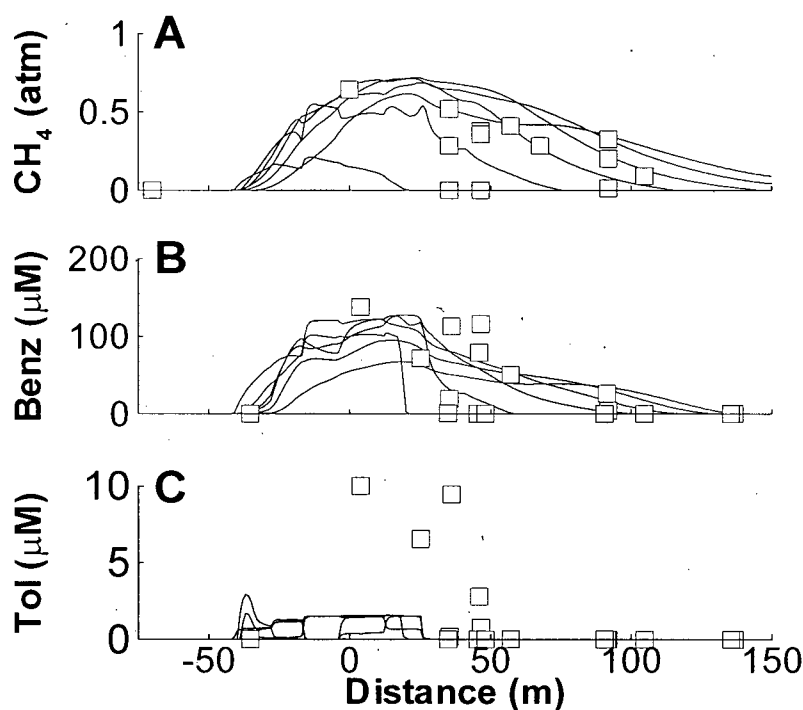
Figure 4-15. Profiles of geochemical constituents along the groundwater flow path for 11 years simulation time (lines) compared to observed data from 1990 for dissolved CH$_4$ (A; Revesz et al., 1995), 'benzene' (B; Essaid et al., 2003) and 'toluene' (C; Essaid et al., 2003). For observed data, 'benzene' and 'toluene' refers to the sum of benzene and ethylbenzene, and the sum of toluene and xylenes, respectively. For simulated data, each line represents a horizontal transect through the model domain as shown by the dashed lines in Figure 4-11J.

4.7.2.3   17 years simulation time

The simulated vadose zone plume at 17 years is similar to that at 11 years (Compare Figures 4-12 and 4-16). The most noticeable differences are the decrease in volatile hydrocarbon concentrations, and increase in CH_4 concentrations, in the core of the plume (Figures 4-16A and B). The increase in CH_4 is due mainly to the build up of gas over time as the rates of methanogenic degradation do not increase between 11 and 17 years (data not shown). Volatile hydrocarbons continue to decrease as they are depleted form the NAPL phase.

The simulated volatile hydrocarbon, CH_4, CO_2 and O_2 plumes reproduce the general character of the observed plumes in 1997 (Figure 4-17; Chaplin et al., 2002). The most noticeable discrepancy is the over-estimation in volatile hydrocarbon concentrations, with simulated concentrations exceeding 300 g m^{-3} (Figure 4-16A), while observed concentration reach a maximum of only 50 g m^{-3}. This discrepancy is again due to the difficulty in representing the array of volatile components in the oil with a single component in the simulations. In general, the simulation reproduces the main processes occurring at this stage of the geochemical evolution at the site, namely the persistence of an anaerobic plume supported mainly through the production of CH_4 (Chaplin et al., 2002).

Previous simulation of unsaturated zone processes at the Bemidji site assumed that all anaerobic degradation was through methanogenesis (Chaplin et al., 2002). Using the unified conceptual model in both the saturated and unsaturated zone, including Mn(IV) and Fe(III) reduction in both zones, as considered here; however, clearly shows that Fe(III) reduction can be an important degradation process in the unsaturated zone,
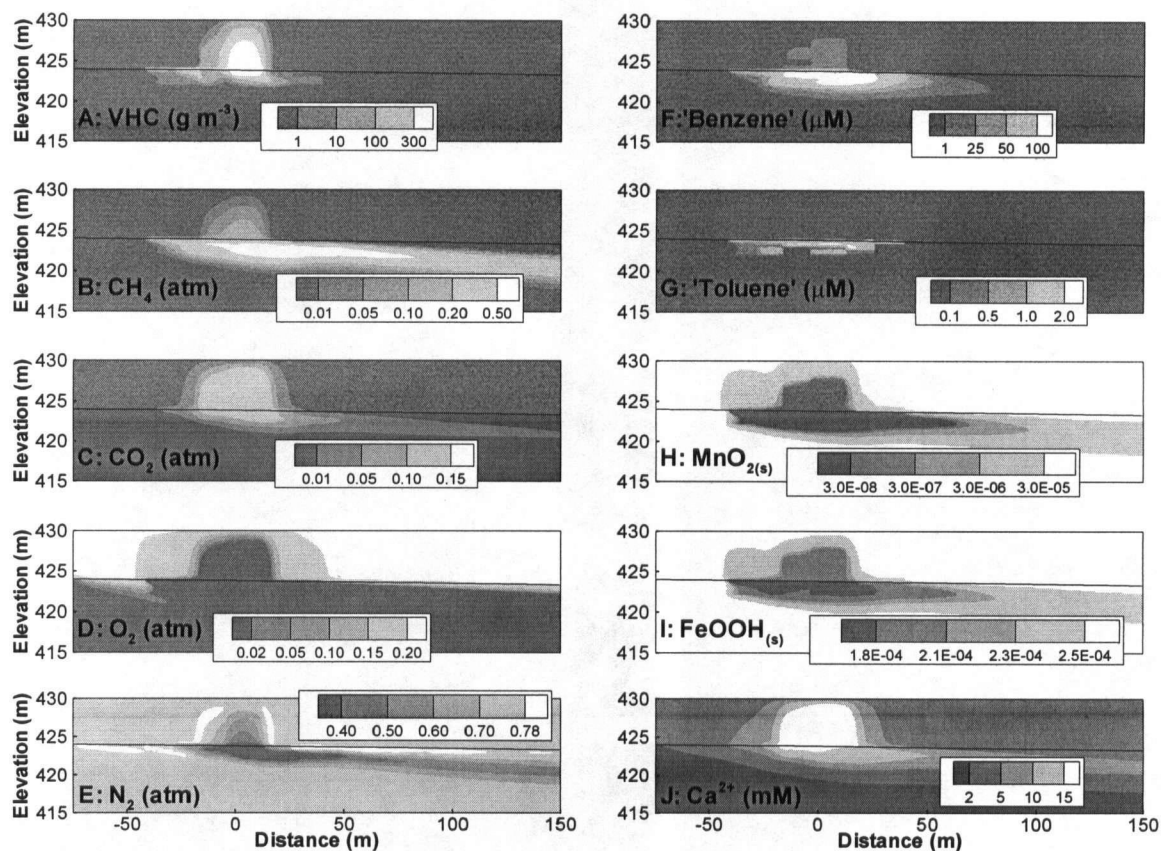
Figure 4-16. 2-D plots of geochemical results at 17 years of simulation time. Distance is from the center of the oil body. VHC refers to volatile hydrocarbons.

164
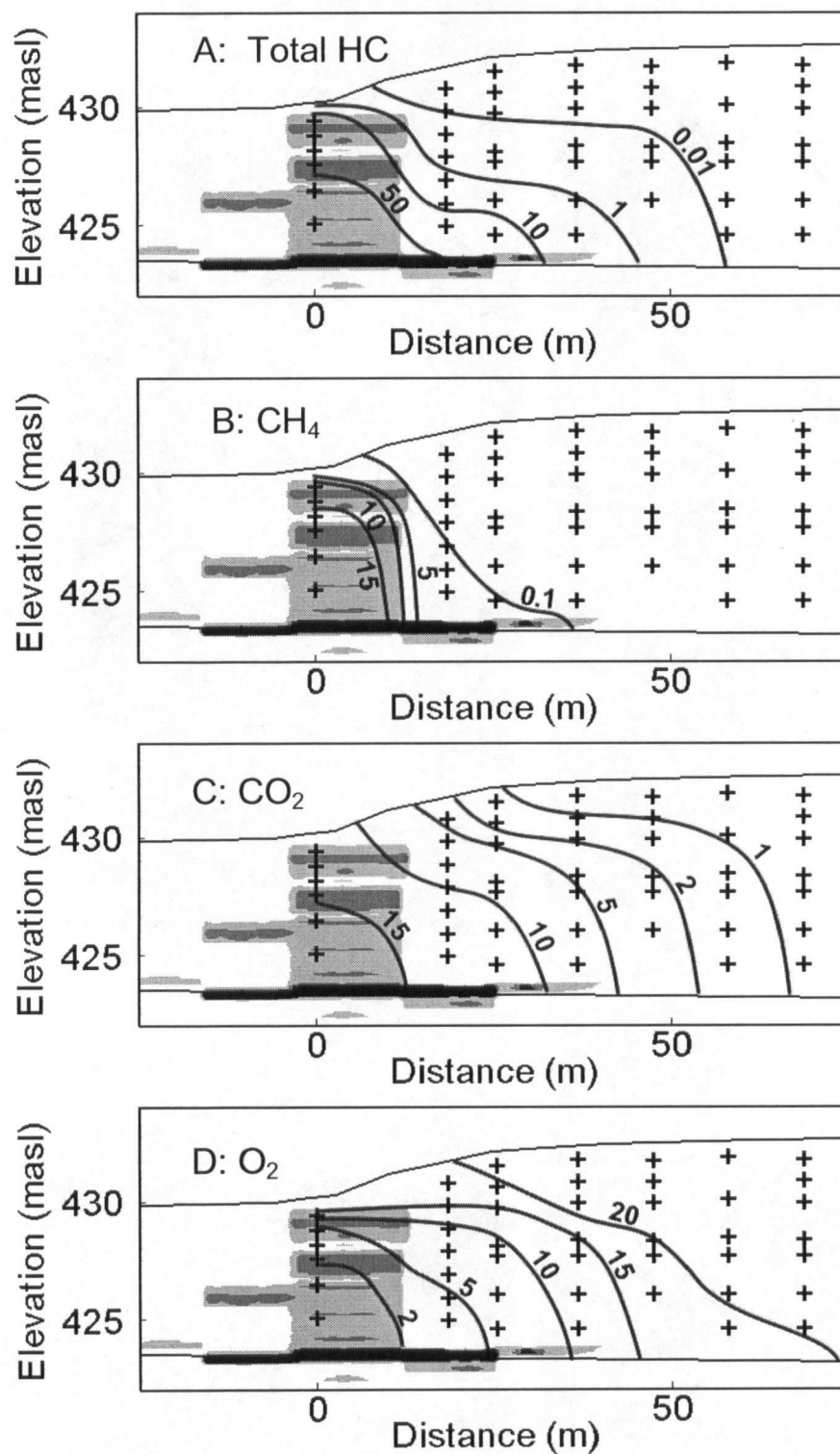
Figure 4-17. Cross sections of unsaturated zone showing contours of vapour phase data collected in 1997. All data is in percent by volume except total hydrocarbons (A) which is in g m-3. Modified from Chaplin et al. (2002). Oil saturation contours, from lightest to darkest, are 0.1, 0.2 and 0.3. Sampling points are marked with '+'.

165

indicated by the depletion in $FeOOH_{(s)}$ above the water table (Figure 4-16I). This conceptual model is consistent with the work of Bekins et al.(1999) who found 10^2 g^{-1} sediment iron reducing microbes in two unsaturated zone samples using MPN analysis. These MPN numbers are above background, but lower than the numbers of methanogens from the same sample, up to 10^4 g^{-1} sediment, suggesting that Fe(III) reduction was less important than methanogenesis at these locations. Data from unsaturated zone lysimeters collected in 2004 (Figure 4-5) showed elevated levels of Fe, again indicating that Fe(III) reduction is a significant degradation process in the unsaturated zone.

The geochemistry of the groundwater plume at 17 years of simulation time has not changed in general character from 11 years (Compare Figures 4-12 and 4-16). However, volatile hydrocarbon concentrations are lower than at 11 years (Figures 4-12A and 4-16A), due mainly to a decreased loading from recharge water as a result of depletion of volatile hydrocarbons in the unsaturated zone. Elevated CH_4 concentrations are migrating further downgradient (note the 0.20 contour in Figures 4-12B and 4-16B), and similarly the depleted N_2 plume is also migrating further (note the 0.50 contour in Figure 4-12E and 4-16E).

At 17 years the volume fraction of $FeOOH_{(s)}$ continues to decrease, with 0.6×10^{-4} moles consumed in the core of the plume. This value is inconsistent with 0.5 M HCl extractions performed on core samples taken from 1993 to 1996 which suggest that solid phase Fe(III) depletion in the core of the plume was equivalent to 2.5×10^{-4} mole of $FeOOH_{(s)}$ (Tuccillo et al., 1999). This discrepancy is potentially a result of inaccurate hydrocarbon dissolution and degradation rates used in the simulations. If so, this indicates that total hydrocarbon degradation through Fe(III) reduction is underestimated in the

simulations by a factor of 5. It is possible that the discrepancy is due to a sampling bias toward sediment more depleted in Fe(III). Given that sediment extractions on a limited sample set cannot accurately capture the inherent heterogeneity of the aquifer, and resulting heterogeneity in mineral dissolution, the magnitude of this discrepancy is not surprising.

Simulated groundwater O_2, 'benzene' and 'toluene' concentrations at 17 years are compared to observed concentrations in 1995 in Figure 4-18. Consistent with previous results, the simulations show a rebound in O_2 concentrations downgradient of the source that is not shown in the field data, simulated 'benzene' concentrations show a reasonably good fit, and 'toluene' concentration are lower than observed (Figure 4-18C). Note that maximum observed 'toluene' concentrations are higher in 1995 than in 1990, while the simulated concentrations remain relatively stable (Figure 4-15C and 4-18C). The change in observed concentrations is potentially a function of sampling bias and not necessarily a change in process rates.

The simulation results at 11 and 17 years suggest that the vadose zone and groundwater plumes are becoming more geochemically stable. Up to 11 years, both the unsaturated and saturated zone plumes are characterized by transitions to more reducing conditions. After this point, the conditions are much more consistent, with both plumes being dominated by a combination of methanogenic and Fe(III) reducing conditions. Bekins et al. (1999) used MPN analysis on core samples collected from 1994 to 1997 to show that on a plume scale, Fe(III) reduction and methanogenesis were occurring concurrently, but on a smaller scale, zones of Fe(III) reducing activity transition to methanogenic activity over time. The simulation cannot capture the small scale details of

these findings but is consistent with the plume scale conceptual model. Based on aqueous Fe^{2+} concentrations Cozzarelli et al., 2001 estimated that the rate of growth for the BTEX plume to be ~3 m yr^{-1}, suggesting that significant solid phase iron exists to retard the plume significantly for an extended period of time. This result has important implications on predictions of source longevity. Specifically, because the geochemistry is not predicted to change drastically, the rates of degradation can also be assumed stable, at least for the compounds simulated, and therefore future degradation can be predicted through extrapolation.
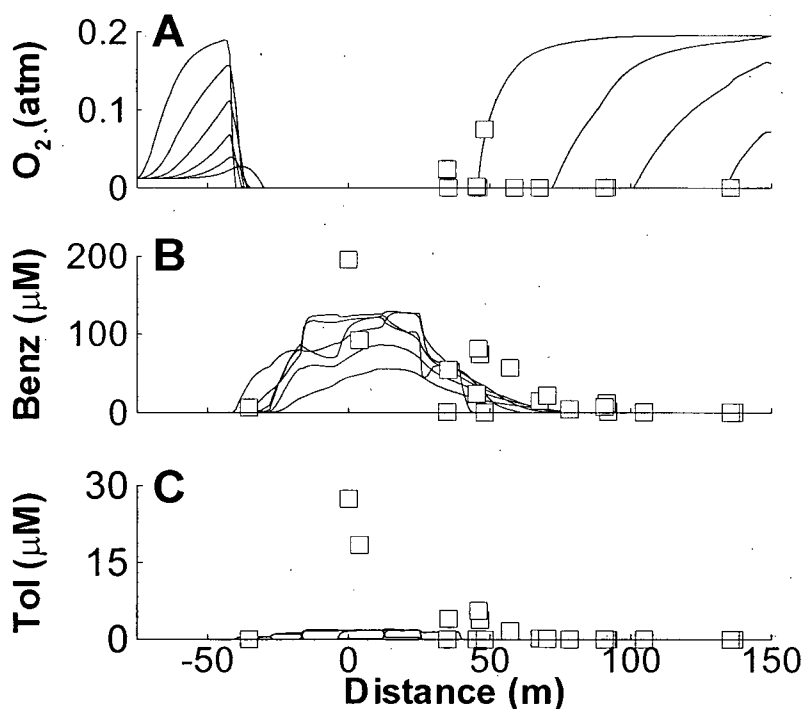
Figure 4-18. Profiles of geochemical constituents along the groundwater flow path for 17 years simulation time (lines) compared to observed data from 1995 for dissolved O_2 (A; Cozzarelli et al., 2001, benzene (B; Essaid et al., 2003) and toluene (C; Essaid et al., 2003). For observed data, 'benzene' and 'toluene' refers to the sum of benzene and ethylbenzene, and the sum of toluene and xylenes, respectively. For simulated data, each line represents a horizontal transect through the model domain as shown by the dashed lines in Figure 4-11J.

4.7.2.4   24 years simulation time

The vadose zone and groundwater plumes at 24 years simulation have not changed significantly from the plumes at 11 years (compare Figures 4-16 and 4-19). Minor changes include the further reduction in volatile hydrocarbon concentrations in the unsaturated zone (Figures 4-16A and 4-19A), a slight retardation of the dissolved N_2 plume in the groundwater (note 0.50 atm contour in Figures 4-16E and 4-19E), and a further decrease in the volume fraction of $FeOOH_{(s)}$ in the core of the unsaturated and saturated zone plumes (Figures 4-16I and 4-19I).

Comparison of the simulated vadose zone gas plumes (Figures 4-19B-E) to observed gas concentrations in 2003 (Figures 4-20A-D; Amos et al., 2005) shows that the simulations compare well with observed data in general character but some discrepancies are noted. As with previous results (i.e. 7 and 17 years), the observed lateral extent of the vadose zone plume is not well reproduced, and the simulated concentration gradients are too sharp (note CO_2 and O_2 plumes in Figures 4-19C-D and 4-20B-C). Also, the CH_4 concentrations reproduced in the unsaturated zone are somewhat too low (see the 0.10 atm contour in Figures 4-19B and 4-20A).

The observed spatial distribution of N_2 concentrations in the unsaturated zone are not well reproduced by the simulations; however the general pattern of simulated N_2 enrichment and depletion is consistent with the observed. Specifically, where CH_4 is produced N_2 concentrations are depleted, and where CH_4 is depleted, due to aerobic oxidation, N_2 is enriched. The simulated magnitude of depletion in the methanogenic zone is somewhat overestimated; simulated concentrations drop below 0.6 atm, while observed concentrations reach a minimum of approximately 0.70 atm. The maximum
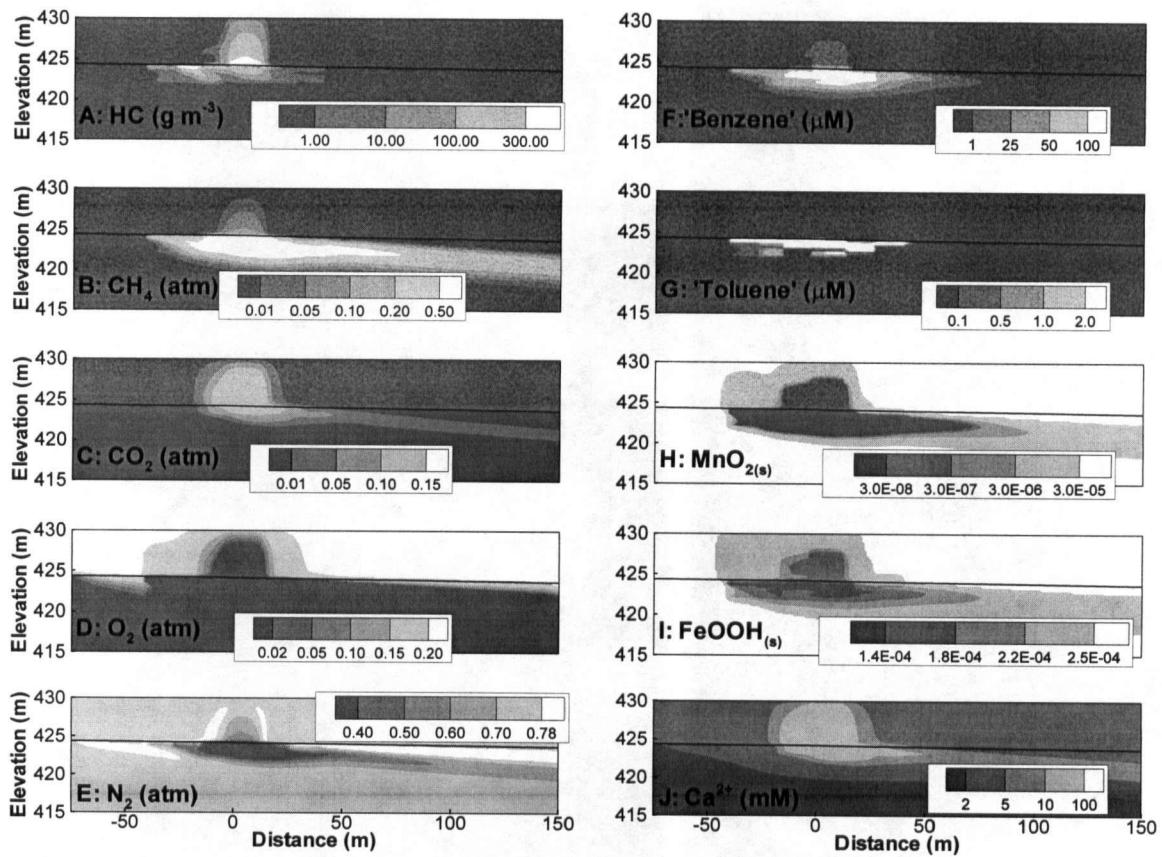
Figure 4-19. 2-D plots of geochemical results at 24 years of simulation time. Distance is from the center of the oil body. VHC refers to volatile hydrocarbons.
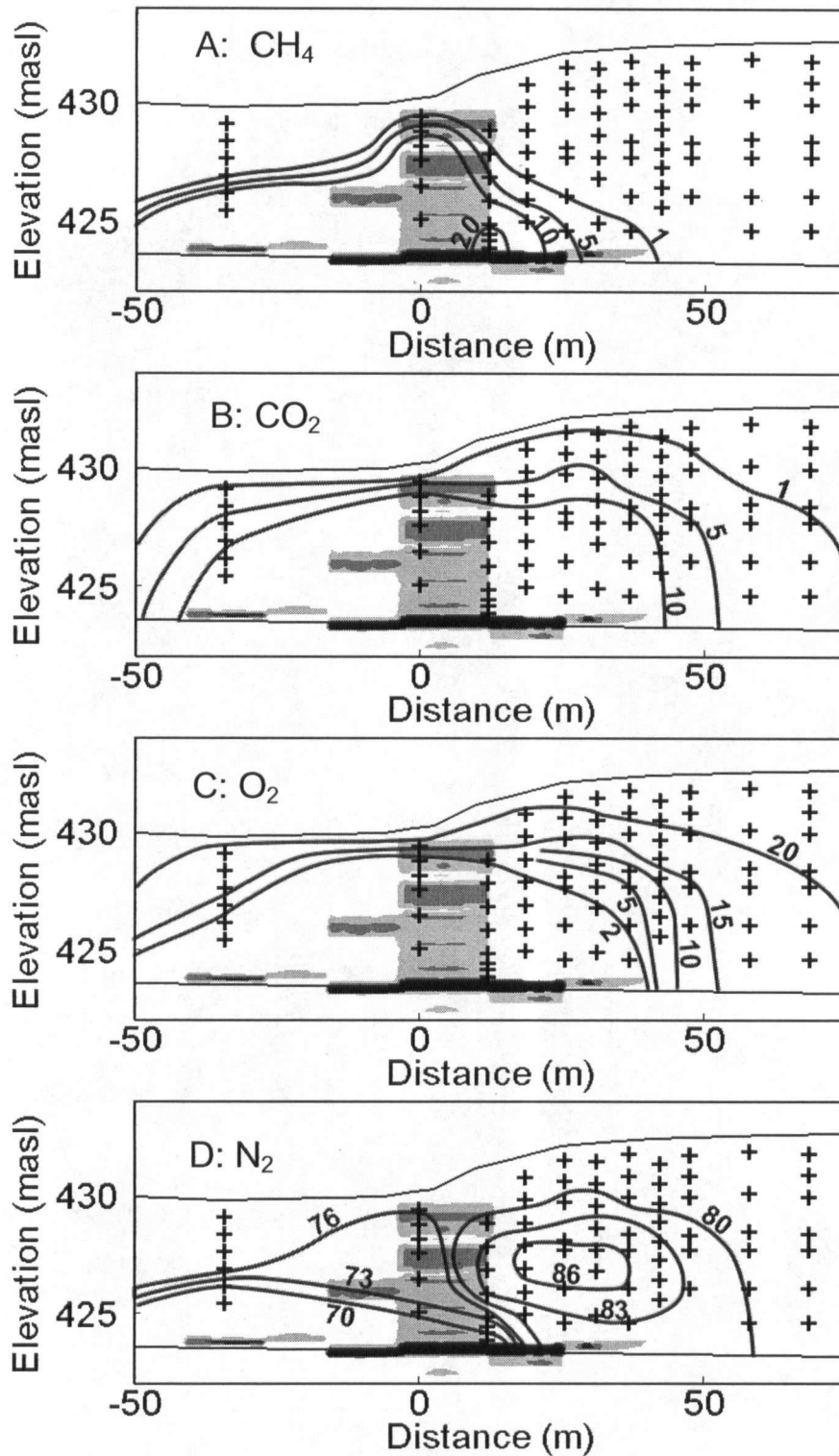
Figure 4-20. Cross sections of unsaturated zone showing contours of vapour phase data collected in 2003. All data is in percent by volume. Modified from Amos et al. (2005). Oil saturation contours, from lightest to darkest, are 0.1, 0.2 and 0.3. Sampling points are marked with '+'.

171

observed enrichments of 0.86 atm, are underestimated by the simulation, which show a maximum concentration of 0.78 atm. Reproducing the detailed pattern of N2 concentrations is difficult without including physical heterogeneity in the model.

Simulated vadose zone pH, alkalinity, and dissolved Ca^{2+} concentrations are compared to observed data from unsaturated zone lysimeters collected in 2004 in Figure 4-21. Similar to saturated zone data (i.e. 7 years and 24 years (shown below)), pH is reasonably well reproduced in the contaminant zone but alkalinity and Ca^{2+} concentrations are overestimated.
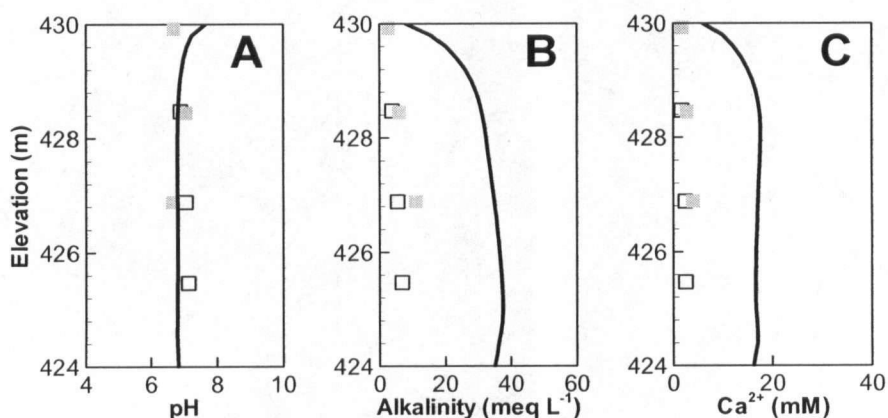
Figure 4-21. 1-D profiles of pH, alkalinity and Ca^{2+} data collected in 2004 at lysimters L9014 (grey squares) and L303 (open squares), and simulated data along a vertical transect through the unsaturated zone at 0 m, 24 years simulation time (black lines). Lysimiters L9014 and L303 are above the floating oil.

Fe^{2+} and Mn^{2+} data collected in lysimeters in 2004 indicate that both Fe(III) and Mn(IV) reduction are degradation pathways in the unsaturated zone (Figure 4-5 and corresponding discussion in Section 4.5.2), and indicate a significant degree of geochemical heterogeneity. This is in contrast to simulation, which shows that Mn(IV) reduction is no longer an important degradation pathway; indicated by the complete depletion of $MnO_{2(s)}$ in the core of the unsaturated zone plume (Figure 4-19H). This

discrepancy illustrates the inability of the simulation to capture small scale heterogeneity; but also highlights the need to consider multiple TEAPs in the unsaturated zone. The assumption that other electron accepting processes are no longer important because CH_4 is present in high concentrations appears flawed.

Simulated saturated zone geochemistry is compared to observed dissolved gas data collected in 2003 (Figures 4-22A-D; Amos et al., 2005), and pH, alkalinity and Ca^{2+} data collected in 2004 (Figures 4-22E-G). In general, the comparison of the observed and simulated data is as expected based on previous results; namely, simulated O_2 concentrations show a rebound downgradient of the source that is not reflected in the field data, pH is reasonably well simulated through the source zone, alkalinity and Ca^{2+} are overestimated by the simulation, and CO_2 partial pressures are accurately simulated.

Of further interest are the simulated and observed CH_4 and N_2 partial pressures. N_2 partial pressures are controlled in the simulations by physical processes. Namely, the depletion of N_2 in the source zone is a result of the formation of gas bubbles, due to CH_4 and CO_2 production, and partitioning of N_2 into the bubbles. The replenishment of N_2 downgradient of the source is partially a result of the hydraulic isolation of the source zone, due to the formation of gas bubble, and interaction of trapped bubbles rich in N_2 near the water table. Also the concentration of N_2 in the recharge water will affect simulated N_2 concentrations. The good match of the simulated and observed data (Figure 4-22D) suggests that the physical processes occurring in the field have been adequately represented in the simulation. This result lends support to the conceptual model of O_2 transport below the water table as a result of bubble entrapment and oxygenated recharge, as is suggested by the simulated rebound in O_2 concentrations noted in Figure 4-22C.
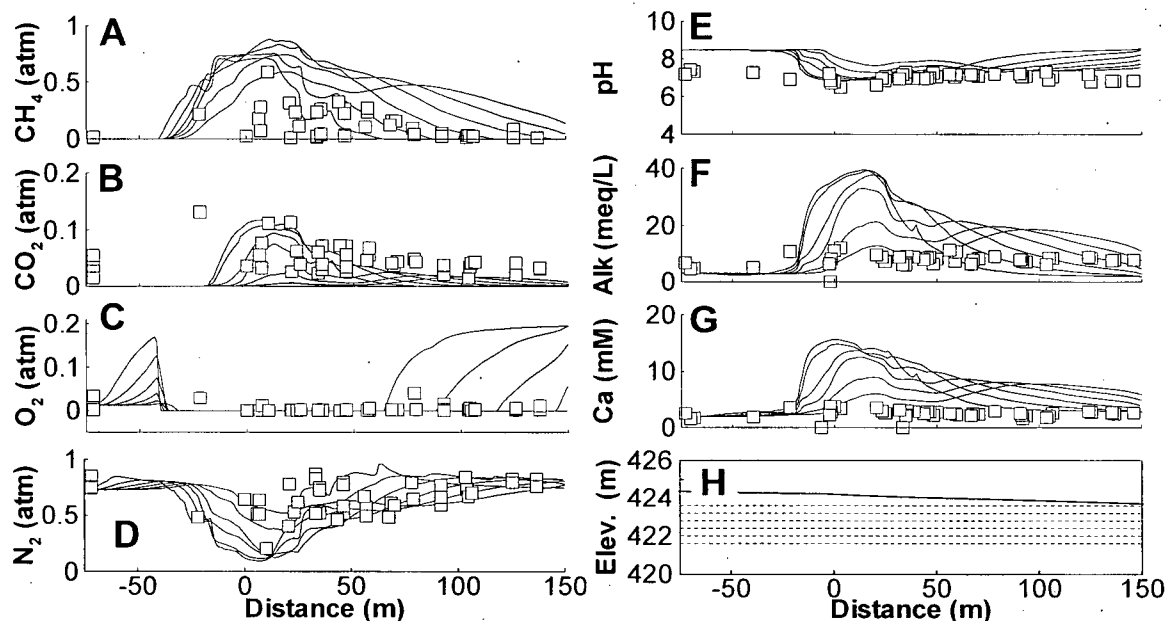
Figure 4-22. Profiles of geochemical constituents along the groundwater flow path for 24 years simulation time (lines) compared to observed data from 2003 for dissolved gases (B-E; Amos et al, 2003), and 2004 for all other data. For observed data, 'benzene' and 'toluene' refers to the sum of benzene and ethylbenzene, and the sum of toluene and xylenes, respectively. For simulated data, each line represents a horizontal transect through the model domain as shown in H.

Simulated CH_4 partial pressures are overestimated in the source zone and the transport of dissolved CH_4 through the downgradient aquifer is also overestimated (Figure 4-22A). In the field, the concentration of CH_4 in the groundwater will potentially be controlled by a number of processes, including the production of CH_4 and formation of gas bubbles in the source zone, the concentration of CH_4 in the recharge water and the rate of recharge, and also the entrapment of gas bubble near the water table and the O_2 concentration in those bubbles. Each of these processes is included in the simulation, and constrained by the field data. The discrepancy in observed and simulated data therefore suggests that the conceptual model used in the simulation is incomplete. It is difficult to

174

speculate on the reasons for the discrepancy; however, processes that could potentially affect dissolved CH_4 concentrations that have not been included in the simulation include, gas bubble ebullition from the source zone (Amos et al., 2006b), or the oxidation of CH_4 by an electron acceptor other than O_2 (Raghoebarsing et al., 2006).

This analysis of CH_4 production and transport demonstrates an advantage of integrated saturated and unsaturated zone modeling. Previous models of the groundwater at the Bemidji site (i.e. Essaid et al., 1995; 2003), and analysis of the effects of bubble formation and entrapment on geochemistry (Amos and Mayer 2006a), have made assumptions about the water table boundary and have speculated on the affects of those assumptions. Although we have not been able to reproduce the dissolved CH_4 plume with complete accuracy, more of the relevant processes have been included, removing some of the speculation and uncertainty.

4.7.3   Dynamic water table hydrology and geochemistry

A primary advantage of the integrated modeling approach is the dynamic treatment of the water table from both a hydrological and geochemical standpoint. There are two main advantages of this approach. Firstly, transient conditions at the water table, including water level fluctuations and chemical changes, make using the water table as a boundary condition for simulating either saturated or unsaturated zone processes difficult. By including both the saturated and unsaturated zones in the simulations, appropriate boundary conditions are much easier to simulate and become more realistic (Figure 4-8). Essaid et al. (1995) simulated the geochemical evolution in the saturated zone at the Bemidji site using a spatially variable recharge boundary, assuming no O_2 above the source zone, but noted that neglecting spatially and temporally variable CH_4

concentrations in the recharge water may have lead to inaccuracies in their simulated CH_4 plume. Similarly, Amos and Mayer (2006a) simulated bubble entrapment near the water table, but were unable to adequately represent the spatial and temporal variability in the composition of the entrapped bubbles, leading to potential inaccuracies in the demonstrated effect of trapped bubbles on the groundwater plume. Here we have been able to reasonably simulate unsaturated zone geochemistry so that spatial and temporal variations in the composition of recharge water and entrapped bubbles have been taken into account. The benefits of this approach, specifically in relation to the simulation of dissolved CH_4 concentrations, were discussed in the previous section.

A second advantage of simulating the water table within the model domain is that water table elevation can be determined dynamically based on prevailing hydrological conditions. In the simulation we were able to qualitatively reproduce the observed water table fluctuations based on scaling measured precipitation rates with the known ratio of average precipitation to average recharge. This allows for a more realistic representation of processes occurring near the water table and within the capillary fringe. Specifically, this includes the entrapment of gas bubbles near the water table as a result of water table rise, and release of gas bubbles formed in the saturated zone, into the unsaturated zone, upon a decrease in water table elevation. Both of these processes can change the hydrological and geochemical conditions near the water table and affect contaminant transport.

4.7.4 Sequential TEAPs in the unsaturated zone.

A significant difference between the simulation presented here and previous work is that the spatial and temporal evolution of unsaturated zone chemistry is explicitly

considered, including the sequential use of TEAPs, consisting of aerobic oxidation, Mn(IV) reduction, Fe(III) reduction and methanogenesis. Although this evolution is not well constrained by field data in the unsaturated zone, the simulations provide insights into the relevant processes. The simulations have shown; that the initial composition of the oil, specifically the high fraction of volatile components, is essential in forming and maintaining an anaerobic plume; that the delay in elevated CH_4 concentrations observed in the unsaturated zone compared to the saturated zone, is due to the higher rate of gas transport in the unsaturated zone; and that methanogenic degradation within the residual oil retained above the water table may be a significant process, despite concentration profiles that may suggest otherwise.

The sequential use of TEAPs is a well proven conceptual model in the saturated zone at Bemidji (Bennett et al., 1993; Baedecker et al., 1993; Revesz et al., 1995; Bekins et al., 1999; Cozzarelli et al., 2001; Bekins et al., 2001), but investigation of unsaturated zone processes have focussed on aerobic oxidation and methanogenesis as degradation pathways (Chaplin et al., 2002; Amos et al. 2005), although there is some evidence of Fe(III) reduction (Bekins et al., 2001). In the simulation presented here, the transition to methanogenic activity observed in the field was reasonably reproduced in both the saturated and unsaturated zones using a similar conceptual model for both zones, including aerobic oxidation, Mn(IV) reduction, Fe(III) reduction and methanogenesis, with only minor adjustments. This result highlights a benefit of using an integrated modeling approach, in that saturated and unsaturated zone conceptual models can be compared and significant differences in processes between the zones can be isolated. In this simulation the only major difference in saturated and unsaturated zone processes

needed to reproduce the observed geochemistry was a higher rate of methanogenesis in the unsaturated zone.

4.7.5 Gas Bubble formation and entrapment

An important difference between the current modelling study and previous studies is the incorporation of bubble formation due to in-situ gas production and bubble entrapment due to water table rise. These processes dramatically change the hydrogeology of the site and contribute to attenuation of the contaminants. Previous field and modeling studies at the site have suggested that degassing due to biogenic CH_4 and CO_2 production is occurring at the site (Baedecker et al., 1993; Essaid et al., 1995; Curtis et al., 1999). While previous studies have attempted to quantify the effects of degassing on the mass balance of CH_4 and CO_2, they have not constrained the results with independent data, i.e. stable gas concentrations, or attempted to quantify the effects of bubble formation on groundwater flow.

In this study we have used N_2 concentrations to constrain the degree of bubble formation as well as the effects of bubble formation on permeability, and the degree of bubble entrapment near the water table. In the source zone the primary control on N_2 is the formation of gas bubbles due to in-situ gas production. Thus, the observed depletion in N_2 concentrations provide a good constraint of the degree of gas bubble formation, allowing the amount of reactive gases partitioned into the bubbles (Equations 5-7), and the effect on permeability (Equation 1), to be estimated. Downgradient of the source, the N_2 concentrations will be controlled by the flow of groundwater depleted in N_2 out of the source zone, and potentially the interaction with bubbles trapped near the water table as a result of water table fluctuations. Amos and Mayer (2006a) showed that both of these

178

processes can be important in controlling the downgradient N_2 concentrations at the Bemidji site. The good match of simulated and observed N_2 concentrations suggest that these processes have been adequately represented in the simulation (Figure 4-11 and 4-21). Note that measure Ar concentration in 2002 and 2003 showed similar trends to N_2 concentrations, in terms of % depletion, so that N_2 can be viewed as a conservative component in this system.

The effect of bubble formation on groundwater flow in the simulations is demonstrated in Figure 4-23. Initially, i.e. before 7 years, the rate of methanogenesis in the groundwater is low so that the production of gas bubbles is minimal (Figure 4-23A), and the groundwater tends to flow more or less horizontally through the source zone and groundwater plume (Figure 4-23E). As methanogenesis rates increase, and time passes, the accumulation of gas bubbles increases (Figures 4-23B-D) resulting in groundwater flow being deflected around the source zone where gas bubble generation is most pronounced (Figures 4-23F-H). In the simulations, this hydraulic isolation of the source zone leads to decreased loading of contaminants from the source zone to the downgradient aquifer, providing a physical means of attenuation.

The entrapment of gas bubbles near the water table can lead to the introduction of O_2 into the saturated zone downgradient of the source zone, as is demonstrated by the simulations (i.e. Figures 4-11, 4-18 and 4-22). This can result in aerobic degradation of CH_4 and organic contaminants. Because 'toluene' is readily degraded anaerobically this

179
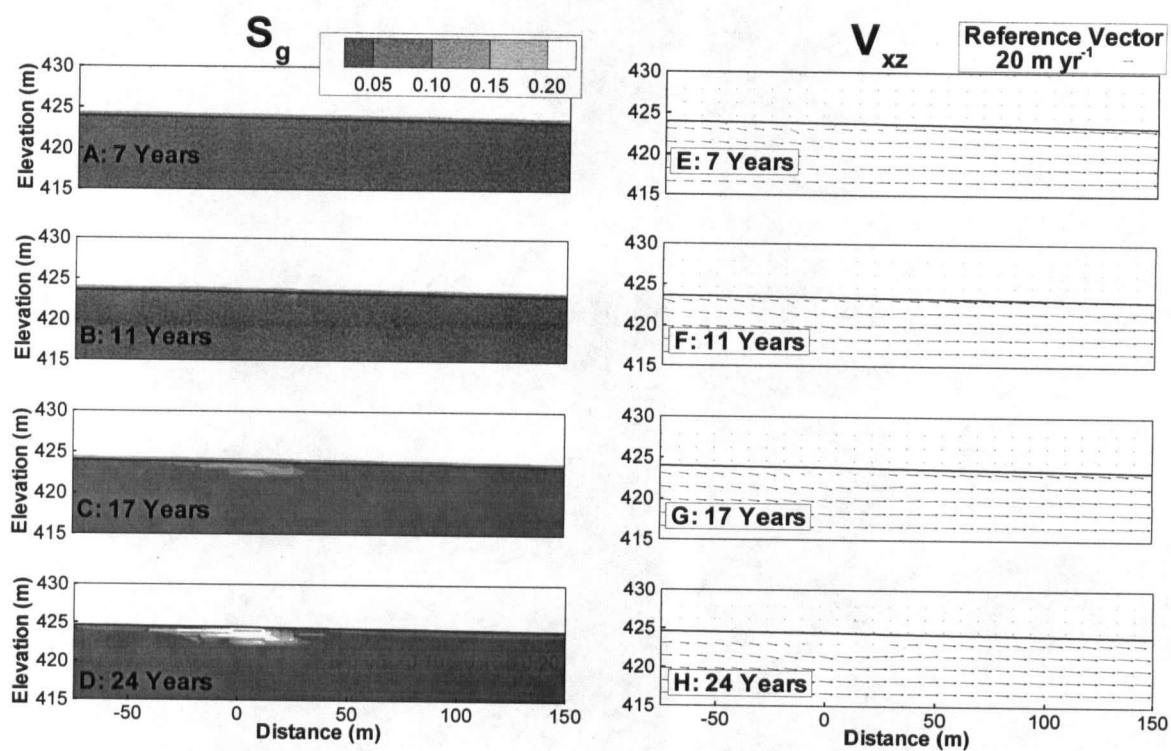
Figure 4-23. 2-D plots of simulated gas phase saturation (S_g) and groundwater velocities (V_{xz}) at 7, 11, 17 and 24 years. Distance is from the center of the oil body.

plume does not extend far into the downgradient aquifer. On the other hand, the simulated 'benzene' plume generally extends over 100 m downgradient of the center of the source zone (Figures 4-9, 4-12, 4-16 and 4-19). Figure 4-24 shows the aerobic degradation of CH_4 and 'benzene' throughout the simulations. Note that throughout the simulations both these components are degraded aerobically near the water table. Essaid et al. (2003) noted temporal variations in benzene concentrations of up to 90 μM in a well screened across the water table 46 m downgradient from the center of the source zone. They attempted to reproduce the variability in concentrations based on changes in flow pattern and dilution effects due to water table fluctuations, but were unable to do so. They noted that the fluctuation in water table would likely result in changes in redox conditions that could explain the observed variability. The results shown here are consistent with this conceptual model and offer an explanation for the changes in benzene concentrations. Note that between 11 and 17 years the simulated 'benzene' plume shortened, but that the highest concentration contour extends further downgradient, demonstrating the variability in 'benzene' concentrations due partially as a result aerobic oxidation near the water table. We must note; however, that while the agreement between simulated and observed N_2 partial pressures suggests that bubble entrapment is occurring in the field, the enrichment of O_2 in the groundwater due to this process cannot be verified with field data. Therefore, we emphasize that the aerobic oxidation of CH_4 and 'benzene', as suggest by the simulations, is a possible but unproven hypothesis.

4.7.6   Implications for Source Longevity

The simulation presented here gives an assessment of hydrocarbon degradation through multiple pathways over the 24 year history of the Bemidji oil spill site, and

181
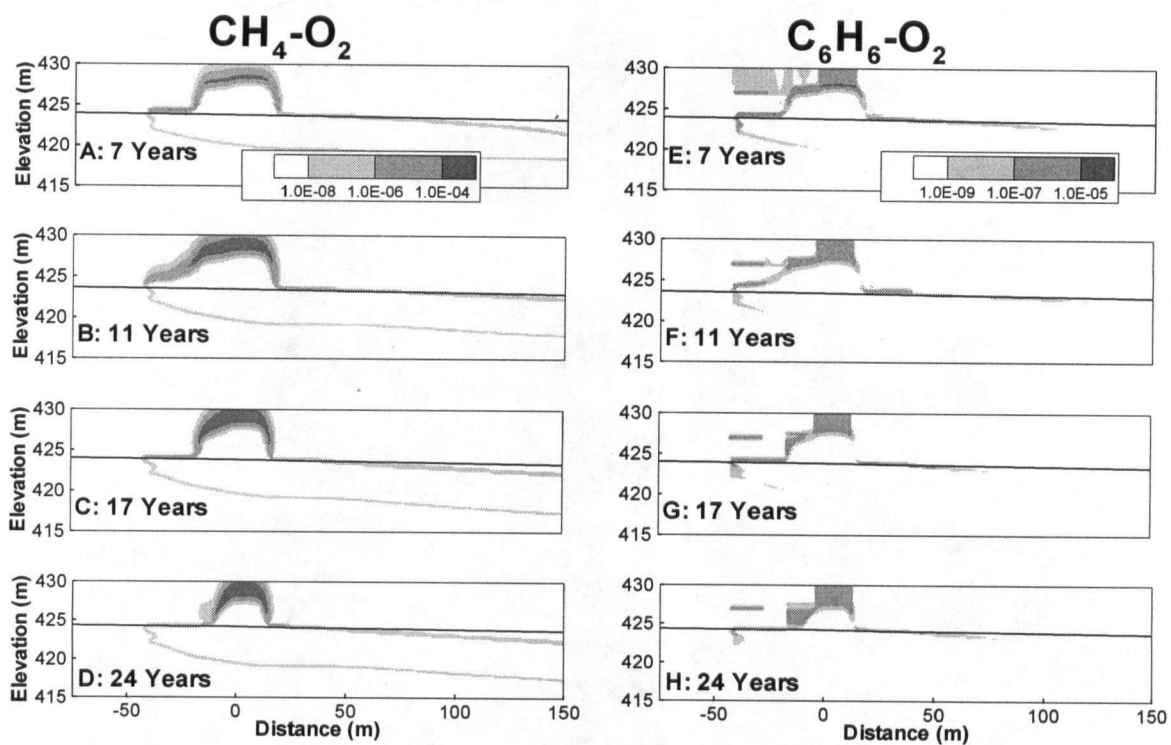
Figure 4-24. 2-D plots of simulated aerobic degradation rates for CH_4 and C_6H_6 at 7, 11, 7 and 24 years. Distance is from the center of the oil body.

includes both saturated and unsaturated zone degradation processes, as well as volatilization in the unsaturated zone. The simulation shows that for the three compounds simulated, after 24 years, 19% of the 'benzene', 6% of the 'toluene' and 48% of the 'butane' has been removed from the source. By simple linear extrapolation this would suggest that BTEX compound could persist in the oil for up to 400 years. It is difficult to extrapolate 'butane' loss since the majority of the initial loss is through volatilization in the unsaturated zone, which has slowed considerably over time.

This estimate is consistent with that of Essaid et al. (2003) who used inverse modeling to determine that 18 years after the spill 10.2% of benzene, 8.6% of toluene, 1.2% of ethylbenzene, 1.4% of *m,p*-xylene and 2.7% of *o*-xylene had been removed from the oil body. Their simulations included saturated zone processes only.

Based on 1990 1-D carbon flux calculations horizontally through the saturated source zone and vertically above the floating oil, Revesz et al. (1995) estimated the life expectancy of the source to be 110 years, but acknowledge that this is a minimum estimate since the more volatile and reactive components will slow down with time. This estimate is not directly comparable with our estimate because Revesz et al. (1995) accounted for the entire oil mass while we only consider the BTEX compounds and volatile alkanes. Similarly, Chaplin et al. (2002) used 1-D gas flux modeling to estimate that unsaturated zone volatilization and degradation in 1997 accounted for 0.2% yr^{-1} of the original total oil mass. If mass removal continued at a similar rate the entire source would be removed in 500 years. Both these estimates predict much faster source removal than the estimate provided by the simulation presented here, since they predict removal of the entire source within 110-500 years while our estimate suggest that over 400 years is

required to remove BTEX compounds, which make up only a small fraction of the original oil. These results suggest that the 1-D carbon flux estimates are optimistic predictions.

4.7.7 Uniqueness, uncertainty and model limitations

The simulated geochemistry is quite complex and given the number of parameters and the interaction of numerous geochemical reactions, it is difficult to claim that the simulations provide a unique solution to the geochemical evolution observed in the field. A more rigorous sensitivity analysis of the various parameters is warranted; however, given the complexity of the model and the long simulation times, typical model runs took 3-4 weeks to complete, a thorough sensitivity analysis is prohibitive. However, considering the wealth of spatial and temporal data, and the reasonably good fit of the simulations to the data, we can be confident that the simulations capture the major geochemical processes occurring at the site and offer insights into the controlling factors.

A limitation of the MIN3P model that becomes apparent in these simulations is that it is a single phase model, meaning that the primary unknowns are considered in the aqueous phase only. This has several implications on the simulations, including an immobile NAPL phase, no advective gas flux, and an imprecise representation of volatilization in the unsaturated zone. In general, the free phase NAPL floating on the water table or suspended in residual saturation in the unsaturated zone does not appear to have moved a significant distance laterally since the time of the spill. However, the observed fluctuations in the water table will likely cause similar fluctuation in the horizontal position of the floating oil and potentially lead to smearing and enhanced volatilization or degradation in the smear zone. This process is not reproduced by the

184

model. In addition, the fluctuating water table in the simulations causes the water table to move around the NAPL phase so that the amount of NAPL exposed to dissolution varies with time.

Neglecting the advective gas flux term has likely led to an underestimation of gas fluxes and as a consequence, possibly aerobic degradation rate in the unsaturated zone may also have been underestimated. The magnitude of this uncertainty is not well defined; however, analytical calculations comparing diffusive and advective CH_4 fluxes based on a 1-D transect suggest that the diffusive fluxes are more important (Amos et al., 2005). At earlier times when volatile hydrocarbons are more abundant, gas advection may have played a more important role.

Because MIN3P does not explicitly simulate volatilization, to reproduce the high observed hydrocarbon concentrations (Hult and Grabbe, 1988, Figure 4-10) in the unsaturated zone, 'butane' dissolution rates were set to four orders of magnitude above those in the saturated zone (Table 4-2, Reaction 17). This formulation will potentially overestimate hydrocarbon concentration in recharge water and therefore hydrocarbon loading to the saturated zone.

In these simulations we have focused on the volatile and soluble components of the oil, namely short chain alkanes and BTEX compounds, and have assumed the remainder of the oil to be non-degradable. However, Bekins et al. (2005) showed that longer straight chain n-alkanes, C10 to C25, will also degrade under methanogenic conditions, and furthermore, these compounds are partially or almost completely depleted from the majority of the oil samples extracted from the sediment throughout the source zone. It is unclear what fraction of the oil is made up of these compounds; however, the

185

potential exists for the degradation of these compounds to influence the geochemistry of the site to a more significant degree than has been included in these simulations. If these compounds do make up a significant fraction of the oil then we may have underestimated the total amount of CH_4 production, or overestimated the degradation of other compounds through methanogenesis.

The simulation shows a significant amount of gas production in the methanogenic zone beneath the floating oil, resulting in a gas phase saturation of up to 0.20. Studies of ebullition in column experiments (Amos and Mayer, 2006b) showed that in medium grained sand significant ebullition occurs when gas phase saturations exceed 0.20, and that maximum gas phase saturation is ~ 0.30. These experiments and the high gas phase saturations suggested by the modeling indicate that ebullition may be an important process at the Bemidji site. Ebullition would reduce the predicted gas phase saturations, limiting the permeability effects induced by the formation of the gas phase below the water table, and create a flux of CH_4 and CO_2 to the unsaturated zone from the saturated zone. Amos and Mayer (2006b) have modeled ebullition using an empirical formulation in a modified version of the reactive transport model MIN3P; however, the formulation is unproven in real geological media and use of it would be speculative in the current modeling study.

4.8 Summary and Conclusions

The modeling study presented here has provided a comprehensive simulation of the geochemical evolution of natural attenuation processes at the Bemidji oil spill site, including volatilization, aerobic oxidation, Mn(IV) reduction, Fe(III) reduction, and methanogenesis in both the saturated and unsaturated zones. Furthermore, the simulation

186

spans the timeframe from the time of the spill, 1979, until recent time, 2003. This approach has provided additional insights into the geochemical evolution at the site, allowed for a more complete analysis of hydrocarbon degradation at the site and over time, and highlighted the strengths and weaknesses of modeling this degree of complexity using reactive transport models.

The conceptual model used in this modeling effort has included fundamental enhancements over previous modeling studies at this site, and over reactive transport modeling of contaminated sites in general. These include; integration of saturated and unsaturated zone processes into a single model, explicit simulation of the evolution of unsaturated zone degradation processes, and incorporation of gas bubble formation and entrapment.

The integration of saturated and unsaturated zone processes has provided a more complete representation of the geochemical evolution of the site, reducing the uncertainty due to estimating spatially and temporally variable geochemical conditions at the water table, and offered a comparison between saturated and unsaturated zone degradation processes. Specifically, the simulation showed that saturated and unsaturated zone processes could be simulated using a conceptual model that is fundamentally the same in both zones. This result has important implications for future work in that unsaturated and saturated zone processes can be simulated in an integrated manner, without adding additional complexity. Moreover, using such an approach could allow for more subtle differences in biochemical controls between the zones, such as the availability of nutrients, to be investigated.

The detailed representation of unsaturated zone degradation processes and the sequential use of TEAPs have provided addition insights into the geochemical evolution of the sight. The simulation suggests that in the early stages of plume development, volatilization is an important process, not only in terms of a hydrocarbon loss mechanism, but also in terms of developing an anaerobic plume that later transitions to methanogenic activity. Comparison of simulated methanogenic rates and CH_4 concentrations suggest that the observed CH_4 concentration profiles through the unsaturated zone do not give a good indication of the spatial or temporal distribution of degradation rates. Simulation of the geochemical evolution over time suggests that the observed CH_4 build up in the unsaturated zone may take years to develop. Simulating the evolution of TEAPs, including aerobic oxidation, Mn(IV) reduction, Fe(III) reduction and methanogenesis, showed that this conceptual model provides a plausible representation of unsaturated zone degradation processes and provides motivation for further investigation of Mn(IV) reduction and Fe(III) reduction in the unsaturated zone.

This simulation has included bubble formation below the water table due to in-situ gas production, bubble entrapment near the water table due to water table fluctuations, and permeability effects due to trapped bubbles. Each of these physical processes has implications on geochemistry, including providing a sink for CH_4 and other gases, restricting the flow of highly contaminated water from the source zone, and potentially introducing O_2 into the aquifer. The good agreement between simulated and observed N_2 data suggests that these physical processes have been reasonably well represented in the simulation, and therefore, provides confidence in the representation of

geochemical processes also. Including these processes in the simulation suggests that the observed CH_4 plume is affected by additional processes not included in the simulation.

The degradation of hydrocarbons and geochemical evolution in the saturated and unsaturated zones is simulated starting at the time of the spill up to present day conditions. The extent of this simulation, from both a spatial and temporal point of view, has not been previously accomplished, and provides a more integrated estimate of total mass removal from the source than previous estimates, which have included only saturated or unsaturated zone processes, or have considered limited timeframes or snapshots in time. The simulation estimates that after 24 years, 19% of the 'benzene', 6% of the 'toluene' and 48% of the 'butane' has been removed from the source.

This integrated modeling approach has distinct limitations in that various assumptions and simplifications were necessary to either accommodate the abilities of the model or reduce the CPU requirements of the simulations. Furthermore, interpretation of the results can be difficult when detailed geochemical processes are incorporated into such a broad spatial and temporal scale. The Bemidji site has been thoroughly investigated for over 20 years, including field and modeling studies in both the saturated and unsaturated zones. This previous work has provided significant data and insights into the relevant geochemical processes, and has made the modeling work presented in this study feasible. Furthermore, given the extensive research previously done, a more comprehensive modeling study was warranted to integrate the available data and test the validity of the conceptual model. Under these circumstances a modeling effort of this complexity has been a useful endeavour. However, given that most contaminated sites do

not have the same degree of available data, it is likely that more narrowly defined

modeling studies, would offer greater insights into the relevant geochemical processes.

4.9 Acknowledgements

4.10 References

Allison, J. D., Brown, D. S., Novo-Gradac, K. J. (1991), MINTEQA2/PRODEFA2, A geochemical assessment model for environmental systems: Version 3.0 Users's Manual, U.S Environmental Protection Agency: Washington, DC, 1991, EPA/600/3-91/021.

Amos, R.T., Mayer, K.U., Bekins, B.A., Delin, G.N., Williams, R.L. (2005), Use of dissolved and vapor-phase gases to investigate methanogenic degradation of petroleum hydrocarbon contamination in the subsurface, *Water Resour. Res.*, *41*, W02001, doi:10.1029/2004WR003433.

Amos, R. T., Mayer, K. U. (2006a), Investigating the Role of Gas Bubble Formation and Entrapment in Contaminated Aquifers: Reactive Transport Modelling. *J. Contam. Hydrol.*, *in press*, 47 pages.

Amos, R.T., Mayer, K.U. (2006b), Investigating Ebullition in a Sand Column Using Dissolved Gas Analysis and Reactive Transport Modeling. *Submitted to Environ. Sci. Technol.*, May 2006, 19 pages.

Baedecker, M.J., Cozzarelli, I.M., Evans, J.R., Hearn, P.P. (1992), Authigenic mineral formation in aquifers rich in organic material, in Kharaka, Y.K., and Maest, A.S., eds., Proceedings of the 7th International Symposium on Water-Rock Interaction, Park City, Utah, July 9-23, 1992: A.A. Balkema, Rotterdam, 257-261.

Baedecker, M.J., Cozzarelli, I.M., Eganhouse, R.P., Siegel, D.I., Bennett, P.C. (1993), Crude oil in a shallow sand and gravel aquifer - III. Biogeochemical reactions and mass balance modeling in anoxic groundwater, *Appl. Geochem.*, *8*, 569-586.

Bekins, B.A., Godsy, E.M., Warren, E. (1999), Distribution of microbial physiologic types in an aquifer contaminated by crude oil, *Microbial Ecology*, *37*, 263-275.

Bekins, B.A., Cozzarelli, I.M., Godsy, E.M., Warren, E., Essaid, H.I. Tuccillo, M.E. (2001), Progression of natural attenuation processes at a crude oil spill site: II: Controls on spatial distribution of microbial populations, *J. Contam. Hydrol.*, *53*, 387-406.

Bekins, B.A., Hostettler, F.D., Herkelrath, W.N., Delin, G.N., Warren, E., Essaid, H.I. (2005), Progression of methanogenic degradation of crude oil in the subsurface. *Environ. Geosci*, *12*, 139-152.

Bennett, P.C., Siegel, D.E., Baedecker, M.J., and Hult, M.F. (1993), Crude oil in a shallow sand and gravel aquifer – I. Hydrogeology and inorganic geochemistry, *Appl. Geochem.*, *8*, 529-549.

Bilir, S.H. (1992), Hydrogeologic characterization of a glacial aquifer contaminated by crude oil near Bemidji, Minnesota, M.A. thesis, The University of Texas at Austin.

Chaplin, B.P., Delin, G.N., Baker, R.J., Lahvis, M.K. (2002), Long-term evolution of biodegradation and volatilization rates in a crude oil-contaminated aquifer, *Bioremediation Journal*, *6*, 237-255.

Cozzarelli, I.M., Eganhouse, R.P., Baedecker, M.J. (1990), Transformation of monoaromatic hydrocarbons to organic acids in anoxic groundwater environment, *Environ. Geol. Water Sci.*, *16*, 135-141.

Cozzarelli, I.M., Bekins, B.A., Baedecker, M.J., Aiken, G.R., Eganhouse, R.P., Tuccillo, M.E. (2001), Progression of natural attenuation processes at a crude-oil spill site I. Geochemical evolution of the plume, *J. Contam. Hydrol.*, *53*, 369-385.

CRC Press (2004), *CRC Handbook of Chemistry and PhysicsI*, 84th ed., Boca Raton, Fla.

Curtis, G.P., Cozzarelli, I.M., Baedecker, M.J., Bekins, B.A. (1999), Coupled biogeochemical modeling of ground-water contamination at the Bemidji, Minnesota, crude oil spill site. Water-Resources Investigations - U. S. Geological Survey, Report: WRI 99-4018-C, p.153-158.

Curtis, G.P. (2003), Comparison of approaches for simulating reactive solute transport involving organic degradation reactions by multiple terminal electron acceptors, *Comp. Geosci.*, *29*, 319-329.

Delin, G.N., Essaid, H.I., Cozzarelli, I.M., Lahvis, M.H., Bekins, B.A. (1998), USGS Fact Sheet 084-98, Ground Water Contamination by Crude Oil near Bemidji, Minnesota. http://mn.water.usgs.gov.

Dillard, L.A., Essaid, H.I., Herkelrath, W.N. (1997), Multiphase flow modeling of a crude-oil spill site with a bimodal permeability distribution, *Water Resour. Res., 33,* 1617-1632.

Eganhouse, R.P., Baedecker, M.J., Cozzarelli, I.M., Aiken, G.R., Thorn, K.A. (1993), Crude oil in a shallow sand and gravel aquifer - II. Organic geochemistry, *Appl. Geochem., 8,* 551-567.

Eganhouse, R.P., Dorsey, T.F., Phinney, C.S., Westcott, A.M. (1996), Processes affecting the fate of monoaromatic hydrocarbons in an aquifer contaminated by crude oil, *Environ. Sci. Technol., 30,* 3304-3312.

Essaid, H.I., Bekins, B.A., Godsy, E.M., Warren, E., Baedecker, M.J., Cozzarelli, I.M. (1995), Simulation of aerobic and anaerobic biodegradation processes at a crude oil spill site, *Water Resour. Res., 31,* 3309-3327.

Essaid, H.I., Cozzarelli, I.M., Eganhouse, R.P., Herkelrath, W.N., Bekins, Delin, G.N. (2003), Inverse modeling of BTEX dissolution and biodegradation at the Bemidji, MN crude-oil spill site, *J. Contam. Hydrol., 67,* 269-299.

Fayer, M.J., Hiller, D. (1986), Air encapsulation: I. Measurement in a field soil, *Soil Sci. Soc. Am. J., 50,* 668-572.

Franzi, D.A. (1988), Surficial and subsurface distribution of aquifer sediments at the Bemidji, Minnesota research site, *in U.S. Geological Survey Toxic Waste--Ground Water Contamination Program--Proceedings of the technical meeting, Cape Cod, Massachusetts, October 21-25, 1985: U.S. Geological Survey Open-File Report 86-481,* edited by S.E. Ragone, p.C5-C10.

Fry., V.A., Selker, J.S., Gorelick, S.M. (1997), Experimental investigations for trapping oxygen gas in saturated porous media for in situ bioremediation, *Water Resour. Res., 33,* 2687-2696.

Heilweil, V.M., Solomon, D.K., Perkins, K.S., Ellett, K.M. (2004), Gas-partitioning tracer test to quantify trapped gas during recharge, *Ground Water, 42,* 589-600.

Herkelrath, W.N., Delin, G.N. (2001), Long-term monitoring of soil-moisture in a harsh climate using reflectometer and TDR probes, in Dowding, C.H., eds., Proceedings of the Second International Symposium and Workshop on Time Domain Reflectometry for Innovative Geotechnical Applications, September 5-7, 2001: Evanston, Illinois, Northwestern University, Infrastructure Technology Institute, p.262-272.

Hult, M.F., Grabbe, R.R. (1988), Distribution of gases and hydrocarbon vapors in the unsaturated zone, in U.S. Geological Survey Toxic Substances Hydrology Program; Proceedings of the Technical Meeting, Cape Cod, Massachusetts, October 21 –25, 1985: U.S. Geological Survey Water Resources Investigations Report 81 –4188 , edited by S.E. Ragone, p.C21 –C26.

Jakobsen, R., Postma, D. (1999), Redox zoning, rates of sulfate reduction and interactions with Fe-reduction and methanogenesis in a shallow sandy aquifer, Romo, Denmark, *Geochimica et Cosmochica Acta, 63*, 137-151.

Landon, M.K. (1993), Investigation of mass loss based on evolution of composition and physical properties of spilled crude oil contaminating a shallow outwash aquifer, in Faculty of the Graduate School., University of Minnesota. 276 pages.

Li, X., Yortos, Y.C. (1995), Theory of multiple bubble growth in porous media by solute diffusion, *Chem. Eng. Sci., 50*, 1247-1271.

Mayer, K.U., Frind, E.O., Blowes, D.W. (2002), A numerical model for the investigation of reactive transport in variably saturated media using a generalized formulation for kinetically controlled reactions, *Water Resour. Res., 38*, 1174-1194.

Postma, D., Jacobsen, R. (1996), Redox zonation: Equilibrium constraints on the Fe(III)/SO_4-reduction interface, *Geochimica et Cosmochica Acta, 60*, 3169-3175.

Raghoebarsing, A.A., Pol, A., van de Pas-Schoonen, K.T., Smolders, A.J.P., Ettwig, K.F., Rijpstra, W.I.C., Schouten, S., Sinninghe Damsté, J.S., Op den Camp, H.J.M., Jetten, M.S.M., Strous, M. (2006), A microbial consortium couples anaerobic methane oxidation to denitrification. *Nature, 440*, 918-921.

Revesz, K., Coplen, T.B., Baedecker, M.J., Glynn, P., and Hult, M. (1995), Methane production and consumption monitored by stable H and C isotope ratios at a crude oil spill site, Bemidji, Minnesota. *Appl. Geochem., 10*, 505-516.

Ryan, M.C, MacQuarrie, K.T.B., Harman, J., Mclellan, J. (2000), Field and modeling evidence for a "stagnant flow" zone in the upper meter of sandy pheatic aquifers, *J. Hydrol., 233*, 223-240.

Thorstenson, D.C., Pollock, D.W. (1989), Gas transport in unsaturated zones: multicomponent systems and the adequacy of Fick's Laws, *Water. Resour. Res., 25*, 477-507.

Tuccillo, M.E., Cozzarelli, I.M., Herman, J.S. (1999), Iron reduction in the sediments of a hydrocarbon-contaminated aquifer, *Appl. Geochem., 14*, 655-667.

Williams, M.D., Oostrom, M. (2000), Oxygenation of anoxic water in a fluctuating water table system: an experimental and numerical study, *J. Hydrol.*, *230*, 70-85.

Weiss, R.F. (1970), The solubility of nitrogen, oxygen and argon in water and seawater. *Deep-Sea Res.*, *17*, 721-735.

Wösten, J.H.M., van Genuchten, M.T. (1988), Using texture and other soil properties to predict the unsaturated soil hydraulic functions, *Soil Sci. Soc. Am. J.*, *52*, 1762-1770.

Yamamoto, S., Alcauskas, J.B., Crozier, T.E. (1976), Solubility of methane in distilled water and seawater, *J. Chem. Eng. Data*, *21*, 78-80.

Zachara, J.M., Kukkadapu, R.K., Gassman, P.L., Dohnalkova, A., Fredrickson, J.K., Anderson, T. (2004), Biogeochemical transformation of Fe minerals in a petroleum-contaminated aquifer, *Geochimica et Cosmochica Acta*, *68*, 1971-1805.

5 Investigating Ebullition in a Sand Column Using Dissolved Gas Analysis and Reactive Transport Modeling

5.1 Introduction

Ebullition, the vertical transport of gas bubbles driven by buoyancy forces, can have important implications on gas transport to the atmosphere from aquifers and within the aquifer and soil zone. Methane is an important greenhouse gas, accounting for approximately 22 % of the greenhouse effect at present (Lelieveld et al., 1998), with natural and managed wetlands (rice paddies) accounting for about 37 % of total emissions to the atmosphere (Whalen, 2002). In these environments, ebullition greatly enhances CH_4 transport to the atmosphere as gas bubbles rapidly bypass CH_4 oxidation zones, and can account for up to 85% of emissions (Walter and Heimann, 2000; Whalen, 2002).

The formation and ebullition of gas bubbles in aquifers also affects groundwater flow and transport of dissolved species and gases through the aquifer and into the soil zone (Ryan et al., 2000; Williams and Oostrom, 2000; Heilweil et al., 2004; Amos et al., 2005). In contaminated aquifers these processes can be of particular significance as there can be a large supply of substrate and/or electron acceptors for gas producing biogenic processes (Revesz et al., 1995; Blicher-Mathiesen et al., 1998; van Breukelen et al., 2003). At a crude oil spill site near Bemidji, MN, methanogenesis has led to gas bubble formation below the floating oil body for a period of over 15 years (Amos et al., 2005; Revesz et al., 1995). In a modeling study, Amos and Mayer (2006) showed that gas phase saturations in this zone could possibly exceed 30%. This high volume of gas suggests that gas ebullition may be an important process and could substantially affect gas transport and rates of biogeochemical processes in the system.

Previous researchers have investigated bubble growth and motion based on pore-scale processes and monitoring of individual bubble movement (Hawes et al., 1996; McDougall et al., 1996; Roosevelt and Corapcioglu, 1998; Corapcioglu et al., 2004). While these studies are important to fully understand the physical processes controlling ebullition, they are difficult to upscale due to pore-scale heterogeneity and the possibility of erratic bubble movement (Hawes et al., 1996; McDougall et al., 1996; Corapcioglu et al., 2004). Other research has focused on the movement of gases in air sparging systems, but these systems use large air-injection rates and are not directly analogous to systems where gases are produced biogenically (Hawes et al., 1996; McDougall et al., 1996; Corapcioglu et al., 2004). Our approach is to infer the presence and migration of gas bubbles based on the composition of dissolved gases throughout the water column. This approach is useful in that it provides a means of quantifying bubble movement based on observations of bulk-scale properties. Although this approach does not strictly account for pore-scale processes, insights into the controls on bubble movement can be inferred.

Column experiments are advantageous in that they provide a controlled, simplified environment and facilitate the collection of well-resolved spatial and temporal data. Here we reproduce methanogenic conditions in a stagnant (i.e., no water flow) volume of water-filled sediment and monitor dissolved gas concentrations in the methanogenic zone and overlying clean sand column to quantify gas bubble formation and ebullition.

The reactive transport code MIN3P (Mayer et al, 2002) is broadly applicable to geochemical problems in variably saturated media involving kinetically controlled redox and mineral dissolution/precipitation reactions along with equilibrium hydrolysis,

aqueous complexation, ion exchange, and surface complexation reactions. Amos and Mayer (2006) recently modified the code to include gas bubble formation/dissolution in the saturated zone in response to changes in total dissolved gas pressures. Here the code is further enhanced to include ebullition of the bubbles. We must emphasize that the proposed formulation is not intended as a predictive model but is rather used as a tool to investigate and quantify the relationship between gas bubble movement and dissolved gas concentrations.

The primary objective of this contribution is to investigate gas bubble formation and ebullition in a sand column by using dissolved gas analysis and reactive transport modeling to elucidate important controls on the rate of ebullition and gas composition. As a secondary objective, we aim to show that dissolved gas analysis and the proposed reactive transport model are effective tools for investigating these processes.

5.2   Column Experiments

5.2.1   Experimental set-up

The column experiment was conducted in a 122 cm-long, 8.225 cm-diameter column, constructed of 2 cm-thick clear Plexiglas. The column was fitted with sampling ports at 5 cm intervals along the height of the column, and a syringe septa and pressure gauge at the top of the column (Figure 5-1). The sampling ports consisted of 1/8" I.D. PVC tubing fitted on one end with a 2-way Luer valve and sealed through the side of the column with Swagelok compression fittings. The other end of the tubing extending into the column was slotted along its length and covered with fine nylon meshing. The column was also fitted with a 150 ml graduated cylinder connected to the port at 107 cm
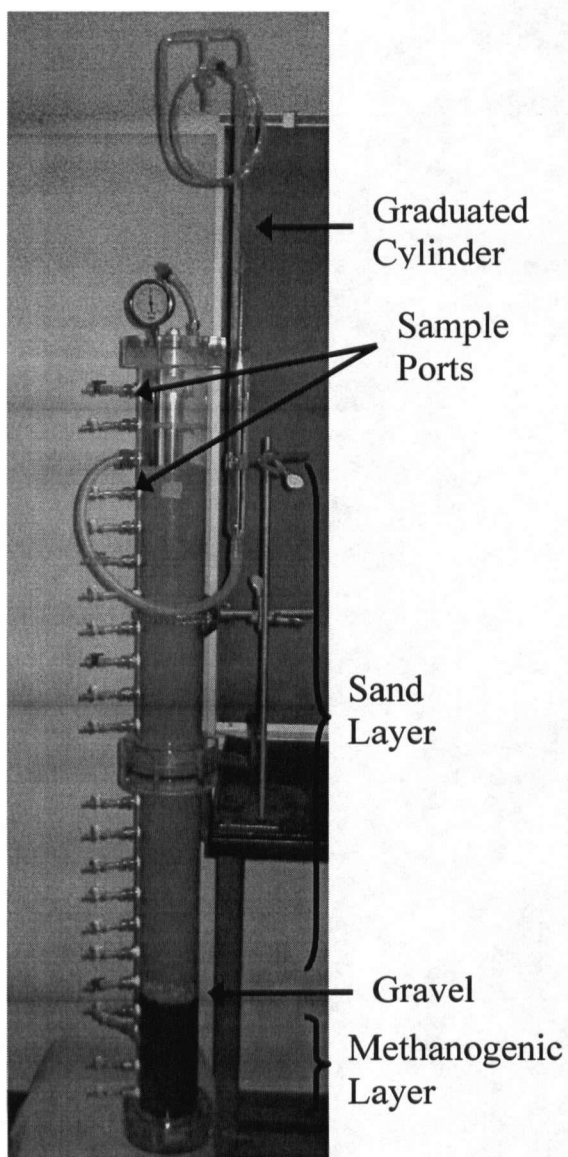
Figure 5-1. Experimental setup of laboratory column.

through a length of tubing. This allowed water to be displaced by gas bubble growth and facilitated the quantification of the amount of displacement, corresponding to the volume of produced gas. The column was filled to approximately 24 cm with a mixture consisting of 50% methanogenic organic-rich sediment and 50% 20/30 mesh Ottawa sand measured by weight. The organic mixture was overlain by a 2.5 cm gravel layer, then

filled to approximately 105 cm with clean 20/30 mesh Ottawa sand. Initially the column was fully saturated to the top. Column preparation procedures are outlined in Appendix 5-1.

5.2.2 Sample collection

Sampling of the column included weekly or bi-weekly collection of water samples for dissolved gas analysis at 15 cm intervals along the column, monitoring of water levels in the graduated cylinder to determine the volume of gas bubbles produced in the columns, and quantitative removal of gas accumulated at the top of the column. Details of the sampling procedure are included in Appendix 5-2.

5.2.3 Results and discussion of column experiments

5.2.3.1 Bromide

Bromide was added to the methanogenic mixture (lower 24 cm) as a transport tracer. Since there is no significant water flow through the column, bromide transport will be primarily through diffusion. The removal of column water at the various ports for sampling and addition of WEA at the top of the column would have created a small advective flow, downward through the column. Bromide concentrations along the profile of the column at various times throughout the experiment are shown in Figure 5-2H. The data clearly show that bromide is transported upward under a diffusive gradient over time but that the transport is minimal.
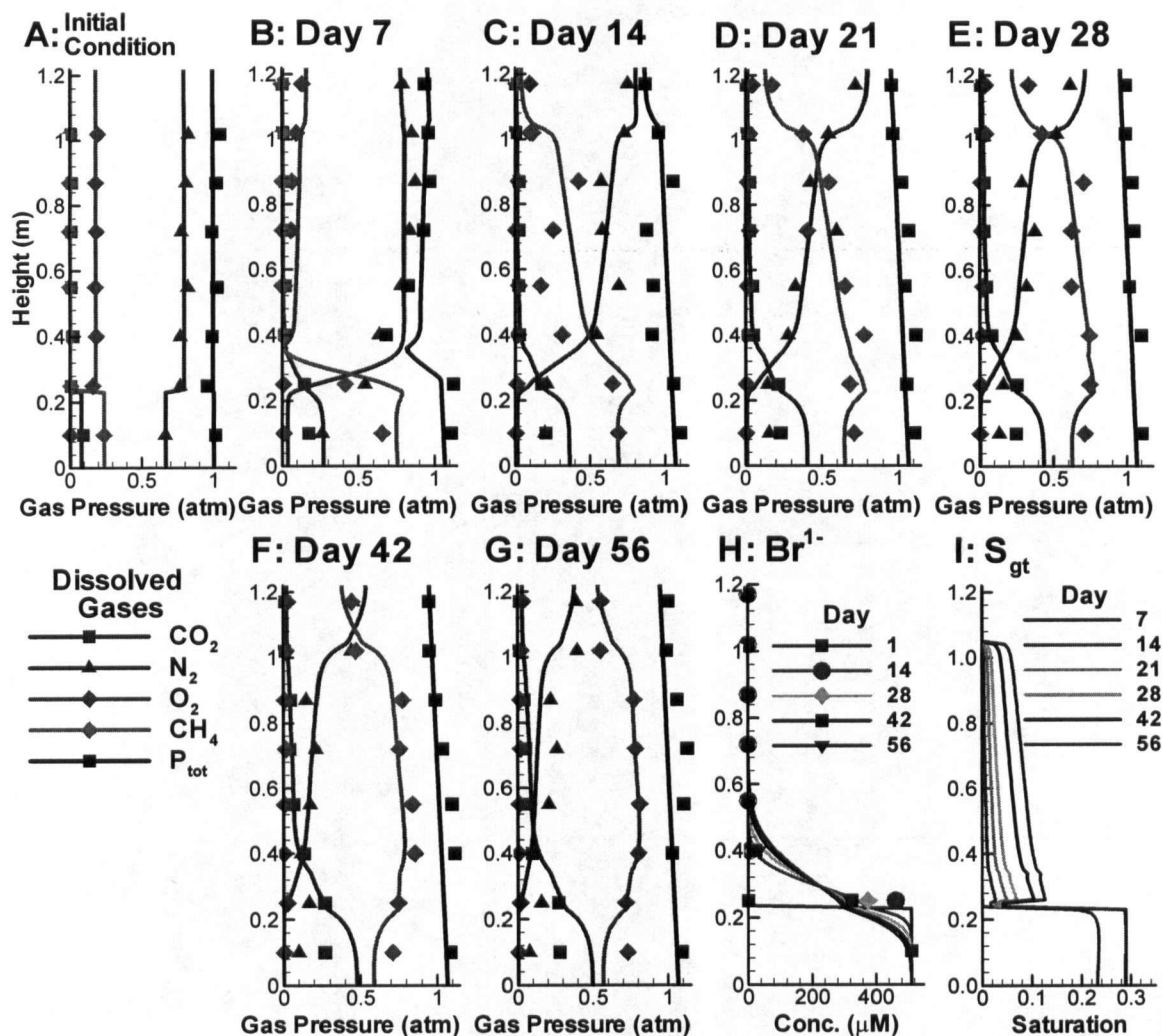
Figure 5-2. A-G: Dissolved gas profiles for observed (symbols) and simulated (lines) data. **H:** Bromide concentrations at various times for observed (symbols) and simulated (lines) data. **I:** Gas saturation profiles for simulated data only.

5.2.3.2 Gas Saturation

Increases in gas phase saturation over time are shown in Figure 5-3A. The data indicate that initially gas bubble growth occurred at a rate of ~12 ml per day (0.4% of porosity per day) and slowed down to ~6 ml per day. The total gas volume produced is 439 ml, which is ~15.5 % of the porosity of the column. Figure 5-3B shows the cumulative volume of gas removed from the top of the column over time. The total

amount of gas removed was 224 ml (4.21 ml cm^{-2} cross sectional area), equivalent to ~51% of the total gas volume produced, indicating that ebullition is an important gas transport mechanism in the column.

5.2.3.3 Dissolved Gases

Profiles of dissolved CH_4, CO_2, O_2 and N_2 along the length of the column are shown in Figures 5-2A-G for each sampling event through the experiment. Both dissolved Ar and N_2 are used as non-reactive tracers in this experiment; however, since Ar concentrations do not show significantly different results from N_2 they are omitted from the figures for clarity. Initially dissolved gas concentrations above the methanogenic layer are near WEA, while in the methanogenic layer CH_4 and CO_2 concentrations are elevated, O_2 nearly depleted, and N_2 is slightly depressed (Figure 5-2A).

The formation of gas bubbles due to biogenic gas production will lead to the stripping of non-reactive gases from the water. This phenomenon has been used to identify and quantify the formation of gas bubbles in a variety of aquifers (Blicher-Mathiesen et al, 1998; Amos et al., 2005; Fortuin and Willemsen, 2005). The CH_4, CO_2 and N_2 data in the bottom 0.24 m of the column demonstrate this effect quite clearly, indicating the formation of gas bubbles within the column (Figure 5-2A-G). In the methanogenic zone, CH_4 and CO_2 concentrations increase over time, exceeding 0.75 and 0.25 atm respectively at 56 days. Simultaneously, N_2 concentrations decrease over time, reaching ~0.1 atm at 56 days (Figure 5-2G). Because CO_2 is very soluble, its partial pressure generally remains lower than CH_4, so that the production of CH_4 is generally a more important contributor to the build-up of gas pressure and the formation of gas bubbles.
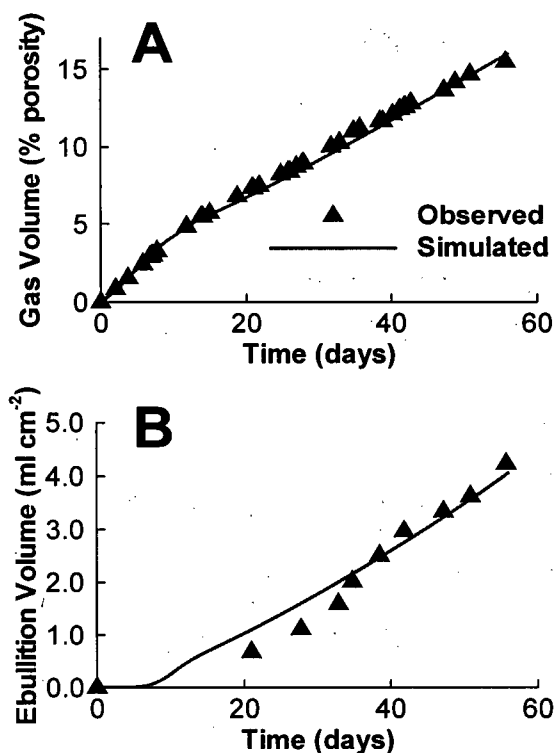
Figure 5-3. A: Gas volume produced in % of porosity for observed and simulated data. B: Ebullition volume in ml of gas per cm^2 of column cross section for observed and simulated data.

Dissolved gas data above an elevation of 0.24 m (Figure 5-2) indicate that ebullition is occurring, most notably through the increase in CH_4 concentrations at successively higher elevations over time (Figures 5-2A-G). Given that CH_4 is only produced in the methanogenic layer, the slow rate of diffusion, as shown by the bromide tracer and noting that CH_4 and bromide have similar aqueous phase diffusion coefficients (1.84×10^{-9} and 2.080×10^{-9} m^2 s^{-1}, respectively), cannot account for the observed migration of CH_4 through the column over the duration of the experiment. Furthermore, because CO_2 is significantly more soluble than CH_4 at the circum-neutral pH range

203

measured in the columns, ebullition will tend to favour the transport of CH_4 over CO_2 as can be seen clearly in Figure 5-2.

5.3   Reactive Transport Model Development

A new formulation to describe the ebullition of gas bubbles through porous media has been implemented in the reactive transport code MIN3P (Mayer et al., 2002). This formulation builds on previous enhancements to MIN3P that describe gas bubble formation due to in-situ gas production as is outlined in Chapter 3.2. Here we describe specific additions to the model formulation that are relevant to the problem of ebullition.

The objective for developing the model was to find a formulation that could describe gas bubble movement on the macro-scale, constrained by dissolved gas data observed in the column experiments. To achieve this, we have employed an empirical approach that describes gas movement but does not take into account the physical forces acting on the bubbles such as buoyancy and capillarity. This approach distinctly differs from previous attempts at modeling bubble movement that use physical constraints on bubble movement (Corapcioglu et al., 2004), but offers advantages in that difficult-to-measure parameters needed for more physically based representations, such as the number of bubbles, bubble size and pore throat dimensions, are not needed. Nevertheless, application of the model is restricted to where well resolved spatial and temporal dissolved gas data are available. While this approach offers insights into the rate and degree of gas movement, predictive capabilities of the model are limited.

To describe gas movement we have developed an expression for the flux of gas out of a control volume due to ebullition;

$$F_{ij}^E = V_i \phi_i T_{ij}^g R_i^{Sgt} \left(\frac{S_{gt,i}}{S_{gt,i}^{max}} \right)^{E_F} + F_{i-1,j}^E \left(1 - R_E \Delta z_i \right) \qquad j = 1, N_C \quad (1)$$

where F_{ij}^E [mol day^{-1}] is the ebullition flux of component j leaving control volume i, T_{ij}^g is the total component concentration in the gas-phase [mol L^{-1} gas], $S_{gt,i}$ is the corresponding trapped gas phase saturation, V_i is the volume [L] of the control volume, ϕ_i is porosity, the subscript $i-1$ refers to the control volume immediately below the current control volume, and R_i^{Sgt} [L air L^{-1} void space day^{-1}] is the rate of gas volume increase given by $d\bar{S}_{gt,i}/dt$ where t is time and $d\bar{S}_{gt,i}$ is the change in trapped gas saturation before ebullition is considered. This term includes gas produced through biogenic reactions, plus gas retained from ebullition from lower control volumes, minus gas dissolved into the water through equilibration.

The first term in the expression describes the volume of gas bubble ebullition from control volume i. The parameter $S_{gt,i}^{max}$ defines the maximum gas phase saturation, beyond which the porous medium is unable to retain more gas bubbles and further gas production will result in ebullition of that gas. The concept of a maximum gas phase saturation is suggested by mass balance calculations of the column data. To account for the observed CH$_4$ mass through the column at later times in the experiment, i.e. after 14 days, it must me assumed that all the gas produced, as constrained by the gas volume data (Figure 5-3A), is transported upward. The parameter E_F describes the degree of gas bubble ebullition prior to the $S_{gt,i}$ reaching $S_{gt,i}^{max}$. This parameter is necessary because some ebullition is observed at early times in the experiment, i.e. before 14 days (Figure 5-2B and C). An exponential function was chosen because the rate of ebullition appears to be a non-linear function of $S_{gt,i}$. The effects of the parameters $S_{gt,i}^{max}$ and E_F on ebullition

205
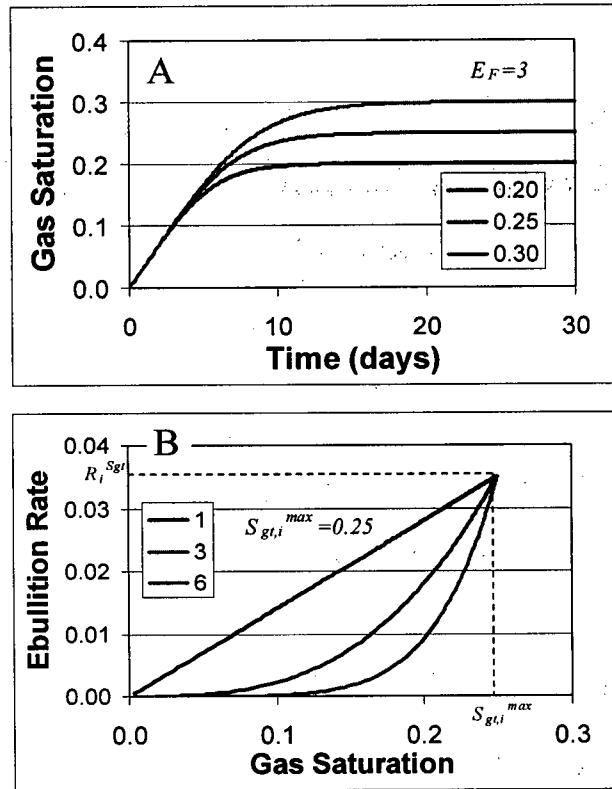
Figure 5-4. A: $S_{gt,i}$ versus time for control volume i with R_i^{Sgt} is equal to 0.035 day^{-1} and E_F equal to 3 for various values of $S_{gt,i}^{max}$. **B:** Ebullition rate, in units of saturation per day, versus $S_{gt,i}$ for control volume i with R_i^{Sgt} is equal to 0.035 day^{-1} and $S_{gt,i}^{max}$ equal to 0.25 for various values of E_F.

are demonstrated graphically in Figure 5-4A and B, respectively, for a control volume

where R_i^{Sgt} is equal to 0.035 day^{-1}, a rate similar to that of the column experiments. Figure

5-4A shows $S_{gt,i}$ over time and demonstrates that gas phase saturation increases until

$S_{gt,i}^{max}$ is reached. Figure 5-4B shows the volume of gas bubble ebullition, in units of

saturation per day, as a function of saturation. A high value of E_F, i.e., six, limits

ebullition at low saturations, and is representative of fine-grained sediment where

capillary forces are high. A lower E_F, i.e., one, will promote ebullition at low saturations,

and can be used to describe coarse sediment where capillary forces do not significantly

inhibit ebullition. The second term in Equation 1 is controlled by the ebullition

attenuation factor R_E (m^{-1}) and accounts for the retention and re-equilibration of gas

bubbles in control volume i during upward transport through the sediment from control

volume i-1. This term was included because dissolved gas data clearly shows that

attenuation of the rising bubbles is occurring (Figure 5-2B-G).

For simplicity the ebullition fluxes are calculated at the beginning of each time

step based on values of T_j^g, S_{gi} and R_{Sgi} from the previous time step. To minimize

numerical error due to this simplification, the time step is limited to restrict saturation

changes to less than 0.1 % per time step. Reducing the time step further did not affect

simulation results.

5.4   Reactive transport modelling of column experiments

5.4.1   Model Parameters

The experiments were modeled as a 122 cm long, 1-D vertical column discretized

into 1 cm control volumes. The model domain is broken up into 4 physical and chemical

zones to represent the methanogenic layer, the gravel layer, the clean sand layer, and the

ponded water on top of the column. Physical and ebullition parameters used to represent

each of these zones are shown in Table 5-1. Flow and transport parameters such as

hydraulic conductivity and dispersivity are unimportant in these simulations since water

flow through the column is negligible and gas migration is exclusively controlled by the

parameters $S_{gt,i}^{max}$, E_F and R_E. The simulations include eight primary components; HCO_3^-

, N_2, Ar, CH_4, H^+, O_2, Br^{-1} and dissolved organic matter represented by CH_2O, three

secondary species; CO_3^{2-}, $H_2CO_3(aq)$, and OH^-, and five gases; CO_2, N_2, Ar, O_2 and CH_4.

Diffusion coefficients and Henry's Law constants used for components and gas species

are shown in Table 5-2. Component dependent diffusion coefficients are used to

highlight the potential differences between the diffusion rates of each component; however, we have not considered the effects of electrochemical migration in these simulations. Secondary species are assumed to diffuse at the same rate as the corresponding primary components.

Table 5-1. Porosity and ebullition parameters for reactive transport modeling.

	Methanogenic Layer	Gravel Layer	Sand Layer	Ponded Water
porosity	0.30	0.40	0.36	1.0
ebullition parameters				
- S_{gt}^{max}	0.29	0.05	0.15	0.001
- E_f	5	1	2	1
- R_E (m^{-1})	0.95	0.75	0.95	1

The degradation of organic matter is modelled as a two-step process where an immobile solid fraction is initially degraded to produce dissolved CH_2O which is subsequently degraded methanogenically. To represent the initially higher rate of gas production in the column, a bi-modal organic carbon decomposition model is used. A labile organic carbon fraction is readily degraded at the beginning of the experiment but is quickly exhausted, and a second more recalcitrant fraction degrades at a slower rate throughout the duration of the experiment. The volume fractions of organic matter in the methanogenic layer were calibrated to 1.4×10^{-4} and 1.4×10^{-1} for the labile and recalcitrant fractions respectively. Solid organic matter was assumed to be absent from all other layers. In the aqueous phase three microbially mediated redox reactions are considered in the simulations. These include methanogenic degradation of organic matter, aerobic oxidation of CH_4, and aerobic oxidation of organic matter. The last reaction is

208

generally unimportant in the experiment but is included for completeness. Reaction

stoichiometries, rate expressions and reaction constants are shown in Table 5-3. A

constant head flow boundary of 133 cm is set at the top of the column, to represent the

approximate average water level in the graduated cylinder throughout the column

experiments, and all other boundaries are considered no-flow. Gas volume transported

past the upper boundary was monitored to determine total volume of gas ebullition.

Table 5-2. Reactive transport parameters for components and gases.

Component	Diffusion Coefficient ($m^2 \, s^{-1}$)	Gas Species	Henry's Law Constant ($mol \, L^{-1} \, atm^{-1}$)
N_2	$2.00 \times 10^{-9,\,a}$	N_2	$6.45 \times 10^{-04,\,b}$
O_2	$2.42 \times 10^{-9,\,a}$	O_2	$1.27 \times 10^{-03,\,b}$
CH_4	$1.84 \times 10^{-9,\,a}$	CH_4	$1.41 \times 10^{-03,\,c}$
Ar	$2.50 \times 10^{-9,\,a}$	Ar	$1.39 \times 10^{-03,\,b}$
HCO_3^-	$1.185 \times 10^{-9,\,a}$	CO_2	$3.41 \times 10^{-02,\,a}$
H^+	$9.311 \times 10^{-9,\,a}$		
CH_2O	$1.089 \times 10^{-9,\,a}$		
Br^-	$2.080 \times 10^{-9,\,a}$		

[a] From CRC Press (2004) at 25 °C.

[b] From Weiss (1970) calculated for 25 °C.

[c] From Yamamoto et al. (1976) calculated for 25 °C.

5.4.2   *Model Calibration and Discussion*

Calibration of model parameters was performed manually by visual inspection.

This approach allowed to investigate the sensitivity with respect to the individual

parameters and aided in the development of the model formulation.

Table 5-3. Reaction stoichiometries, rate expressions, rate constants and half saturation constants used in reactive transport simulations.

Reaction	Rate Expression	Constants
1. $Organic\,Matter_{(Labile)} \rightarrow CH_2O_{(aq)}$	$R_1 = k_1 \left(\dfrac{F_{OM(L)}}{K_{OM(L)} + F_{OM(L)}} \right)$	$k_1 = 4.6 \times 10^{-09}$ $K_{OM(L)} = 1.00 \times 10^{-05}$
2. $Organic\,Matter_{(Recalcitrant)} \rightarrow CH_2O_{(aq)}$	$R_2 = k_2$	$k_2 = 4.0 \times 10^{-09}$
3. $CH_2O_{(aq)} + 0.5H_2O \rightarrow 0.5CH_{4(aq)} + 0.5HCO_3^- + 0.5H^+$	$R_3 = k_3 \left(\dfrac{\{CH_2O_{(aq)}\}}{K_{CH_2O} + \{CH_2O_{(aq)}\}} \right)$	$k_3 = 2.0 \times 10^{-07}$ $K_{CH_2O} = 1.00 \times 10^{-05}$
4. $CH_{4(aq)} + 2.0O_{2(aq)} \rightarrow HCO_3^- + H^+ + H_2O$	$R_4 = k_4 \left(\dfrac{\{CH_{4(aq)}\}}{K_{CH_4} + \{CH_{4(aq)}\}} \right)\left(\dfrac{\{O_{2(aq)}\}}{K_{O_2} + \{O_{2(aq)}\}} \right)$	$k_4 = 3.0 \times 10^{-9}$ $K_{CH_4} = 1.00 \times 10^{-05}$ $K_{O_2} = 3.12 \times 10^{-06}$
5. $CH_2O_{(aq)} + O_{2(aq)} \rightarrow HCO_3^- + H^+$	$R_5 = k_5 \left(\dfrac{\{CH_2O_{(aq)}\}}{K_{CH_2O} + \{CH_2O_{(aq)}\}} \right)\left(\dfrac{\{O_{2(aq)}\}}{K_{O_2} + \{O_{2(aq)}\}} \right)$	$k_5 = 3.0 \times 10^{-8}$ $K_{CH_2O} = 1.00 \times 10^{-05}$ $K_{O_2} = 3.12 \times 10^{-06}$

The volume fraction of organic matter is designated by F_{OM}.

5.4.2.1 Diffusion

Spatial profiles of simulated bromide concentration at various times are compared to measured concentrations in Figure 5-2H. The good agreement between the simulated and measured concentrations strongly suggests that the diffusion parameters and formulation used in MIN3P, including tortuosity correction after Millington (1959), are adequate representations of the physical system.

5.4.2.2 Gas bubble formation and ebullition

Important model calibration parameters include ebullition parameters (Table 5-1) and the kinetic rate constants (Table 5-3). Simulated and observed gas production, shown in Figure 5-3A, show good agreement, including the initially high gas production rate followed by a period of lower production, suggesting that rate parameters used for Reactions 1, 2 and 3 (Table 5-3) accurately reproduce the amount of CH_4, CO_2, and the volume of gas produced in the system. Accurately reproducing the rates of CH_4 and CO_2 production is important since the amount of ebullition is directly related to the amount of gas produced. Kinetic parameters for the aerobic oxidation reactions (Table 5-3, Reactions 3 and 4) are less important since the amount of O_2 in the system is limited.

The ebullition parameters are calibrated to provide a best fit to the ebullition volume (Figure 5-3B) and dissolved gas concentrations along the column (Figure 5-2A-G). The simulated gas volume accumulated at the top of the column is compared to experimental results in Figure 5-3B. The simulation reproduces the amount of ebullition at later times (i.e., after ~35 days), but over predicts ebullition at earlier times. Using the present model, a better fit to this early data (before 35 days) could not be achieved without under-predicting ebullition at later times and adversely affecting the fit to the dissolved gas data. Furthermore, the experiments showed periodic release of large gas volumes while the simulations show a gradual release over time. These results highlight the inability of the model to capture the erratic bubble movement typically observed in real systems. Nevertheless, the model is capable of adequately simulating gas release and attenuation over time. It must be noted; however, that simulation of ebullition was only made possible by collecting sufficient spatial and temporal data from the experiments

including the volume of gas production (Figure 5-3A) and dissolved gas concentrations (Figure 5-2A-G). Application of the model to cases where these data are not available would be speculative.

The simulated dissolved gas concentrations also show a good match to observed data (Figure 5-2A-G) indicating that the model adequately reproduces the distribution of gas through space and time. Simulated and observed results differ most significantly for N_2 concentrations in the methanogenic zone, with simulated concentrations being consistently lower than those observed. The most likely explanation for this discrepancy is contamination from atmospheric gases. During the column experiments, sampling of the ports in the methanogenic layer produced only gas so that the sampling port was always filled with gas. Although the port valve was closed between sampling events, this possibly provided a conduit for gas entrance into the column, replenishing N_2 concentrations to a degree. The initial nitrate concentration in the methanogenic layer was measured and was below the detection limit of 50 μM, suggesting that nitrate reduction could not be a significant process in these sediments, and therefore, could not account for the discrepancy in the N_2 concentrations.

The solution provided here cannot be considered unique; however, the good match of the simulated dissolved gas concentrations, gas phase saturation and ebullition volume to the experimental observations strongly suggests that the model presented here adequately reproduces the important processes occurring in the column experiment.

Analysis of the ebullition parameters (Table 5-1) and inspection of the modeled gas phase saturations through the column (Figure 5-2I) can provide insights into the mobility of gas bubbles in the system. The most critical parameters in the simulations are

the parameters for the methanogenic and sand layers. For the methanogenic layer S_{gt}^{max} and E_F are calibrated to 0.29 and 5, respectively, suggesting that gas phase saturations reach high levels before ebullition becomes significant. This can be seen in the saturation profiles at 7 and 14 days, which show that gas phase saturations in the methanogenic zone reach 0.24 and 0.29 respectively, while the saturations in the remainder of the column remain very low, i.e., below 0.05. In the sand layer, S_{gt}^{max} and E_F are set to 0.15 and 2, respectively, highlighting the physical differences between the methanogenic and sand layers, and suggesting that this zone does not retain gas as readily as the methanogenic layer. The ebullition attenuation factor for the sand layer is another important calibration parameter because much of the bubble transport is through this zone. For this zone R_E was calibrated to 0.95 m^{-1}, indicating that some gas bubbles will travel a vertical distance of up to 0.95 m before attenuation. This suggests that gas bubbles are highly mobile through the column. Due to the small vertical thickness of the gravel layer, the model is insensitive to the parameters used for this zone. Nevertheless, S_{gt}^{max} and E_F are set to 0.05 and 1.0 respectively, to represent the low capillary forces and the low retention potential in the coarse grained material. This results in a sharp drop in gas phase saturation above the methanogenic zone (Figure 5-21).

For the ponded water S_{gt}^{max} is set to a very small value, 0.001, to represent the quick movement of bubbles through this zone. A value greater than zero must be used to satisfy Equation 1. At the low value of S_{gt}^{max} used for the ponded water, E_F becomes an unimportant parameter. In the ponded water R_E is set to 1.0 suggesting that retardation of bubbles is significant in this zone. This is presumably due to dissolution of trapped gas bubbles at the top of the column into the ponded water. Trapped bubbles were removed

from the top of the column whenever observed, but possibly sat at the top of the column one to three days. Mixing of the surrounding water by rising gas bubbles may also contribute to dissolution of the gas bubbles in this zone.

Analysis of simulated CH_4 transport provides a measure of the significance of ebullition as a transport mechanism. At 56 days, the total CH_4 produced was 1.22×10^{-5} mol g^{-1} sediment. Of this amount 83% entered the gas phase, and 36% was transported to the top of the column through ebullition. Over time these percentages will increase as the column approaches bubble saturation. These numbers indicate that ebullition is a significant transport mechanism for CH_4 in this system.

The simulations also indicate that a significant amount of CO_2 can be transported through ebullition despite the high solubility of the gas. The amount of CO_2 produced in the column is slightly higher than that of CH_4 due to aerobic degradation reactions. Of the 1.26×10^{-5} mol g^{-1} sediment produced, 36% entered the gas phase, of which 19% was transported to the top of the column through ebullition. The simulations likely overestimate the degree of CO_2 ebullition since the partial pressure of CO_2 in the methanogenic layer is also overestimated. This is likely due to some unidentified buffering mechanism in the laboratory column that is not captured by the simulation. Nevertheless, the simulations indicate the potential for CO_2 transport through ebullition.

The analysis presented here has shown that dissolved gas analysis and reactive transport modeling can provide effective means of investigating ebullition and quantifying gas transport. Further work along these lines using different porous materials and gas production rates will lead to a better understanding of the controls on ebullition.

5.5 Acknowledgements

Appendix 5-1: Column Preparation

To minimize entrapment of gas bubbles and avoid contamination of the clean sand layer with organic matter during column preparation, the following procedure was employed. The methanogenic mixture was made into a slurry using organic-rich water collected with the methanogenic sediment and added to the column. Potassium bromide was added to the methanogenic mixture as a tracer. The gravel and clean sand were then added to the column dry, followed by flushing with CO_2 through the section of the column that contained clean sand and gravel. The CO_2 was then displaced from this section of the column with ~1 pore volume of water equilibrated with the atmosphere (WEA). After allowing ~ 24 hrs for any trapped CO_2 to dissolve into the water, the clean sand layer and gravel were flushed several times to ensure the water remaining was WEA. Flushing of the column was always from top to bottom to ensure that organic matter was not transported upwards through the column. The sand used for the clean sand layer was initially sterilized in an oven at $120\,^0C$ for ~2 weeks. WEA was prepared with distilled water. The column was covered with aluminum foil to prevent photosynthetic processes. Porosity of the porous material was determined experimentally by weight.

Appendix 5-2: Sample collection and analysis

Water samples for dissolved gas analysis were collected weekly to bi-weekly at 15 cm intervals in 10 ml gas-tight syringes through the sampling ports in the sides of the column. An 8 ml sample was collected, then the syringe was fitted with a red rubber septum and 2 ml of helium were added. After shaking for 8 minutes, a 1.5 ml gas sample was extracted from the 10 ml syringe with a 2.5 ml gas-tight syringe. Sample handling was done inside a glove-bag purged with helium to prevent contamination of the sample with atmospheric gases. The 2.5 ml syringe was then transferred outside the glove-bag for injection into the gas chromatograph (GC). The 8 ml water sample was stored in a Nalgene sample bottle and refrigerated for later bromide analysis.

At the 10 cm sampling port, and at various times at the other sampling ports, sample collection yielded only gas due to the build-up of gas bubbles around the sampling port. In this case the gas sample was analysed directly with the GC.

Analysis for Ar, O_2, N_2, CH_4, and CO_2, was performed on a Varian CP-4900 dual channel gas chromatograph equipped with TCD detectors, a Molsieve 5A PLOT column to separate Ar, O_2, and N_2 and a PoraPLOT U column to separate CH_4 and CO_2. The carrier gas used for both columns was helium. The molsieve column is capable of baseline separation of Ar and O_2 at ambient temperatures. This instrument was calibrated with air and Supelco calibration mix #234 consisting of approximately 5 % N_2, 5 % O_2, 4 % CH_4, and 5 % CO_2 in He. Bromide analysis was done on a Dionex, DX-100 ion chromatograph.

The water level in the graduated cylinder was monitored regularly (approximately 1-3 days apart) to monitor the amount of gas produced in the column. If a gas bubble was

present at the top of the column it was removed using a gas-tight syringe through the top septum of the column to quantitatively monitor the volume of gas ebullition.

5.6   References

Amos, R.T., Mayer, K.U., Bekins, B.A., Delin, G.N., Williams, R.L. (2005), Use of dissolved and vapor-phase gases to investigate methanogenic degradation of petroleum hydrocarbon contamination in the subsurface, *Water Resour. Res., 41*, W02001, doi:10.1029/2004WR003433.

Amos, R. T., Mayer, K. U. (2006), Investigating the Role of Gas Bubble Formation and Entrapment in Contaminated Aquifers: Reactive Transport Modelling. *Submitted to J. Contam. Hydrol.*, 47 pages.

Blicher-Mathiesen, G., McCarty, G.W., Nielsen, L.P. (1998), Denitrification and degassing in groundwater estimated from dissolved dinitrogen and argon, *J. Hydrol., 208*, 16-24.

Braida, W., Ong, S.K. (2000), Modeling of air sparging of VOC-contaminated soil columns, *J. Contam. Hydrol., 41*, 385-402.

Burns, S.E., Zhang, M. (2001), Effects of system parameters on the physical characteristics of bubbles produced through air sparging, *Environ. Sci. Technol., 35*, 204-208.

Corapcioglu, M.Y., Cihan, A., Drazenovic, M. (2004), Rise velocity of an air bubble in porous media: Theoretical studies, *Water Resour. Res., 40*, W04214, doi:10.1029/2003WR002618.

CRC Press (2004), *CRC Handbook of Chemistry and PhysicsI*, 84th ed., Boca Raton, Fla.

Fortuin, N.P.M., Willemsem, A. (2005), Exsolution of nitrogen and argon by methanogenesis in Dutch ground water, *J. Hydrol.*, *301*, 1-13.

Hawes, R.I., Dawe, R.A., Evans, R.N. (1996), Theoretical model for the depressurisation of waterflooded reservoirs. *Transactions of the Institute of Chemical Engineers, March,* 197-2005.

Heilweil, V.M., Solomon, D.K., Perkins, K.S., Ellett, K.M. (2004), Gas-partitioning tracer test to quantify trapped gas during recharge, *Ground Water*, *42*, 589-600.

Lelieveld, J., Crutzen, P.J., Dentener, F.J. (1998), Changing concentration, lifetime and climate forcing of atmospheric methane, *Tellus*, *50B*, 128-150.

Mayer, K.U., Frind, E.O., Blowes, D.W. (2002), A numerical model for the investigation of reactive transport in variably saturated media using a generalized formulation for kinetically controlled reactions, *Water Resour. Res.*, *38*, 1174-1194.

McCray, J.E., Falta, R.W. (1996), Defining the air sparging radius of influence for groundwater remediation, *J. Contam. Hydrol.*, *24*, 25-52

McDougall, S.R., Sorbie, K.S. (1996), Estimation of critical gas saturation during pressure depletion in virgin and water flooded reservoirs, *Petrol. Geosci.*, *5*, 229-233.

Millington, R.J. (1959), Gas diffusion in porous media, *Science*, *130*, 100-102.

Revesz, K., Coplen, T.B., Baedecker, M.J., Glynn, P., Hult, M. (1995), Methane production and consumption monitored by stable H and C isotope ratios at a crude oil spill site, Bemidji, Minnesota, *Appl. Geochem.*, *10*, 505-516.

Roosevelt, S.E., Corapcioglu, M.Y. (1998), Air bubble migration in a granular porous medium: Experimental Studies, *Water Resour. Res.*, *34*, 1131-1142.

Ryan, M.C, MacQuarrie, K.T.B., Harman, J., Mclellan, J. (2000), Field and modeling evidence for a "stagnant flow" zone in the upper meter of sandy pheatic aquifers, *J. Hydrol.*, *233*, 223-240.

van Breukelen, B.M., Roling, W.F.M., Groen, J., Griffioen, J., van Verseveld, H.W. (2003), Biogeochemistry and isotope geochemistry of a landfill leachate plume, *J. Contam. Hydrol.*, *65*, 245-268.

Walter, B.P., Heimann, M. (2000), A process-based, climate-sensitive model to derive methane emissions from natural wetlands: Application to five wetland sites, sensitivity to model parameters, and climate, *Global Biogeochem. Cy.*, *14*, 745-765.

Weiss, R.F. (1970), The solubility of nitrogen, oxygen and argon in water and seawater, *Deep-Sea Res.*, *17*, 721-735.

Whalen, S.C. (2005), Biochemistry of methane exchange between natural wetlands and the atmosphere, *Env. Engineer. Sci.*, *22*, 73-94.

Williams, M.D., Oostrom, M. (2000), Oxygenation of anoxic water in a fluctuating water table system: an experimental and numerical study, *J. Hydrol.*, *230*, 70-85.

Yamamoto, S., Alcauskas, J.B., Crozier, T.E. (1976), Solubility of methane in distilled water and seawater, *J. Chem. Eng. Data*, *21*, 78-80.

6   Summary and Conclusions

An important aspect of this research has been to better understand the processes affecting CH_4 production, transport, and degradation, and determine rates of these processes. Inherent in the investigation of CH_4 fate and transport is the study of gas bubbles formed below the water table or entrapped due to water table rise, and their role on natural attenuation processes. Field work conducted at the Bemidji site identified a variety of processes that affect the mass balance of CH_4 in the contaminated subsurface. In the unsaturated zone, methanogenesis and methanotrophy produce and consume CH_4, respectively, and both diffusion and advection are responsible for the transport of CH_4 and other gases. In the saturated zone, the formation of gas bubbles provides a significant sink for dissolved CH_4.

Modeling work suggests that the production of gas bubbles due to methanogenesis in the source zone can lead to a reduction in hydraulic conductivity in this zone, which partially isolates the most heavily contaminated portion of the aquifer, leading to a reduction in contaminant loading to the downgradient aquifer. The entrapment of gas bubbles, of atmospheric composition, due to water table fluctuations can enhance O_2 transport from the unsaturated to the saturated zone and increase in the aerobic degradation of CH_4 or other contaminants, particularly those that are more recalcitrant and do not degrade readily under anaerobic conditions.

The entrapment of gas bubbles near the water table is an example of the interaction between unsaturated and saturated zone processes. Particularly near the source zone, the composition of entrapped bubbles, and therefore their effect on saturated zone geochemistry, will be determined by unsaturated zone natural degradation processes that are temporally and spatially variable. The chemistry of recharge water will also be

221

affected by unsaturated zone processes and can potentially have a significant impact on saturated zone geochemistry.

Another aspect of the relationship between saturated and unsaturated zone processes that has not previously been investigated at the Bemidji site is the consistency between the conceptual models used for degradation processes. The modeling work described in Chapter 4 demonstrated that the geochemical evolution in the saturated and unsaturated zones can be adequately described using the same conceptual model and very similar reaction rates.

In this study, stable gases, specifically N_2 and Ar, are used extensively in field and modeling work to quantify physical processes related to bubble formation and entrapment, and gas transport in general. In the source zone, observed stable gas concentrations are used to quantify degassing. Downgradient of the source, the replenishment of Ar and N_2 along the flowpath is used to quantify the effects of bubble entrapment on gas transport. The quantification of these physical processes also enables biogenic processes to be better quantified. For example, by determining the extent of bubble formation using stable gases, the rates of methanogenesis can be better quantified. Similarly, the extent of Ar and N_2 replenishment is used to quantify the effects of bubble entrapment, which provides an estimate of the potential for aerobic oxidation of CH_4 and other contaminants downgradient of the source near the water table.

The modeling work in Chapter 4 integrates previous studies at the Bemidji site, including investigations of natural attenuation processes in the saturated and unsaturated zones, with additional insights identified in this work, including an enhanced understanding of the rates of CH_4 production, transport and degradation, and the effects

of gas bubble formation and entrapment, into a single conceptual model. The resulting model provides a comprehensive picture of the hydrology and geochemistry at the site, accounting for the evolution of the contaminant plumes in both the saturated and unsaturated zones, as well as interaction between the zones.

Field and modeling evidence in this study suggest that ebullition may be a significant process at the Bemidji site. However, ebullition is not well understood, particularly at the field scale. Therefore, a laboratory column experiment was conducted to provide insights into the factors controlling the extent and rate of ebullition in saturated sediments. This experiment suggests that for the medium sand used, ebullition is an important gas transport mechanism when trapped gas phase saturation exceed 0.20, and that the maximum trapped gas phase saturation is ~0.30. Furthermore, the experiment showed that once ebullition began, over 50% of the gas produced traveled over 1 m through the column.

Despite the site specific nature of this work, the processes discussed are of a fundamental nature and applicable to a wide variety of contaminated sites and geochemical environments, and furthermore, the tools developed to investigate these processes are also widely applicable.

The processes occurring at the Bemidji site are relevant to other sites where gas production occurs. This can include landfill leachated plumes (van Breukelen et al., 2003), nitrate contaminated aquifers (Blicher-Mathiesen et al., 1998) and organic rich natural aquifers (Fortuin and Willemsen, 2005). Although, the process of degassing has been noted at each of these environments, the effects of gas bubble production on contaminant transport have not been fully investigated. The insights gained in this study

223

will help to evaluate other sites and identify processes that could potentially enhance or retard contaminant transport and/or degradation.

The use of dissolved gases to investigate geochemical processes in groundwater is becoming an increasingly important research tool. For example, Manning and Solomon (2003) used dissolved noble gases to estimate groundwater recharge temperature and elevation to constrain the fraction of mountain block recharge in the Salt Lake Valley. Stute and Talma (2000) used measured excess Ne in an aquifer in Namibia to infer a period of increased recharge 6000 years before present. In this work we have expanded the role of dissolved gases as a research tool in contaminated aquifers. In particular, this study was the first to map the spatial distribution of Ar and N_2 along a flow path to determine the extent of degassing, and investigate attenuation of the plume high in CH_4 and depleted in stable gases. Methods developed in this study were employed by Williams et al. (2005) who used dissolved Ar, N_2 and CH_4 to quantify degassing and determine the consumption of organic matter through methanogenesis in a permeable reactive barrier treating acid rock drainage.

This study also demonstrated the use of stable gases, Ar and N_2, as indicators of unsaturated zone processes. Previously, Thorstenson and Pollock (1989) had theorized that stable gas concentrations would be affected by advective gas transport; however, this study was the first to our knowledge to demonstrate this phenomenon in the field. Furthermore, collecting thorough spatial vapour phase data allowed us to qualitatively infer reactive zones and determine the direction of advective gas transport. This data has been further used in the development of a reactive transport model simulating gas

advection in a complex geochemical framework (Molins, 2006), which will allow quantification of advective gas transport in a variety of geochemical settings.

In addition to field based methods, this research has also focused on the development of modeling techniques to simulate gas bubble formation, due to in-situ gas production or bubble entrapment, and the effects of gas bubbles on geochemistry and hydrogeology, including relative permeability changes. These processes were incorporated into the reactive transport code MIN3P, which provides a tool for the investigation of the formation and effects of gas bubbles in complex geochemical and hydrological environments.

This research has also endeavoured to introduce a new approach for investigating ebullition on a macro-scale. The use of dissolved gases as a tracer for ebullition provides a unique perspective in that gas transport can be monitored and measured without the need to capture instantaneous gas movement or decipher pore scale processes. The development of a reactive transport model able to simulate ebullition, although empirical in nature, provides a means of quantifying the rate of ebullition and provides insights into the properties of a porous material with respect to ebullition. The column experiments and reactive transport simulations provide a means of investigating ebullition at the macro-scale but are limited by the lone application to nearly homogenous sediment. Further laboratory experiments in a variety of sediment types, including more complicated stratigraphies, and using different gas production rates, may provide more meaningful constraints on the parameters controlling ebullition, which could potentially lead to field scale investigations

6.1 References

Blicher-Mathiesen, G., McCarty, G.W., Nielsen, L.P. (1998), Denitrification and degassing in groundwater estimated from dissolved dinitrogen and argon, *J. Hydrol.*, *208*, 16-24.

Fortuin, N.P.M., Willemsem, A. (2005), Exsolution of nitrogen and argon by methanogenesis in Dutch ground water, *J. Hydrol.*, *301*, 1-13.

Manning, A.H., Solomon, D.K. (2003), Using noble gases to investigate mountain-front recharge, *J. Hydrol.*, *275*, 194-207.

Molins, S., Mayer, K.U. (2006), Coupling between geochemical reactions and multi-component gas diffusion and advection in porous media – A reactive transport modeling study, *submitted to Water Resources Research*, May 2006.

Stute, M., Talma, A.S. (1998), Glacial temperatures and moisture transport regimes reconstructed from noble gases and $\delta^{18}O$, Stampriet Aquifer, Namibia, in Proceedings Series - International Atomic Energy Agency, Report: STI/PUB/1024, p.307-318

Thorstenson, D.C., Pollock, D.W. (1989), Gas transport in unsaturated zones: multicomponent systems and the adequacy of Fick's Laws, *Water. Resour. Res.*, *25*, 477-507.

van Breukelen, B.M., Roling, W.F.M., Groen, J., Griffioen, J., van Verseveld, H.W. (2003), Biogeochemistry and isotope geochemistry of a landfill leachate plume, *J. Contam. Hydrol.*, *65*, 245-268.

Williams, R.L., Mayer, K.U., Amos, R.T., Blowes, D.W., Ptacek, C.J. (2005). Using dissolved gas analysis to investigate the performance of an organic carbon permeable reactive barrier for the treatment of mine drainage. *Submitted, Appl. Geochem., Sept. 2005.*